

Thesis for the degree of Doctor of Philosophy

The Molecular Modelling of Calixarene Inclusion Complexes

Darren Fayne, B.Sc, MRSC

Dublin City University
School of Chemical Sciences

Supervisors: Prof. Dermot Diamond and Dr. Joshua Howarth

March 2001

I hereby certify that this material, which I now submit for assessment on the programme of study leading to the award of Doctor of Philosophy is entirely my own work and has not been taken from the work of others save to the extent that such work has been cited and acknowledged within the text of my work.

Signed:

Darren Fayne

Darren Fayne

ID No.:

95970665

Date:

24-5-01

Dedicated to the memory of Niall Naughton (1973-2001).

Our life is ours, alone to live,
Friends are there, to love and to give,
We will never forget, the memories remain,
Without you, we will never be the same.

ACKNOWLEDGEMENTS

It is people that make a place enjoyable to work in. In DCU there's a lot of people still here, and those who made their escape, that have made being here a much more.....what's the phrase I'm looking for...interesting experience! A few people who have accompanied me down the narrow slippery path when I needed it, and a lot more who have rushed headlong, arm-in-arm down the broad well-trodden road, when I probably would have been better off without it, but life wouldn't have been nearly as much fun! There are too many people to mention but I'll see how many I can get through in the next half an hour or so!

Fran "Mobile phones, 5 for 50" the Man, the football crew (my toe, ankles and knees have fond, cherished memories), the bouncy toed diddley-eye boy, ye olde AS4's/STOCS/Twerg (aka Jobble)/Deno (aka rasher)/bloke with no name/Le hindian/Laner and his pot-bellied Vietnamese lady friend/black hole/Mick (aka Luke)/Larkin (How you survived I'll never know)/Moses (currently Ms. Moses)/Melon, and their card playing marathons in the 'real' canteen smokers section (You nearly cost me my second year exams!), Dr. Lukeimus (Go on the Kingdom) 'Kiwi' O'Brien, philowaffle Fiona (thanks for listening), Fraggers united – Shane "I appreciate Prince's music" O'Neill, Mr. Duff (your turn...), Nick, Hogie Bear and Big Joe – Doom made the prefab bearable!!, the honoured members of Loserville...who have all miraculously turned into winners...Beverly Hills 90210 will never seem the same to me again and Bobs will always be Bad (but MT's worse!), young Wilson and his "Just out for one pint", Andrea "One pint more"...we were the classiest people in Roskilde!, Johan who has being chilled out down to a refined art-form (Danish, old-folks retirement home, islands here I come!), Damo "Jimi" Lynch, Luisimo, Eadain and her evil laugh, the poker heads – Ger, Cotsey, Frank (Naaaavaaaan), Adrian – some good nights/early mornings, Eimear (That smirnoff ice wasn't too bad!!!), Michaelhaha with her sheepy jackets and fluffy, yellow slippers. Marion "Just one more spin around the dancefloor", Wavey Davey with his ear-breaking rendition of Twist and Shout, the Canoers...Honest, I have been in a canoe...Achill was the best, all in the "foreign" student's house,

Belfast...the international food day nearly was the death of me! And, yep you were right, I was employed by the university to get you all out as often as possible!, The Prinsengrachtians, the hip-hop happening crew – Martina, Paula, Jill‘or’, Eavan (I knew I shouldn’t have left you five unguarded!!!) and Emma – for a good night out that helped relax me before the main event and all the unsung heros...

We all made it back basically intact, well, ignoring the sticks in the park, 40 winks in phone boxes, ladies of a foreign persuasion, the rants & raves, “Whelans isn’t too far, honest”, Friday slops in the Kipper, and God knows what happened in the bushes. Thanks to all the technicians also, especially Damo (the tongue) McGuirk (Oooooook!!) and Ambrose...I’ll come back next year to help get revenge in the soccer tournament...we may even get some sweet, amber nectar next time! The BEST centre office crew have also been great...especially when it came to calming me down when the printer just sat there laughing at me! And as for Paddy with his bananas, I’ll be having nightmares about them for years to come. A special appreciation goes out to all those who were there for me during the last couple of months. To all those in DCU and The Free World, thanks for a great few years.

Now that I’ve finished with the saints, it’s time to move onto the scholars... My thanks go out to Dermot for his faith and trust in me, advice to me...and also for the few pennies that flew my way every once in a while! But there shall be no more playing certain games which involve me buying loads of drinks, only one of which for myself, after Christmas dinner! Thanks to Josh for introducing me to the wonders of synthetic chemistry and for letting me get away from it also. His Christmas drinks, sorry meal, were always interesting! I’d also like to thank the two men that allowed me into Queens University, Belfast. Dr. Bell and Prof. McKervey. They were of great help to me as I was starting out on the twisty postgrad road.

Lastly, my family. Who have kept me going and believed in what I could do. Support and advice when I needed it, but the latter tended to fall on deaf ears! I can’t thank you guys enough.

Sláinte,

Darren Fayne

PUBLICATIONS

1. Howarth, J., Fayne, D., Hanlon, K. and McCormac, P., "Moisture stable dialkylimidazolium salts as heterogeneous and homogeneous Lewis acids in the Diels-Alder reaction", *Tetrahedron Letters*, **1997**, 38, 17, 3097-3100.
2. Bell, S.E.J., McKervey, M.A., Fayne, D., Kane, P. and Diamond, D., "Molecular modelling of calixarenes with group 1 metal ions", *J. Molecular Modeling*, **1998**, 4, 44-52.
3. Kane, P., Fayne, D., Diamond, D., Bell, S.E.J. and McKervey, M.A., "Modelling of the sodium complex of a calixarene tetraester in the 1,3-alternate conformation", *J. Molecular Modeling*, **1998**, 4, 259-267.
4. Kane, P., Kincaid, K., Fayne, D., Diamond, D. and McKervey, M.A., "Modelling metal complexes of calixarene esters and phosphine oxides using molecular mechanics"; *J. Molecular Modeling*, **2000**, 6, 272-281.

CONFERENCES AND MEETING ATTENDED

- Attended the Irish postgraduate chemistry colloquia in Cork (2000), Dublin DIT colleges (1999), Galway (1998), DCU (1997) and Cork (1996).
- Attended a Schrödinger Inc. workshop in London where various aspects of their new software (Titan and Jaguar) were discussed (June, 1999).
- Presented a poster entitled "Amino acid:chiral calixarene interactions investigated by fluorescence and molecular modelling studies" at the Royal Society of Analytical Chemistry conference held in DCU on 25-30th July 1999.
- Contributed the molecular modelling section to a body of work that won best poster (Entitled "Enantiomeric Selectivity by Calixarenes") at the CALIX '99 conference in Perth, Australia.
- Attended the Irish Atomistic Simulation Conference, University College Cork, 21st December 1998.
- I was involved in the organisation of the "Training Of Teachers" seminar in which myself and colleagues explained various aspects of molecular modelling to staff and postgraduate students from the chemistry and biology departments in DCU. I gave a talk entitled "Determination of NMR, UV and IR spectra utilising molecular modelling software" (Dublin City University, January 15-16th, 1998).

TABLE OF CONTENTS

| | |
|---|----------|
| Declaration----- | ii |
| Dedication----- | iii |
| Acknowledgements----- | iv |
| Publications and meetings----- | vi |
| Table of contents----- | vii |
| Abstract----- | xi |
| Abbreviations----- | xiii |
| Contents of CD----- | xvi |
| | |
| 1. MOLECULAR MODELLING: THEORY AND LITERATURE----- | 1 |
| 1.1 INTRODUCTION ----- | 2 |
| 1.2 A BRIEF HISTORY OF MOLECULAR MECHANICS ----- | 3 |
| 1.3 WHY PERFORM MOLECULAR MECHANICS CALCULATIONS?----- | 4 |
| 1.4 ISSUES WITH MOLECULAR MECHANICS ----- | 9 |
| 1.4.1 Global minimum problem----- | 9 |
| 1.4.2 Parameterisation----- | 9 |
| 1.4.3 Molecular interactions----- | 10 |
| 1.4.4 Electron density ----- | 10 |
| 1.4.5 Polarisation----- | 10 |
| 1.5 FORCE FIELDS ----- | 10 |
| 1.5.1 Bond stretching----- | 12 |
| 1.5.2 Angle bending ----- | 14 |
| 1.5.3 Torsional terms ----- | 16 |
| 1.5.4 Van der Waals' interactions ----- | 18 |
| 1.5.5 Electrostatic and hydrogen bonding terms----- | 20 |
| 1.5.6 Additional terms----- | 24 |
| 1.5.7 Problems with X-ray crystallography ----- | 24 |

| | | |
|----------|---|----|
| 1.5.8 | Neutron diffraction spectroscopy ----- | 25 |
| 1.6 | THE QUEST FOR THE GLOBAL ENERGY MINIMUM ----- | 27 |
| 1.6.1 | Molecular Dynamics ----- | 28 |
| 1.6.2 | Metropolis Monte Carlo ----- | 31 |
| 1.6.3 | Simulated Annealing ----- | 33 |
| 1.6.4 | Dynamic Monte Carlo ----- | 34 |
| 1.6.5 | Genetic Algorithms ----- | 34 |
| 1.7 | AVAILABLE MINIMISATION ALGORITHMS ----- | 35 |
| 1.7.1 | Steepest Descent ----- | 36 |
| 1.7.2 | Polak Ribiere ----- | 37 |
| 1.7.3 | Newton Raphson ----- | 38 |
| 1.8 | TO SOLVATE OR NOT TO SOLVATE? ----- | 39 |
| 1.8.1 | Explicit inclusion of solvent molecules ----- | 41 |
| 1.8.2 | Continuum methods ----- | 41 |
| 1.8.3 | Application to Monte Carlo methods ----- | 44 |
| 1.9 | METHODS FOR CALCULATING ATOMIC CHARGES ----- | 45 |
| 1.9.1 | Point charges ----- | 46 |
| 1.9.2 | Mulliken method for charge partitioning ----- | 47 |
| 1.9.3 | Charges based on fits to electrostatic potentials ----- | 48 |
| 1.9.4 | Which method is better? ----- | 49 |
| 1.9.5 | Effect on the conformational energy by variation in charge sets ----- | 49 |
| 1.10 | MOLECULAR MODELLING OF CALIXARENES AND RELATED COMPLEXES ----- | 50 |
| 1.10.1 | Uncomplexed calixarene tetrol ----- | 52 |
| 1.10.1.1 | Recent experimental work on the parent calixarene tetrol ----- | 53 |
| 1.10.2 | Calixarene:amine inclusion complexes ----- | 56 |
| 1.10.2.1 | Lower rim functionalisation ----- | 57 |
| 1.10.2.2 | Upper rim functionalisation ----- | 58 |
| 1.10.2.3 | Sulfonate calix[6]arene ----- | 62 |
| 1.10.2.4 | Calix[5]arene complexing three amines ----- | 62 |

| | | |
|-----------|--|-----------|
| 1.10.2.5 | Chiral calixarenes incorporated into chromatographic separations ----- | 63 |
| 1.10.3 | Dihomooxacalix[4]arene and resorcarene studies ----- | 64 |
| 1.10.4 | Crown ether studies ----- | 65 |
| 1.10.5 | Cyclodextrin studies ----- | 68 |
| 1.11 | CHIRAL RECOGNITION AND SELECTIVE COMPLEXATION ----- | 70 |
| 1.11.1 | Tools for structural recognition ----- | 74 |
| 1.11.2 | Preorganisation ----- | 76 |
| 1.11.3 | Complementarity ----- | 78 |
| 1.11.4 | The physical chemistry of molecular recognition ----- | 78 |
| 1.12 | HYDROGEN BONDING ----- | 81 |
| 1.12.1 | Role in intermolecular interactions ----- | 82 |
| 1.12.2 | Types of hydrogen bonds ----- | 83 |
| 1.12.3 | The structure of hydrogen bonds ----- | 85 |
| 1.12.4 | Length of hydrogen bonds ----- | 86 |
| 1.12.5 | Strength of hydrogen bonds ----- | 87 |
| 1.12.6 | Directionality of hydrogen bonds ----- | 90 |
| 1.12.7 | Bifurcated bonds ----- | 90 |
| 1.12.8 | The Hydrophobic Effect ----- | 91 |
| 1.12.9 | X-ray diffraction studies ----- | 92 |
| 1.12.10 | Computational considerations ----- | 93 |
| 1.12.11 | <i>p-tert.</i> -butyl calix[4]arene tetrol ----- | 94 |
| 1.13 | INCORPORATION OF FLUOROPHORES /CHROMOPHORES INTO SENSORS ----- | 95 |
| 2. | MOLECULAR MODELLING STUDYS ON CALIX[N]ARENES | |
| | COMPLEXING ALKALI METAL CATIONS ----- | 99 |
| 2.1 | CALIXARENE CONFORMATION ----- | 100 |
| 2.2 | INTRODUCTION ----- | 101 |
| 2.3 | EXPERIMENTAL ----- | 103 |
| 2.4 | RESULTS ----- | 105 |

| | | |
|--|---|-----|
| 2.4.1 | Calix[4]arenes ----- | 105 |
| 2.4.1.1 | <i>p-tert.</i> -butylcalix[4]arene tetrol ----- | 105 |
| 2.4.1.2 | Tetramethyl <i>p-tert.</i> -butylcalix[4]arene tetraether ----- | 110 |
| 2.4.1.3 | Tetramethyl <i>p-tert.</i> -butylcalix[4]arene tetraester ----- | 113 |
| 2.4.1.4 | Tetraethylamide <i>p-tert.</i> -butylcalix[4]arene ----- | 117 |
| 2.4.1.5 | Tetraethyl <i>p-tert.</i> -butylcalix[4]arene tetraester ----- | 119 |
| 2.4.2 | Penta <i>p-tert.</i> -butylcalix[5]arene pentaketone ----- | 122 |
| 2.5 | CONCLUSIONS ----- | 124 |
| 3. ENANTIOSELECTIVE COMPLEXATION OF CHIRAL AMINES BY CHIRAL | | |
| CALIX[4]ARENES: A COMPUTATIONAL INVESTIGATION ----- 126 | | |
| 3.1 | INTRODUCTION ----- | 127 |
| 3.1.1 | Requirements for enantioselective complexation ----- | 127 |
| 3.2 | EXPERIMENTAL ----- | 129 |
| 3.3 | RESULTS ----- | 131 |
| 3.4 | CONCLUSIONS ----- | 146 |
| 4. IONIC LIQUIDS ----- 149 | | |
| 4.1 | INTRODUCTION ----- | 149 |
| 4.2 | EXPERIMENTAL ----- | 149 |
| 4.2.1 | NMR data ----- | 150 |
| 4.2.2 | Experimental procedure ----- | 151 |
| 4.3 | RESULTS AND DISCUSSION ----- | 151 |
| 5. BIBLIOGRAPHY ----- 153 | | |
| 6. REFERENCES ----- 155 | | |

The Molecular Modelling of Calixarene Inclusion Complexes.

ABSTRACT:

Darren Fayne

School of Chemical Sciences,
Dublin City University

Chapter 1:

This consists of a literature review and an introduction into the variety of computational techniques and methodologies available.

Chapter 2:

The molecular modelling of alkali metal complexes with calixarenes. We have published three papers in this area¹.

The HyperChem molecular modelling software package has been demonstrated to be a straightforward and computationally undemanding technique that is surprisingly good at reproducing the structures of a range of metallo-calixarenes.

Chapter 3:

The molecular modelling of the enantioselective complexation of chiral amines by chiral calix[4]arenes.

With reference to the enantioselective complexation studies we have shown that by using molecular modelling software, an insight can be gained into the interactions that occur on complexation of chiral amines by chiral calixarenes. By observing the hydrogen bonding patterns formed between the host and guest we can postulate why one enantiomer interacts more strongly than the other and, hence, provide a plausible explanation for the observed enantiomeric selectivity observed in the fluorescence quenching experiments.

Chapter 4:

The catalysis of the Diels Alder reaction by ionic liquids. The first example of the usage of dialkylimidazolium salts ($R_2Im^+X^-$) as heterogeneous and homogeneous Lewis acids catalysts in the Diels-Alder reaction is detailed in a published paper².

¹ (a) Bell, S.E.J., McKervey, M.A., Fayne, D., Kane, P. and Diamond, D., "Molecular modelling of calixarenes with group 1 metal ions", *J. Molecular Modeling*, **1998**, 4, 44-52; (b) Kane, P., Fayne, D., Diamond, D., Bell, S.E.J. and McKervey, M.A., "Modelling of the sodium complex of a calixarene tetraester in the 1, 3-alternate conformation", *J. Molecular Modeling*, **1998**, 4, 259-267; (c) Kane, P., Kincaid, K., Fayne, D., Diamond, D. and McKervey, M.A., "Modelling metal complexes of calixarene esters and phosphine oxides using molecular mechanics", *J. Molecular Modeling*, **2000**, 6, 272-281.

² Howarth, J., Fayne, D., Hanlon, K. and McCormac, P., "Moisture stable dialkylimidazolium salts as heterogeneous and homogeneous Lewis acids in the Diels-Alder reaction", *Tetrahedron Letters*, **1997**, 38, 17, 3097-3100.

ABBREVIATIONS

E_{bond} : Bonding energy,

E_{angle} : Valence angle energy,

E_{torsion} : Torsional angle energy,

E_{vdW} : van der Waals interaction energy,

$E_{\text{electrostatic}}$: Electrostatic interaction energy,

$E_{\text{H-bond}}$: Energy derived from hydrogen bonding interactions,

k_{rij} : Bond stretching potential constant,

r_{ij} : Calculated bond length between atoms i and j,

r_0 : Equilibrium bond length,

θ_{ijk} : Calculated bond angles between the atoms i, j and k,

θ_0 : Equilibrium bond angles between the atoms i, j and k,

$k_{\theta_{ijk}}$: Angle bending potential constant,

E_{sb} : Stretch bend interaction energy,

k_{sb} : Stretch bend potential constant,

r_1 , r_2 and θ : Explained in **Figure 5**,

r_{01} , r_{02} and θ_0 : Ideal values of the variables shown in **Figure 5**,

V_n : n -fold barrier to torsional rotation,

n : Usually 1, 2 or 3,

s : +1 or -1 according to whether a staggered (+1) or eclipsed (-1) conformational is the most stable,

ω : Torsional angle,

A_{ij} : A parameter that controls the depth of the potential energy well between two atoms, i and j,

B_{ij} : A parameter that controls the position of the potential energy well between two atoms, i and j,

A'_{ij} , B'_{ij} and C_{ij} : Constants relevant to the atoms i and j,

c_1 , c_2 and c_3 : universal constants,

ε^* : Reflects the pair potential well depth,
 ε_i and ε_j : Well depths of the individual atoms, i and j ,
 r^* : Sum of the van der Waal radii for atoms i and j ,
 ε : Dielectric constant,
 q_i and q_j : Partial charges of atoms i and j ,
 C_{ij} and D_{ij} : Coefficients depending on the atoms i and j ,
 F : Force exerted on the atom,
 m : Mass of the atom,
 a : Atom's acceleration,
 V : Potential energy at position r ,
 Δt : Small time step,
 d_i : Atomic velocities,
 R : Gas constant,
 T : Simulation temperature,
 $\text{RAN}[0,1]$: A random number between 0 and 1,
 x_0 : Initial atomic coordinates,
 Δx : Change in atomic coordinates,
 h_{i+1} : The conjugate gradient,
 g_{i+1} : The gradient at the point $i+1$,
 h_i : The previous search direction,
 β : An indication how much the previous search direction influences the current direction,
 g_i : The gradient at the point i ,
 r_i : Minimum at the i th point in **Section 1.7.3**,
 r_{i-1} : Minimum at the previous step,
 $A(r_{i-1})$: Matrix of the second partial derivatives of the energy with respect to the coordinates at r_{i-1} ,
 $\nabla E(r_{i-1})$: Gradient of the potential energy at r_{i-1} ,
 G_{elec} : Energy of electrostatic interaction,
 a : Radius of the solvent cavity,
 q : Charge on the solvated cation,
 $G_{\text{solvation}}$: Energy of solvation,

$G_{\text{dispersion}}$: Dispersion energy,

$G_{\text{electrostatic}}$: Electrostatic energy.

Files included on the CD inside the back cover of the thesis

An electronic version of the full thesis.

The ChemDraw structures of the relevant figures.

The modelled structure of the calixarenes structures. These are saved as the pdb file format. A Windows version of Rasmol is also included for the visualisation of the files but all molecular modelling software packages should have the ability to read in and display the files. The numbering scheme illustrated in **Figure 55** is relevant to the file names.

A movie file of R-phenylglycinol docking with L1 was generated by slowly moving the amine into the calixarene inclusion cavity, saving the images as it progressed and generating an avi file afterwards.

The numbers on the journal articles in my lab (XG25) refer to their reference number in the thesis.

1 MOLECULAR MODELLING: THEORY AND
LITERATURE

1.1 INTRODUCTION

The underlying physical laws necessary for the mathematical theory of a large part of physics and the whole of chemistry are thus completely known, and the difficulty is only that the exact application of these laws leads to equations much too complicated to be solvable...Dirac, 1929 [1].

But the creative principle resides in mathematics. In a certain sense, therefore, I hold it true that pure thought can grasp reality, as the ancients dreamed...Albert Einstein.

We are now reaching the time that by using only the equations and theories given by mathematicians to theoretical chemists, biologists and physicists we can predict and verify observations in the astronomical, physical, chemical and biological worlds. Great progress has been made in these areas and even though many of the equations are still too complicated to be completely solvable, approximate solutions are accessible, and using computers these approximations are approaching ‘chemical accuracy’ [2]. In computational chemistry one does not directly develop new theoretical methods. It can, however, suggest where improvements can be made to the underlying theory. Computers just generate numbers; it is people that actually solve the problems. The hardware and software generate data that a human may use to gain insight into the behaviour of molecules.

The expanding role of computational methods in chemistry has been fuelled by the steady and rapid increase in computing power over the last fifty years as illustrated in **Figure 1**. The ratio of performance to price has increased by an order of magnitude every five-to-seven years, and there is no weakening in this trend. The introduction of massive parallelism in computer architecture will easily maintain the present growth rate. Parallelism involves a group of processors working on different parts of a calculation and

combining the results at the end. Improvements in the computational and theoretical methodologies allows a more refined application of these techniques to the study of chemical systems. This means that more complex molecular systems may be simulated over longer periods of time, or that it will be possible to handle more complex interaction functions in the years to come.

1.2 A BRIEF HISTORY OF MOLECULAR MECHANICS

The earliest reference to molecular mechanics that I have found is in a paper by Andrews [3], which was written with reference to vibrational spectroscopy. But as this was in 1930, computational power, and the software, was not yet available to efficiently solve the relevant equations. It was a further sixteen years until Hill, Dostrovsky and Westheimer & Mayer published three separate papers [4], which taken together provide a very substantial basis for molecular modelling. What these papers basically demonstrated was that if one included van der Waals' interactions in the vibrational spectroscopist's force fields, structures of molecules, energy relationships between conformations, vibrational and thermodynamic information could be obtained. However, the computational power was still beyond them so they could only test out these ideas on very simple or idealised cases.

Fifteen more years passed before Hendrickson [5], in 1961, published an application of these calculations to a study of the geometries of medium sized cycloalkanes, utilising a computer for the extensive calculations. This started the ball rolling and in 1965, Wilberg [6] published the results and description of a general computer program for optimising molecular geometries. It was very simplistic but may be viewed as the basis for all subsequent development in this area.

The crucial factor which enabled a set of reasonably well established ideas to be turned, in the space of a few years, into the very broad and widely used discipline was not due to some sudden improvement in the available theories. In common with many other branches of science (such as spectroscopy), which are heavily dependent on instrumentation, it was a consequence of improvements in the equipment available to perform the experiments. Which, in this case, was the emergence of digital computers, which offered sufficient power to perform the calculations required, in a reasonable amount of time and not at an exorbitant cost.

Since then various research groups tackled the problem of developing widely applicable and accurate force fields. Initially, the force fields created took very different forms but as time proceeds they are becoming more similar to each other and the differences between them will probably continue to narrow as a function of time. Ideally, one hopes that such refinements will eventually lead towards a unified computational model that can successfully mimic nature on a routine basis.

1.3 WHY PERFORM MOLECULAR MECHANICS CALCULATIONS?

The basis presupposition behind molecular mechanics is that the atoms in a molecule can be treated as a collection of spherical masses interacting through a variety of simple electrostatic and harmonic forces. The form taken by these equations is described in **Section 1.5**. Conversely to the Born-Oppenheimer approximation, which allows one to treat the electrons in a molecule explicitly for ab initio/semi-empirical calculations, molecular mechanics calculations are concerned with the positions of the nuclei and does not deal with electron distribution.

Due to the fact that molecules tend to be composed of subunits which are structurally similar in different molecules a set of parameters, or ideal values, can be compiled for bond lengths, angles etc which can be broadly applied over a wide range of molecules. An example of this is the C–H bond length. In different molecules, values for it range from 1.06 to 1.10 Å (For example: C_{sp3}–H=1.06 Å, C_{sp2}–H=1.08 Å [7]). When being attached to single, double or triple bonded carbon atom is taken into account the variation between these values decreases even more. It is now conceivable that a set of parameters can be accurately determined for a group of molecules and subsequently applied to molecules which were not included in the parameterisation set.

The overall energy of the molecule thus takes the form shown in **Equation 1**.

$$E = E_{\text{bond}} + E_{\text{angle}} + E_{\text{torsion}} + E_{\text{vdW}} + E_{\text{electrostatic}} + E_{\text{H-bond}} + \dots \quad \text{Equation 1}$$

Where E_{bond} is the bonding energy, E_{angle} the valence angle energy, E_{torsion} the torsional angle energy, E_{vdW} the van der Waals interaction energy, $E_{\text{electrostatic}}$ the electrostatic interaction energy, $E_{\text{H-bond}}$ the energy derived from hydrogen bonding interactions and "... indicates that further interactions can also be included in this equation as deemed appropriate. **Equation 1** details the various structural features that parameters are required for. Some idea of the complexity of the task is given in **Table 1**, as the number of parameters required for a highly accurate force field is relatively large.

| Term | Estimated number of parameters | Actual number of parameters |
|----------------------|--------------------------------|-----------------------------|
| E_{vdW} | 142 | 142 |
| E_{bond} | 900 | 290 |
| E_{angle} | 27,000 | 824 |
| E_{torsion} | 1,215,000 | 2466 |

Table 1. A comparison of the possible and the actual number of MM2(91) [8] parameters [9].

As can be seen, only 0.3% of the estimated total torsional space is parameterised. The reason for the increase in the number of parameters as we go from van der Waals to torsional parameters is because the number of atoms involved in the corresponding interactions increases. In the case of the vdW term only one atom is needed but for torsional terms, four different atoms are involved, which can be combined in different arrangements. Hence, the great increase in the number of parameters required. In order to obtain a value for one parameter at least 3 or 4 independent sets of data should be used. A further problem is the fact that the dihedral/torsional parameters are the hardest ones to obtain experimental data for. There is a great discrepancy between the possible and actual parameters shown above but it has been estimated that ~20% of the ~15 million known compounds can be modelled with MM2 parameters. MM2 is one of the most commonly used force fields for general organic compound modelling. See **Section 1.5** for further information regarding force fields.

Now that we have a set of parameters we need to consider how long it will take to evaluate their contribution to the energy of the molecule. When we consider a set of linear alkanes, $\text{CH}_3(\text{CH}_2)_{n-2}\text{CH}_3$, we can see that E_{vdW} requires, by far, the greatest amount of computational effort as shown in **Table 2**. For large molecules most of the atoms are not bonded to each other, or to a common atom, so they interact through E_{vdW} terms. The use of non-bonded cut-offs or keeping a non-bonded list can help to alleviate this problem.

| n | N_{atoms} | E_{bond} | E_{angle} | E_{torsion} | E_{vdW} |
|--|--------------------|-------------------|--------------------|----------------------|------------------|
| 10 | 32 | 31 | 60 | 81 | 405 |
| 20 | 62 | 61 | 120 | 171 | 1710 |
| 50 | 152 | 151 | 300 | 441 | 11025 |
| 100 | 302 | 301 | 600 | 891 | 44550 |
| Formula to calculate the number of terms | N | $(N-1)$ | $2(N-2)$ | $3(N-5)$ | $N(N-1)/2-3N+5$ |

Table 2. The number of terms for each energy contribution in $\text{CH}_3(\text{CH}_2)_{n-2}\text{CH}_3$ [10].

What follows is a list of advantages and benefits with respect to the use of molecular modelling techniques.

- ◆ Modelling may be performed on highly reactive molecules and on transition states (if parameters are available) as easily and reliably as on stable species; experiments become increasingly more difficult with increasing reactivity and can only be applied to transition states under special circumstances.
- ◆ Models can be analysed in great detail to understand the origin of chemical phenomena. Simplified systems and/or systems with specific structural features may easily be considered. A single parameter can be changed and its effect on the rest of the system can be monitored.
- ◆ The amount of computer time required increases with the square of the number of atoms in the molecule of interest. With molecular orbital methods the increase is to the 3rd-6th power of the number of orbitals (more precisely, the number of basis functions used to describe each orbital) present. So molecular mechanics calculations are much less computationally expensive than their molecular orbital counterparts and can study much larger molecular systems.

- ◆ Software and algorithms are available that allow one to simulate and study molecules of the size of proteins.
- ◆ Studies can be performed on the conformational flexibility of relatively large molecules. Methods such as Molecular Dynamics, Metropolis Monte Carlo simulation (see **Section 1.6**) and free energy perturbation calculations are all readily accessible.
- ◆ Modelling is becoming less and less costly to perform largely due to a constant decrease in hardware price:performance ratios, while experimental chemistry is becoming ever more expensive; especially with environmental concerns increasingly being considered.
- ◆ As the sophistication of the molecular modelling software increases, instead of going through the procedure of synthesising many different compounds and testing them to see if they have properties of interest, such as in combinatorial chemistry currently utilised in the pharmaceutical industry, they can be modelled initially which yields information on their structural features and certain chemical properties.
- ◆ Along with spectroscopic and crystallographic techniques, molecular modelling helps the experimental chemist in the elucidation of 3D chemical structures and bonding patterns.
- ◆ It is a very useful tool to aid in the visualisation of the 3D structure of molecules. Even before the consideration of electronic factors, the structural features of the molecule may be examined to see if they preclude the reaction of interest occurring. Previously, chemists had to rely upon Dreiding or CPK hand held models in order to examine the conformations of a molecule.

1.4 ISSUES WITH MOLECULAR MECHANICS

Molecular mechanics calculations are a lot more straightforward (theoretically and computationally) to apply than *ab initio* or semi-empirical calculations but there are still a number of pitfalls inherent in the procedure [11]. People utilising these methodologies need to be aware of potential problems.

1.4.1 Global minimum problem

Large molecules can adopt many millions of conformations, but only a small proportion of these will contribute significantly to the ground state properties of the molecule. A straightforward geometry optimisation will not necessarily yield the global minimum so other approaches need to be implemented. Methods for surmounting this problem are dealt with in **Section 1.6**.

1.4.2 Parameterisation

Molecular mechanics is parameterised with reference to experimental and/or *ab initio* data for a select ‘training set’ of molecules (**Section 1.5**). The quality of these parameters depends on how accurate these calculated data are and new molecules may not necessarily have all the required parameters in the force field. Swapping and guessing parameters constitutes one of the major abuses of molecular mechanics. Parameterisation should involve fits to databases that may include molecular structure, vibrational data, heats of formation, molecular dipole moments, heats of sublimation, or rotational barriers from NMR or other spectroscopic measurements. It is often difficult to obtain all the relevant data needed to generate reliable parameters.

1.4.3 Molecular interactions

Electronic properties are not dealt with explicitly because molecular mechanics is based on nuclear positions only; electrons are not taken into account. Effective parameterisation may provide reliable results but a much more effective method is the usage of semi-empirical or ab initio methods. Comparison to experimental results needs to be performed as a form of validation before new molecules can be examined.

1.4.4 Electron density

Related to this is the fact that molecular mechanics cannot deal with chemical reactions as changes in bonding connectivity cannot be modelled. Atomic charges and electron density maps, as discussed in **Section 1.9**, cannot be calculated by molecular mechanics methods either.

1.4.5 Polarisation

In most force fields a change in the molecular structure does not effect the partial charges assigned to the various atoms in the molecule [12]. This is an unrealistic way of dealing with conformational changes and, especially, complexation interactions as the electron distribution around the molecule(s) can be significantly altered.

1.5 FORCE FIELDS

Strictly speaking, each molecule should have its own unique force field. Fortunately, however, the interpolation, or sometimes extrapolation, of existing data is usually adequate to describe related families of molecules. The parameterisation of the

force field relies heavily on experimental, or ab initio computational, data collected over the years, and judicious choice must be made in sorting out good and bad data because the reliability of the method implemented can be no better than the data used for parameterisation.

In the following equations the “ k ” values in the various equations will be referred to as “potential constants”. The reader will be more familiar with the term “force constants” but this term refers to a spectroscopists force field, and potential constants refer to molecular mechanics force fields. As spectroscopic force constants cannot be directly transferred into molecular mechanics force fields it would be misleading to refer to both constants in the same way.

Figure 2 shows a schematic diagram of some of the various interactions that are taken into account in a force field model and **Table 3** shows some experimentally determined bond lengths and energies.

| Bond lengths | | Diatomic bonds | | Polyatomic bonds | |
|--------------|------|----------------|----------|------------------|----------|
| | Å | | (kJ/mol) | | (kJ/mol) |
| H-C | 1.09 | H-H | 435 | H-C | 414 |
| H-N | 1.00 | O=O | 498 | H-N | 389 |
| H-O | 0.96 | N=N | 946 | H-O | 464 |
| C-C | 1.54 | H-F | 565 | C-C | 347 |
| C-N | 1.47 | H-Cl | 431 | C-N | 305 |
| C-O | 1.43 | H-Br | 368 | C-O | 360 |
| C-Cl | 1.76 | H-I | 297 | C-Cl | 339 |
| P-O | 1.57 | F-F | 155 | C-F | 485 |
| C=C | 1.35 | Cl-Cl | 243 | C=C | 611 |
| C=N | 1.30 | Br-Br | 193 | C=N | 615 |
| C=O | 1.22 | I-I | 151 | C=O | 749 |
| P=O | 1.47 | - | - | C≡C | 837 |

Table 3. Some experimental bond lengths and energies [13].

1.5.1 Bond stretching

Either the exponential Morse potential function or the much simpler Hooke's Law can represent the bond stretching potential. A Morse potential has been used in Urey-Bradley and other early force field calculations but (owing to its more complicated nature) requires greater computation, without significant increase in accuracy. The potential has been extensively replaced by the simpler Hooke's Law expression given in **Equation 2:**

$$E_{\text{bond}} = \sum_{r_{ij}} k_{r_0} \frac{1}{2} (r_{ij} - r_0)^2 \quad \text{Equation 2}$$

Where $k_{r_{ij}}$ is the bond stretching potential constant, r_{ij} is the calculated bond length between atoms i and j , and the r_0 is the equilibrium bond length.

The agreement between the two curves (the experimental and theoretical) is good for near equilibrium bond lengths (**Figure 3**), although problems may occur for molecules with exceptionally long bonds (where the strain is overestimated). Cubic (and higher) terms may be added to **Equation 2** to improve the potential curve at longer bond lengths, offering considerable improvement for sterically crowded molecules. However, the cubic term overcompensates for the excess repulsion incurred at long distances with the result that a bad starting geometry (very long bonds) may result in atoms flying apart. Therefore, this term should be used later in the optimisation procedure when the geometry has improved somewhat.

Some sample values for the equilibrium bond lengths and potential constants are detailed in **Table 4**.

| Bond | R_0 (Å) | k (kJ mol ⁻¹ Å ⁻²) |
|------------------------------------|-----------|---|
| Csp ³ -Csp ³ | 1.523 | 1326 |
| Csp ³ -Csp ² | 1.497 | 1326 |
| Csp ² =Csp ² | 1.337 | 2887 |
| Csp ² =O | 1.208 | 3251 |
| Csp ³ -Nsp ³ | 1.438 | 1536 |
| C-N- (amide) | 1.345 | 3008 |

Table 4. Selected equilibrium bond lengths and potential constants for the MM2 [8] force field.

We can see how the potential constants vary with the bond order and the atoms involved in various bonds.

1.5.2 Angle bending

Valence angle bending is dealt with in a manner exactly analogous to bond lengths and is shown in **Figure 4**.

$$E_{\text{angle}} = \sum_{\theta_{ijk}} k_{\theta_{ijk}} \frac{1}{2} (\theta_{ijk} - \theta_0)^2 \quad \text{Equation 3}$$

θ_{ijk} and θ_0 represent calculated and equilibrium bond angles, respectively, $k_{\theta_{ijk}}$ is the angle bending potential constant and with cubic (and higher) additions to the simple Hooke's Law relationship possible for better consideration of distorted valence angles in strained molecules.

Table 5 shows some typical values of the potential constants and equilibrium angles for a variety of angle bending terms. When compared to **Table 4** it can be seen that the potential constants are significantly smaller than those associated with bond stretching potential constants.

| Angle | θ (°) | k (kJ mol ⁻¹ deg ⁻¹) |
|--|--------------|---|
| Csp ³ -Csp ³ -Csp ³ | 109.47 | 0.0414 |
| Csp ³ -Csp ³ -H | 109.47 | 0.0331 |
| H-Csp ³ -H | 109.47 | 0.0293 |
| Csp ³ -Csp ² -Csp ³ | 117.2 | 0.0414 |
| Csp ³ -Csp ² =Csp ² | 121.4 | 0.0506 |
| Csp ³ -Csp ² =O | 122.5 | 0.0423 |

Table 5. Selected equilibrium bending angles and potential constants for the MM2 force field.

Several points concerning bending and stretching forces should be made.

(a). More energy is required to stretch a bond than to bend it for equal atomic displacements. Basically, $k_{r_{ij}} > k_{\theta_{jk}}$ by about a factor of 10. Therefore, if the molecule is deformed we would expect to find most of the distortion in the bond angles, rather than bond lengths.

Also, in general it takes less energy to distort a torsional angle (single bond) than it does to shift a bond angle from its natural value. Therefore, a molecular distortion will usually show up more in the torsional energy of a molecule. In the treatment of very large molecules it is common to hold the bond lengths and angles fixed and to vary only the torsional angles [14].

(b). Hooke's Law overestimates the energies required to achieve large distortions. When bond angles, or lengths, are greatly deformed from their natural values the atomic orbitals no longer efficiently overlap, leading to a reduction in the potential constant. **Equations 2** and **3** assume constant values for potential constants regardless of how severe the angle is deformed or the bond is stretched. In order to correct the Hooke's Law potentials, cubic terms are usually added to **Equations 2** and **3**.

(c). When a bond angle is compressed the two associated bond lengths become longer. Two ways for accounting for this are:

(i) Assign a natural distance between two atoms bonded to a common atom, thus these interactions contribute to the steric energy through this non-bonded term. This form of force field is known as a Urey-Bradley force field [15].

(ii) Include a stretch-bend energy "cross term" equation in the overall energy expression (e.g. **Equation 4** for an A-B-C atomic sequence). Cross terms make structural features such as bond lengths and angles dependent on the neighbouring

structural features. As two atoms bound to a common atom are brought closer together (i.e., the bond angle decreases) their corresponding bond lengths should increase to compensate for this. An equation of the form shown below should be used. Most force fields do not incorporate this effect however.

$$E_{sb} = k_{sb}(\theta - \theta_0)[(r_1 - r_{01})(r_2 - r_{02})] \quad \text{Equation 4}$$

Where E_{sb} is the stretch bend interaction energy, k_{sb} is the associated potential constant, r_1 , r_2 and θ are explained in **Figure 5**. r_{01} , r_{02} and θ_0 are the ideal values of the variables shown in **Figure 5**.

Figure 6 illustrates how by increasing the value of the potential constants the steepness of the potential energy curve is also increased.

1.5.3 Torsional terms

For four atoms directly and sequentially bonded together rotation about the central bond necessitates the surmounting of one or more potential energy barriers. The potential energy depends on the relative orientation of the first and fourth atoms with respect to each other, which is termed the dihedral (or torsional) angle. If A–B–C–D represents the directly bonded atoms being considered in a rotation about the B–C bond, then the torsional angle corresponds to the angle between the A–B–C atomic plane and the B–C–D atomic plane. Torsional potential energies are by far the most important of all molecular mechanics terms in determining molecular conformation. Distortions in geometry will be more readily apparent in the torsional potential energy term, as much less energy is required to distort a torsional angle than a bond angle, i.e. most torsions have relatively low barriers, *ca* 0–8.3 kJ, to rotation.

Torsional terms are particularly useful in distinguishing between the in-plane and out-of-plane bending potential constants at sp^2 hybridised atoms. This is important for cyclic compounds with adjoining double bonds.

Exceptions to this occur for cases where the central bond is of sp^2 or sp character, as the barrier is made correspondingly higher. For these reasons torsional terms are essential for the appropriate molecular flexibility and fundamental for good agreement with experimental geometries and conformational equilibria. The most common method of representing torsional potential energies is a discrete Fourier series, **Equation 5**.

$$E_{\text{torsion}} = \sum_{\omega} \frac{V_n}{2} (1 + s \cos n\omega) \quad \text{Equation 5}$$

Where V_n is the n -fold barrier to rotation; n is usually 1, 2 or 3; s will be +1 or -1 according to whether a staggered (+1) or eclipsed (-1) conformational is the most stable; and ω is the torsional angle. Usually one, and occasionally two, of the n -fold potentials will typically represent the conformational preference for a single torsional angle. If the atoms are not successively bonded together, then this is termed an improper torsion. Two-fold improper torsions are required for maintaining the planarity of sp^2 hybridised atoms in cyclic and acyclic molecules. **Figure 7** represents a typical change in a torsional profile.

Experimental estimations of torsional barriers are sometimes known from microwave studies, or from thermodynamic studies, and are more now becoming available from Raman and far-infrared spectroscopy. But for molecules that have large values for two or more of the torsional coefficients, one usually cannot formulate the force field without more experimental, or ab initio molecular orbital, information than can be found in the current literature.

1.5.4 Van der Waals' interactions

The interactions between atoms that are not bound to each other or to a common atom are generally referred to as *van der Waals' interactions*. Together with the electrostatic term they describe the non-bonded energy. They lead to the non-transferability of spectroscopists force constants, and they have major effects on the structures of congested molecules. They have also proven difficult to determine accurately.

Theory says that the van der Waals' potential (E_{vdW}) should be composed of two parts. It is an electrostatic interaction, and the first term of the attractive part (between neutral atoms) is proportional to r_{ij}^{-6} . This is sometimes called the *induced dipole-induced dipole interaction* or *London Dispersion Forces*.

The other term is the inter-electron cloud repulsion, which results when one tries to put two atoms in the same place at the same time. It is well represented over the range of interest by either an exponential function, or by r_{ij}^{-n} . Just what value should be used for n , or the corresponding exponential, depends on what it is one wants to fit. For molecular mechanics calculations n is usually defined as 12 and this value also helps to simplify the mathematics of the resultant equation. One common way of dealing with these interactions is to use a Lennard-Jones potential, **Equation 6**.

$$E_{\text{vdW}} = \sum_{r_{ij}} \frac{A_{ij}}{r_{ij}^{12}} - \frac{B_{ij}}{r_{ij}^6} \quad \text{Equation 6}$$

where the A_{ij} and B_{ij} parameters control the depth and position (interatomic distance) of the potential energy well for a given pair of non-bonded interacting atoms (e.g. C:C, O:C, O:H, etc.). This is schematically shown in **Figure 8**. In effect, A_{ij} determines the degree of “softness” of the van der Waals attraction and B_{ij} determines the degree of “hardness” of the atoms (e.g. marshmallow-like, billiard ball-like, etc.). r_{ij} represents the distance between atoms i and j .

The “ A ” parameter can be obtained from atomic polarisability measurements, or it can be calculated using quantum mechanics. The “ B ” parameter is typically derived from crystallographic data so as to reproduce observed average contact distances between different kinds of atoms in crystals of various molecules.

Alternative functions for representing van der Waals interactions are the Buckingham potential, **Equation 7**, which retains the r^{-6} attractive term but replaces the r^{-12} repulsive term by an exponential function. A'_{ij} , B'_{ij} and C_{ij} are constants relevant to the atoms i and j . This is justified due to the fact that as two atoms approach the repulsive energy increases approximately exponentially. The Hill equation, **Equation 8**, which is similar in functional form can also be used.

$$E_{\text{vdW}} = \sum_{r_{ij}} A'_{ij} \exp\left(\frac{B'_{ij}}{r_{ij}}\right) - \frac{C_{ij}}{r_{ij}^6} \quad \text{Equation 7}$$

$$E_{\text{vdW}} = \sum_{r_{ij}} \varepsilon \left[-c_1 \frac{r^*}{r_{ij}^6} + c_2 \exp\left(-c_3 \frac{r^*}{r_{ij}}\right) \right] \quad \text{Equation 8}$$

In **Equation 7**, like the Lennard-Jones potential, the coefficients are explicit atom-pair coefficients. The Hill equation (**Equation 8**), however, uses universal constants c_1 , c_2 and c_3 , with the parameter ε^* ($= \left(\frac{\varepsilon_i}{\varepsilon_j} \right)^{\frac{1}{2}}$) which reflects the pair potential well depth, where ε_i and ε_j are the well depths of the individual atoms and r^* is the sum of the van der Waal radii for atoms i and j . It is also possible to use the exponential-based Morse potential function to represent non-bonded interactions [16].

1.5.5 Electrostatic and hydrogen bonding terms

For molecules containing polar groups, the resultant asymmetrical charge distribution necessitates the use of another term. This will have to represent the attraction and repulsion of the charges associated with these groups. A simple Coulombic treatment in which an atom is assigned a hypothetical partial charge (or each atom pair is assigned a bond dipole) is sufficient to represent many polar interactions. The extent of the interaction can be adjusted by the (effective) dielectric constant, ε , enabling the simulation of a solvent if ε is made proportional to the distance between interacting atoms:

$$E_{\text{electrostatic}} = \sum_{r_{ij}} \frac{q_i q_j}{\varepsilon r_{ij}} \quad \text{Equation 9}$$

q_i and q_j correspond to the atomic partial charges. The source of the monopolar partial charges for substitution into **Equation 9** is an important issue and is considered in **Section 1.9**.

Due to the fact that most force fields do not have parameters for bond lengths and angles for hydrogen bonds molecular mechanics calculations, in general, do not actually treat hydrogen bonds as bonds. If hydrogen bonds were included in the connection table for a molecule, then different hydrogen bonding patterns would be considered to be different molecules. By treating hydrogen bonds mainly as electrostatic interactions, there is no need to specify whether or not a bond is there, and so their formation need not be explicitly included at the start of the calculation.

The van der Waals and electrostatic functions together do not mimic hydrogen bonds correctly if ϵ is made greater than unity, causing them to form unrealistically close distances. So a slightly more repulsive term may be employed. Commonly this takes the form of a 10–12 potential^a which, like the 6–12 potential, is given adjustable coefficients for various atom pair combinations:

$$E_{\text{H-bond}} = \sum_{ij} \frac{C_{ij}}{r_{ij}^{12}} - \frac{D_{ij}}{r_{ij}^{10}} \quad \text{Equation 10}$$

C_{ij} and D_{ij} are coefficients depending on the atoms i and j . Adjustment of D_{ij} allows the hydrogen bonds to be ‘fine-tuned’ to best fit the experimental data. The use of **Equation 10** in place of **Equation 6**, for example, would be governed by imposing a distance limit beyond which **Equation 6** becomes inoperative for a hydrogen-bond donor and acceptor atom pair, and the less specific non-bonded potential given in **Equation 10** is then employed for that atom pair. Additionally, only predefined atom types would be parameterised to use **Equation 10** in the first place.

^a 10–12 refers to the powers on r in **Equation 10** and 6–12 refers to **Equation 6**.

A point of note here is that while in reality van der Waals and electrostatic interactions extend to infinity, normally some limit (cut-off) must be placed on these interactions to render them computation feasible. While it may be desirable to extend these interactions as far as possible, in practice this is computationally expensive and so these interactions often have cut-offs at around 10–12 Å. A sharp cut-off will cause problems for atoms around the cut-off distance, as during energy minimisation they will move from feeling significant forces to feeling no force whatsoever, or vice versa. Therefore, cut-offs for these interactions are normally made more gradual ('soft') with an additional distance dependence around the cut-off limit. However, truncation of these long-range interactions, that is, the use of cut-offs, significantly affects results [17], even when tapering functions are utilised [18].

Two assumptions are made in the implementation of non-bonded functions. The first of these is that non-bonded parameters, derived from e.g. intermolecular crystal contacts, can reasonably represent intramolecular interactions. Second, non-bonded interactions are assumed to be pair wise additive and only succeed in molecular mechanics as a result of the large number of adjustable parameters within the remaining force field terms.

Molecular mechanics potential constant parameters are typically derived from vibrational spectroscopy while estimates of bond lengths, angles and barriers to rotation come from microwave and X-ray crystallographic studies. Non-bonded parameters are the most difficult to derive *a priori*. They are typically obtained from crystallographic non-bonded contacts and interpolation or extrapolation of van der Waal contact data for rare gas elements. These parameters are then further refined by their ability, in conjunction with the other force field parameters, to reproduce experimental observations.

Hagler has described a method of deriving potential constants and optimum force field functions from ab initio potential surfaces for small molecules [19]. The use of

(accurate) semi-empirical methods will permit the extension of the theoretical derivation for significantly larger molecules or simply faster parameterisation. The use of AM1-derived parameter sets for organic species of similar quality to some experimentally derived parameter sets has been reported [20].

Sharp and Honig [21] have reviewed the difficulties and successes of applying electrostatic theory to problems in molecular biophysics. They found that it is possible to account for a wide range of phenomena that are primarily electrostatic in origin and that depend critically on the details of the three-dimensional structure of a macromolecule and on the properties of the surrounding solvent.

The fundamentals of classical electrostatics, like those of thermodynamics, are well known and can be stated concisely with a few elegant equations. The apparent simplicity of these equations, however, can hide the difficulties in applying them to complex systems.

Gilson [22] has reviewed relatively recent advance in the efficient computation of long-range electrostatic interactions; the application of the Poisson-Boltzmann model in conformational analysis and in quantum chemistry calculations; the development of atomic parameters and finally, the modelling of ionisation equilibria in proteins.

Electrostatic interactions may be defined as the forces and energies that result when a solute possesses an asymmetric charge distribution or a non-zero net charge. These interactions are critical to the structure and function of molecules, and are challenging to model accurately.

1.5.6 Additional terms

However, when we enter the realms of inorganic and organometallic chemistry more problems are encountered. Force fields are generally inadequate at reproducing a metal ion-ligand complexes potential energy surface. The multiple minima needed to describe ligand directionality around the metal centre are not well treated by existing organic force fields. Additional parameters, and even extra force field equations, need to be added to account for these interactions.

Various force fields have been developed over the years, amongst which are MM2 [23], MM3 [24], MM4 [25], AMBER [26] (with a united atom approach for aliphatic hydrogen atoms [27]), CHARMM [28], TRIPOS [29] and GROMOS [30]. Pettersson and Liljefors have discussed comparisons made in the literature by different authors between a variety of these force fields and experimental data [31]. Allinger's MM2/3 programs were shown to be among the best available but none of the studies discussed incorporated the modelling of hydrogen bonds. The version of AMBER incorporated into MacroModel was shown to be only slightly less accurate than the MM2/3 force fields. As the objective of this research is not an intense relative conformational energy study and, in my opinion, AMBER models the hydrogen bond interactions more accurately than the MM2/3 force fields, AMBER was the force field of choice for the chiral recognition studies.

1.5.7 Problems with X-ray crystallography

Experimentally, or computationally, there are a lot of problems involved in deciding just where an atom is located. Much of the problem stems from the fact that atoms vibrate, and the amplitude is usually of the order of 0.05-0.10 Å. Therefore, to determine an atomic position accurately one has to average over the vibrational motion. Depending on the calculation or experiment, this averaging is done in different ways, and hence the atomic positions obtained depend on the method used.

In general, force field parameters are developed utilising X-ray crystallography data. Therefore, when performing a molecular mechanics calculation without any explicit inclusion of a specific environment it is not strictly accurate to refer to the calculation as being in vacuo. Interactions with neighbouring molecules, included solvent molecules, hydrogen bonds to counter ions, etc are present in crystal lattices and, therefore, are incorporated to some extent in the force field parameter set.

The major difference between bond lengths found by X-ray crystallography and by gas-phase (or neutron crystallography) is in the C–H bond length. X-ray crystallography works by locating the distribution of electron density around the molecule and for a C–H bond this density is located about 0.1 Å closer to the carbon atom than the position of the hydrogen nucleus as measured by the other experimental methods. This is due to the fact that the only electron the hydrogen atom has is used in bonding and is, therefore, displaced towards the carbon atom. Crystal packing forces also have an effect on the calculated positions and bond lengths in molecules, whereas molecular mechanics calculations consider isolated molecules. X-ray crystallography experiments also have problems in determining accurately the position of atoms that have lone pair electrons due, again, to the fact that it deals with electron density and not nuclear position. The lone pair of electrons offsets the electron density from the nucleus, and for the nitrogen atom of amines this difference may amount to 0.01–0.02 Å.

One last problem with X-ray crystallography structural determination is that it is usually measured at room temperature. So these structures need to be corrected for thermal vibrational motion which is typically of the range of 0.005–0.015 Å.

1.5.8 Neutron diffraction spectroscopy

In many ways the principles of neutron diffraction are similar to those of X-ray diffraction, but there are some important differences. **Table 6** lists some of the abilities of

both methods. A nuclear reactor is required to produce a sufficient amount of neutrons for diffraction purposes. The beam of neutrons is weak when compared to a beam of X-rays, about 10^3 – 10^4 times weaker, so a broader beam, and hence, a larger detector needs to be utilised.

| X-ray diffraction | Neutron diffraction |
|--|--|
| X-rays are readily available from laboratory instruments | Neutrons are only available from national or international centres |
| The data collection time is a few days, or even hours | Data collection time can be up to a few weeks |
| Temperatures below 120 K are not generally available | Temperatures down to 10 K are conveniently available |
| Hydrogen atoms are poorly located, especially when bound to electronegative atoms. Accuracy ~ 0.1 Å | Hydrogen positional parameters are comparable to those for carbon, nitrogen etc; ~ 0.001 Å |
| Small crystals can be used (~ 0.01 mm ³ , ~ 0.01 mg) | Large crystals are required (~ 4 mm ³ , ~ 5 mg) |
| It is not necessary to make deuterium substitution | If the structure contains many hydrogen atoms, deuterium substitution may be essential to reduce incoherent background |
| Careful absorption corrections are necessary | Absorption is negligible, except for crystals containing B, Cd, Sm or Li (corrections for hydrogen are advisable for molecules with a large hydrogen atom content) |
| Radiation damage can occur | No radiation damage |

Table 6. A comparison of X-ray and neutron diffraction single crystal analysis.

Neutron diffraction structures are determined by nuclear scattering, and hence they are comparable with the gas-phase structures rather than with the X-ray diffraction structures (as they more accurately resolve the nuclear positions).

1.6 THE QUEST FOR THE GLOBAL ENERGY MINIMUM

Perhaps the biggest challenge in molecular mechanics calculations is to find the global energy minimum. As the size of the molecule of interest increases, many more potential conformations (local minima) become available for the molecule to adopt and finding the lowest energy conformation becomes a problem that can severely tax the commonly available computational resources.

The five techniques described here are all designed to fully sample the potential energy surface of the molecule of interest and generate an ensemble of states [32]. An ensemble refers to a set of configurations which best represents a system at a given temperature, in which the frequency of occurrence of each configuration is in accordance with the Boltzmann population. For a molecule at non-zero temperatures intermediate conformations, as well as local minima, will be significantly populated and an accurate description of the molecule will require contributions from these non-equilibrium structures.

There are two distinct statistical methodologies for the generation of Boltzmann-weighted ensembles: Molecular Dynamics [33] (MD) and Metropolis Monte Carlo [34] (MC). The MC method is stochastic, in that random steps are taken on the potential energy surface to sample the configurational space. MD, in contrast, is a deterministic process that seeks to generate a dynamic trajectory for the system by following the path of each atom over time. This leads to the major difference in the applicability of the two methods, in that MD can be used to study both static properties and also time-dependent processes such as diffusion. The ensembles generated by MC simulations can only be

used for the calculation of static properties of the system (e.g. energies and equilibrium structures).

There have been various reviews on the different methods of searching conformational space published [35]. None of these methods are guaranteed to find the global minimum, but they may in many cases, generate a local minimum which is close in energy to the global minimum.

1.6.1 Molecular Dynamics

MD is a powerful computational technique in which kinetic energy is introduced to the simulation and Newton's laws of motion are solved for each atom to generate a dynamic trajectory for the molecule. Each atom moves in response to its own kinetic energy and the force field generated potential energy surface.

Newton's second law,

$$F = ma \quad \text{Equation 11}$$

where F is force, m is the mass of the atom and a is the atom's acceleration, can also be written as:

$$-\frac{dV}{dr} = m \frac{d^2r}{dt^2} \quad \text{Equation 12}$$

where V is the potential energy at position r . The vector r contains the coordinates for all the particles.

Given a set of particles with positions r_i , their positions after a small time step, Δt , are given by a Taylor expansion:

$$r_{i+1} = r_i + v_i \Delta t + \frac{1}{2} a_i (\Delta t)^2 + \frac{1}{6} b_i (\Delta t)^3 + \dots \text{Equation 13}$$

The velocities, v_i , are the first derivatives of the positions with respect to time (dr/dt) at time t_i , the accelerations, a_i , are the second derivatives (d^2r/dt^2) at time t_i , b_i are the third derivatives etc.

The positions at a small time step, Δt , earlier are derived from **Equation 13**, by substituting Δt with $-\Delta t$.

$$r_{i-1} = r_i - v_i \Delta t + \frac{1}{2} a_i (\Delta t)^2 - \frac{1}{6} b_i (\Delta t)^3 + \dots \text{Equation 14}$$

Addition of **Equations 13** and **14** gives:

$$r_{i+1} = (2r_i - r_{i-1}) + a_i (\Delta t)^2 + \dots \text{Equation 15}$$

This is the Verlet algorithm [36] for solving Newton's equations numerically. As Δt is decreased, the trajectory becomes a better and better approximation to the 'true' trajectory, until problems of finite numerical accuracy arise. However, smaller time steps mean that more steps are necessary to cover a specific time span. A similar equation that takes into account the frictional influence of the surrounding solvent is known as the Langevin equation.

Initial velocities are assigned to each atom at random, consistent with a Maxwell-Boltzmann distribution at the desired simulation temperature. This integration time step is of crucial importance. It must be an order of magnitude shorter than the periodicity of the highest frequency vibration (bond stretching), that effectively limits it to approximately 10^{-15} seconds (1 femtosecond). The SHAKE algorithm [37] can be used to constrain hydrogen bond lengths to their equilibrium values throughout the simulation; this allows a longer time step, typically 2–3 fs, to be used. The necessity of taking short time steps, coupled with the computation of the energy gradients, severely limits the length of trajectory that can be simulated by MD. For molecules the size of proteins, 100 ps to 1 ns simulations (1 million iterations) are possible on modern hardware platforms.

MD simulations can be run at constant temperature (canonical ensemble), constant energy (microcanonical) and constant pressure (involving periodic boundary condition). During the initial equilibration phase of the simulation, the temperature must be carefully controlled, usually by direct velocity scaling. Once the system is fully relaxed, a more gentle method can be employed, such as coupling to an external heat bath that gradually adds or removes energy to/from the system [38]. In order to obtain physical properties from the simulation the trajectory should be sufficiently long enough to have sampled fully the configuration space.

MD is also commonly adapted for use as a local minima hunter [39]. For these purposes it is more efficient if artificially high temperatures are used, often 600–900 K or higher. Dynamics simulations can overcome energy barriers of the order of RT , where R is the universal gas constant, and therefore, if the temperature is raised, higher energy barriers can be overcome and the potential energy surface traversed more rapidly. Because of the non-physical temperatures, the actual ensemble generated has little meaning, and energy minimisations must be employed to periodically sample the underlying minima located by the trajectory. These minima can then be analysed by energy and conformation.

1.6.2 Metropolis Monte Carlo

MC simulations based on the methods of Metropolis et al. [40] have been widely used for the generation of Boltzmann-weighted ensembles since the earliest days of digital computers. The general method is as follows. From a given starting configuration, a trial-configuration is generated by a small random displacement of one or more of the atoms. The energy change over the step is calculated, ΔE , and the trial accepted either if the energy has decreased ($\Delta E < 0$) or the Metropolis test is passed:

$$\exp\left(\frac{\Delta E}{RT}\right) > \text{RAN}[0,1] \quad \text{Equation 16}$$

where R is the gas constant, T is the simulation temperature and $\text{RAN}[0,1]$ is a random number between 0 and 1. This only allows uphill steps on the potential energy surface with a certain probability, depending on the magnitude of the energy change and the nominal temperature at which the simulation is conducted. If the trial is accepted, the coordinates are updated and used as the starting coordinates for the next random displacement; otherwise the previous configuration is re-used and counted again in any statistical averaging. The nature of the Metropolis test ensures that, over a sufficient number of trials (often 10^5 – 10^6), each configuration is visited with a frequency equal to its Boltzmann's population at the sampling temperature. Thus, physical properties can be determined by a straight average over the simulation, with no need to further weight the configurations.

The acceptance rate for the Metropolis test (the ratio between the number of accepted steps and the total number of trials) is dependent on the maximum allowed random displacement and must be carefully controlled to achieve the most efficient sampling. It is generally believed that an acceptance rate of 50% gives the optimum balance between large but infrequent steps and very small, frequent steps on the potential energy surface [41]. For cycloheptadecane it was shown that the maximum atomic

movement should be between 2.7 and 3.1 Å. Larger steps distorted the molecule so badly that the average time for energy optimisation was increased dramatically. The probability of falling back to the starting geometry increased when kicks smaller than 1.5 Å were applied [42].

Treasurywala et al. [43] studied the stochastic methods available in SYBYL and MacroModel. Both methods gave quite different results when performed on a comprehensive test set of molecules. This indicates that it would be prudent to perform the search from several starting conformers and to compare the results or, alternatively, to perform the search with as many different stochastic methods as possible so as to avoid generalisations from incomplete data. The methods are stochastic and thus, by their very nature, cannot assure the user of a complete search - although the probability of finding a low energy conformer by either method is very high. The stochastic methods are generally regarded as faster but less thorough than systematic methods [44].

A limiting feature of systematic methods is that the optimal choices of parameters and step sizes vary from case to case and no method is available for predicting ideal values in advance. For stochastic methods, the energy window by which it is decided if a new conformer is considered energetically favourable was found to be a strong factor in determining the number of low energy conformers reported.

Meza et al. compared the genetic search algorithm (GA) and parallel direct search methods on 7 small, 8 medium and 4 large sized molecules [45]. They found that both methods were good for generating a set of low energy conformations for small to medium molecules.

Other studies [46] have shown that both GAs and simulated annealing outperformed pure random search for large molecules. Also, GA was demonstrated to be better than simulated annealing in several conformation search applications. Various authors [47] have compared GA with several other methods for searching databases

containing flexible three-dimensional structures and found it to be superior to all but a direct tweak method [48], to which it was comparable.

A variety of methodologies for searching conformational space have been developed incorporating MC simulation [49].

1.6.3 Simulated Annealing

The powerful technique of simulated annealing has been applied to problems of global optimisation in many areas of science, not just in chemistry [50]. It is based on the application of statistical mechanics techniques to the generation of Boltzmann ensembles, usually by MC sampling but MD may also be utilised, and the control temperature is gradually lowered [51]. At the highest temperatures gross changes in conformation are possible, allowing the molecule to overcome large energy barriers. As the temperature is lowered, the molecule is less able to surmount the highest energy barriers, and becomes progressively trapped in deeper and deeper energy wells. Under the correct conditions the final state of the system will have a high probability of being the global minimum. Infinitely slow cooling would be needed for this to be completely true.

In practice, it is necessary to perform a number of runs from the same starting structure and take the lowest energy found as the global minimum. The number, and length, of runs required is dependent on the size of the molecule and the complexity of the potential energy surface.

1.6.4 Dynamic Monte Carlo

The Dynamic Monte Carlo (DMC) conformational search algorithm [52] combines aspects of both MD and MC sampling with a simulated annealing protocol. Trial configurations are generated by short bursts of coherent molecular dynamics, with the kinetic energy concentrated into one randomly selected bond spin, fragment rotation or fragment translation. This approach leads to more rapid conformational transitions than does standard molecular dynamics, while still allowing bond lengths and angles to relax. A key feature of the method is that favourable dynamics trajectories are allowed to continue for as long as the energies of the new structures satisfy the Metropolis test, thus allowing low-energy regions of the conformational space to be located more rapidly. Following an unsuccessful trial, a new motion is selected for dynamics initialisation.

1.6.5 Genetic Algorithms

This method is based on ideas from biological evolution. A population of structures is initially randomly generated and their corresponding energies are calculated. Lower energies indicate that a more “evolved” molecule has been attained. These structures are then “cross-bred” in order to obtain lower energy structures. A fragment from one low energy molecule is linked to the corresponding fragment from another low energy molecule forming the original molecule under study. A minimisation is then performed and if the energy of this newly generated molecule is in the low energy region of the potential energy surface of the molecule it is included in any further “crossovers”. See the preceding Sections for an indication of this methods effectiveness.

1.7 AVAILABLE MINIMISATION ALGORITHMS

The potential energy surface of a molecule can be very complex, consisting of a multitude of peaks and troughs. The initial starting structure will, generally, have a configuration somewhere above this surface due to the fact that some of the bond lengths, torsions, etc will be unrealistically large after the initial model building procedure. By utilising a variety of minimisation algorithms one can quickly refine this structure (bring it down onto the potential energy surface) and then travel down the surface to the nearest trough (minima). There are a number of algorithms that can accomplish this feat, which can be divided into two classes: Steepest descent and Polak-Ribiere, which are first-derivative techniques; Newton Raphson that is a second derivative technique.

But first, the basic idea behind travelling down the surface will be discussed. In principle, it is easy enough to do. The potential energy minimum is a place where the derivatives of the potential energy with respect to all of the coordinates are simultaneously equal to zero. So, again in principle, all one has to do is write down a trial structure for the molecule, which can be generated, for example, by using standard bond angles, standard bond lengths and staggered torsional angles relevant to the compound under study. Since we have equations, which describe the change of energy with changes in internal coordinates, we can take the derivatives of the energy with respect to these coordinates, find which way the slope lies, and then move down the slope from each coordinate until we locate an energy minimum.

An energy minimum can be characterised by a small change in energy between steps and/or by a zero gradient of the energy function. The gradient usually provides the best indication for completion of the minimisation (convergence) because very small changes in the gradient are much more significant than small changes in the energy function itself. Precise convergence can, thus, be achieved with a non-zero gradient.

Energy minimisation algorithms often limit the calculations to a set computer time and/or a set number of steps/iterations by default. Ordinarily, these limits should be substantially increased. If iterations are the “fuel” of an energy minimisation, an empty tank should not be assumed to mean the end of the trip.

1.7.1 Steepest Descent

Wilberg used the steepest descent method with numerically calculated first derivatives of the energy in the first general computer program for energy minimisation [53]. The energy is calculated for the initial coordinates $[f(x_0)]$, and then again when an atom was moved in turn by small increments $[f(x_0+\Delta x)]$. This is, in essence, a numerical determination of the first derivatives. The process is repeated for all the atoms, which are finally moved simultaneously to new positions downhill on the energy surface by an amount dictated by the steepness of the surface. The entire sequence is repeated until the predetermined minimum condition is fulfilled. The method is shown schematically in **Figure 9**.

The steepest descent algorithm converges rapidly and reliably when the derivatives are large (i.e. the molecule is far from a minima), but convergence is slow when the derivatives are small, which they are when close to a minima or in a valley with a shallow slope.

The main problem with steepest descent techniques is their scale dependence. There are two critical processes, the numerical determination of the first derivatives and the step-size for moving the atoms. If the search increments are too large, minimisation — especially that of torsional strain — is hampered. In the latter case the energy increase due to bond stretching and angle bending may easily be larger than the energy gained from relieving torsional strain [54], and torsional angles are often not well minimised by his procedure.

1.7.2 Polak Ribiere

This conjugate gradient method is a modified steepest descent technique. Here the program 'remembers' its last step and uses this additional information to accelerate movement, especially along valleys in the energy surface. A conjugate gradient method is a first order minimiser. As before, the direction of steepest descent is sought for one atom, which is then moved to an improved position, but the size and direction of the movement is saved. After the program has cycled through all atoms, in the next cycle the atoms are moved by the sum of the new steepest descent step plus the last step, and so on, thus accumulating a moving pattern.

The first step is equivalent to a steepest descent step, but the remaining searches are equivalent to a mixture of the current negative gradient and the previous search direction (**Equation 17**).

$$h_{i+1} = g_{i+1} + \beta_i h_i \quad \text{Equation 17}$$

where h_{i+1} is the conjugate gradient, the new direction vector leading from the point $i+1$, g_{i+1} is the gradient at the point $i+1$ and h_i is the previous direction.

There are a variety of methods for choosing β , which dictates how much the previous search direction influences the current direction. The Polak-Ribiere method is discussed here (**Equation 18**).

$$\beta = \frac{(g_{i+1} - g_i) \cdot g_{i+1}}{g_i \cdot g_i} \quad \text{Equation 18}$$

The pattern is abandoned when the direction of steepest descent changes. This method is illustrated in **Figure 10**. Fletcher-Reeves is also an optimiser of this type but it is not as refined a method as Polak-Ribiere.

1.7.3 Newton Raphson

The Newton Raphson block diagonal method is a second order optimiser. It calculates both the first and second derivatives of potential energy with respect to Cartesian coordinates. These derivatives provide information about both the slope and curvature of the potential energy surface. The complete second derivative matrix defines the curvature in each gradient direction. The inverse of the second derivative can be multiplied by the gradient to obtain a vector that translates in the direction of the nearest minimum (**Equation 19**).

$$r_i = r_{i-1} - A^{-1}(r_{i-1}) \cdot \nabla E(r_{i-1}) \quad \text{Equation 19}$$

where r_i is the minimum at the i th point, r_{i-1} is the minimum at the previous step, $A(r_{i-1})$ is the matrix of the second partial derivatives of the energy with respect to the coordinates at r_{i-1} , and $\nabla E(r_{i-1})$ is the gradient of the potential energy at r_{i-1} .

Unlike a full Newton Raphson method, the block diagonal algorithm calculates the second derivative matrix for one atom at a time, avoiding the second derivative with respect to two atoms. Block diagonal methods require less computer time than the full procedure but it suffers from the problem that it does not deal with cooperative movement of atoms; this is especially noticeable when torsional angles must be adjusted.

It has been reported that in the case of a very flat energy surface, the block diagonal scheme approaches the energy minimum rapidly to within a value of about 0.04 kJ mol⁻¹, but torsional angles were found to change from such a position by up to 10° when a full-matrix Newton Raphson minimisation was employed afterwards [55]. But within the context of molecular mechanics an energy difference of 0.04 kJ mol⁻¹ is not very significant.

The choice of minimisation algorithm should be matched to the problem at hand. A good strategy is to switch minimisers as the calculation progresses, so that each algorithm operates in the region for which it was designed. This is done by successively running each algorithm for a preset number of iterations. The final minimisation session should be a balance between attaining a reasonably accurate result and avoiding unnecessary computations when there is no discernible change in the conformation of the molecule [56].

1.8 TO SOLVATE OR NOT TO SOLVATE?

It is easy, when discussing the energetics of complex formation, to forget the crucial role played by the solvent (generally water). It cannot be emphasised enough that water plays a vital part in the energetics of complexation, both entropically and enthalpically.

Water is the solvent of virtually every biological process. Whether inside or outside a living cell, water surrounds the proteins, nucleic acids and the small molecules necessary for life. In many cases, water molecules make specific hydrogen bonds and electrostatic interactions with the surface atoms of these molecules. More generally, water is responsible for the hydrophobic effect that stabilises the structure of proteins and drives many macromolecular interactions.

It is, therefore, appropriate to consider how accurately force field calculations performed *in vacuo* approximate reality. The electrostatic influence of the solvent surrounding a complex permeates the entire ligand, affecting the dielectric within the interaction site. Gas-phase calculations overestimate electrostatic effects, especially when there are ions in the system. Water strongly influences hydrogen bonding patterns and charge-charge interactions. This is significant in conformational studies on small molecules.

It is important to recognise the influence of water on the kinetics of association. In the formation of a complex, both the interaction site and the guest molecule are likely to become desolvated. This is probably a cooperative process. The removal of water molecules from reactant surfaces prior to binding would lead to a massive kinetic barrier to the formation of a complex. A more plausible model is that the interaction site squeezes out the water molecules between it and the guest slowly, utilising the dynamic changes in hydrogen bonding patterns, and replaces them with a similar polar environment [57]. Dynamic simulations of bulk water indicate that water is a random tetrahedral network with defects, where pentacoordinated water molecules and bifurcated hydrogen bonds were found [58]. The presence of bifurcated hydrogen bonds means that hydrogen bonds may be swapped between water molecules very quickly, leading to increased mobility and, hence, entropy. In the hydration of a molecule's surface, part of the coordination shell of each water molecule is occupied by bulky solute, which sterically disfavours the formation of high coordination number shells. Hence, there are fewer defects and lower mobility. This accounts for the increase in entropy on desolvation and complex formation, and suggests a mechanism whereby hydrogen bonding groups within an interaction site may aid the process of gradual desolvation.

Pitera and Kollman [59] have developed a technique for describing the average structure of the hydration shell of a solute. Data on the average orientation of the water molecules and approximate lifetime information is also provided.

1.8.1 Explicit inclusion of solvent molecules

Conceptually, the simplest way to allow for the effect of a solvent is just to include the solvent explicitly in the calculation. Water molecules can be added one at a time to the system until the property under study remains constant. This requires quite complicated computational methods, however, and as hundreds of water molecules may need to be included it is very hardware intensive.

A group of solvent molecules with the molecule of interest in the middle is constructed, and placed in some sort of 'box' in order to stop the solvent boiling away (periodic boundary condition can also be used). Solvent properties can then be found by considering many different arrangements of the solvent molecules in the box. Molecular dynamics (**Section 1.6.1**) is a convenient method of modelling solvent effects using this approach. Conformational searching methods cannot do this very well, because of the difficulty in figuring out how to fit the molecules into the box. It works well with molecular dynamics, because it is easier to move from one reasonable arrangement to another, similar, reasonable arrangement, than to generate new reasonable arrangements from scratch. Since a great many solvent molecules must be considered, these calculations are very slow, but they can give useful results that are compatible with experiments.

1.8.2 Continuum methods

Solvents have a major effect on electrostatics [60], because they alter the effective dielectric of the medium. Ways of modelling solvents as a continuum are being developed, and such a method has been published by Still et al. [61] This model can reproduce molecular dynamics studies of solvated small molecules, which use large

numbers of solvent molecules around the molecule of interest and, consequently, are very slow. The Still model has the advantage of being very fast (about a million times faster than modelling explicit solvent molecules and only about 50% slower than gas phase calculations).

The model has three components. Solvent effects depend on the surface area of a molecule, because a molecule represents a hole in the solvent, and the area of the interface between solvent and molecule will be the same as the surface area of the molecule. Calculation of the exact surface area of a molecule, defining the surface as the van der Waals surface or something similar, is possible by the use of long and tedious geometry. This accurate calculation is too slow to be useful for most molecular mechanics investigations, but there are approximations which can be calculated very quickly and which are reasonably accurate. In the Still model this component of the solvation energy is taken to be proportional to the surface area of the system, which is calculated by a fast, but approximate, method. This creation of a cavity costs energy which involves the work done in order to create the cavity against the solvent pressure and the entropy penalty associated with the reorganisation of solvent molecules around the solute. The cavity, and also the dispersion, energy terms are approximately proportional to the surface accessible surface area of the solute. The proportionality constants are usually calculated from the free energies of transfer of alkanes from vacuum to water. This needs to be compensated for by attractive interactions between the solute and solvent.

Dispersion interactions between the solvent and solute add to the stabilisation. Charge on a solute will polarise the solvent around it yielding an electrostatic stabilisation. This effect is also included in the model, using an approximation to the generalised Born equation (**Equation 20**) for the energy of an ion in a medium.

$$G_{elec} = -\frac{q^2}{2a} \left(1 - \frac{1}{\epsilon} \right) \quad \text{Equation 20}$$

where G_{elec} is the energy of electrostatic interaction, q is the charge on the ion and a is the radius of the cavity.

Together, these terms give a good approximation to the energy of the system.

$$\Delta G_{solvation} = \Delta G_{cavity} + \Delta G_{dispersion} + \Delta G_{electrostatic} \quad \text{Equation 21}$$

Hydrogen bonds are weakened, not because their interaction energy becomes smaller, but because breaking them creates a favourable component in the polarisation term, and so the energy required to break a hydrogen bond can be regained by the interaction of the two broken ends with the solvent.

One of the simplest ways to account for solvent effects is just to change the dielectric constant, relevant to the particular solvent, in the Coulomb law equation (**Equation 9**) [62]. In atomic units, the dielectric of the vacuum is one. Alternatively, the dielectric can be made distance dependent, and so the electrostatic effects are reduced with increasing distance much more rapidly than they would be in a vacuum. **Table 7** shows a few typical dielectric constant values.

| Solvent | Dielectric constant (ϵ) |
|-------------------|------------------------------------|
| Hexane | 1.9 |
| Benzene | 2.3 |
| Diethyl ether | 4.3 |
| Chloroform | 4.8 |
| Ethyl acetate | 6.0 |
| Acetone | 20.7 |
| Dimethylformamide | 38 |
| Dimethylsulfoxide | 48 |
| Acetic acid | 6.2 |
| <i>t</i> -butanol | 10.9 |
| Ethanol | 24.3 |
| Methanol | 33.6 |
| Formic acid | 58 |
| Water | 80.4 |

Table 7. Some typical dielectric constant values.

A rather severe way of dealing with problems of charges and solvation is to perform the calculation without taking the charges into account. This can yield acceptable results but, of course, hydrogen bonding, ion-ion interactions, etc cannot be taken into account.

1.8.3 Application to Monte Carlo methods

The Metropolis Monte Carlo method has been applied to liquid simulations, using simplified force fields consisting only of intermolecular Lennard-Jones and Coulombic non-bonded potentials and, optionally, torsional terms to describe internal rotations. Jorgensen and co-workers have developed highly optimised parameters for Monte Carlo

simulations of many organic solvents [63], designed to reproduce dimerisation energies, radial distribution functions and thermodynamic properties. The original parameter sets were referred to as Transferable Intermolecular Potential Functions (TIPS) [64]; these have now been largely superseded by the Optimised Potentials for Liquid Simulations (OPLS) series [65]. A hybrid AMBER/OPLS force field has been developed for the study of proteins in a full solvent environment [66].

When a guest molecule is being docked into a host trial configurations are generated by randomly selecting a molecule, translating it along all three Cartesian axes, rotating it about an arbitrary axis and performing any appropriate internal rotations. The maximum allowed displacements for each type of move are optimised to give a trial acceptance rate of 0.4–0.5. The bulk solvent environment is simulated with the use of periodic boundary conditions.

1.9 METHODS FOR CALCULATING ATOMIC CHARGES

The main problem with molecular mechanics is the treatment of non-bonded interactions. This is a consequence of the way it is set up. 1:2 interactions, 1:3 interactions and 1:4 interactions are all given separate functions to account for them, but the 1:5 interactions and all long-range interactions are treated in the same way. The method used to model these medium- to long-range interactions must be a simple one, so that it does not slow down the calculation to a great extent.

Molecules can interact well beyond their van der Waals surfaces (Up to and beyond 10 Å as electrostatic interactions scale to r^{-1}). Positively charged molecules are attracted to negatively charged ones. π -systems tend to stack in particular orientations and hydrogen bonds can form between suitable sites. The strength of these interactions will be moderated by the dielectric constant of the intervening regions, but dielectric

constants are measured for the bulk properties of materials and so are hard to define on an atomic level. Some equations must be added to the model for 1:2, 1:3 and 1:4 interactions that can account for all these effects.

Generally, non-bonded interactions are treated as a combination of van der Waals repulsions and electrostatic interactions (**Equation 7**), for which each atom is given a partial charge and the interactions calculated from Coulomb's law (**Equation 9**). This model works well, considering its simplicity, but is probably the weakest link in the molecular mechanics description of molecules.

1.9.1 Point charges

Electrostatic interactions are usually modelled by point charges being placed on atoms. This is the simplest possible way of accounting for electrostatics, and it gives reasonable results. Allinger has used bond dipoles instead — for example, in the MM2 force field — but this approach is very similar to using point charges. However, the assumption that the electrostatic effect of a molecule can be reasonably represented by the superposition of spherical, nucleus-centred potentials is not well founded. This is a particular problem when dealing with π - π interactions and hydrogen bonds.

Hunter and Saunders [67] developed a simple way for modelling these π - π interactions. The single partial charge most force fields place on each carbon atom is replaced by three charges, a large positive charge on the carbon atom of a π system which is flanked by two negative charges, each half the size of the positive one, in the π electron cloud of the system. This increase in complexity gives excellent agreement with experimental data. In this case, it seems that the improvement in the results outweighs the increase in complexity of the model, and also gives a qualitative way of understanding π - π interactions, in terms of π - π repulsions and π - σ attraction.

Additional charges have also been used to try and improve the electrostatic description of lone pairs by placing negative partial charges as shown in **Figure 11**.

It is possible to mimic the electrostatic potential around the molecule more closely by making the model more complicated, but the extra effort seems to have only a small reward in terms of increased accuracy. Placing a small negative charge as shown in **Figure 11** may seem to have some relationship to reality, but it is also possible to put a positive charge on the opposite side of the atom in question, and get a similar directionality for the hydrogen bond. This approach has been used by Legon and Millen to model gas phase dimers [68], and also is used in some of the standard force fields.

In addition, the electrostatic properties of a molecule vary with its conformation, and as it interacts with other molecules [69]. However, for such a simple model, it behaves rather well, and can be regarded as giving excellent value for money.

1.9.2 Mulliken method for charge partitioning

The electron density function $p[\mathbf{r}]$ for a molecule is given by the square of the wavefunction, and the probability of finding an electron at \mathbf{r} is given by $p[\mathbf{r}]d\mathbf{r}$, where $d\mathbf{r}$ is the small volume centred at \mathbf{r} . Summing over all space necessarily gives the total number of electrons contained in the molecule. The wavefunction can now be expressed as a linear combination of atomic orbitals. The electron density function defined by the square of the wavefunction involves a summation that contains terms that are products of the atomic orbitals. Some of these products involve orbitals located on the same atom, and the electron density associated with these terms can reasonably be assigned to this atom. However, some of the orbitals are on different atoms, and it is not at all obvious how to distribute this electron density (referred to as the “overlap population”) between the two atoms. This was first recognised by Mulliken [70], who proposed that each atom be given half of the overlap population. This scheme, which allows all of the electron

density to be assigned to specific atoms and generate a specific set of atom charges, is referred to as 'Mulliken Population Analysis'. Another popular charge set is known as Natural Atomic Orbital Charges.

1.9.3 Charges based on fits to electrostatic potentials

This alternative method of obtaining atomic charges is not a partitioning scheme as is the Mulliken procedure, but a scheme in which the electrostatic potential, the energy of interaction of a point positive charge with the nuclei and electrons of a molecule, is fitted to atomic charges [71]. One can then think of the method as providing that set of atomic charges that best reproduces the "exact value" of the electrostatic potential.

Several steps are involved in its implementation after a molecular orbital wavefunction has been obtained:

[1] Define a grid of points around the molecule. Choice of the grid obviously introduces ambiguity into the method. In practice, several thousand points make up the grid, and these are primarily located in a belt 2–5 Å thick above the van der Waals surface.

[2] Calculate the electrostatic potential at each of these points, using the nuclear charges and electronic wavefunction.

[3] Fit the calculated potential to a potential based on atomic charges (treated as variables), subject to the constraint that the sum of the atomic charges is equal to the total charge on the molecule.

A weakness of this procedure is that in polar molecules these charges are generally too large and need to be scaled back accordingly.

1.9.4 Which method is better?

They all have relative strengths and weaknesses. The principle advantage of Mulliken analysis is that it is computationally simple. These charges are perhaps as good as electrostatic fit charges for qualitative assignments, but generally fail to provide a good account of electric dipole moments.

The electrostatic potential fitting procedure, while computationally much more expensive is the obvious method of choice if the reason of calculating charges in the first place is to use them in the construction of empirical energy functions, i.e., to reproduce intra and intermolecular electrostatic interactions. Electrostatic fit charges typically provide a good account of dipole moments.

However, the point charge model is intuitive and easy to calculate. There is always a balance to be found between simplicity and accuracy, and in the case of charges a simple model gives good results and so is widely used, with minor modifications. More complicated procedures have been tried, but the increase in accuracy generally seems to be quite small, compared with the increase in complexity.

1.9.5 Effect on the conformational energy by variation in charge sets

Yates and Richardson have studied the effect that various methods of calculating charges for a number of conformations of cyclododecane, 12-crown-3, 13-crown-4, 16-crown-4, 12-crown-4 and its sulfur analogue [72] (**Figure 12**). They found that only in the case of the sulfur analogue was there any reordering of conformational energies due to the change in charge sets. This indicates that in this study relative conformational energies are, generally, not highly sensitive to changes in the atomic charges.

1.10 MOLECULAR MODELLING OF CALIXARENES AND RELATED COMPLEXES

Modification of the size of the calix[n]arene [73] molecule [by changing the value of n (the number of aryl groups forming the hydrophobic cavity)] and the introduction of various functional groups makes it possible to 'tailor' calixarenes to a variety of applications, such as catalysts, ligands and molecular hosts. See **Section 2.1** for conformational details of the calixarenes. To suppress oxygen-through-the-annulus rotation in calix[4]arenes it is necessary to substitute the phenoxy oxygen atoms with, at the smallest, propyl groups [74]. NMR studies have shown that isomerisation does not occur in these calix[4]arene at temperatures even above 100°C which indicates that the calix[4]arene is conformationally locked [74].

The main use of molecular mechanics, with reference to calix[n]arenes, has been in exploring the conformations of the metal-free complexes [75], but with improving parameter sets and modelling software it is being increasingly implemented towards inclusion complexes [76]. Thondorf and Brenn [77] examined the parent *p*-methylcalix[5]arene and the pentamethyl ether *p*-methylcalix[5]arene (**Figure 13**) by means of molecular mechanics calculations using the TRIPOS and the MM3 force fields. MD calculations showed that both calix[5]arenes are very conformationally flexible species. The basic calix[5]arene can have 32 different conformations but these can be assigned as variations on the four basic calix[4]arene conformations. The TRIPOS force field did not adequately reproduce the conformational energy profile for the parent calix[5]arene while MM3 calculations agreed reasonably well with experimental data.

By examining a variety of molecular mechanics force fields and semi-empirical methods Lipkowitz and Pearl showed that semi-empirical methods are not necessarily better than molecular mechanics methods for studying metal free calixarenes [78]. However, to the best of my knowledge, ab initio methods are currently too

computationally expensive to be used in the exploration of the properties of calix[*n*]arenes as only approximately 50 heavy atoms can be studied at a reasonable level of theory.

A coordinate driver method, incorporating the MM3(92) force field, was developed by Thondorf and Brenn [79] to explore the conformational space of five simple *p-tert.*-butyl calix[4]arenes (phenoxy substituent: OH, H, SH, CH₃ and NH₂). The results obtained were in reasonable agreement with the experimental data available.

Gundertofte et al. [80] have also demonstrated that semi-empirical methods are not more reliable than molecular mechanics methods for reproducing experimental rotational barriers and conformational energies for a varied set of test molecules. MM2(85) was shown to be more reliable than Sybyl, ChemX, AM1 and PM3.

Various force fields, e.g. AMBER [81], MM2P [82], CHARMM [83], MM3 [84], MM2 [85] and CVFF [86] have been employed for the study of molecular properties of calix[4]arenes. A variety of methods [TRIPOS, AMBER, MM2(85), PM3] have been used on an exploration of a dissymmetric calix[4]arene and its methyl ethers [87]. Other studies have been published in which the calculated relative stability of the calix[4]arene conformations were not reproduced by NMR spectroscopy [88].

Calix[*n*]arenes have been shown to form inclusion complexes with fullerenes [89]. Schlachter et al. [90] utilised a molecular dynamics simulation with the AMBER force field to study the relative stabilities between complexes formed between calix[4,6,8]arenes and C₆₀ and C₇₀. The calculated data correlated with the experimentally observed equilibrium constants (See **Table 8**). The experimentally determined complexation constants are compared to the interaction energies [$\Delta E(\text{interaction}) = E(\text{calix/fullerene}) - E(\text{calix}) - E(\text{fullerene})$]. For a comparison of the results for C₆₀ and C₇₀, the average interaction energy per carbon atom is given. The last column shows a detailed description of the interaction energy. "Arene" indicates the central

phenyl unit inclusive of hydrogen atoms, whereas the “rest” corresponds to the *t*-butyl, the OH group and the methylene bridges.

The trend of the calculated interaction energies per atom is in agreement with the experimentally observed complex constants, i.e. the values for the complexes of C₆₀ are larger than for C₇₀. By considering the distribution of the interactions, all complexes show a uniform pattern. The arene’s part equals barely 60%, emphasising the influence of the alkyl substituents in stabilising the complex.

| Complex of fullerene and <i>p</i> - <i>tert</i> .-butylcalix[<i>n</i>]arene | Equilibrium constant | Interaction energy, ΔE [kJ/mol] | Interaction energy per carbon atom [kJ/mol] | % distribution arene/rest |
|---|----------------------|---|---|---------------------------|
| C ₆₀ + [4] | - | -53.35 | -0.88 | - |
| C ₆₀ + [6] | 230 | -262.0 | -4.35 | 58/42 |
| C ₆₀ + [8] | 381 | -282.88 | -4.69 | 60/40 |
| C ₇₀ + [6] | 154 | -271.21 | -3.89 | 57/43 |
| C ₇₀ + [8] | 179 | -289.03 | -4.10 | 59/41 |

Table 8. A comparison of complexation constants with computationally calculated interaction energies.

1.10.1 Uncomplexed calixarene tetrol

Harada and Shinkai undertook a comprehensive computational study on unmodified calix[*n*]arenes (*n*=4-7) (**Figure 14**) [91]. They utilised the MM3(92) force field as this has been shown to give the most reliable results for conformational studies of calix[*n*]arenes [92]. They showed that the small ring calix[4,5]arenes keep their high molecular symmetry because of stable intramolecular hydrogen bond formation, whereas the large-ring calix[6,7]arenes lose their molecular symmetry and tend to adopt a pinched

conformation because the formation of stable intramolecular hydrogen bonds inevitably induces ring deformation. The computational results were reinforced by NMR and X-ray crystallography data. **Figure 15** shows the NMR spectra, in the regions of interest, of the calix[4-7]arenes. By observing the Ar–OH spectral patterns we can gain an insight into the type of hydrogen bonding patterns formed. For **1₄** and **1₅** a singlet is obtained which indicates that a cyclic hydrogen bond array is formed with all the phenoxy protons being equivalent. For **1₅**, the signal is shifted to a higher magnetic field which indicates that weaker hydrogen bonds are formed. This is expected due to the greater dimensions of the lower rim cavity. **1₆** shows three singlets of equal intensity at a comparable downfield shift to **1₄**. This indicates that **1₆** does not try to retain the cone conformation, but adopts a pinched cone conformation (as shown in **Figure 16**) and the hydrogen bonds formed are more stable than those in **1₅**. Seven singlet peaks (only six are easily visible) are obtained for **1₇**, that shows that none of the phenoxy protons are equivalent in this molecule.

Figure 16 shows the X-ray structures overlaid with the MM3(92) optimised structures. Overall there is a very good agreement between the two structures, but the rings in the X-ray structures have a tendency to be somewhat more flattened.

1.10.1.1 Recent experimental work on the parent calixarene tetrol

Benevelli et al. [93] have performed a series of solid state studies on the alkali metal complexes of *p-tert.*-butylcalixarenes. The parent calixarenes, containing only phenolic functional groups, show ambidentate character having two different sites for complexation: Endo and exo. In exo complexes [see **Figure 59(b)** for an example] the phenolic oxygen atoms are capable of ‘hard’ electrostatic interactions with small ‘hard’ cations, such as Li⁺ [94] and Na⁺ [95], while the phenyl π electrons participate in endo complexes (see **Figure 56** for an example) with soft dispersion and induction [96] interactions with large ‘soft’ cations, such as Cs⁺ [97]. The rubidium cation has been shown to be too large to form stable exo complexes and too small to have enough

polarisability to form endo complexes with *p-tert.*-calix[4]arene tetrols. Solid-state NMR analysis of the alkali metal cation series confirms this. For Li⁺ complexation was observed with all the calixarenes, with the relative complexation affinity decreasing as *n* increases. The spectral intensity ratios are 1:0.46:0.15 and the spectra are shown in **Figure 17**.

This same trend was followed for Na⁺ complexes with spectral intensity ratios of 1:0.74:0.08, shown in **Figure 18**. A slight shift in the peak's position is probably due to a difference in the distance to the phenoxy oxygen atoms between the two calixarene complexes.

All the calixarenes interacted very weakly with Rb⁺, in the order calix[4]arene>calix[8]arene>calix[6]arene.

¹³³Cs spectra of calix[4]arene indicate that both endo and exo complexation occurs (as indicated by peaks at +218 and -200), in the ratio of 92:8. In the case of the calix[8]arene both the oxygen atoms and the phenyl rings are involved in the binding (**Figure 19**). Very weak signals are obtained for the calix[6]arene complex and are similar to those just discussed. The relative binding affinity for Cs⁺ is the same as for Rb⁺.

The very poor tendency of *p-tert.*-butyl-calix[6]arene to form complexes when the calix π -electrons are involved has already been observed [98]. It has been suggested that the pinched cone conformation of this calixarene prohibits easy access of the cation to the calixarene cavity [99].

An X-ray crystallographic study [100] of the 1:1 Cs⁺ complex of *p-tert.*-butyl-calix[4]arene monoanion reveals an inclusive (endo) structure, where the Cs⁺ cation is found inside the cone form calixarene, closer to the aromatic carbon atoms than to the phenolic oxygen atoms, and coordinated to one CH₃CN molecule (**Figure 20**). The

separation of the cation to the phenoxy oxygen atoms is close to 4 Å, which is much longer than Cs–O distances of 3.0–3.3 Å identified with typical coordinate bonds [101].

In chloroform solution, ^{133}Cs NMR measurements indicate that this structure is retained, i.e. that the caesium remains bound to the soft, phenyl- π -electron site, and this would appear to be true to at least some degree of a number of related Cs^+ complexes of bridged calix[4]arene derivatives also used in cation transport studies [102]. In the better donor solvent acetone [103], however, the ^{133}Cs NMR shifts are consistent with oxygen ligand coordination, suggesting that the complex isomerises on dissolution to the phenoxide bound form or dissociates to a solvent-separated ion pair. Phenoxide (exo) coordination is the mode of binding revealed by X-ray crystallography in the solid state structures [104] of the Na^+ complex of the anionic host and the (di) Li^+ complex of the diprotonated calixarene, but the nature of the K^+ complex has, to the best of my knowledge, not been established, so that the exact point at which there is a change from endo to exo bonding is unknown. The previously mentioned data for the rubidium complex indicates that this is a “borderline” exo/endo inclusion cation.

NMR, UV spectrophotometry and computational studies on the *p-t*-butyl-calix[4]arene monoanion (one deprotonated phenolic group) complexing a variety of alkali metal cations has shown the same trend as above for the uncharged calixarene [105]. The nature of the solvent also had a large bearing on the endo or exo nature of complexation and on the equilibrium constants as shown in **Table 9**.

| Solvent | Li^+ | Na^+ | K^+ | Rb^+ | Cs^+ |
|----------------------|----------------|---------------|--------------|---------------|---------------|
| Acetonitrile (298 K) | 760 ± 35^b | 19 ± 5 | 18 ± 2 | $< 10^c$ | $< 10^c$ |
| Acetone (293 K) | – | 301 ± 64 | – | – | 160 ± 120 |

Table 9. Estimated equilibrium constants ($\text{mol}^{-1} \text{l}$), by NMR titration with the metal triflates in acetone and UV spectrophotometry in acetonitrile, for the complexation of alkali metal cations with the calix[4]arene monoanion.

^b For Li_2 :calix[4]arene monoanion complexes, overall equilibrium constant $(1.1 \pm 0.5) \cdot 10^4$.

In polar solvents all the cations are complexed in an exo manner (see **Section 1.10.1.1**), and when the cation solvation energies are small, such as in non-polar solvents, the endo form is preferred.

1.10.2 Calixarene:amine inclusion complexes

Organic amines are easily dissolved in water and can be oxidised to nitrite compounds that are harmful pollutants in the environment. Many pharmaceutically important compounds contain an amino moiety. Amines, including amino acids [106], noradrenaline, norephedrine and so on, play critical roles not only in the field of chemistry but also in biological systems. A simple monitoring system for the discrimination between enantiomers is one of the most pressing challenges in the design of molecular sensors [107]. Such a system may also be most welcome in pharmacology and in environmental protection.

Analogous to enzymes and substrates in biological chemistry, the terms host and guest are applied to the molecular complexes studied in synthetic chemistry. A host contains convergent binding sites and concave surfaces while the guest possesses divergent binding sites as part of convex surfaces [108]. Calixarene:amine complexes have been studied by various research groups [109].

Zhang et al. [110] have written a comprehensive review on the enantiomeric recognition of amine compounds by a variety of chiral macrocyclic receptors. The review is relatively recent and even though it is nearly 50 pages in length, less than one page details calixarene complexation chemistry which is indicative of the amount of research performed in the area to date!

^c Spectral changes too small to allow precise estimation.

Up until now very little research has centred on the selective complexation of chiral amines by chiral calixarene host molecules. But there has been interest in the binding of non-chiral amines and amino acids by calixarenes. The binding interactions have been observed to occur at both the upper and lower functionalised rims. Work performed by various research groups on these complexes shall now be detailed.

1.10.2.1 Lower rim functionalisation

The complexation behaviour of 5,17-Di-*tert.*-butyl-26,28-bis[(methoxycarbonyl)methoxy]calix[4]-26,28-diquinone (**Figure 21**) has been studied with NH_4^+ and $\text{Bu}_n\text{NH}_{4-n}^+$ ($n=0,1,2,3$) [111]. ^1H NMR data shows that NH_4^+ and BuNH_3^+ form inclusion complexes with the calix[4]diquinone but Bu_2NH_2^+ and Bu_3NH^+ do not. NH_4^+ can form four hydrogen bonds with the quinone and the ether lower rim substituents, BuNH_3^+ can form three bonds while secondary and tertiary alkylammonium ions can only form two and one hydrogen bond respectively. The length of the alkyl chain does not significantly effect the complexation behaviour. However, due to the calix[4]diquinone being difunctionalised with *tert.*-butyl groups this would significantly inhibit the inclusion of the ammonium cations in the aryl cavity.

Mohammed-Ziegler et al. investigated the UV/Vis spectra of two calix[4]arenes (**Figure 22**) in the presence of alkali/alkaline earth metals and aliphatic amines in a variety of solvents [112]. Two para-substituted $-\text{NO}_2$ groups, connected to the phenolic hydroxyl groups through conjugated electron systems, provided the signalling element of the calixarene. A bridging amide linkage between opposite rings (**1**) and in the other calixarene ester groups in the same two positions (**2**) provided the complexation site.

In the case of amines, complex formation is strong not only in acetone and acetonitrile (aprotic, polar solvents) but also in ethanol (protic solvent) as well. The effect is weaker in apolar solvents, particularly in carbon tetrachloride. This is thought to be due

to the amine being protonated before complexation, so the complex is stabilised by electrostatic and hydrogen bonding interactions with the solvent. The strength of the complex formation depends primarily on the order of the amine. Primary monoamines are complexed strongly, the reaction with diethylene triamine is partial, whereas only a small proportion of triethylamine is complexed.

For the metal cations, formed from their bromide salts, the dependence on the solvent was also similar, in polar solvents the complex formation with lithium and calcium was effective, while in apolar solvents it was poor. Except for in the case of Ca^{2+} where the more rigid structure of the bridged calixarene yielded a significant enhancement in the stability of the complexes formed.

1.10.2.2 Upper rim functionalisation

Ungaro et al. [113] have shown that tetrasulfonatocalix[4]arenes [114], substituted with esters/acids on the lower rim (**Figure 23**), can complex a variety of L- α -amino acids. The postulated mechanism of interaction involves the inclusion of, (1) the aromatic, or aliphatic, apolar group of the amino acid in the aromatic cavity and, (2) a simultaneous interaction of the polar groups of the amino acid with the sulfonate groups and the polar medium surrounding the calixarene. NMR studies confirm that (1) occurs and removal of the sulfonate groups stops any complexation occurring, thus verifying (2).

Sansone et al. [115] studied the inclusion properties of an L-alanine upper rim functionalised calix[4]arene (**Figure 24**) with several guest molecules. In water no evidence for the inclusion of L-phenylalanine or its methyl ester hydrochloride was observed. Also, association constants for trimethylanilinium and benzyltrimethylammonium cations were lower than those obtained with the tetrasulfonate derivative (**Figure 25**). This could be due to the fact that the peptidocalix[4]arene has an inherent conformational flexibility [116].

Two short di(ethylene glycol) units were linked to proximal positions on the lower rim to inhibit this flexibility (**Figure 26**) [115]. The association constants obtained for this rigidified host with a variety of amine guests showed that it is a much more efficient host than its conformationally mobile analogue, demonstrating the importance of rigidity in the recognition process.

α -amino acids are complexed via their apolar moiety. They are more efficiently complexed as their methyl esters rather than in their zwitterionic form. Also, aromatic amino acids are more strongly complexed than the aliphatic ones. Only a very modest chiral discrimination is observed between L- and D-amino acids.

This above work shows the remarkable influence of subtle conformational changes of the cone calix[4]arene platform, which can be tuned by the nature of the functionalisation at the lower rim, on the recognition properties of peptidocalix[4]arenes towards ammonium cations and amino acids. These researchers also found that when the recognition process involves more directional hydrogen bonding, a better binding is found with more flexible hosts [117].

Calix[4]arenes functionalised with ureas on the upper rim have self-complementary recognition sites and can assemble into dimeric structures [118]. A “tongue-in-groove” hydrogen bonding pattern is formed between two identical calix[4]arenes producing a capsule that is S_8 -symmetric and achiral. When the capsule is assembled from two different halves, a chiral, C_4 -symmetric heterodimer results. The head-to-tail urea directionality of its hydrogen bonding seam defines enantiomers. Equal populations of both clockwise and anticlockwise species exist as there are no energetic differences between them. However, stereocentres near the ureas serve to introduce a second chiral element, beyond the urea directionality, and diastereomeric complexes are generated. Just as with conventional diastereomers, the energies and populations of these assemblies are not expected to be equal. Castellano et al. [119] reported molecules that

not only heterodimerise with exclusivity but also have a single-handed direction to their urea rotation (**Figure 27**). The resulting capsules are non-racemic and are capable of discriminating between enantiomers of guest molecules. However, heterodimerisation was only observed when $R=1$ (not 2) for assemblies formed between those calixarenes and a variety of eight β -branched amino acid substituted calixarenes.

The weak interactions that result in this selectivity are sensitive to subtle changes in structure and medium; they are highly cooperative systems. If β -branched amino acid derivatives are used, in the heterodimeric state they form, exclusively, one diastereomeric assembly in C_6H_6 . When the β -branching is removed or $CDCl_3$ is utilised as the solvent this selectivity falls off.

The discrepancy between C_6H_6 and $CDCl_3$ in promoting heterodimer formation illustrates the fragility of these systems and the weak forces that hold them together. Molecular modelling indicates that the volume of the heterodimer cavity is smaller ($\sim 20 \text{ \AA}^3$) than that of the homodimer so the size and fit of the solvent/guest in each of these cavities may play a role in determining which capsule emerges. It also appears that polarity differences between the two solvents result in significant selectivity differences; the more polar solvent disrupting the non-covalent interactions between the urea and the amino acid side chains of the substituted calix[4]arenes. Also, the addition of a 4% methanol solution to the heterodimeric complex in chloroform results in no circular dichroism [120] (CD; see **Section 1.11.1**) activity. As no CD activity is observed unless the two calixarenes are added together, the species are monomeric.

Chiral guests within these heterodimeric assemblies can sense the hydrogen bond directionality that defines the capsule's chirality, and they are observed to bind selectively [121]. Because the chiral heterodimers have a defined urea direction, a mixture of enantiomeric guests produces two diastereomeric capsules. But these capsules are formed in different proportions so only a modest discrimination is observed.

Urea bimolecular complexes are created by the formation of hydrogen bonding patterns on self-complementary molecules. The moderate directionality and reversible formation of hydrogen bonds by the ureas gives rise to a seam of hydrogen bonds between the hemispheres. Böhmer also published results on a related series of capsular systems [122] after initially disagreeing with Rebek [123] when he first talked about it at a conference in 1995 [124]. They mixed two very similar calixarene dimers that yielded a heterodimeric system. An X-ray structure with an included benzene guest molecule was published soon after [125]. Reinhoudt also published research on such a system after his original scepticism [126].

Competition by solvent molecules for encapsulation is a large problem for these systems. Still and Chapman [127] had shown that concave surfaces into which solvents do not fit tended to show high affinities for other small molecules that do. This scenario was staged by the use of solvents that are too large to be accommodated into the cavity, providing that they still dissolve the components of the system. These observations concerning solvent size versus cavity size are generally applicable to encapsulation phenomena. In the current case, solvents such as CDCl_3 are efficiently complexed guests and exist in a concentration that would give them an insurmountable advantage. Deuterated *p*-xylene or mesitylene are non-competing solvents that have been used.

The calixarene tetraureas derived from norleucine, in its optically active form, showed a very high preference for forming heterodimers with the parent aryl urea. Within these, the head-to-tail arrangement of the eight ureas appeared entirely to be oriented in one direction. In other words, the peripheral point chirality of the amino acid was being transmitted to the capsule's lining. This heterodimerisation was shown to be exclusive to other amino acids that have β -branched side chains, like isoleucine and valine [128]. The side chains of the amino acids provide contacts that are vital in the dimeric assembly and eventually lead to instruction of the clockwise or anticlockwise arrangement of the ureas.

These asymmetric microenvironments distinguish only moderately between enantiomeric guests. Norcamphor shows only an excess of 15% of one diastereomeric complex.

1.10.2.3 Sulfonate calix[6]arene

The design of water soluble synthetic receptors is a topic of current interest in supramolecular chemistry since they allow the study of host-guest interactions in a solvent where most biological processes take place [129].

For the lower rim unsubstituted sulfonated calix[6]arene (**Figure 28**) the degree of intramolecular hydrogen bonding, and hence preorganisation, has been shown to have an effect on the complexation abilities of the calix[6]arene [130]. Molecular modelling studies (MC conformational searching using MacroModel) suggests that when two of the phenolic OH groups are deprotonated the calix[6]arene exists in a partial cone conformation with three of the sulfonate groups on one side of the cavity and the other three groups on the opposite side. The two negatively charged phenolate groups are hydrogen bonded to their adjoining two phenolic OH groups. This stabilises the conformation and produces two arene regions that are available to partake in complexation. When the phenolic OH groups are fully protonated or methylated the calix[6]arene adopts conformations that were not ideal for the inclusion of guest molecules. This computational data was found to be in agreement with voltammetric experimental results obtained for the complexation of four ferrocene-based guests.

1.10.2.4 Calix[5]arene complexing three amines

An appropriately functionalised calix[5]arene (11.23-*m*-hydroxycarbonylphenyl-5,17,29-trimethyl-31,32,33,34,35-pentahydroxycalix[5]arene) (**Figure 29**) has been

studied both experimentally and computationally by Haino et al. [131] with regards to its complexation abilities with three amines [(Figure 29) 2-aminopyrimidine **1**, 9-ethyladenine **2** and imidazole **3**]. The upper rim of the calix[5]arene was substituted with two benzoic moieties and these were shown to form efficient hydrogen bonds with the relevant hydrogen and nitrogen atoms of the amines. The two larger amines were not included in the cavity of the calix[5]arene. The benzoic acid groups effectively bound them and this binding process was also driven by the fact that a stabilising lower rim hydrogen bonding network was also formed.

1.10.2.5 Chiral calixarenes incorporated into chromatographic separations

Chiral calixarenes have also been used in investigations of enantioselectivity and discrimination of chiral amines as molecular recognition of biorelevant molecules is an important and expanding area of research [132].

A variety of chromatographic techniques have been used, incorporating chiral calixarenes, in the separation of enantiomers. The first report of chiral separation using a chiral calixarene as a chiral medium in capillary electrophoresis [133] was the separation of racemic 1,1'-binaphthyl-2-2'-diyl hydrogen phosphate (BNHP). The separation of enantiomers on chiral calixarenes has been investigated by electrokinetic chromatography. Thus, several atropisomeric binaphthyl compounds have been resolved by the addition of (N-L-valinoacyl)calix[4]arene [134]. In liquid chromatography a new chiral calixarene derivative functionalised with (-)-ephedrine and chemically bonded to silica has been used for enantiomer separation of S-(+)-1-phenyl-2,2,2-trifluoroethanol [135].

Gas chromatographic techniques have also been used. The poor solubility of calixarenes in polysiloxanes restricted their use to gas-solid chromatography [136]. The solubility problem can be alleviated by the introduction of long alkyl chains into the

molecules [137] (**Figure 30**), or by chemically linking calixarenes to polysiloxanes [138]. Iki et al. [139] have used a chiral thiacalixarene to achieve separations. A collection of N(O,S)-TFA-D,L-amino acid methyl esters were resolved with the use of a resorc[4]arene which had its eight hydroxy groups modified with L-valine-*tert.*-butylamide moieties and four long ω -unsaturated alkyl chains attached to the lower rim [140] (**Figure 31**). Surprisingly however, amino acids containing aromatic moieties were badly resolved with reference to the remainder of the amino acids. According to the authors, this could be due to the fact that the L-valine-*tert.*-butylamide moieties are very bulky attachments and it is likely that strong hydrogen bonding is occurring between these groups, which, when taken into consideration together, may be blocking the arene cavity, thus preventing host-guest π - π interactions.

Chen et al. [141] studied five calixarene coated PQC sensors for the detection of organic amines in liquids (**Figure 32**). The strongest responses were observed for small amine molecules that are easily included in the calixarene cavity. So, these calixarenes provided a shape discrimination of analytes via the inclusion of organic amines into the apolar cavity of the calixarene.

1.10.3 Dihomooxacalix[4]arene and resorcarene studies

Bernardino et al. [142] performed a theoretical study on the molecular properties of *p-tert.*-butyl-dihomooxacalix[4]arene (same structure as in **Figure 33**, except for a hydrogen atom instead of the benzyl group). This system, when compared to *p-tert.*-butylcalix[4]arene has one of the methylene bridges substituted by a CH₂-O-CH₂ group which gives more flexibility to the macrocycle, and increases the size of the cavity [143]. Particular attention was paid to the analysis of the hydrogen bonding patterns formed. A comparison of bond angles found using the AM1 semi-empirical method and X-ray crystallography data is shown in **Figure 34**.

Their calculations showed that the cone conformation was the most stable and that the thermodynamic stability of this conformer is related to the formation of intramolecular hydrogen bonds. The results obtained compared favourably with X-ray crystallography [144] and NMR data [145].

Conflicting results were found by Santos et al. [146] when they performed MM/MD simulations on the tetrabenzyl ether of *p-tert.*-butyl-dihomooxalix[4]arene (**Figure 33**) using the CVFF and AMBER force fields. ¹H NMR data indicates the presence of the cone conformation but the computational study indicated that the 1,3-alternate is the thermodynamically most stable conformation, followed by one of the two partial cone conformations.

The apparent discrepancy between theory and available experimental data could be attributed inherent deficiencies in the force fields utilised, or to different control procedures. Which means that the relative stability of the model is only thermodynamically controlled while the actual conformational preference of the product should be kinetically controlled during the derivatisation procedure.

Thondorf et al. [147] performed MM3 calculations on *p*-methylresorcarene (**Figure 35**) [148]. The intramolecular hydrogen bond stabilised cone conformation was found to be the most stable; mirroring results found for *p-tert.*-butylcalix[4]arene.

1.10.4 Crown ether studies

Nature makes extensive use of weak interactions such as π -forces, cation-interactions and hydrogen bonding in order to control and to fine-tune structures and functions of the species involved in many important biological processes.

In a very recent review Schalley [149] discussed the use of mass spectroscopic methods in determining the structure of supramolecular architecture and their complexes formed. Most of the examples discussed in the review refer to crown ether complexes but the same methodologies have been, and continue to be, applied to calixarene chemistry **Figure 36** shows one of the crown ethers investigated by Schalley. The involvement of the aryl rings of the unsubstituted calixarene in the binding of alkali and silver cations has been shown mass spectroscopically [150]. For the conformations of the calixarene shown in **Figure 37** its affinity for K^+ and Ag^+ appears in the order 1,3-alternate>partial cone>>cone.

Armentrout [151] discussed the trends in bond dissociation energies (as shown in **Table 10**) for the binding of the alkali metal cations, Li^+ , Na^+ , K^+ , Rb^+ and Cs^+ , to a series of ethers, 1-4 dimethyl ethers (DME), 1 and 2 dimethoxy ethanes (DXE), and the crown ethers 12-crown-4, 15-crown-5 and 18-crown-6 in the gas phase (**Figure 38**).

| | M | | | | |
|--------|----------------|----------------|----------------|----------------------|----------------------|
| x L | Li | Na | K | Rb | Cs |
| 1 DME | 164.99 (10.61) | 91.66 (4.82) | 73.33 (3.86) | 61.75 (8.68) | 56.93 (4.82) |
| 2 DME | 120.61 (5.79) | 82.01 (4.82) | 68.50 (4.82) | 55.00 (4.82) | 47.28 (5.79) |
| 3 DME | 88.77 (7.72) | 69.47 (4.82) | 56.93 (7.72) | 36.66 (10.61) | 39.56 (0.09) |
| 4 DME | 67.54 (9.65) | 60.79 (3.86) | 50.17 (7.72) | 38.59 est | 35.70 est |
| | | | | | |
| 1 DXE | 241.21 (18.33) | 158.24 (3.86) | 118.68 (3.86) | 93.59 (8.68) | 56.93 (4.82) |
| 2 DXE | 138.94 (11.58) | 115.78 (7.72)) | 88.77 (11.58) | 49.21 (11.58) | 54.03 (6.75) |
| | | | | | |
| 1 12c4 | 371.47 (51.14) | 251.83 (12.54) | 189.11 (11.58) | 92.63 (12.54) | 84.91 (8.68) |
| 1 15c5 | – | 294.28 (18.33) | 204.55 (14.47) | 113.85 (6.75) | 100.34 (5.79) |
| 1 18c6 | – | 296.21 (19.30) | 234.46 (12.54) | 191.04 (12.54) | 167.88 (8.68) |

Table 10. Bond dissociation energies (in kJ mol^{-1}) at 0 K of $M^+(L)_x$ for the loss of a single ligand^d.

^d The uncertainties are in parentheses. The values in bold exceed theoretical values by an average of 73%. The values in italics are ~40% higher than theory. Est: Estimated value.

The experimental values in **Table 10** are taken from Ref. [152]. For Li^+ , Na^+ and K^+ complexes the theoretical results are $12\pm 8\%$ higher than the experimental values. The discrepancies illustrated appear to be due to the measurements being performed on complexes that are not in their ground state. It was shown that bond energies fall in the order $\text{Li}^+ > \text{Na}^+ > \text{K}^+ > \text{Rb}^+ > \text{Cs}^+$. This is expected for electrostatic interactions because the smaller the ion is, the closer the metal-ligand bond distance and the stronger the electrostatic interaction. It was also shown that the bond energies gradually decrease as the number of ligands around the metal ion increases. This is also typical behaviour for electrostatic interactions. The bond energies decrease because of electron delocalisation at the metal centre and due to ligand-ligand repulsions. The weakening in bond energy upon increasing ligation trend is observed most strongly for Li^+ . This is due to more severe ligand-ligand repulsions around the smallest cation.

Calculations indicated that the DME ligands bind to the metal cation by directing the oxygen atom towards the metal ion [153]. Thus, the dipole moment of DME is aligned in the most favourable orientation.

For ligands bigger than DME, such as DXE, the bond energies are generally lower than the sum of the DME bond energies by 10–20%. This difference can be rationalised on the basis that the C–C bond along the DXE backbone constrains the orientation of the oxygen atoms toward the metal ion. In essence, the local dipoles in DXE cannot simultaneously orient themselves toward the metal ion and maintain the optimal M–O bond distance because of the restriction in geometry. The DME ligands are not constrained and can optimise both the orientation and M–O bond distance. This trend is also seen for the crown ethers but to a varying extent.

In an aqueous environment 18-crown-6 binds K^+ selectively over Rb^+ , Cs^+ and Na^+ [154]. However, the bond energies determined in the gas phase clearly indicate that Na^+ is the most strongly bound by a considerable margin. This phenomenon can be

understood by considering the competition between solvation of the cations by water and complexation by the crown ether [155][156]. It has been shown that complexation of Na^+ by 18-crown-6 is favoured until the number of water molecules that have to be displaced nears a complete solvent shell. At this point K^+ is selectively bound by the crown ether, in agreement with the findings in solution. Another factor governing the selectivity is that in complexes of K^+ , Rb^+ and Cs^+ with 18-crown-6, the metal is exposed and can be directly solvated, while the 18-crown-6 surrounds the smaller Na^+ cation, shielding it from being solvated directly [157]. This should stabilise the larger metal ion crown ether complexes relative to $\text{Na}^+:\text{18-crown-6}$. Overall, this comparison demonstrates that the selective binding of K^+ by 18-crown-6 in aqueous media is a delicate balance of solvation versus complexation enthalpy, entropic effects and the solvation of the resultant complex. Clearly, these factors depend critically on the identity of the solvent.

Grootenhuis and Kollman described the first general application of free energy perturbation methods to a wide series of alkali metal cation:dibenzo-crown ether complexes. They showed that a combination of MM and MD calculations can qualitatively reproduce experimental trends with respect to dibenzo-18-crown-6 binding alkali cations in methanol solution [158].

1.10.5 Cyclodextrin studies

Most of the 1000 or so papers published each year on cyclodextrins concern cyclodextrin inclusion complexes and only a few deals with cyclodextrin metal complex chemistry. The metal ion can assist the host-guest interactions often enhancing the properties of cyclodextrins as chiral receptors and enzyme models. Computational approaches are increasingly being applied to the study of cyclodextrin inclusion complexes [159].

Rizzarelli and Vecchio [160] have reviewed various experimental studies on the metal complexes of functionalised cyclodextrins acting as enzyme models and chiral receptors. Due to the inherently chiral nature of their cavity they have been often used as chiral receptors, particularly in the area of chromatography.

Alvira et al. [161] performed calculations on the interaction of R and S equol (**Figure 39**) with β -cyclodextrin. Using the AMBER force field a breakdown of the energy contributions for both enantiomers is shown in **Table 11**. They stated that the van der Waals term is the main contributor to the total energy of the inclusion complex and that it was the electrostatic term that causes the difference between the most stable complexes formed of the R- and S-equol. On analysing the results, their reasoning appears to be flawed as the electrostatic term stabilises inclusion of the S enantiomer with respect to the R enantiomer and it is the van der Waals term that contributes to a more stable R enantiomer complexation process. As can be seen, once the equol molecule is included in the cyclodextrin cavity no hydrogen bonding occurs, even though it does happen as the guest approaches the cavity. Perhaps its influence in the complexation process is orientational in nature.

| | <i>E</i> | <i>vdW</i> | <i>Electrostatic</i> | <i>H-bonding</i> |
|---------|----------|------------|----------------------|------------------|
| R-equol | -103.12 | -77.21 | -25.90 | 0.0 |
| S-equol | -99.56 | -64.25 | -35.31 | 0.0 |

Table 11. The total energy and contributions of van der Waals, electrostatic and hydrogen bonding terms in the complexes formed (in kJ mol^{-1}).

However they assumed that inclusion complex formation did not affect the structure of either molecule, so they kept the internal coordinates of both the host and guest molecules fixed. Numerous studies on enantiodiscrimination based on molecular mechanics methods concluded that, in general, the chromatographic retention order predicted by the lowest computed energies using rigid molecules are unable to reproduce

experimental results [162]. Also, solvent effects were not taken into account during the modelling process.

Cozzini et al. [163] studied the complexation behaviour, both experimentally and computationally, of 2,6-di-O-methyl-3-O-trifluoroacetyl- β -cyclodextrin (**Figure 40**) with 20 chiral guests. In the case of the proline derivatives and γ -lactones a good correlation was obtained between the gas chromatographic elution order and the energies of the host-guest complexes calculated by molecular modelling. However, aliphatic amino acids containing $-NH$ groups did not follow this dependence. As the study performed seems to rely on a size-fit relationship when obtaining the computational data, hydrogen bond formation would disrupt this theory.

1.11 CHIRAL RECOGNITION AND SELECTIVE COMPLEXATION

The propagation of all life is dependent upon the recognition/response phenomenon. Molecular recognition is the cause of the specificity seen during neurotransmitter response, cell-cell, antigen-antibody, the restoration of genetic code, substrate-enzyme and hormone-receptor interactions [164]. It is not a new concept, having occupied the minds of notable 19th century scientists like Pasteur and Ehrlich. Indeed, Ehrlich is widely credited with developing the concept of the pharmacophore. In a paper in 1900 [165], he reasoned that toxins possessed two different combining groups, a heptaophore that bound the toxin to the cell and a toxophore that was responsible for the toxic action.

Emil Fisher introduced the lock and key concept almost 100 years ago [166]. A significant extension was Koshlands proposal of induced fit [167] in which the receptor adapts its conformation so as to achieve optimal binding with the substrate.

One of the fundamental components of systems that exhibit molecular recognition is non-covalent interactions [168]. Such interactions involve a subtle interplay of entropic and enthalpic effects that are difficult to separate.

Living organisms may be taken as amazingly complicated yet highly perfected molecular systems, where molecular recognition is essential. Nowadays, sophisticated receptor molecules are purposefully synthesised and their complexation behaviour has been investigated to obtain a better understanding of the mechanisms of molecular recognition phenomena [169]. Among them, simple in concept but often most difficult in practice, is chiral recognition in which a chiral host molecule selectively binds one of the enantiomers of a racemic mixture [170].

The chiral nature of a drug molecule is essentially required after synthesis and during *in vivo* and *in vitro* studies due to the fact that the physiological effects of the enantiomers may significantly differ [171]. Thus, the determination of enantiomeric purity has become one of the most important strategies in pharmaceuticals. Several techniques have been developed for the determination of enantiomeric purity: Specific rotation [172], circular dichroism and separation techniques including liquid and gas chromatographies [173].

Compounds that exist in two forms that are non-superimposable mirror images (enantiomers) are optically active, rotating plane polarised light in different directions. Many compounds, such as drugs, agrochemicals and food additives have been marketed as racemic mixtures but the often dramatic difference in biological effects of the enantiomers of a chiral compound demonstrates the need for methods capable of discriminating between them. Presently, the use of HPLC is the most common means of achieving enantioselective separation. A large number of different chiral stationary phases (CSPs) are available, classified according to their separation mechanisms and, thus, the structural requirements of the analyte [174].

Molecular recognition is thought to be predominantly electrostatic at long range [175], with steric and electronic requirements becoming important as the guest approaches the active site. The global minimum conformation of an isolated drug, or guest, molecule is not necessarily equivalent to its binding conformation in the complex. The guest molecule may induce significant conformational changes. In addition, the host molecule itself may relax to accommodate the docking of the guest into the complexation site.

Ideally, it should be possible to use truly unrestrained simulations to model the recognition process: i.e. to determine the lowest-energy bound conformations (if indeed binding is favourable) of two initially uncomplexed molecules, allowing full flexibility in each molecule. In practice, the global minimum problem is usually virtually intractable in a reasonable time due to the amount of degrees of freedom in any reasonably sized system that necessitates the use of restraints, particularly in enzyme/protein docking procedures.

The study of weak interactions is a topic of great current interest because it is these non-covalent interactions which determine the stability, for example, of DNA duplexes, of the folded states of proteins, of enzyme–substrate complexes, and of ligand–receptor interactions. A deeper understanding of weak interactions is highly desirable not simply because of the intellectual drive to understand the above systems, but also because of the wish of the pharmaceutical industry to ‘rationally’ design new drugs.

Williams and Westwell [176] discussed the play-off or compensation between electrostatic binding and the restriction in motion of the interacting species. They have obtained promising results using a semi-empirical approach for the estimation of binding affinities.

Topiol and Sabio [177] have written an interesting review discussing the general principles governing chiral recognition. They outlined a number of principles that can aid in the understanding of chiral discrimination processes, illustrated with some examples from the literature.

Molecular chirality is a fundamental concept in chemistry which is well established and whose existence has pervasive ramifications. Of particular interest is the chiral nature of many drugs. Differences in pharmacological activities of enantiomers can often be traced to their different interactions with chiral macromolecular systems such as proteins. Depending on the relative profiles of activities of the enantiomers of a given drug, it is often necessary to separate the enantiomers by physio-chemical means (e.g., chiral chromatographic columns) so that only the active enantiomer can be isolated. While the chiral nature of such compounds is well established, the underlining principles for chiral discrimination, e.g., at proteins or with resolving agents, is still poorly understood. This understanding is critical to further rational approaches in drug design and the development of separation techniques.

A “three-point model” generally describes chiral discrimination [178] (**Figure 41**). One of these three simultaneous interactions should be stereochemically dependent. While this model seems almost intuitively obvious, there are examples in the literature that question both whether ‘three points’ is a necessary or, indeed, a sufficient condition. On the one hand, using formal, computational approaches, Salem and co-workers have suggested that three points are the minimal requirement for chiral discrimination [179]. Similar conclusions are implicit in the model of Meyer and Rais [180]. Topiol and Sabio have stated that in fact four points are needed for chiral discrimination [181]. On the other hand, chiral stationary phase experiments have been conducted which support two and even one-point models [182]. Even analyses that cite three point models can be misleading. For instance, Pirkle and co-workers have analysed results of models of chiral stationary phase complexes whose chiral discrimination properties were attributed to a three-point model [183]. Topiol et al. [184] later showed that the complexes described

were not operating via a three-point model, but rather a "pseudo-two-point model". Computational studies by Lipkowitz and Baker [185] decomposed the interactions of model chiral complexes into three fragments and analysed the contributions of these with respect to chiral discrimination. In such studies, the concept of chiral discrimination residing in, e.g., a single fragment of the molecule, is similarly unclear in terms of basic principles.

It is common practice to invoke three-point models (e.g., Easson and Stedman [186]) in the description of the recognition of chiral molecules, wherein the points are taken to be atoms, fragments, etc. Topiol proposed [187] a distinction in the terms interactions versus contact points to help clarify chiral discrimination. Specifically, the term interactions should be taken to refer to the actual physical interactions that take place between all particles (atoms, electrons, etc) in a given molecular complex. These interactions are well defined by basic physicochemical principles. Contact points are defined as the primary interactions between molecular systems. An important distinction is that the actual assignment of the contact points in a given system is generally subjective whereas the interactions are rooted in physical principles.

For a further discussion on the nature and measurability of chirality see Buda et al. [188] Breckenridge [189] has written an informative review on the area of molecular recognition.

1.11.1 Tools for structural recognition

3D structural information now plays an integral role in the comprehensive understanding of molecular interactions. Over the last 25 years there has been an explosion in structural information generated by a combination of experimental and theoretical techniques. There are a variety of sources of structural information available:

- (1) X-ray and crystallography (see **Section 1.5.7**).
- (2) Neutron diffraction (see **Section 1.5.8**).
- (3) Structures derived from NMR methods.
- (4) Fluorescence studies (see **Section 1.13**).
- (5) IR/UV-Vis/Raman spectroscopic studies.
- (6) LC-MS.
- (7) Circular dichroism: Chiral molecules respond differently to radiation depending on whether it is left or right circularly polarised. The differential absorption of light of these two polarisations is known as circular dichroism (CD), and the differential refraction as optical rotation.
- (8) Theoretical methods, based upon mathematical principles: Molecular modelling software provides elegant and powerful tools for building, visualising, analysing and storing models that can be used to interpret host-guest relationships.

Each provides a different but complementary perspective of molecular interactions. Recent advances in computer technology have also directly benefited all the technologies to rapidly generate structural information.

Filippi et al. [190] have reviewed the most important experimental methodologies in determining the intrinsic non-covalent interactions governing chiral recognition in diastereomeric complexes mainly in the gas phase.

Quantification of non-covalent interactions in diastereomeric aggregates in the condensed phase represents a formidable task because of the transient character of the adducts and the unavoidable interference from the medium [191]. To overcome these difficulties increasing attention is being paid to gas-phase techniques, chiefly mass spectrometry. In fact, these techniques allow observation of long-lived diastereomeric aggregates and the evaluation of their intrinsic interactions by eliminating the interfering effect of the solvent.

Non-covalent interactions constitute the basis for information transfer between molecules in living systems as well as in synthetic supramolecular structures. Despite an ever more accurate description of biological systems and their modelling by synthetic host/guest complexes, a systematic and general understanding of the underlying forces is still in its infancy. A major problem is presented by the unpredictable action of the solvent, which mitigates specific intermolecular interactions, fundamental in biological and host/guest aggregates, so as to make the entropy term sometimes predominant.

1.11.2 Preorganisation

Selective complexation of inorganic cations and anions is by far the most developed aspect of supramolecular chemistry. General rules based on such principles as chelation and Hard/Soft Acid-Base (HSAB) phenomena have been worked out largely in the framework of inorganic coordination chemistry [192].

Size-dependant selectivity is observed if the ligands conformation is rather fixed, such as with Lehn's cryptand [193]. However, Hancock and Martell [192] have shown conclusively how simple rules of size matching can break down with more flexible ligands such as crown ethers and azamacrocycles. These general findings can be explained and substantiated by molecular mechanics calculations [194].

Cram's preorganisation principle [195] which is demonstrated by spherand encapsulation of Li^+ , **Figure 42**, which calls for cooperative attraction between binding sites and guest molecule without the development of non-bonded repulsions.

The spherand possesses a single conformation ideally arranged for binding Li^+ and Na^+ . Its oxygen atoms are deeply buried within a hydrocarbon shell. The orbitals of their unpaired electron pairs are in a microenvironment whose dielectric properties are between those of a vacuum and of a hydrocarbon. No solvent can approach these six

oxygen atoms, which, therefore, remain unsolvated. This spherand was the first host system to be designed and synthesised which was completely organised for complexation during synthesis, rather than during complexation. The free energy costs of organising the spherand into a single conformation and of desolving its six oxygen atoms was paid for during its synthesis. Thus, this spherand is preorganised for binding [196].

Cram concluded that both selectivity and complexation strength increase generally in the order podands < coronands (crown ethers, etc.) < cryptands < spherands due to the corresponding increase in attainable preorganisation. However, this low conformational flexibility is only favourable when the host molecule has an appropriately complementary shape and electrostatic surface with the guest molecules.

Comba [197] discusses molecular mechanics modelling of the selective coordination of specific metal ions by a variety of host molecules. He highlights some limitations of the model.

- The coordination of ligand molecules to a metal ion induces strain by the metal centre to the ligand molecule and strain by the ligand to the metal centre [198]. The loss of steric energy is compensated for by the bonding energy that results from the metal to ion-donor atom bond formation.

- Preorganisation refers to a specific metal ion/ligand pair, and it involves the size and the shape of the binding cavity of the ligand and the preferences of the metal ion. Size- and shape-selective ligands need to be highly preorganised and the energy cost for their structural reorganisation needs to be large, or else they will not discriminate enough. Basically, what we require is a metal ion selective ligand with a high degree of preorganisation for a specific metal ion and also a high degree of 'disorganisation' or 'mismatch' for other metal ions.

- In contrast to simple predictions, additional binding sites do not necessarily lead to enhanced binding, in line with the general chelation equation. This is demonstrated by weaker Li^+ complexation with the spherand in **Figure 43** as compared to in **Figure 42** due to build up of strain energy in order to attain full interaction with the Li^+ cation whereas simultaneous interaction with all of the oxygen atoms is possible with Na^+ .

1.11.3 Complementarity

Just as preorganisation is a central determinant of binding power; complementarity is the central determinant of structural recognition [199]. The binding energy at a single interaction site is, at most, a few kilocalories per mole, much lower than that of a covalent bond. Interactions at several sites between hosts and guests are required for structuring of complexes. Such interactions depend on complementary placements of binding sites in the complexing partners.

The binaphthyl crown ether shown in **Figure 44** displays a high degree of chiral recognition towards valine [200]. However, when the crown ring contains one more or one less ethyleneoxy unit the resulting macrocycle no longer enantioselectively complexes valine [201]. Molecular models suggest that the smaller crown cannot accommodate the ammonium group while in the larger crown the three oxygen atoms bonding with the ammonium cation are too far removed from the chiral barrier.

1.11.4 The physical chemistry of molecular recognition

The rules governing all physical chemical processes can also be applied to molecular recognition. The Gibbs free energy, ΔG , (equivalent to the binding energy) is composed of two opposing terms.

$$\Delta G = \Delta H - T\Delta S$$

Equation 22.

where ΔH is the enthalpy component, ΔS the entropy component and T is the absolute temperature.

When ΔG is negative we have a thermodynamically feasible spontaneous process. The conditions for a negative ΔG are (1) if ΔH and ΔS are both negative and the absolute magnitude of ΔH is greater than that of ΔS , or (2) if ΔH is negative and ΔS is positive.

Molecular recognition is a complex process involving solvation/desolvation, global changes in translation and rotation degrees of freedom well as internal modifications to rotation and vibration modes [202]. Van der Waals and electrostatic interactions between a host and guest molecule contribute positively to enthalpy (H). It compensates for similar interactions that occurred between the two molecules and the surrounding solvent, and also for any structural changes required for complexation to happen. Upon complexation the two molecules lose degrees of freedom, a decrease in entropies, while the release of interacting solvent molecules counteracts this effect. The process of spontaneous binding requires that the drug and receptor molecule have a complementarity of shape and charge which leads to an overall negative interaction energy ($\Delta G < 0$). The classical law relating the free energy of dissociation (free energy at constant pressure of Gibbs free energy) to an equilibrium constant K , thus governs bimolecular complex formation,

$$\Delta G = -RT \ln K$$

Equation 23.

where R is the gas constant and T is the absolute temperature.

Electrostatic effects, apart from making a significant contribution to the binding energy, are also involved in the orientation of molecules and the recognition processes that lead to binding [203].

Spichiger-Keller [204] discussed the play-off between thermodynamics, electrostatic interactions and solvent with reference to host-guest reactions. They suggest that fast kinetics are essential in order to apply host-guest chemistry to sensor technology. The thermodynamic properties of a large variety of ionophores was studied [205] and a positive ΔS value at $\Delta H=0$ was found, which implies an entropy-stabilised association mechanism where the predominant conformer of the free ionophore in pure solvent is less stabilised than that of the complex, which means that the associate is entropically favoured. The polarity and hydrogen donicity of the solvent exert a strong influence on the preformation of the ionophore, and therefore, the free energy of interaction.

An interesting slant on this docking procedure is the use of virtual reality systems [206], where the user can physically interact with the molecules, “feeling” and “seeing” where repulsive and attractive interactions occur through a sensor glove and VR helmet [207]. This immersive technology provides a rapid method of generating starting structures for further simulation, but suffers from subjective user bias and the lack of conformational flexibility of the two molecules.

Rzepa has written an interesting and informative review on the development of the Internet along with its application as a computational chemistry tool [208].

Our present understanding of the subtle events that drive the molecular recognition path is still in its infancy but our database of knowledge is continuing to be expanded upon.

1.12 HYDROGEN BONDING

Moore and Winmill made the first description of what is now recognised as hydrogen bonding [209] in 1912. However, it was not until Latimer and Rhodebush [210] postulated hydrogen bonding in 1920 that the concept gained widespread recognition and attention. Up until the mid-1930's researchers had not referred to hydrogen bonds as such in the literature. The phenomenon had been observed but was not definitively named until Huggins used the term "Hydrogen Bridge" [211] in 1936.

The modern concept of the hydrogen bond has its basis in the principle of relative atomic electronegativities (shown in **Table 12**) as put forward by Pauling in 1939 in his book "The Nature of the Chemical Bond" [212].

| | | | | | |
|-----------|-----------|-----------|-----------|-----------|-----------|
| H 2.1 | | | | | |
| Li 1.0 | B 2.0 | C 2.5 | N 3.0 | O 3.5 | F 4.0 |
| Na 0.9 | Al 1.5 | Si 1.8 | P 2.1 | S 2.5 | Cl 3.0 |
| K 0.8 | Ga 1.6 | Ge 1.8 | As 2.0 | Se 2.4 | Br 2.8 |
| Rb 0.8 | In 1.7 | Sn 1.8 | Sb 1.9 | Te 2.1 | I 2.5 |

Table 12. The electronegativities of some of the elements.

A hydrogen bond basically consists of a donor group, X-H, where X is more electronegative than the hydrogen atom and will, therefore, draw electron density away from the hydrogen atom forming a dipole (a hydrogen donor). Another nearby electronegative atom (a hydrogen acceptor) can then coulombically interact with the $H^{\delta+}$

atom. Hydrogen bonding donor-acceptor nomenclature has been discussed in detail by researchers [213].

Hydrogen bonding is a very common interaction for host:guest complexation. An analysis of such structures [214] has shown that complexation energies in this case correlate linearly with the corresponding number of hydrogen bonds, at least in the absence of other effect such as steric hindrance, charge transfer, stacking interaction, etc. It must be noted that the complexation constants decrease sharply even with slight increases in hydrogen bond donor or acceptor power of the solvent. Thus, the addition of ~5% methanol to a carbon tetrachloride solution destroys amide hydrogen bonded complexes completely. In chloroform, one observes a rather constant increment of 5 ± 1 kJ mol⁻¹ per hydrogen bond, which is approximately doubled in carbon tetrachloride.

If a large solvent molecule is unable to enter the cavity of a host, the result may be a higher binding constant. Such solvent-selecting behaviour has also been observed in hydrogen-bonded complexes [215].

Subramanian and Zaworotko [216] have written a review on hydrogen bonding and its applications to crystal engineering that details how hydrogen bonding affects crystal architecture.

1.12.1 Role in intermolecular interactions

Due to the fact that hydrogen bonding is a weak interaction, with respect to covalent or ionic bonds, it can easily be disrupted and is, therefore, ideal when involved in molecular recognition interactions. It is also essential for the multitude of interactions that occur in a living organism as these need to occur in a rapid and reversible time-scale [217]. For stereo specific interactions to occur multiple simultaneous hydrogen bonds need to be formed due to their aforementioned weak strength.

1.12.2 Types of hydrogen bonds

Hydrogen bonds are the most important 'weak' interactions encountered in solid, liquid and gas phases. They define the crystal packing of many organic and organometallic molecules, the 3D structure of biological macromolecules, as well as modulate the reactivity of different groups within a molecule. In the rank of interactions among atoms, the hydrogen bond falls between covalent bonds and non-bonding interaction, such as van der Waals forces. In general, a hydrogen bond is characterised by: (1) a weak to medium interaction energy [218]; (2) a considerable interpenetration of the isolated electronic clouds of the two moieties involved; (3) a certain amount of electron transfer between the two moieties, and (4) a preferred geometry [219].

Table 13 shows some properties of hydrogen bonds. The donor atoms are in bold font. The variables D , d and θ are displayed in **Figure 45**. This table should only be viewed as a guideline and not as a definitive classification of the three types of hydrogen bonds. The categorisation of hydrogen bonding is a highly subjective art and various authors have quite different views on the classifications. For example, Hibbert and Emsley [218] define three kinds of hydrogen bonds according to the following criteria. Between 10 and 50 kJ mol⁻¹ are defined as weak hydrogen bonds, those with energies between 50 and 100 kJ mol⁻¹ are defined as strong hydrogen bonds and those with energies greater than 100 kJ mol⁻¹ are considered very strong hydrogen bonds.

| | Strong | Moderate | Weak |
|------------------------------|--|-------------------|--------------------------|
| Bond energy (-kJ/mol) | 60–170 | 16–60 | <16 |
| Examples | [F ···H··· F] ⁻ | O -H···O=C | C -H··· O |
| | [N ···H··· N] ⁺ | N -H···O=C | O -H··· π |
| | P -OH···O=P | O -H···O-H | Os -H··· O |
| IR ν_s relative shift | >25% | 5–25% | <5% |
| Bond lengths | H···A \approx X-H | H···A>X-H | H···A \gg X-H |
| Lengthening of X-H (Å) | 0.05–0.2 | 0.01–0.05 | \leq 0.01 |
| <i>D</i> (X···A) range (Å) | 2.2–2.5 | 2.5–3.2 | 3.0–4.0 |
| <i>d</i> (X···A) range (Å) | 1.2–1.5 | 1.5–2.2 | 2.0–3.0 |
| Bonds shorter than vdW | 100% | Almost 100% | 30–80% |
| θ (X-H···A) range (°) | 175–180 | 130–180 | 90–180 |
| Covalency | Pronounced | Weak | Vanishing |
| Electrostatics | Significant | Dominant | Moderate |

Table 13. A selection of properties strong, moderate and weak hydrogen bonds [220].

Alkorta et al. have reviewed the various kinds of non-conventional hydrogen bonds (See **Table 14**) [221] and other authors have written detailed reviews on conventional and **D**-H···**A** hydrogen bonds [222]. Conventional hydrogen bonds generally consist of ‘traditional’ donors such as **N**-H, **O**-H and **halogen**-H; and the acceptor atoms consist of the atoms labelled in bold in a different hybridisation state. Non-conventional hydrogen bonds have donor atoms such as **C**-H, **Si**-H and **P**-H; and acceptor groups like **O**, **P**, **Se** and π .

| | D -H... A hydrogen bonds | A -H...H- D dihydrogen bonds |
|------------------------------------|---|--|
| Protic | A=isonitriles [223] | |
| | A=carbanions [224] | Ref. [225] |
| | A=carbenes [226] | |
| | A= π -systems [227] | |
| Solvent and electric field effects | D -H... A \rightarrow D ...H- A ⁺ | D -H...H- A \rightarrow D ...H-H... A ⁺ |
| | Ref. [228] | Ref. [229] |
| Hydric (inverse) | D -H... A \rightarrow D ⁺ -H... A ⁻ | |
| | Ref. [230] | |

Table 14. Non-conventional hydrogen bond donors (**D**) and hydrogen bond acceptors (**A**).

1.12.3 The structure of hydrogen bonds

The terminology used in describing the structure of hydrogen bonded complexes shall now be discussed. To obtain an overall view of the molecule(s) involved in the interactions the term constitution is used. This details the types of donor and acceptor hydrogen bonding functional groups concerned. Configuration refers to the connectivity of the functional groups and conformation describes the stereochemistry in terms of hydrogen bond length, bond angles and torsional angles. Until recently this terminology has not been used with reference to hydrogen bonds as computer graphics were not available and, therefore, it was difficult to visualise hydrogen bonding patterns.

When chains of hydrogen bonds are being formed quantum mechanical calculations [231] have shown that, in the case of water, that the structure shown in **Figure 46** is the most energetically favourable. (The experimentally determined length

and energy of such a bond is 2.02 Å and 22.6 kJ mol⁻¹ respectively). Rather than the (a) alternative double bond or (b) double acceptor hydrogen bonding patterns, **Figure 47**. In **Figures 46-48** the bond directionalities are shown arbitrarily as linear. It is not a necessity in the formation of these bonds.

In cyclic systems semi-empirical calculations suggest that the hydrogen bonding pattern shown in **Figure 48** (a homodromic conformation [232]) is the most stable of the available conformations [233] which is relevant to the hydrogen bonding patterns found in the parent phenolic calix[4]arene.

The relatively wide bond energy range and their inherent directionality makes them exploitable, controllable and versatile. However, their relatively weak strength compared with covalent bonds means that steric [234] and other weak non-covalent bonding forces [235] have to be accommodated and external factors such as temperature [236] and pressure [237] can be important.

1.12.4 Length of hydrogen bonds

Some general hydrogen bond donors and acceptors are listed in **Table 15**. The hydrogen bond distances associated with these groups are in the range of 1.5 to 3 Å but the initial attraction can occur at much longer distances than these can. Ab initio calculations at the Hartree-Fock level of theory with a 6-31G basis set on a water dimer has supported this fact [238]. On separating the potential energy curve generated into its components the electrostatic component is seen to decrease as r^{-1} (r is the distance between the two atoms) as opposed to the exchange and dispersion components which fall off at a much greater rate. This implies that there will still be a significant interaction at a separation distance of 3.5 Å. It has also been suggested that aromatic rings can act as weak hydrogen bond acceptors; such as in the case of molecular mechanics study with a NH donor group [239]. Experimental evidence comes from a calixarene hydrate study

[240]. Halide ions are also known to be strong hydrogen bond acceptors in the order: $\text{Cl}^- > \text{F}^- > \text{Br}^- > \text{I}^-$ [241].

Crystal field packing forces have an effect on the length of the bond so that the bond length observed in X-ray crystallography is an average equilibrium value.

| Donors | Acceptors |
|----------------------------|---|
| O -H | $\overset{-}{\text{O}}=\text{P}$ |
| N -H | $\overset{-}{\text{O}}=\text{C}$, $\text{O}=\text{C}$, C - O -H, C - O - C |
| $\overset{+}{\text{N}}$ -H | $\overset{-}{\text{O}}=\text{S}$ |
| S -H | - N =, N \equiv |
| C -H | S = C |
| | Halides |

Table 15. Functional groups typically involved in hydrogen bonding interactions. Donor and acceptor atoms are shown in a bold font.

1.12.5 Strength of hydrogen bonds

The atoms involved determine the strength of a hydrogen bond. When fluorine atoms are attached to the hydrogen donor atom and also act as the acceptor atom a very strong, ionic like, interaction occurs. A similar interaction is seen to occur if the donor atom is a cation or the acceptor is an anion. The weaker bonds generally have stretching and bending force constants that are about 15 times smaller than for covalent bonds. With reference to the $\text{NH}\cdots\text{O}=\text{C}$ bonds, a range of values have been found for its length (due to the fact that it is such a weak bond, other intermolecular effects can significantly effect it; a 20% expansion or contraction of its length can be observed), forming a Morse type potential curve which does yield an equilibrium bond length [242]. A general pattern for

the strength of hydrogen bonds is $\text{OH}\cdots\text{C} < \text{O}_w\text{H}\cdots\text{O}_w < \text{NH}\cdots\text{O}=\text{C} < \text{NH}\cdots\text{N}$, where O_w refers to a water oxygen atom, but no general quantitative relationship can be proposed.

As bond lengths and energies depend on the surrounding environment, the pattern of bonding in the molecules of interest, crystal forces when examining X-ray data, the most consistent values for energies and bond lengths will come from high level ab initio calculations on dimers of a wide variation of molecules. Studies on strong hydrogen bonds in several aprotic solvents have shown that the stability of these bonds in solution is highly solvent-dependent [243]. Very weak hydrogen bonds have been shown to exist in the gas phase [244] but, for the most part, do not survive in protic or very polar solvents.

High-level ab initio and density functional theory (DFT) calculations have been performed on strong hydrogen bonds. A correlation has been obtained between the bond strength and proton NMR chemical shift. Hydrogen biformate [245] and enol-enolate anion [246] systems have both been studied and a linear dependence was found between bond strength and varying $\text{p}K_a$ of the donor/acceptor complex. This relationship has also been found for weak hydrogen bonds [244].

With reference to **Sections 1.12.4** and **1.12.5**, **Table 16** illustrates the energies and distances for different hydrogen bonds.

| Hydrogen bond | Energy (-kJ/mol) | <i>D</i> (Å) (Figure 45) | Reference |
|---|------------------|--------------------------|-----------|
| [F–H ⁺ ⋯F] ⁻ | 163.2 | 2.30 | [247] |
| [OH ₃ ⁺ ⋯OH ₂] ⁺ | 138.1 | 2.48 | [248] |
| [NH ₄ ⁺ ⋯NH ₃] ⁺ | 100.4 | 2.85 | [251] |
| [OH ₂ ⁺ ⋯OH] ⁻ | 96.2 | 2.44 | [250] |
| NH ₄ ⁺ ⋯OH ₂ | 79.1 | 2.77 | [249] |
| OH ₂ ⁺ ⋯Cl ⁻ | 56.5 | 3.27 | [252] |
| [NH ₃ ⁺ ⋯NH ₂] ⁻ | 42.7 | 2.91 | [250] |
| O=C–O–H ⁺ ⋯O=C–O–H ⁺ ^c | 31.0 | – | [250] |
| Cl–H ⁺ ⋯OH ₂ | 22.6 | – | [251] |
| H ₂ O ⁺ ⋯H ₂ O | 20.9 | – | [252] |
| N≡C–H ⁺ ⋯OH ₂ | 15.9 | 3.12 | [253] |
| Me–OH ⁺ ⋯Ph | 11.7 | – | [254] |
| OH ₂ ⁺ ⋯F–CH ₃ | 10.0 | – | [255] |
| H–C≡C–H ⁺ ⋯OH ₂ | 9.2 | 3.26 | [258] |
| Cl–H ⁺ ⋯SeH ₂ | 8.4 | – | [256] |
| H–C≡C–H ⁺ ⋯C≡C–H | 5.9 | – | [256] |
| H ₂ S ⁺ ⋯H ₂ S | 4.6 | 4.16 | [257] |
| CH ₄ ⁺ ⋯OH ₂ | 2.5 | – | [258] |
| CH ₄ ⁺ ⋯SH ₂ | 1.7 | – | [259] |
| CH ₄ ⁺ ⋯FCH ₃ | 0.8 | – | [258] |

Table 16. Calculated energies and equilibrium distances for a variety of hydrogen bonds.

^c Cyclic dimer.

1.12.6 Directionality of hydrogen bonds

Weaker bonds generally have a X-H...A angle in the range $160\pm 20^\circ$ as they are more electrostatic in nature and, therefore, have less directional characteristics. A comparison between the hydrogen bond acceptor properties of sp^2 versus sp^3 oxygen atoms suggested that there was little difference between the directionality of the bonds formed [260]. It was over a range of $\pm 50^\circ$ from the axis of the acceptor groups; carbonyl or ethers. Even before high precision X-ray and neutron diffraction studies were available it was already considered that the X-H...A angle may not be linear [261]. Crystal field packing forces have an even more pronounced effect on the directionality of a bond than on the length of the bond, so it is very hard to obtain any characteristic trends from X-ray crystallographic data.

1.12.7 Bifurcated bonds

It is not necessarily the case, however, that there has to be only one acceptor atom for each hydrogen donor. Surveys of various hydrogen bond forming complexes, including bonds in peptides (NH...O=C) [262] and amino acids [263], indicated that between 25 to 40% of the bonds formed may be of a bifurcated type (**Figure 49**). The type of bond shown in **Figure 49** was first seen in the X-ray crystal structure of α -glycine in 1939 [264] and was confirmed in 1972 [265]. The term bifurcated bond was used to describe it but as this term has also been used with reference to interactions involving two donor atoms and one acceptor atom the description three-centred has been used when the hydrogen atom is situated between three electronegative atoms. There are also a few examples of two and three acceptor atoms interacting with a hydrogen donor atom. This type of structure has been seen in the nucleosides [266].

An analysis of neutron diffraction data of carbohydrates and amino acids [267] has shown that these three-centred bonds are more common in complexes where there are an excess of acceptor over donor atoms. Four centred bonds may also be formed. This consists of a hydrogen donor atom interacting with three neighbouring acceptor atoms. It is a very rare phenomenon, however, as a study of 1352 $\text{NH}\cdots\text{O}=\text{C}$ hydrogen bonds, yielded only 6 that were possibly of this type. A sufficiently exact analysis was unfortunately not performed.

1.12.8 The Hydrophobic Effect

This phenomenon is concerned with the ease of solvation of molecules in water. For solvation to occur, firstly, a cavity has to be formed in the solvent. This is energetically unfavourable as strongly interacting hydrogen bonded water molecules need to be separated. Once the cavity is formed the solute is then enclosed into it. This is an energetically desirable process and compensates for the cavity formation energy expenditure. If the solute is polar then further favourable hydrogen bonds can be formed between it and the solvent. But, if the solute is nonpolar only a weak van der Waals attraction occurs between it and the solvent so the water molecules have to arrange themselves around the solute so that the greatest amount of hydrogen bonds is formed. However, this ordering of water molecules is entropically unfavourable. So, to compensate for this the solute molecules aggregate together, releasing water molecules into the bulk solvent and, therefore, partially (or wholly) negating the previous entropy problem. This is the main driving force for the “hydrophobic effect” [268]. The free energy of transfer from an organic solvent to water depends linearly on the accessible surface area of a solute molecule [269].

This effect is of particular relevance with respect to the 3D structure of globular proteins. The non-polar side chains are directed towards the interior of the molecule and, thus, are shielded from the surrounding hydrophilic environment. Polar or charged side

chains are on the outer surface, interacting with the aqueous solvent. The formation of membranes or micelles have also to owe their existence to the hydrophobic effect, as they are amphiphilic molecules, consisting of polar and nonpolar moieties [270].

1.12.9 X-ray diffraction studies

The precision with which hydrogen atoms are located is, generally, from 0.1–0.3 Å, while it is ~0.005 Å for non-hydrogen atoms. This error generally places the hydrogen atom closer to its donor atom, hence, increasing the length of the associated hydrogen bond by a corresponding value. As measurements are increasingly been made at lower and lower temperatures this error will decrease. But as neutron diffraction does not include this inherent error it is the optimal experimental technique for studying hydrogen bonding patterns. This difference between X-ray and neutron diffraction is illustrated by Taylor and Kennard for the N-H...O=C bond [271]. The errors varied between 0.02 and 0.17 Å. These errors can be reduced by normalising [272] the covalent bond lengths to “standard” neutron diffraction values; 0.97 Å for O–H, 1.03 Å for N–H and 1.10 Å for C–H (depending on other neighbouring electronegative atoms). There is only about 0.1 Å of an error in C–H bond lengths however.

Because of the crystal field distortion, hydrogen bond lengths tend to be shorter in crystals than observed experimentally or predicted experimentally in hydrogen bonded dimers. However, information from gas-phase diffraction and microwave spectroscopy is much less abundant than that obtained from X-ray and neutron diffraction. A statistical average that could cancel out these perturbing crystal field forces, which are unique to each crystal [273], would appear to be needed over a large number of crystal structures for a particular type of hydrogen bond. This does not seem to be the case however due to the fact that, (1) the influence of many atom effects, and (2) all the other atom pair interactions are trying to obtain their equilibrium minimum. This leads to an overall distortion in the molecule [274]. But, if a large distribution of hydrogen bond lengths and

angles is examined for each particular variety of hydrogen bond in each class of molecules a Gaussian curve of the values is obtained and the effective equilibrium geometrical properties of the particular hydrogen bond can be determined.

1.12.10 Computational considerations

Molecular mechanics will only explicitly include hydrogen bonding if the appropriate force field functions and parameters are included in the methodology.

The molecular modelling of hydrogen bonding is more difficult than the modelling of covalent bond modelling for a variety of reasons. Firstly, hydrogen bonding can be either inter- or intramolecular. Studying intermolecular bonding necessitates the inclusion of additional molecules that have a detrimental effect on the computational costs. Secondly, as hydrogen bonding is a more diffuse, weaker attraction it has a much shallower potential energy minimum than a covalent bond. Therefore, a relatively large change in the configuration of the bond does not necessarily result in a noticeable energy change.

A problem to bear in mind is that atomic charges are not defined physical properties and, therefore, they cannot be calculated experimentally. There are a variety of methods for calculating them and placing them on the appropriate atoms [275] (see **Section 1.9**). As they are essential for calculating the Coulombic interactions their magnitude and distribution around the molecule of interest is important. A further problem is that hydrogen bond formation distorts the electronic distribution, and hence the atomic charges, around the molecule. An induced dipole term can be added to simulate this effect. In some hydration studies a polarisable dipole has been added to each atom [276].

When developing force fields some researchers include explicit functions describing hydrogen bonding [277]. These equations take the form of either a Morse function or a Lennard-Jones potential. For stronger hydrogen bonds angular dependence parameters may be necessary.

Theoretical studies have indicated that the hydrogen bond may best be described as electrostatic in origin [278], although very strong hydrogen bonds may be regarded as having some covalent nature [279].

1.12.11 *p*-tert.-butyl calix[4]arene tetrol

The “flip-flop” hydrogen bond network observed at the lower rim of the *p*-tert.-butylcalix[4]arene tetrol [a name given by C.D. Gutsche in his book (Bibliography Section, book 21, pg. 9)] has also been studied in cyclodextrin molecules [280] and the information discussed here is relevant to both calixarene and cyclodextrin chemistry. Flip-flop means that the hydrogen atom involved in hydrogen bonding alternates in position between two adjacent oxygen acceptor atoms. There are two different possible mechanisms to explain this. (1) Configurational mechanism: A covalent O–H bond is broken and the hydrogen atom is transferred across the O–H...O bond. (2) Conformational mechanism: None of the covalent bonds are broken. The hydroxy groups rotate from one possible hydrogen bonding position to the other. These are also entropically favourable processes. For medium to weak bonds (2) should be preferable due to the large energy expenditure required for (1). In the case of strong hydrogen bonds (1) could come into dominance due to the already weakened covalent bond. These mechanisms do not occur in isolation but all the way around the hydrogen bonding ring.

1.13 INCORPORATION OF FLUOROPHORES /CHROMOPHORES INTO SENSORS

A particularly difficult challenge in the design of molecular sensors is to achieve visual and spectroscopic discrimination between enantiomers. A simple monitoring system for distinguishing between the left- and right-handed forms of chiral drugs would be extremely useful in pharmacology [281]. The development of molecular sensors capable of visual discrimination between enantiomers of chiral guest species has attracted considerable attention because it is a convenient method for monitoring the chirality of molecules. The design and synthesis of such molecules constitutes a timely and challenging research topic.

In order for a molecule to be fluorescent it is believed that, besides the presence of conjugated double bonds, rigidity is an important factor. Fluorescent quenching occurs when the excited molecule and the quencher are within each others active sphere. It involves an energy transfer between the fluorescing molecule and the quencher that is detected by a decrease in the observed fluorescence. There are a variety of energy transfer mechanisms that can cause fluorescent quenching. When the excited state fluorophore and the quencher meet due to diffusions processes dynamic quenching occurs. There is no chemical change during this process. Static quenching takes place when the fluorophore and quencher form a complex. Excited charge-transfer complexes (exciplex) can also be formed. This involves electron transfer between the fluorophore and the quencher that leads to fluorescence quenching. Dynamic quenching is thought to be the method of quenching that the molecules undergo in Chapter 3. Studies are ongoing to confirm this.

Calixarenes are a particularly attractive framework for the construction of artificial receptors [282]. It is a notable advantage for the use of calixarenes that the size

of the internal cavity and the chemical modification of the binding sites around it can be varied in a very flexible manner using numerous synthetic methods. This means that the frameworks would be quite useful for building optical sensory systems [283]. The 1,1'-binaphthyl unit possesses unique properties which induce not only chirality in a structure but also a hydrophobic microenvironment.

Optical chemosensors which selectively complex heavy metal ions are being increasingly studied by researchers [284]. Fluorogenic reagents are prepared by the attachment of fluorophore moieties to a platform of a macrocyclic or chelating complexant. The result of this is two fold. The host molecule can selectively bind the cation of choice yielding the spectral response of the fluorophore to environmental changes upon metal cation complexation.

Fluorogenic calixarenes designed for the complexation of alkali metal cation [285], Zn(II) and Ni(II) [286], or organic species [287] have appeared in the literature. Talanova et al. [288] developed the first fluorogenic calixarene for Hg(II) recognition (**Figure 50**). The observed quenching was unaffected by the presence of other cations in solution.

Kubo et al. [289] synthesised a chiral calix[4]crown, in the cone conformation, containing an optically active 1,1'-binaphthyl subunit and two indophenol chromophores substituted in the para position of the calix[4]arene. When R-phenylglycinol was added to a red coloured ethanol solution of the calixarene this resulted in an immediate colour change to violet-blue. The same experiment was carried out with the S enantiomer and no colour change was observed in the solution. To this solution the R amine was added, and the previous colour change was seen again. These results show that distinction between enantiomers can be successfully achieved by the naked eye. Selectivity was not just obtained with one substrate. Phenylalaninol and phenylglycine were also enantioselectively complexed demonstrating the aforementioned colour change.

The mechanism for binding is thought to be that the amine group of the amine becomes protonated and interacts with the crown ether group, and a phenoxy group of the calixarene loses a proton and hydrogen bonds to the hydroxy group of the amine. Studies on phenylethylamine showed no selectivity, which support the latter argument. This system represents a rationally designed colorimetric sensor for chiral substrate recognition.

Cram et al. utilised a binaphthyl-derived chiral crown ether in the enantioselective complexation of 1-phenylethylammonium hexafluorophosphate (**Figure 51**), with an energy difference of $\sim 1250 \text{ kJ mol}^{-1}$ between the R and S complexed formed, with the R complex being more stable [290]. Modification of the host allowed the optical resolution of primary amine salts and amino acid esters [291]. Binaphthyl-derived cyclophanes [292], clefts [293] and metallomacrocycles [294] are also known as excellent chiral hosts.

It is an important approach for optical recognition that makes use of the fluorescent properties of chromophores. From the point of view of an analytical method, fluorescence is of great value because of its high sensitivity and the variety of signalling modes involving quenching, enhancement, excimer, and so on. Since the binaphthyl ring possesses a fluorescent ability, binaphthyl-derived receptors are quite useful as fluorescent sensor materials. Excellent work has been carried out by Shinkai's research group on the synthesis of binaphthyl-derived sensors [295] that can discriminate between sugar enantiomers (**Figure 52**). The tetra-(S)-di-naphthylprolinol calix[4]arene, being an analogue for binaphthyl appended receptors, exhibits a significant ability to discriminate between enantiomers of chiral amines by the quenching of the fluorescence emission [296]. It has also been shown to enantioselectively discriminate R-phenylglycinol over the S enantiomer [297].

Optical reporting of anion recognition typically involves quenching or enhancement of a chromophore's absorption or a fluorophore's fluorescence emission

upon proximal association of the analyte. Such reporter groups are generally incorporated into the covalent framework of the recognition molecule.

Snowden and Anslyn [298] reported an overview of recent progress in the design and evaluation of synthetic receptors for anion sensing. They concluded that although some promising results have been obtained to date there is still much room for further development in this relatively new field of research.

2 MOLECULAR MODELLING STUDYS ON
CALIX[N]ARENES COMPLEXING ALKALI
METAL CATIONS

2.1 CALIXARENE CONFORMATION

Before discussing the calixarene molecular modelling results we need to detail the conformations attainable by the calix[4]arenes and calix[5]arenes.

Calix[4]arenes can exist in four distinct conformations due to the soft hinging motions of the $\text{CH}_2\text{-Ar-CH}_2$ moieties depending on the substituents on the phenolic oxygen atoms. The para substituent does not have a significant effect on them. The conformations are cone, partial cone, 1,2-alternate and 1,3-alternate as shown in **Figure 53**. These are readily interconvertible as shown by Kammer et al. [299] by dynamic ^1H NMR studies. Bauer and Gutsche [300] have shown, also by using dynamic ^1H NMR studies, that a facile interconversion among the various conformers occurs with an inversion barrier of $65.69 \text{ kJ mol}^{-1}$ for *p-tert.*-butylcalix[4]arene tetrol in CDCl_3 .

In the solid state calix[5]arene parent alcohols exist in a cone-like conformation. $\text{O}\cdots\text{O}$ distances are obviously greater than that in calix[4]arenes which indicates a weaker intramolecular hydrogen bonding network. Molecular modelling indicates that these lengths are about 3.5 \AA , whereas they are about 2.8 \AA for the calix[4]arene tetrol. Calix[5]arene without this hydrogen bonding network have longer $\text{O}\cdots\text{O}$ distances due a lack of intramolecular hydrogen bonding and also repulsions between the phenoxy oxygen atom substituents [301]. Due to the greater size of the apolar cavity the conformational stability depends on the size of the substituents on the phenolic oxygen atoms and also on the meta and para positions of the aryl rings forming the calix[5]arene apolar cavity.

2.2 INTRODUCTION

The ability of molecular mechanics to reproduce the geometry of a given conformation of a metal-free calixarene has already been widely demonstrated in the literature (see **Section 1.10**).

The non-chiral work presented in this section is part of our validation work into the applicability of molecular modelling techniques to studies on calixarene inclusion complexes [302]. As we obtained good agreement between experimental and computational data we then applied this methodology to the study of the enantioselective complexation of chiral amines by two different chiral calix[4]arenes.

All the metal-free calix[4]arenes discussed here (except the alcohol, which is strongly intramolecularly hydrogen bonded) have an approximately C_{2v} (rectangular cone) symmetry, while their metal complexes are approximately C_{4v} (square cone) (**Figure 54**. This figure was produced using Chem3D Pro [303]). The calix[5]arenes have no regular geometry, but are cone-like with reference to the positioning of the phenoxy substituents. Several of the metallo-calixarenes whose crystal structures have been determined crystallise with solvent molecules in their cavities and/or have closely-associated counterions. For this reason we felt it necessary to include appropriate solvent molecules and/or counterions in the calculations of the structures of the complexes. This is a reasonable step since the purpose of the calculations reported here is not to predict whether solvent/counterions will associate with the calixarenes in the solid state but rather is to determine if a simple force field can predict the structure of such an assembly. Excluding encapsulated solvent molecules from molecular modelling calculations when it is known they are present, results in calculated structures which should be compared with hypothetical solvent-free complexes rather than the actual data available. The most straightforward examples are, of course, those complexes with no included solvent molecules and where the counterions are sufficiently distant from the encapsulated metal

ions that they can be safely excluded from the calculations. A 2D representation of the non-chiral calixarenes studied is shown in **Figure 55**. Related studies have also been performed on tetra- and pentaphosphine oxide calix[*n*]arenes (*n*=4, 5). They have helped to explain the observed selectivity of the tetramer and the pentamer with two methylene spacer groups in their pendant groups for the Ca²⁺ cation over other monovalent and divalent cations [304].

2.3 EXPERIMENTAL

All calculations were carried out using the HyperChem [305] molecular modelling package (Release 4) running on a 180 MHz Pentium Pro PC. Metal-free calixarenes were geometry optimised using the default MM+ force field within HyperChem, which is a modified version of the MM2 force field developed by Allinger. For optimisation the metal-free calixarenes dipole/dipole interactions were used without any artificial distance cut-off.

Partial charges were calculated for each of the ligands using a single point (as opposed to a geometry optimisation) AM1 calculation (utilising the AM1 method incorporated in HyperChem) on a symmetrical fragment of the parent compound (normally one full aryl ring and its substituents plus ethyl groups at the bridging methylene positions). These charges were then transferred, with some averaging and rounding off, to the entire parent compound, which meant that the equivalent atoms in each aryl ring in the calixarene were assigned the same charge. It is more straightforward to calculate partial charges on the full complex with no encapsulated metal ion and then to use this charge distribution directly in calculations on the metal complexes but this gives unsymmetrical charge distributions (i.e. chemically non-equivalent binding sites) unless the structure used has a suitably high symmetry axis (a C_4 axis in the calix[4]arenes, for example), which is not normally the case.

Since the default force field only contains parameters for neutral Group 1 metal atoms the metal ions were replaced, for the purposes of the calculation, with the closest-lying noble gases which are isoelectronic with them. The default parameters for properties such as the van der Waals radii of the noble gases are very close to those recommended for Group 1 ions. The noble gas atoms were then assigned a formal +1 charge. To simulate encapsulation of the metal ions the model ions were placed at an

arbitrary position within the calixarene, normally in the vicinity of the expected binding sites, and the complex was molecular mechanics geometry optimised using the assigned partial charges and the atomic charges electrostatics option^f.

The metal-free compounds that were used as the starting points for the complexes had the benzene rings defining the aromatic cavity parallel so as not to form any bias towards having a square or rectangular conformation. In cases where the potentially ligating carbonyl groups in the free calixarene were pointing directly out of the cavity their torsion angles were manually adjusted so that they pointed into the cavity. If this was not performed either the optimisation to the final encapsulating structure took an excessively large numbers of cycles or obvious local minima were encountered. Conformational searching techniques were not utilised as the starting conformation of the complex was adjusted before optimisation with the metal included. Also, more importantly, efficient searching techniques were unavailable in HyperChem and the PC did not have sufficient computational power to complete the calculations in a reasonable amount of time. The geometries and partial charges of solvent molecules were calculated using the AM1 semi-empirical method. In calculations of calixarene structure with solvent molecules, the solvent molecules were inserted directly into the calixarene as described below with no scaling of the AM1 partial charges.

Published crystal structures were taken from the Cambridge Structural Database [306].

^f This is a user defined option within HyperChem for dealing with electrostatics effects. Bond dipoles is another procedure for dealing with these through space effects.

2.4 RESULTS

2.4.1 Calix[4]arenes

The tetraether **5** and tetrol **6** calix[4]arene complexes are structurally the simplest of all the complexes investigated and we might expect that there would be pronounced similarities between them. The observations for both molecules will now be discussed.

2.4.1.1 *p*-*tert*.-butylcalix[4]arene tetrol

The tetrol calixarenes have been shown to transport a variety of alkali cations in liquid membrane systems. Cs⁺ is transported at a much higher rate than the other alkali cations when the source phase was a solution of metal hydroxide. The selectivity for Cs⁺ increased in the order calix[8]arene < calix[6]arene < calix[4]arene, with the Cs⁺ flux increasing in the opposite order [307]. See **Section 1.10.1** for further experimental information on these complexes.

The most difficult complex to model is the simplest of all the structures attempted, the Cs⁺ complex of **6**. The main difficulty is that in its metal-free form the complex contains strong intramolecular hydrogen bonds between the phenolic residues on the lower rim. We have found that the simple MM+ force field does not accurately reproduce the structure of this molecule, which should not be too surprising since it does not contain any explicit hydrogen-bonding interaction terms, (**Section 1.5.5**). Moreover, the Cs⁺ complex of **6** forms only in alkaline solution where it is believed one of the phenolic residues is deprotonated. In order to try to simulate the effect of deprotonating a single phenolic alcohol we placed the calculated partial charges in a 3:1 ratio on the fully protonated calixarene. The calix[4]arene is still fully protonated but there is a larger negative charge on the phenoxy oxygen atoms. This was performed because the proton is not missing from one particular phenolic residue but is transferred around all four of the

phenoxy oxygen atoms thus making all the atomic charges equivalent. The included acetonitrile solvent molecule was placed above the complexed cation in the upper rim in two different positions; with the methyl group or the nitrogen atom pointing downwards towards the cation. The nitrogen atom:cation interaction was found to be more stable than the methyl group one. This is in line with the X-ray crystallography determined data. The structure of the model Cs^+ complex generated through this procedure is shown in **Figure 56**, along with the X-ray data [308] (as discussed in **Section 1.10.1**). de Namor et al. found that, in the case of tetraethyl p-tert.-butylcalix[4]arene tetraacetate, that thermodynamic and ^1H NMR data show that the polar cavity is more preorganised in acetonitrile than in methanol for the complexation of alkali cations [309]. Like in this case an acetonitrile molecule is also thought to be residing in the apolar cavity. The position of the Cs^+ ion within the cavity is close to that found in the crystal structure. The solvent in the model is tilted away from the central symmetry axis by 50° , which is in poor agreement with the crystallographic data, but the nitrogen atom of the solvent in the model structure lies 3.40 \AA from the metal centre. which compares well with the 3.29 \AA value in the known structure so that there is no gross discrepancy in the model. Calix[4]arenes with a hydrogen atom as the para substituent have no included solvent molecule in the solid state [310]. So, as well as aiding in conformationally locking the calix[4]arene the tert.-butyl groups aid in the complexation of solvent molecules in the apolar upper cavity.

In addition, we found that the simpler procedure of treating the calixarene as a simple neutral species and calculating the partial charges on that basis also led to a structure (also shown in **Figure 56**) which is acceptably close to the crystallographic data, although in this case the metal -solvent distance changed to 3.53 \AA , almost twice the error found for the alternative procedure.

Another cation:calixarene interaction that comes into play in solution is π -cation attraction (Ag^+ has been shown to experience such interactions [311]), which will help stabilise the Cs^+ :calixarene inclusion complex. As has been mentioned, molecular

mechanics does not explicitly account for such inherently electronic interactions. But due to the fact that there is a partial negative charge on the phenyl ring carbon atoms, this will interact with the cation, thus yielding some sort of approximation of the π -cation attraction. By far the overriding interaction, however, will be that with any oxygen atoms that are sterically available.

There is no crystallographic data on the Li^+ complex of **6** which can be used to judge the accuracy of the model of this complex, which is shown in **Figure 57**, but it is possible to model this complex completely independently from the molecular mechanics calculation using semi-empirical PM3 methods [312]. Experimental data is also detailed in **Section 1.10.1.1**. The result of this calculation is also shown in **Figure 57**, where it is compared to the MM+ derived structure, and as can be clearly seen there is a very good correlation between the two structures. The PM3 calculation does, however, place the Li^+ ion 0.7 Å lower in the cavity.

The main difference between these Li^+ complexes and the Cs^+ complex of the same calixarene is that both the modelling methods give structures where the Li^+ ion lies between the mean planes defined by the phenolic oxygen atoms and by the bridging carbons while in the Cs^+ complex the metal lies deep within the cavity on the upper rim. This endo:exo complexation has been discussed previously in **Section 1.10.1.1**. This can be easily rationalised by considering the van der Waal radii of the respective ions. HyperChem uses an r^* value to represent the van der Waal's radii of the atoms. It was adjusted during the parameterisation procedure so it is not necessarily equal to the experimentally determined van der Waal's radii. Some r^* values for the studied cations are as follows: Li^+ : 1.53 Å, Na^+ : 1.60 Å and Cs^+ : 2.28 Å. A comparison of r^* diameters with the $\text{O}\cdots\text{O}$ distances for the complexes shows a good correlation. On going from Li^+ to Na^+ the r^* diameter change was 0.14 Å while the $\text{O}\cdots\text{O}$ distance increased by 0.20 Å. The extra size of the cation forces it 0.56 Å higher up in the aromatic cavity. A much more pronounced change is observed on going from Na^+ to Cs^+ . The r^* value increases by 1.36 Å and the $\text{M}^+\cdots\text{O}$ distance enlarges by 1.40 Å. The $\text{O}\cdots\text{O}$ distance approaches close

to that of the free ligand which indicates a lessening of the cation:phenolic oxygen atoms interactions.

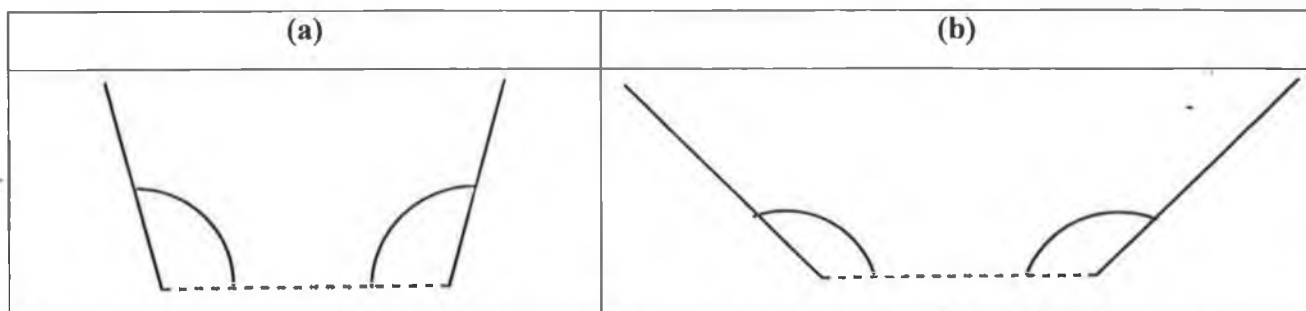


Table 17. Illustration of tilt angles (measured between the plane formed by the methylene linker carbon atoms and the aryl rings) used in the following **Tables 18–22**.

The ring tilt angles were calculated by the following procedure. The C_{4v} structure in **Figure 54** is used to illustrate the method. To calculate the tilt angle of the aryl ring containing the atom labelled Y, the angle between the methylene linked carbon atoms A and B with the atom Y was measured. The same was applied to the atoms C, D and Y and the average result was taken as the tilt angle. This was performed for all four aryl rings forming the upper cavity of the calix[4]arenes and where opposite facing aryl groups had virtually the same angles just the average angle was shown for both the rings.

| | Tilt angles (°) | O...O dist. | M ⁺ ...O dist. | O...N (CH ₃ CN) dist. |
|--|------------------|-------------|---------------------------|----------------------------------|
| Free (MM) | (a) 111.3 | 3.98 | – | – |
| | (b) 111.5 | | | |
| Li ⁺ (MM) | (a) 112.5 | 3.67 | 2.05 | – |
| | (b) 113.0 | | | |
| Li ⁺ (PM3) | (a) 111.6 | 4.02 | 2.02 | – |
| | (b) 111.6 | | | |
| Na ⁺ (MM) | (a) 112 | 3.87 | 2.61 | – |
| | (b) 112 | | | |
| Cs ⁺ (MM) | (a) 112 | 3.92 | 4.01 | – |
| | (b) 112 | | | |
| Cs ⁺ CH ₃ CN (MM) | (a) 110.7, 111.4 | 3.93 | 4.1 | 3.4 |
| | (b) 111.5, 112.7 | | | |
| Cs ⁺ (X-ray) | (a) 114.6 | 3.74 | 4.02 | 3.29 |
| | (b) 114.6 | | | |

Table 18. Geometric data for the parent alcohol calix[4]arenes [All distances are measured in angstroms in the Tables in this Chapter and **Table 17** defines the (a) and (b) tilt angles].

Table 18 shows a more detailed analysis of the geometries of the calixarenes discussed in this Section. As can be seen for the Li⁺ complexes, the ring tilt angles calculated utilising the two molecular modelling methods agree to within 1.4°. The PM3 method yields a more symmetrical molecule, which is in line with the experimental data (**Section 1.10.1.1**), so it could be viewed as a more reliable method for reproducing the Li⁺ tetrol calix[4]arene structure. The metal to oxygen distances are virtually identical and the inter-oxygen distances agree to within 0.35 Å which is an encouraging result.

In the case of the MM optimised Cs⁺ complex with acetonitrile included, the unsymmetrical nature of the solvent complexation yields an unsymmetrical calixarene structure that is illustrated by the variance in the tilt angles. The MM optimised complex

without the solvent molecule has a C_{4v} symmetry that is in line with the X-ray structure. Eventhough the ring tilt angles are not as accurately reproduced as those in the case of the Li^+ there is still a close agreement. For the MM and X-ray determined structures the metal to oxygen atom distances display a high degree of correlation.

The tilt angles for all the complexes formed (and for the free molecular mechanics optimised calix[4]arene) are all very close to each other in value which is an indication of the stabilisation effect of the hydrogen bond network. The network holds the calix[4]arene in a very fixed conformation when compared to the tetramethyl derived calix[4]arene tilt angle data. The Li^+ MM optimised calix[4]arene has shorter $O\cdots O$ contacts than the free ligand, which can be explained by the attractive effect of the included cation. However, the PM3 optimised structure does not show this effect which is indicative of the difference in the ionic radii parameters of the cations utilised by the PM3 and MM methods.

2.4.1.2 Tetramethyl *p-tert.*-butylcalix[4]arene tetraether

Figure 58 shows the molecular mechanics calculated structures for a series of metal complexes of the tetramethylether **5**. These suggest the trend in these structures is to locate the metal ion higher above the ether oxygen plane and into the upper cavity as the cation radius increases. The position of the Cs^+ ion in this simple model agrees rather well with that of the crystal structure of the Cs^+ complex of the tetrol **6** and in both cases the complex has an approximate C_4 axis. However, the model Na^+ complex is very different from the known structure [313]; the position of the Na^+ ion is well above the ether oxygen plane in the model while it is below it in the crystal structure [see **Figure 59**]. Indeed, the position of the Na^+ in the crystal structure is considerably lower than even the position of the Li^+ in the series of models. In order to determine if it was a systematic error in the modelling method which caused this discrepancy we carried out more careful modelling studies on the Cs^+ complex of **6**, the Na^+ complex of **5** and, since

no crystallographic data were available for the Li^+ complex, compared the MM+-derived model Li^+ complex of **6** with a model of the same complex derived from semi-empirical calculations.

Since the trend in metal ion positions in the simple tetrols predicted by the MM+ procedure seems to agree reasonably well with other independent data the disparity between the model and crystal structure of the Na^+ complex of **5** described above is surprising and merits further investigation. **Figure 58** showed the calculated structure of the Na^+ complex of **5** with no solvent or counterion included in the calculation; inclusion of a toluene molecule at the upper rim produces the structure shown in **Figure 59**. There are two distinct groups of stabilising interactions occurring between the toluene molecule and the calixarene cavity. The methyl group of the toluene molecule interacts with the aromatic rings of the cavity and the *p-tert.*-butyl groups of the calixarene interact with the aromatic ring of the toluene molecule.

This structure also reproduces the calixarene aryl ring tilt angles of the crystal but again the Na^+ ion lies above the mean plane of the ether oxygen atoms in the calculated structure while it is below the mean plane in the crystal structure. Closer inspection of the crystallographic data reveals that, in contrast to the structures discussed thus far, the counterion lies only 2.83 Å from the Na^+ ion i.e. little more than the sum of the van der Waals radii of Na^+ and closest carbon atom of the counterion. A counterion in such close proximity to the metal centre might well be expected to have a significant effect on the structure of the complex. For the purposes of these calculations a counterion was placed in position below the complex at the location known from the crystallographic data. After the counterion was placed in position the geometry of the calixarene, solvent and Na^+ ion was allowed to relax.

Figure 59(b) shows the structure of the complex that resulted which is compared to the crystallographic data. Inclusion of the counterion has caused the Na^+ ion to move 1.53 Å lower in the cavity, below the ether oxygen plane and very close to its position in

the crystal structure. In effect, the carbon atom of the counterion that carries a net negative charge has provided an additional electrostatic driving force that pulls the metal ion below the mean ether oxygen plane. However, due to the proximity of the counterion to the calixarene, distortions are introduced into the calixarenes

| | Tilt angles | O...O dist. | M ⁺ ...O dist. | O...Me of tol. |
|---------------------------|--------------|-------------|---------------------------|----------------|
| Free (MM) | (a) 94 | 3.4, 5.1 | – | – |
| | (b) 124 | | | |
| Li ⁺ (MM) | (a) 93.5 | 3.3, 4.9 | 1.86, 2.75 | – |
| | (b) 125.5 | | | |
| Na ⁺ (MM) | (a) 110.4 | 4.1 | 2.46 | – |
| | (b) 112.6 | | | |
| Na ⁺ (toluene) | (a) 112, 113 | 4.3 | 2.4 | 3.3 |
| | (b) 112, 115 | | | |
| Na ⁺ (X-ray) | (a) 107 | 4.47, 4.57 | 2.3 | 4.35 |
| | (b) 115 | | | |
| Cs ⁺ (MM) | (a) 111.2 | 4.1 | 3.9 | – |
| | (b) 112.4 | | | |

Table 19. Geometric data for the tetramethylether calix[4]arenes.

Some geometric data for the complexes modelled in this Section is displayed in **Table 19**. What is readily apparent, from the tilt angles, is that the complexes formed are not as symmetrical as those involving the tetrol calix[4]arene. With the discrepancies lessening as the cation size increases. This effect is particularly prominent in the case of the Li⁺ complex where a rectangular conformation is found. As the cation size increases, it is complexed higher up in the cavity and this pushes the calix[4]arene towards attaining a square conformation. The average O...O distance remains consistent for the various cation complexes (The average distance for the Li⁺ complex is 4.1 Å). The average O...O for the free ligand is also 4.1 Å and its overall geometry is very close to that of the Li⁺ complex.

The effect that the included toluene molecule has on the conformation of the calix[4]arene is more pronounced in the X-ray determined structure than in the structure obtained from molecular modelling calculations, as demonstrated by the difference in the tilt angles. A very close agreement is demonstrated between the Na⁺ to oxygen atom distances obtained utilising the two methods. A large discrepancy is found for the cation to toluene distances. This indicates that the molecular mechanics structure has the toluene molecule more deeply enclosed in the aromatic cavity.

2.4.1.3 Tetramethyl *p-tert.*-butylcalix[4]arene tetraester

This calix[4]arene has been shown to be very efficient in the complexation of Na⁺, over the other alkali and alkali earth metals, and much research interest has centred on the esterified calix[4]arenes [314].

Two different starting geometries were used for the optimisation of the tetramethylester calixarene **3**. The partial charges were calculated as previously detailed. For both methods all eight oxygen atoms were involved in the complexation of the included cations.

Method one:- A structure was built and bond dipoles optimised. The opposite phenyl rings of the 'chalice' were adjusted so as they became parallel. The phenoxy substituents were not adjusted however. This was performed so as not to bias whether or not the optimised conformation was cone or flattened cone. The free ligand was bond dipoles optimised and the Na⁺ cation was placed between the phenoxy and carbonyl oxygen atoms in the starting structure (unoptimised) and an atomic charges optimisation was performed.

Method two:- The starting structure for this method had the phenyl rings adjusted parallel and also the phenoxy substituents were adjusted so that they were symmetrical. The four carbonyl groups were pointing inwards. The Na⁺ cation was placed between the phenoxy and carbonyl oxygen atoms and an atomic charges optimisation was performed.

Tetraester calix[4]arenes, in the cone conformation, are well established as ionophores for the Na⁺ ion [315]. X-ray crystallography data shows that the free ligand is in the cone conformation and is, therefore, quite preorganised for binding a cation (**Figure 60** [315c]). The angles that the four aromatic rings, A–D, make with the ring methylenes mean planes are A (148°), B (94°), C (130°) and D (87°). Rings B and D are basically parallel (interplanar angle 2°), while rings A and C are almost normal to each other (interplanar angle 98°). The torsional angles of the side chains are approaching 180°.

There is very strong evidence, from NMR spectroscopy, that upon complexation with Na⁺, the tetramethylester remains in a ‘cone’ conformation but (unlike the free ligand) has a C_{4v} symmetry and the ion is coordinated by the four phenoxy oxygen atoms and the four carbonyl oxygen atoms [316]. The NMR data shows the *tert.*-butyl peaks become less complicated upon complexation, indicating that the inclusion complex becomes more symmetrical. This eight-fold coordination is found in the energy minimised model of the complex (see **Figure 61**) and in the X-ray structure of the complex formed between the tetraamide analogue of **3** and K⁺ [317] (see **Figure 65** for the K⁺ analogue and **Figure 66** for that of the Na⁺ cation). Thus, it is clear that the Na⁺ ion can be complexed by **3** and other, similar calixarenes in one region only.

For the Na⁺ inclusion complexes, the optimised structures obtained by methods 1 and 2 were very similar. For both methods, the carbonyl groups of both inclusion complexes were offset from the Na⁺ cation, as shown in **Figure 62(a)** and not straight towards the cation as shown in **Figure 62(b)**. The arrows represent the carbonyl groups. However upon overlaying the structures generated by methods 1 and 2, it was noticed

that for the two methods the orientation of the carbonyl groups around the cation were mirror images of each other. A slight reorientation of the direction in which the carbonyl groups were pointing in the starting structure of method one then lead to the same structures being obtained upon optimisation. This shows that a slight change in the starting conformation can lead to distinct changes in the final structure. However, these two minima are obviously separated by a very small energy barrier.

Optimisation of the free ligands utilising both methods is takes a great amount of computational cycles and a rms terminating gradient of $0.001 \text{ kcal mol}^{-1} \text{ \AA}^{-1}$ was only achieved for the symmetrical starting structure. The rms terminating gradient refers to the slope of the potential energy well. The smaller its value the shallower the slope, i.e. the molecule is approaching the bottom of the well rather than occupying the steep sides of the well.

Unsurprisingly, both methods yielded a different optimised structure for the free ligand, but both had flattened cone conformations. For method one, the bond dipoles optimisation procedure yielded three carbonyl groups pointing inwards and one outwards. This implies that the pendant groups can rotate without generating large energy changes.

For method two, the phenoxy oxygen atom substituents were very symmetrical, with the carbonyl groups forming a hydrogen bond type network. This involves the oxygen atoms of adjacent carbonyl groups being attracted to the C=O carbon atom.

A few further calculations were performed to ascertain the effect of atomic charges on the complexation behaviour of the calixarene. Charges were removed from the phenoxy oxygen atoms in the Na^+ complex. On optimisation, it was seen that the carbonyl oxygen atoms were mainly involved in complexation, with the cation being 2.8 \AA away from them.

Charges were then removed from the carbonyl oxygen atoms, (while remaining on the phenoxy oxygen atoms), and on optimisation, the Na⁺ cation was complexed in the upper region of the ‘chalice’, 4.8 Å away from the phenoxy oxygen atoms. This implies that the phenyl rings play a significant role in complexation when the charges are removed from the carbonyl oxygen atoms, even to the extent of masking out the effect of the phenoxy oxygen atoms.

In conclusion, if we start off each study on a calixarene by first molecular mechanics bond dipoles optimising each calixarene in order to obtain the free ligand starting geometry, we cannot be sure if it is actually the global minimum. HyperChem does not have the ability to search for the global minimum and it is my opinion that starting off with a symmetrical calixarene with the four phenyl rings of the ‘chalice’ parallel would be the preferred way to obtain unbiased results.

| | Tilt angles | O···O dist. | M ⁺ ···O=C dist. | M ⁺ ···ether dist. | CO···OC dist. |
|----------------------|--------------|-------------|-----------------------------|-------------------------------|---------------|
| Na ⁺ (MM) | 109.6 | 4.6 | 2.56 | 2.44 | 4.0 |
| Free (MM) | (a) 91 | 4.1, 4.9 | — | — | 2.9, 6.2 |
| | (b) 139 | | | | |
| Free (X-ray) | (a) 87, 94 | | | | |
| | (b) 130, 148 | | | | |

Table 20. Geometric data for the tetramethylester calix[4]arene.

Table 20 shows that, when compared to **5**, the O···O distances are greater for **3**, generally by half an angstrom. This is due to an increase in the repulsion between the lower rim pendant groups when compared to the ether. The distances between the different groups of complexing oxygen atoms are very similar with the cation being slightly closer to the ether complexing groups. This suggests that the aryl groups of the upper cavity may be having an influence on the cation position as the carbonyl groups are inherently stronger complexing groups than the ether groups.

As can be seen for the free ligand (**Figure 60**), it has a square conformation and the carbonyl oxygen atoms are, initially, not ideally placed for complexing the cation. The tilt angles for the X-ray of the free ligand average out to be the same as those for the MM optimised calix[4]arene.

2.4.1.4 Tetraethylamide *p*-*tert*.-butylcalix[4]arene

The crystal structure of the uncomplexed calixarene has been determined by Calestani et al. [317] as is shown in **Figure 63** it displays a rectangular cone conformation. The angles made by the aromatic cavity rings with the mean plane defined by their linking methylene groups is: A (87.4°), B (143.5°), C (89.5°) and D (135.1°). Two opposite aromatic rings (A,C) are almost parallel to each other (the angle between them is 2.2°) and the other two rings (B,D) are almost perpendicular (the angle between them is 92.4°). Molecular mechanics calculations yielded a structure with a rectangular cone conformation and tilt angles of ~123° and ~95°. When these are compared to the tilt angles of the complex it indicates that a relatively high degree of symmetry has been introduced into the molecule upon complexation of K⁺.

Figure 64 shows the calculated structure of the calix[4]arene tetraethyl amide 1 K⁺ complex. The calculated structure has the correct 4-fold symmetry axis, i.e. the structure has 'squared up' on introduction of the metal ion, and the metal lies between the planes defined by the ether and carbonyl oxygen atoms. The distances between opposite ether oxygen atoms and opposite amide oxygen atoms, which define the size of the coordination cavity, are 5.0 Å and 4.7 Å, respectively. The corresponding distances in the X-ray structure are 5.2 Å and 4.7 Å. The K-O bond lengths in the X-ray structure are 2.71 Å and 2.74 Å for the ether and amide oxygen atom respectively. The X-ray structure is shown in **Figure 65**.

The X-ray structure also shows that a methanol molecule is located in the upper cavity. We have found that inclusion of this solvent molecule in the model has a negligible effect on the calculated structure of the complex and concluded that the methanol molecule has no strong intermolecular interactions with the host. Calculations on this complex by Wipff et al. [318] using a similar electrostatic binding approach in the Amber force field gave a similar result.

Figure 66 shows the crystal structure of the 1:Na⁺ complex [319]. An associated iodide ion has no close distances to the calixarene. The refined crystal structure has a high *R* value (a measure of disorder in the crystal) so useful comparisons between bond distances and angles would not be reliable with similar structures.

| | Tilt angles | O...O dist. | M ⁺ ...O=C dist. | M ⁺ ...ether dist. | CO...OC dist. |
|------------------------|--------------------|-------------|-----------------------------|-------------------------------|---------------|
| Free (MM) | (a) 95 (b) 123 | 3.9, 5.3 | — | — | 4.7, 6.5 |
| K ⁺ (MM) | (a) 109 (b) 111 | 4.84 | 2.65 | 2.65 | 4.57, 4.73 |
| K ⁺ (X-ray) | | | 2.74 | 2.71 | |

Table 21. Geometric data for the tetraethylamide *tert.*-butylcalix[4]arene.

The data shown in **Table 21** shows a high degree of correlation with the results shown in **Table 20**. The Na⁺:3 complex has a slightly higher symmetry but it is a smaller molecule than its amide counterpart. The amide groups seems to interact with the cation to a slightly greater extent than a carbonyl group alone, as shown by the equality of the ether and amide to metal distances.

A C_{2v} to C_{4v} symmetry change of the calix[4]arene is observed in going from the free form to the K⁺ modelled complex. The tilt angles and the potential complexing oxygen atoms adopting a more symmetrical conformation demonstrate this.

2.4.1.5 Tetraethyl *p*-*tert*-butylcalix[4]arene tetraester

This calix[4]arene, **4**, has a 1,3-alternate conformation and is referred to as YERFIK in the Cambridge Structural Database [320]. **4** was chosen for study because its structure allows us to explore the possibility of migration of the included cation [321]. As shown in **Sections 2.4.1.3** and **2.4.1.4** the cone conformation with a C_{4v} symmetry coordinates the included cation by the four phenoxy oxygen atoms and the four carbonyl oxygen atoms. As detailed for the other calixarenes studied, calixarenes in the cone conformation complex cations in one region only whereas the 1,3-alternate conformation of **4** creates several possible complexation sites.

The apparent multiple binding sites allow us to test the extent to which the modelling procedure can find the global minimum of an optimised structure more rigorously than is possible in the case of the ‘cone’ calix[4]arenes. In this work, it is assumed that the global minimum corresponds to the X-ray structure. As for the other calixarenes studied in this chapter the modelling procedure uses electrostatic interactions to bind the metal ion within the calixarene, which means that partial charges must be calculated for the ligand. In this work three methods were used to calculate these charges. The first method was to use a single point, semi-empirical calculation (AM1 [322]) on a compound similar to **4** (one full aryl ring and its substituents plus ethyl groups substituted at the methylene linker positions on the ring). These charges (Method 1) were then transferred, with averaging and rounding off, to the entire molecule of **4**, meaning that chemically equivalent atoms were assigned the same charge. The transferring of charges is a labour-intensive process and consequently, partial charges were also calculated on the full ligand with the AM1, MNDO [323] and PM3 [324] semi-empirical methods (Method 2), which was a less laborious process. Another advantage of the latter method is that we can see the effect that assigning slightly different partial charges to atoms that are chemically equivalent but conformationally different has on the optimised geometry of

the complex. This is relevant to the modelling of $4:\text{Na}^+$ as the geometry of the pendant groups in the '2' and '4' positions of **4** is different to that of the pendant groups in the '1' and '3' positions. However, Methods 1 and 2 both suffer from the disadvantage that because the calculations are carried out on the free ligand, they do not take into account withdrawal of electron density from the ligand when it binds with a cation. Accordingly, partial charges were also determined by carrying semi-empirical calculations on the full metal complex using those methods that have parameters for sodium – INDO [325], CNDO [326] and ZINDO/1 [327] (Method 3). The molecular mechanics MM+ force field available with the HyperChem software (and indeed, the other force fields available in HyperChem) contain no parameters for Group 1 metal ions and, therefore, as performed in the case of the previously studied calixarenes, the atom type for neon was used for the sodium ion since neutral neon is isoelectronic with Na^+ . The ion was assigned a formal charge of +1 in the case of Methods 1 and 2. The starting geometry used for the ligand for both the molecular mechanics and semi-empirical calculations was that of the ligand as in the X-ray structure of $4:\text{Na}^+$. Hydrogen atoms needed to be added, as the X-ray structure did not contain them. With Methods 1 and 3, the ion was initially placed in Position 2 only – the position it occupies in the X-ray structure (see **Figure 67**). When partial charges were assigned with Method 2 the initial position of the Na^+ ion was varied as shown in **Figure 67**. The geometry of the structure was subsequently optimised using the MM+ force field. The same algorithms were used for the optimisation as for the previous calixarene studies.

During the course of this investigation it was found that the optimised structure of the complex and the final position of the included ion was independent of the initial position of the ion. These positions are shown in **Figure 67**.

The cation was placed both above and below the two carbonyl and two ether oxygen atoms involved in complexation and upon optimisation it returned to the general region of position 2. However, the impression was given that two oxygen atoms, rather

than four, bound the cation as indicated in the X-ray structure; O1 and O4 in **Figure 68(a)**.

The optimised structure of this complex is virtually independent of the semi-empirical method used to assign partial charges to the ligand. However, Method 3, as judged from the rms overlay values, does not yield as tight a fit as the other two methods. This is mainly manifested in the conformation of the calixarene pendant groups as opposed to the position of the included cation. Differences in partial charge between chemically equivalent atoms in the pendant groups with different conformations, have a small effect on the optimised structure of the ligand in the complex. A very encouraging result is the fact that, when Method 2 was used to assign partial charges, the geometries of the optimised structures of the complex (both in terms of the conformation of the ligand and the position of the ion) are almost identical, regardless of the initial position of the ion (**Figure 67**), for each of the three semi-empirical methods used.

It is very interesting to note that though the conformation of the ligand initially used was that of the X-ray structure, the two pendant groups most involved in the binding of the ion as indicated by the X-ray structure [the '1' and '3' pendant groups (containing O1 and O4 in **Figure 68a**)], are the least involved according to the optimised structures, regardless of the initial position of the ion, i.e., when, for example, the ion was placed initially placed in Position 2 – its position in the X-ray structure – its optimised position was that of Position 3 with the corresponding rearrangement of the both pairs of pendant groups. It is important to realise that in the X-ray structure, the '1' and '3' pendant groups of the ligand have a geometry that is very well suited to complexation with the Na⁺ ion as the ion is approximately equidistant from the carbonyl and phenoxy oxygen atoms of these pendant groups, and the two carbonyl groups and the Na⁺ ion are approximately in the same plane. This movement of the ion from Position 2 to Position 3 suggests that the energy barrier to the migration is relatively small. This is supported by evidence, obtained from dynamic ¹H NMR measurements [328], that the Na⁺ ion oscillates rapidly (163 s⁻¹) across the hydrophobic arene cavity in an intramolecular fashion.

An example of this similarity between the optimised and X-ray structures is shown in **Figure 68(b)**. For the optimised structure, partial charges were obtained by performing a PM3 semi-empirical single point calculation on the whole molecule and the cation was initially placed at position '2'. When the optimised and X-ray structures are overlaid an rms overlay error of 0.731 Å is obtained and the Na⁺ cations differ in position by 0.32 Å which indicates that there is a close match between the experimental and theoretically calculated structures.

Overall, we have shown that the optimised geometry of the ligand in the complex and the final position of the ion is independent of the initial position of the ion and this is a very encouraging result. We have also demonstrated that improved results are obtained when metal cations are assigned formal charges than when partial charges are calculated for both the ligand and the metal ion.

2.4.2 Penta *p-tert.*-butylcalix[5]arene pentaketone

¹H NMR data for the pentaketone indicates that the conformation of the free ligand is a symmetrical cone conformation but solid state IR analysis displays two carbonyl absorptions of unequal intensity [329]. This implies that a rapid conformation average process is occurring in solution. See **Section 1.10** for more information on the pentaketones.

In the solid state the metal-free calix[5]arene **2**, which is a ketone, has a non-regular cone geometry in that one of the aryl rings tilts into the central cavity. The same general conformation is also observed in its Rb⁺ complex, whose crystal structure is shown in **Figure 69(a)** and **(b)**. The Rb⁺ ion lies approximately in the mean plane defined by the four ether oxygen atoms which it lies closest to (i.e. well above the mean carbonyl oxygen plane) and is not coordinated by the oxygen atoms of the inward-tilting ring. The

crystallographic and calculated structures for this complex, both shown in **Figure 69(c)** and **(d)** are very similar. The main features of the geometry (calixarene ring tilting angles and position of the encapsulated metal ion within the calixarene) are well reproduced by the calculated geometry.

This is rather more impressive than the successful prediction of the highly symmetrical calix[4]arene structure shown above since any force field with reasonable ion size parameters for the metal ion and coordinating atoms could well minimise to a symmetrical structure for the calix[4]arene, even if the metal-oxygen interactions were significantly overestimated in the calculation. It is much less likely that a force field with excessively strong attractive interactions could lead to the very irregular structure shown in **Figure 69**.

The single crystal X-ray structure of the Na^+ complex of **2** [**Figure 70(e)** and **(f)**] shows that it is rather different from the Rb^+ complex, the inward tilting aryl ring is much more upright and the metal ion lies farther below the average plane of the four coordinating ether oxygen atoms. However, the complex crystallises with one methanol solvent molecule in the cavity so that these differences could be due either to the change in the central metal ion or to the encapsulated solvent. In the calculated structure of the Na^+ complex with no solvent included, shown in **Figure 70(a)** and **(b)**, the conformation of the calixarene is similar to that of the Rb^+ complex. Inclusion of the methanol solvent molecule brings the calculated structure [**Figure 70(c)** and **(d)**] much closer to that obtained crystallographically, with a more upright displacement of the inward tilting aryl ring and the Na^+ ion lying between the carbonyl and ether oxygen planes. The position of the solvent is also reasonably well reproduced in the calculated structure. Without the included methanol molecule the sodium cation is closer to the complexing ketone carbonyl groups than in the case of complexation of the caesium cation. This indicates that the change in cation leads to the difference in complexation position and the inclusion of a methanol molecule in the apolar cavity shifts the inwardly tilting aryl group slightly out of the cavity.

| Calix[5]arene complex | O...O dist. | M ⁺ ...O=C dist. | M ⁺ ...ether dist. | CO...OC dist. |
|----------------------------|-------------|-----------------------------|-------------------------------|---------------|
| Na ⁺ :MeOH (MM) | 5.6, 5.7 | 2.6 | 2.9 | 3.9, 4.3 |
| Na ⁺ (MM) | 5.3, 5.6 | 2.7 | 2.8 | 4.3, 4.4 |
| Free (X-ray) | 5.2, 6.0 | – | – | 5.2, 7.3 |

Table 22. Geometric data for the calix[5]arene. The calculated distances do not include the pendant group connected to the inward tilting aryl group.

Table 22 shows some of the structural data for the calix[5]arene complexes. As can be seen, the complexation of the Na⁺ cation causes the ether and carbonyl groups to come closer together and also to be more symmetrically arranged in the molecule.

2.5 CONCLUSIONS

Using the HyperChem molecular modelling software package has been demonstrated to be a straightforward and computationally undemanding method which is surprisingly good at reproducing the structures of a range of metallo-calixarenes. This implies that the force field employed is at least reasonably good at balancing the conflicting demands of the electrostatic interactions between the ligating oxygen atoms and the encapsulated metal ions with the stretching/bending forces induced in the calixarene by the metal ion inclusion. The method is not, nor is it intended to be, in any way rigorous or highly accurate. It gives metal ion positions within calix[*n*]arenes in the solid state which, in the worst cases, are up to 0.5 Å in error, although the average error is considerably less. There is clearly potential for refining the method as more crystallographic data becomes available, indeed we found we could adjust the metal ion parameters to make near-perfect fits to the crystallographic data but felt that we could have little confidence in the transferability of these arbitrary parameters to other complexes. However, the method as it stands already provides a simple and inexpensive visualisation tool that should be useful for gaining an insight into the possible 3D

conformation of proposed calixarene derivatives and also as a complementary technique with NMR spectroscopy in the elucidation of calixarene structures.

3 ENANTIOSELECTIVE COMPLEXATION OF
CHIRAL AMINES BY CHIRAL
CALIX[4]ARENES: A COMPUTATIONAL
INVESTIGATION

3.1 INTRODUCTION

In order to enantioselectively complex chiral amines, a chiral receptor is required. Gutsche et al. [330] synthesised the first chiral calixarene in 1979. Since then a variety of approaches have been employed to create chirality in calixarenes [331]. For example, the introduction of chiral moieties onto the upper [332] or lower rim [333] (**Figure 71**) has been used by many research groups. These modifications can be performed on any molecule to induce chirality, but due to the calixarenes non-planar geometry the addition of non-chiral substituents to the meta position of the phenolic rings [334] or to the upper/lower rims of the calixarene, forming an asymmetric substitution pattern, also yields the desired chirality [335]. The first calixarene with chirality of this type was synthesised by Gutsche and No in 1982 [336]. But it was not until 1990 that Shinkai et al. [337] resolved the first enantiomerically pure chiral calixarene (**Figure 72**).

A high level of enantioselectivity can be achieved through the rational design of the molecular system utilising multiple hydrogen bonds as the driving force for stereoselective complexation [338]. In all systems created, directionality and strength of hydrogen bonding between complementary functionalities are the key factors responsible for generating enantioselectivity.

3.1.1 Requirements for enantioselective complexation

With relevance to our current work, and taking into account studies previously performed in the field, a number of prerequisites are necessary for the desired enantioselective recognition to occur. The two chiral calixarenes that we have studied are shown in **Figure 73**. These possess ligating groups with appropriate interacting moieties for selective complexation of the enantiomers of chiral amines with complementary

structure and chirality (e.g. phenylglycinol and phenylalaninol, see **Figure 74**). Both hydrogen bond donor (to interact with the nitrogen and oxygen lone pairs of the chiral amine; in our calix[4]arenes OH groups) and acceptor (to interact with the δ positive hydrogen atoms of the chiral amine; in this case CO, ether and OH groups) are essential for the efficient complexation of our guest molecule. In order to have these groups rigidified in space they are attached to the phenolic oxygen atoms of a calix[4]arene backbone. This provides a chiral 3-D environment capable of enantiomeric discrimination of guest amines. A calix[4]arene was chosen, as opposed to higher homologues in the series, as molecular models indicated that the cavity size for this calixarene was compatible for the complexation of these target amines. *Tert.*-butyl and allyl groups (which can be further reacted to conformationally lock/immobilise the calixarene) substituted at the upper rim fix the calixarene into the cone conformation. Also, these groups do not aid in the complexation of a guest molecule in the arene cavity, a process that may compete with complexation by the lower rim substituted pendant groups. Finally we need a procedure for obtaining a signal indicating that the desired interaction is occurring. Inclusion of naphthalene ring systems in the pendant groups provides us with an easily detectable indicator of the efficiency of binding as the binding process leads to quenching of the fluorescence emission signal.

In designing the two chiral calix[4]arenes presented here we have adhered to the principles detailed above and, as the fluorescence data demonstrates, we have achieved the desired enantioselective complexation of two chiral amines. Molecular modelling was implemented so as to ascertain, mechanistically, the detailed interactions and hydrogen bonding patterns formed upon complexation of these amines by the calix[4]arenes.

3.2 EXPERIMENTAL

For **Section 3** the calculations were performed using the MacroModel v. 6.0 software package [339]. The force field of choice was AMBER* [340], as supplied with MacroModel. Corresponding calculations performed utilising the MM3 force field [341], produced no definitive hydrogen bonding patterns so only results obtained with AMBER* will be discussed here. The complex was modelled in three different environments, chloroform, water and in vacuo. No artificial cut-offs were used. The Polak-Ribiere conjugate gradient minimiser [342] was the minimisation algorithm. Convergence was obtained when the gradient root mean square was below 10^{-4} kJ/mol/Å.

Molecular modelling studies on 3-(S)-acetylamino-7(S)-carboxy-azepan-2-one N-methyl amide (**Figure 75**) show that the MM2 force field over-emphasises the significance of intramolecular hydrogen bonding whereas the AMBER force field satisfactorily predicts the tendency of the lactam to dimerise involving intermolecular hydrogen bonding [343].

The MM2* and MM3* force fields implemented in the MacroModel program resemble the Allinger MM2 and MM3 force fields, but electrostatics and improper torsions are treated differently in the MacroModel version.

Post-simulation rendering was performed with Spartan v. 5.1.1 [344] to generate the 3-D images. These were transferred to Microsoft PowerPoint 97 in order to illustrate the hydrogen bonding patterns.

The starting conformation of the chiral calixarenes had all four of the 'calix' phenyl groups parallel so as not to have any bias towards a rectangular or square cone conformation. The pendant groups had their complexing moieties (the carbonyl, alcohol and/or ether groups) pointing inwards with the naphthalene groups outside the cavity. The

pg/pa guest molecule was introduced at the lower end of the complexation region formed by the pendant groups. The amine and alcohol groups of the chiral amine were level with the alcohol groups of the calixarene, equidistant from each of the pendant groups, and the phenyl group positioned below the cavity. The chiral amine was then rotated by 90° three times (and the corresponding structures were saved separately) to yield four different starting conformations with the chiral amine remaining in the original position with respect to the calix[4]arene. Before the calculations were initiated every complex was checked to confirm that no inter- or intramolecular hydrogen bonding was occurring.

Molecular dynamics and Monte Carlo simulations were carried out to see if they would lead to a highly intermolecular hydrogen bonded inclusion complex as the global energy minimum. Even after adjusting a variety of parameters in the software and using many different starting conformations (both optimised and unoptimised) no definitive results could be obtained. The simulation would, generally, place the guest molecule slightly outside the complexation cavity of the host that would not have been of any help to us in our attempt to rationalise the experimentally determined fluorescence data. Much time was spent trying to optimise these simulation procedures but in the end it was decided that a more “user controlled” optimisation procedure would be more efficient for yielding results.

As the calix[4]arene:amine host:guest complex has a very complex energy surface it is a prodigious task to attempt to ascertain the global minimum, especially considering the conformational sampling techniques appeared to be ineffective in this case. Upon optimisation of the four starting structures the hydrogen bonding patterns formed between the host and guest were analysed. If intramolecular hydrogen bonds were observed to form in the calixarene these were broken and potential hydrogen sites in the amine were moved closer to the relevant calixarene pendant group. Slight bond rotations of the calixarene and/or amine, along with some rotational movement of the amine, were performed to achieve this. Further optimisations were then initiated. Steric hindrance between the phenyl group of the amine and the pendant groups of the calixarene

prevented certain hydrogen bond being formed. A multitude of structures were thus generated, for each amine enantiomer:calix[4]arene complex, and fully optimised.

Upon the generation of a highly hydrogen bonded amine:calixarene complex the amine was removed and the other corresponding enantiomer of the same amine was inserted in the same general region. Successive optimisations were then performed on slightly adjusted starting structures to check if a similar number of hydrogen bonds between the opposite amine enantiomer and the same host formed. Invariably the same hydrogen bonding patterns did not reoccur, even after bond torsional adjustment and translational movement of the amine.

Exhaustive attempts were made to maximise the amount of hydrogen bonds formed between the amines and the two chiral calix[4]arene host molecules. The results discussed here are of the best eight optimised complexes obtained.

The hardware consisted of a SGI O2 workstation with a MIPS R5000 processor, 128MB of RAM and running under IRIX 6.3.

3.3 RESULTS

Figure 73 shows a 2-D representation of the two chiral calixarenes used in the chiral amine recognition study and **Figure 74** shows the corresponding structures of the chiral amines.

Our group performed four different sets of fluorescence studies. A histogram of the Stern-Volmer constants is shown in **Figure 76**. For L1 we have demonstrated that R-pg quenches the fluorescence signal significantly more than the S-enantiomer (ratio of the Stern-Volmer slopes is >2:1), implying that stronger interactions are occurring between the R-enantiomer and the calix[4]arene. However, when R and S pa are used as the chiral

amine guest molecules virtually no quenching is observed. This does not necessarily mean that there is no interactions occurring between the host and guest molecules; just that these interactions do not lead to quenching of the fluorescence signal.

In the case of L2 the opposite trend as seen for L1 is obtained. Interactions are seen to occur between R and S pg but to the same extent for each enantiomer, i.e., no enantioselectivity is observed. However, chiral recognition does occur in the case of R and S-pa. Clearly, the R enantiomer quenches the fluorescence to a greater extent than the S (Stern-Volmer slope ratio is again >2:1) indicating that it is being enantioselectively bound by the calixarene.

We shall now discuss molecular modelling results obtained which aid in our understanding of which interactions are involved and why one enantiomer of a chiral amine is selectively complexed over the other. There are two kinds of comparisons that shall be referred to: (1) Differences between the two chiral calix[4]arenes complexing the same chiral amine; both calix[4]arenes have very similar interacting moieties and, basically, only differ in the length (and the nature) of the spacer between the alcohol and the naphthalene groups of the pendant groups. These relatively small differences in the calix[4]arenes lead to a great change in their interactions with a chiral amine. (2) The two chiral amines, which only differ by one methylene spacer group, interact with the same calix[4]arene very differently. The remarkable fact that there is such a great change in the fluorescence quenching in going from pg to pa being complexed by L1, and the differences seen for L2, shall be discussed.

Out of the three environments used to perform the molecular mechanics calculations in, only the data obtained for the inclusion complex in chloroform was chosen for investigating the binding mechanism and enantioselectivity of the chiral amines with the calixarenes. Initial work with the host:guest complexes in water, in vacuo and chloroform showed that substantially less hydrogen bonds formed in water, with in vacuo being intermediate between water and chloroform. This is due to the fact that as

chloroform is a non-polar solvent, it is not going to lessen the interactions with hydrogen bonding sites on the host or guest molecules. Therefore, an amplification of the hydrogen bonding patterns obtained is observed as compared to that in water and in vacuo.

Other work (not shown) has demonstrated that a pg/pa molecule cannot fit through the upper rim of the chiral calix[4]arene so its most likely point of entry into the complexation region is from below the naphthalene groups. This is why the starting positions for the simulation were chosen. Also, placing pg/pa into the calix[4]arene sideways, by which we mean with the phenyl group placed between the pendant groups at the hydroxy oxygen atoms level and the alcohol group likewise on the other side of the calixarene, is not a feasible proposition due to the great increase in steric interaction energies that occurs.

Pertinent distances between key atoms are displayed in **Tables 23-31**. Schematics for these distances are shown **Figures 77** and **78**.

We shall now discuss (1) mentioned above; the two different chiral calix[4]arenes interacting with the same chiral amine. We shall first look at both enantiomers of pg. According to the energy minimised conformation of the L1-pg complex, **Figure 79**, R-pg is extremely efficiently complexed by the (S) dinaphthyl prolinol groups of the calixarene host. A five-point interaction (all of which consists of hydrogen bonds) takes place between the chiral calixarene and its guest. Two of the bonds formed (**1,2**) are between the hydroxy oxygen atoms of the calixarene and the two amine hydrogen atoms of R-pg. Two more bonds are formed (**4,5**) between the hydroxy hydrogen atom of the amine and carbonyl groups of adjacent calixarene pendant groups. The fifth bond formed (**3**) is between a hydroxy hydrogen atom on the calixarene and the hydroxy oxygen atom of R-pg. The R-pg phenyl group is directed below the calixarene, in the region of three of the naphthalene groups, roughly 3.5 Å away from all of them. We believe that there could be an interaction occurring between the naphthalene and phenyl ring systems resulting in a quenching of the fluorescence but, as mentioned previously, molecular mechanics

simulations do not have specific parameters to give a description of π - π stacking interactions. Three of the calixarene pendant groups seem to be involved in the complexation of R-pg.

In contrast, these interactions were not seen for equivalent simulations involving the complexation of S-pg to such a great extent (see **Figure 80**. This image was generated utilising the POV-ray software program [345]). In this case two hydrogen bonds between the amine hydrogen atoms and the hydroxy oxygen atom and carbonyl group of adjacent pendant groups of the calixarene were formed (**2,3**). A hydrogen bond is also formed (**1**) between the hydroxy hydrogen atom of the amine and the previously mentioned carbonyl group. The remaining hydrogen bonds that are seen to form for the R enantiomer of the chiral amine (**3** and **5** in **Figure 79**) cannot both form simultaneously due to inhibiting interactions that would then occur between the phenyl group of pg and the naphthalene groups of the calixarene. This happens because it is impossible for the pg phenyl group to point straight down the middle of the cavity, as for the R-enantiomer, and thus prevent these unfavourable interactions occurring. In this case, the second of two broad groups of interactions that may occur in stereoselective complexation, steric interactions, do not actually play a constructive role in the binding of the R-enantiomer. Rather, it inhibits the binding of the S-enantiomer.

Tables 23 and **24** show the distances between the most important atoms and the tilt angle of the aromatic cavity benzene rings in the R- and S-pg complexes.

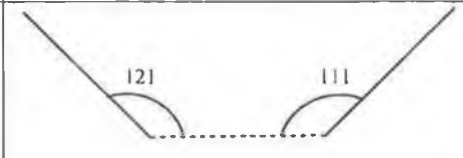
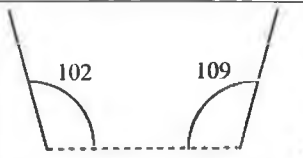
| R-pg | | |
|-------------|--|---|
| Tilt angles |  |  |
| a | 4.4 | 4.8 |
| b | 5.7, 5.9 | 5.9, 6.6 |
| c | 5.9 | 6.8 |
| d | 9.1 | 9.4 |
| e | 5.7 | 7.0 |
| f | 6.4, 7.8 | 7.1, 8.1 |

Table 23. Relevant interatomic distances (Å) and ring tilt angles (°) for the L1:R-pg optimised complex.

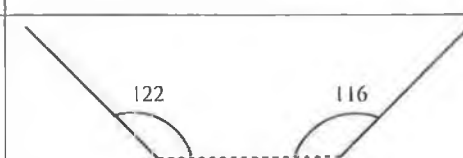
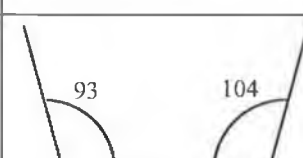
| S-pg | | |
|-------------|--|---|
| Tilt angles |  |  |
| a | 4.4 | 5.3 |
| b | 5.3, 6.4 | 6.7, 7.3 |
| c | 5.8 | 7.3 |
| d | 9.0 | 10.0 |
| e | 6.8 | 7.1 |
| f | 5.7, 8.6 | 7.3, 8.3 |

Table 24. Relevant interatomic distances (Å) and ring tilt angles (°) for the L1:S-pg optimised complex.

As can be seen from **Tables 23** and **24** the two complexes are dimensionally very similar. However, for virtually every geometric parameter the S inclusion complex's

value is slightly longer than the corresponding value for the R complex. Upon examination of the hydrogen bonding data (**Table 31**) it can be seen that there is two extra hydrogen bonds formed during the inclusion of the R enantiomer. So there is a greater interaction between the pendant groups and the amine in the case of the R enantiomer. This would lead to the pendant groups being closer to the guest, which is indicated by the geometric data.

From the various calculations performed on this calix[4]arene it was seen that there is a strongly competing intramolecular hydrogen bonding process occurring; between the hydrogen atom of the alcohol group and the carbonyl group in the same pendant group. Care was taken not to have this type of hydrogen bond preformed in the starting structure of an optimisation. Intra-molecular hydrogen bonds were also observed to occur in L2, but not to such a great extent.

Unlike in cation complexation, the 'calix' of the calixarene adopts a rectangular rather than a square conformation on complexation with the guest amine, such as by the calix[4]arene tetraester. This is due to the fact that the calixarene is now complexing a much larger guest and it is sterically energetically favourable for it to adopt this conformation.

The energy minimised complex obtained with L2 and R-pg (**Figure 81**) shows the formation of four hydrogen bonds between the host and guest. The amine hydrogen atoms form (2,3) hydrogen bonds to a carbonyl group and to the oxygen atom of the ether group connected to a naphthalene group. The hydroxy hydrogen atom of the amine binds to another carbonyl group (4) and the hydroxy oxygen atom interacts with a hydrogen atom of an alcohol group on a pendant group of the calixarene (1). Three of the naphthalene groups are in close proximity to the phenyl group of the amine that is pointing straight down the cavity of the calixarene.

For the S enantiomer of pg four hydrogen bonds are again formed (**Figure 82**). Two carbonyl groups of the calixarene pendant groups form (2,3,4) three hydrogen bonds with the two hydrogen atoms of the amine and the hydrogen atom of the hydroxy group. The fourth bond is between the oxygen atom of the amine hydroxy group and the hydroxy hydrogen atom of a calixarene pendant group (1). Again, the phenyl group of the amine is pointing down the cavity of the calixarene and 3 to 5 Å away from the naphthalene groups.

Both enantiomers of the chiral amine are effectively complexed by L2 to the same extent, as shown by the hydrogen bonding patterns formed. As also mentioned previously the phenyl group of the chiral amine is very close to three of the naphthalene groups of the calix[4]arene which may lead to the observed quenching of the fluorescence.

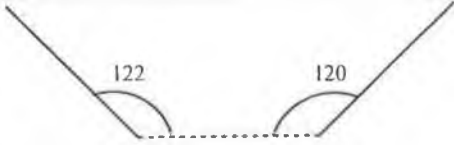
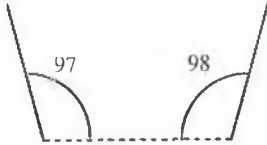
| R-pg | | |
|-------------|--|---|
| Tilt angles |  |  |
| a | 4.1 | 5.4 |
| b | 5.4, 5.6 | 5.8, 6.0 |
| c | 5.4 | 6.2 |
| d | 8.7 | 9.2 |
| e | 7.3 | 9.4 |
| f | 8.9 | 9.5 |
| g | 8.7, 10.6 | 9.2, 10.4 |
| h | 7.3, 8.0 | 9.3, 9.3 |

Table 25. Relevant interatomic distances (Å) and ring tilt angles (°) for the L2:R-pg optimised complex.

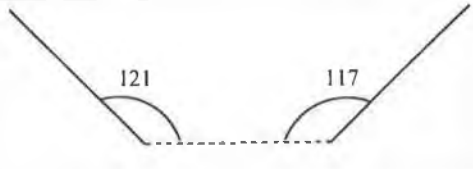
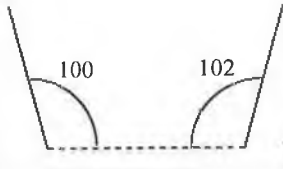
| S-pg | | |
|-------------|--|---|
| Tilt angles |  |  |
| a | 4.1 | 4.9 |
| b | 4.5, 6.4 | 5.9, 6.7 |
| c | 5.7 | 6.9 |
| d | 8.8 | 9.8 |
| e | 10.5 | 12.8 |
| f | 9.8 | 11.5 |
| g | 9.0, 10.5 | 9.3, 11.4 |
| h | 8.7, 9.0 | 9.9, 10.1 |

Table 26. Relevant interatomic distances (Å) and ring tilt angles (°) for the L2:S-pg optimised complex.

The results displayed in **Tables 25** and **26** broadly follow the trend observed for L1 complexing both enantiomers of pg. The cavity size formed by the complexing pendant groups of the calix[4]arene is smaller in the case of the R complex rather than the S. However, in this case as there is an equal amount of hydrogen bonds formed so both amines interact equally with the host calix[4]arene. The average hydrogen bond length is 2 Å for the R-pg complex and it is 1.9 Å for the S-pg complex that also reinforces the fluorescence data. As judged by g, a measure of the length of the complexing cavity, it is around 10 Å for L2. For the L1 inclusion complex, with the same amine, the corresponding distance is ~7.5 Å that indicates that L2 is a more suitable host for complexing guests of a larger size.

The inclusion complexes formed between both the enantiomers of pa and the two chiral calix[4]arenes shall now be discussed. Out of the various optimisations performed, for L1 complexing R-pa, the conformation with the greatest number of hydrogen bonds

formed is shown in **Figure 83**. The amine's hydroxy hydrogen and oxygen atoms are interacting with a carbonyl group and the hydrogen atom of a hydroxy group on a pendant group, respectively (**1,2**). One of the amine hydrogen atoms is hydrogen bonding with the oxygen atom of the same pendant hydroxy group (**3**). As can also be seen the phenyl group of the amine is positioned slightly below the naphthalene ring region of the calixarene. Other conformations have shown the chiral amine to be lower down in the cavity. Even though the carbonyl groups are still involved in the complexation of the amine the extra methylene spacer group of pa (when compared to pg) forces the amine's phenyl group outside the optimal region for interaction with the naphthalene groups and, therefore, this may lead to the observed lack of fluorescence quenching, i.e., complexation does not necessarily lead to quenching. This is a very interesting result, especially considering that an efficient three point interaction takes place between the guest and host molecules.

Optimisations performed with L1 and S-pa also yielded a conformation with three hydrogen bonds formed between the host and guest molecules (**Figure 84**). A hydrogen atom of the chiral amine's amine group and the alcohol hydrogen atom both form a bond with the same carbonyl group (**2,3**). The other hydrogen atom of the amine interacted with the oxygen atom of the alcohol group on the same pendant group of the calix[4]arene as the carbonyl group (**1**). The lack of experimentally observed fluorescence quenching may be explained by the same rationale as mentioned in the previous paragraph.

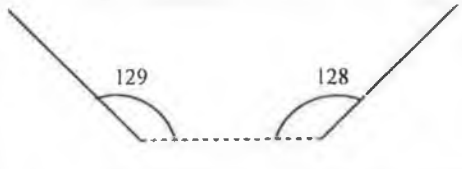
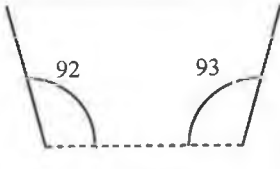
| R-pa | | |
|-------------|--|---|
| Tilt angles |  |  |
| a | 3.3 | 5.4 |
| b | 4.8, 4.9 | 6.8, 6.8 |
| c | 5.3 | 7.8 |
| d | 8.0 | 10.7 |
| e | 6.5 | 7.6 |
| f | 6.8, 7.3 | 7.9, 8.1 |

Table 27. Relevant interatomic distances (Å) and ring tilt angles (°) for the L1:R-pa optimised complex.

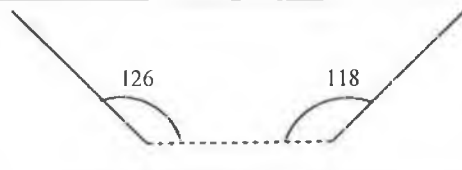
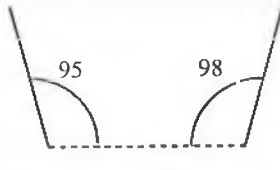
| S-pa | | |
|-------------|--|---|
| Tilt angles |  |  |
| a | 4.1 | 5.4 |
| b | 5.3, 5.7 | 6.5, 7.3 |
| c | 5.8 | 7.6 |
| d | 8.1 | 11.1 |
| e | 5.3 | 8.7 |
| f | 5.4, 7.9 | 8.2, 8.8 |

Table 28. Relevant interatomic distances (Å) and ring tilt angles (°) for the L1:S-pa optimised complex.

Tables 27 and **28** show some of the more pertinent geometric data for the L1:pa complexes. Again, the trend seen for the previous two groups of complexes is observed.

The S inclusion complex has, in general, a larger complexation cavity than the corresponding R complex. On average the cavity size is 7.5 Å, which is the same for the L1:pg complex. This suggests that different guest molecules do not alter the overall length of the host calix[4]arene to any great extent.

The average hydrogen bond length for L1:R-pa is 1.92 Å and for the L1:S-pa complex it is 1.94 Å so, even though there is a significant difference between the individual bond lengths, there is a very close agreement overall.

In contrast to these results, the energy minimised complex obtained with L2 and R-pa (**Figure 85**) suggest that it is the carbonyl groups of the propranolol amide calix[4]arene that are only involved in the complexation of R-pa. Four hydrogen bonds are formed; one of the carbonyl groups forms two hydrogen bonds with an amine group and the hydroxy hydrogen atoms of pa (**1,2**), another carbonyl group, on an adjacent pendant group also hydrogen bonds to the amine hydrogen atom (**3**) and a third carbonyl group bonds to the other amine hydrogen atom (**4**). Three of the naphthalene groups of the calix[4]arene are between 3.5 and 4.5 Å away from the phenyl group of pa. As the chiral amine is complexed so high up in the cavity there is, therefore, no problem with the phenyl group interacting with the naphthalene groups of the calix[4]arene.

With L2 and S-pa, a different mode of complexation was observed compared to the R enantiomer (as shown in **Figure 86**). An alcohol group is now involved in the binding of pa [it binds to the hydroxy oxygen atom of the amine via a hydrogen bond (**1**)]. In addition, two amine hydrogen atoms of pa interact with two carbonyl groups on adjacent pendant groups (**2,3**) and the hydrogen atom of the pa alcohol group also interacts with one of these carbonyl groups (**4**). Due to the mode of complexation experienced by the chiral amine its phenyl group is not directed down the cavity; rather it is pointing out at an angle, thus forcing one of the calixarene's pendant groups away from the cavity. The phenyl group is still in close proximity to a naphthalene group of the

pendant group but as it is away from the centre of the cavity (and the remaining three pendant groups) this could lead to the lessening in the observed fluorescence quenching.

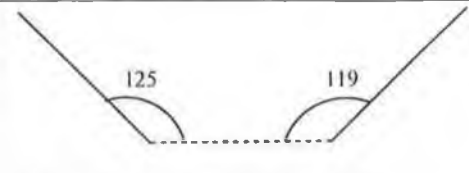
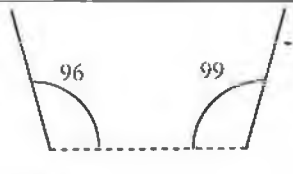
| R-pa | | |
|-------------|--|---|
| Tilt angles |  |  |
| a | 3.9 | 5.2 |
| b | 4.2, 5.7 | 6.2, 6.2 |
| c | 4.4 | 5.9 |
| d | 8.1 | 9.5 |
| e | 7.4 | 10.6 |
| f | 10.4 | 10.8 |
| g | 9.4, 10.4 | 9.3, 10.9 |
| h | 6.5, 8.2 | 8.7, 9.4 |

Table 29. Relevant interatomic distances (Å) and ring tilt angles (°) for the L2:R-pa optimised complex.

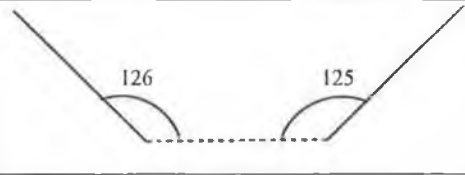
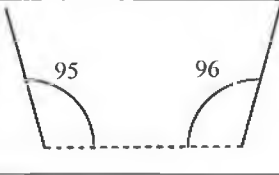
| S-pa | | |
|-------------|--|---|
| Tilt angles |  |  |
| a | 3.4 | 5.4 |
| b | 4.6, 5.0 | 6.5, 6.5 |
| c | 5.1 | 6.5 |
| d | 7.9 | 10.4 |
| e | 8.4 | 8.5 |
| f | 9.9 | 13.2 |
| g | 9.8, 9.8 | 10.3, 10.7 |
| h | 6.6, 7.9 | 8.0, 8.8 |

Table 30. Relevant interatomic distances (Å) and ring tilt angles (°) for the L2:S-pa optimised complex.

Tables 29 and **30** illustrate some of the key interatomic distances measured in the L2:pa complexes. The differences in cavity size are not a significant as in the previous complexes but the S inclusion complex is, overall, slightly bigger than the corresponding R complex. As measured by the g parameter the cavities of both the complexes are ~10 Å. The average hydrogen bond length for the R-pa complex is 2.06 Å and it is 1.97 Å for the S complex which is only a 0.09 Å difference. This does not indicate that the difference in the observed fluorescence for the complexation of the R and S enantiomers is due to the strength or type of hydrogen bonding patterns formed.

Point (2) shall now be expanded upon; the differences between two chiral amines interacting with the same calix[4]arene. L1. as has already been mentioned, displayed strong quenching when interacting with pg but not with pa. These two chiral amines only differ by a methylene spacer group but this seems to be crucial in the positioning of the phenyl group of the amine in proximity to the naphthalene group that causes the quenching of the fluorescence signal (as discussed in **Section 1.13**). There is still a strong

interaction occurring between L1 and the pa molecule, but as no quenching is obtained during the process, no definitive conclusions can be inferred. As stated previously, it is possible for binding to occur without quenching also taking place.

For pa the presence of this methylene spacer does not effect the fluorescence quenching due to the extra length of L2's pendant groups. Therefore, quenching is obtained using both chiral amines. However, it can be seen experimentally that enantioselective complexation is not occurring for pg and molecular modelling data gives an insight into why this is so. Both enantiomers of the amine are equally as efficiently complexed.

Table 31 shows the length of each of the hydrogen bonds found in all the complexes modelled. Note that the numbering of the hydrogen bonds in corresponding R and S enantiomers does not necessarily refer to the same bond as different atomic groups are involved in some of the bonds formed. As can be seen for the L1-pa and the L1-pg complexes the main bond lengths are on par with each other. In the case of the R enantiomer of L1-pg two extra, longer, bonds are also formed which may be the underlying reason for the observed enantioselective complexation.

| Inclusion complex | Distance (Å) | |
|-------------------|--------------|-----------|
| | R | S |
| L1-pg | (1) 1.960 | (1) 1.989 |
| | (2) 1.885 | (2) 1.897 |
| | (3) 1.950 | (3) 1.857 |
| | (4) 2.279 | – |
| | (5) 2.095 | – |
| L1-pa | (1) 1.795 | (1) 1.962 |
| | (2) 2.060 | (2) 2.032 |
| | (3) 1.905 | (3) 1.833 |
| L2-pg | (1) 1.977 | (1) 2.154 |
| | (2) 2.266 | (2) 1.790 |
| | (3) 1.998 | (3) 1.805 |
| | (4) 1.792 | (4) 1.823 |
| L2-pa | (1) 1.957 | (1) 1.933 |
| | (2) 2.333 | (2) 2.218 |
| | (3) 1.925 | (3) 1.774 |
| | (4) 2.028 | (4) 1.961 |

Table 31. Hydrogen bond distances for interactions formed between the host and the guest molecules in studied inclusion complexes.

As can be seen for L2-pg for every bond of corresponding length, the bonds formed with the S enantiomer are slightly shorter than those for the R. This suggests that stronger bonds are formed and it is also reflected in the fluorescence selectivity data. On the same basis, for the L2-pa complex there is stronger binding of the S-enantiomer. This increase in the binding strength may also lead to, and energetically compensate for the fact that,

the phenyl group of the chiral amine being directed outside the central cavity of the calixarene and interacting with just one of the naphthalene groups. As can be seen from this example, a stronger interaction with the included amine does not necessarily lead to a greater amount of quenching. The R-enantiomer being able to interact with more of the naphthalene groups could lead to the observed fluorescence quenching pattern.

3.4 CONCLUSIONS

With reference to the enantioselective complexation studies we have shown that by using molecular modelling software, an insight can be gained into the interactions that occur on complexation of chiral amines by chiral calixarenes. Prior to commencing the computational study we were unsure as to what interactions were occurring between the calixarene and pg/pa, where the chiral amine was positioned in the calixarene and the reason as to why one enantiomer was preferred over the other. Now, by observing the hydrogen bonding patterns formed between the host and guest we can postulate why one enantiomer interacts more strongly than the other and hence provide a plausible explanation for the observed enantiomeric selectivity observed in the fluorescence quenching experiments. In particular, we can give a possible rationalisation as to why the fluorescence signal changes to such a great extent when the (S) dinaphthyl prolinol calix[4]arene interacts with pg as opposed to pa.

Further studies (also NMR and IR work) are ongoing into the binding mechanisms and enantioselectivities of a group of related chiral amines to investigate if this molecular modelling procedure can be applied to a wide group of chiral amines and to other small chiral guest molecules.

The growing need for enantiomerically pure chiral compounds for use in the medical and research areas will drive further research in this field. The ability of molecular mechanics to provide a picture of the possible interactions occurring in

host:guest complexation should make it a valuable tool from a predictive and mechanistic viewpoint. Advances are still continuing in many areas that will make 3D structural visualisation more generally applicable.

(1) The parameter sets available, for bond length, angle, hydrogen bonding interactions, etc. As the sophistication and power of the experimental techniques (i.e. NMR, X-ray crystallography, etc) for probing the detailed structure of molecules increases more accurate and reliable data will be made available for the parameterisation process.

(2) Currently the functional form of the molecular mechanics force field equations has to be very simple (i.e. Hookes Law) in order to facilitate the completion of calculations in a reasonable amount of time. More complex equations can be used as increasingly more powerful computers come on the market.

(3) The computational power price to performance ratio over the last 50 years has increased by an order of magnitude every 5-7 years.

(4) High-resolution graphics aid in the visualisation and manipulation of modelled structures.

(5) MM/Quantum mechanics methodologies are continually in development. They enable one to treat the region of interest at an ab initio/DFT level of theory while the remainder of the molecule is modelled utilising molecular mechanics methods. This allows larger, more complex, systems to be studied.

(6) More efficient algorithms for accurately and quickly determining the global minimum and nearby local minima, i.e. efficient sampling of configuration space, are constantly being produced.

(7) Methods for the more effective treatment of solvation are needed. Many solvents are not available in the current software packages; both pure solvent and mixed solvent systems. Faster algorithms for the explicit inclusion of solvent molecules are needed.

(8) Our understanding of chiral interactions at a mechanistic level needs to deepen. Improvements in various spectroscopic techniques are aiding in this exploration.

With these advances in mind, in the future it may be possible to tailor-make a chiral calixarene on a computer, adjust its interacting moieties so that it will specifically complex the desired enantiomer of a chiral molecule and, as calixarene synthetic methods have been efficiently optimised, it should be possible to then synthesise the desired calixarene.

As the technology already exists for the incorporation of calixarenes into ion-selective electrodes and solid-state sensors [346], and as has been demonstrated, there is a lot of ongoing research in the area of preparing calixarene derivatives containing fluorophores and chromophores, in the near future, accurate and sensitive sensors for the detection of chiral neutral molecules should be available.

4 IONIC LIQUIDS

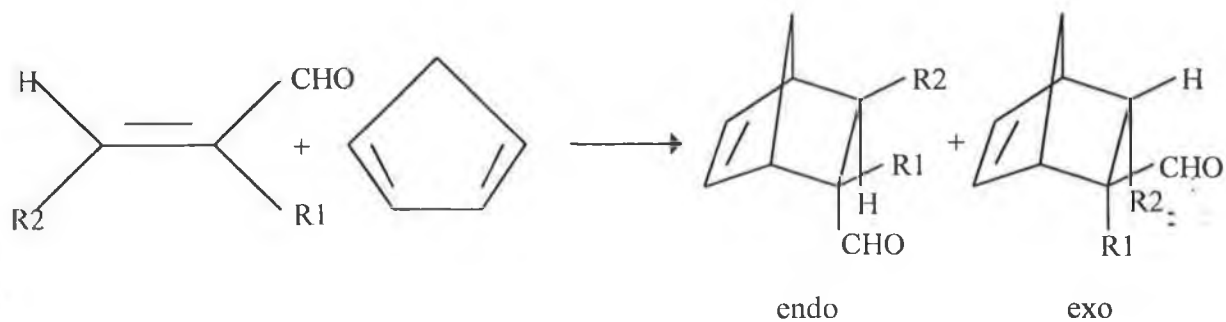
4.1 INTRODUCTION

Now we will discuss the first example of the usage of dialkylimidazolium salts ($R_2Im^+X^-$) as heterogeneous and homogeneous Lewis acids in the Diels-Alder reaction [347]. This class of compound is otherwise known as Ionic Liquids [348], but they can also have the form of low melting point solids.

There has been interest in these compounds previously, but this mainly deals with their physical properties, such as conductivity [349] and stability [350], and also their use in polymerisation and hydrogenation catalysis[351][352]. Unlike these ionic liquids, we are interested in use of water stable salts such as dialkylimidazolium bromides and trifluoroacetates as the catalytic Lewis acid centre rather than using these ionic liquids as solvents for Lewis acids or other reactive species as has been the case to date.

4.2 EXPERIMENTAL

The Lewis acidity of three dialkylimidazolium salts, compounds **1-3** (**Figure 87**), was investigated in the Diels- Alder reaction between crotonaldehyde **4** or methacrolein **5** with cyclopentadiene **6**, **Scheme 1**. The diethylimidazolium bromide **1** was produced in a yield of 46% and the diethylimidazolium trifluoroacetate **2** was produced in 89% yield from **1** on addition of silver trifluoroacetate to an aqueous solution of **1** following the method of Harlow et al. [353] The chiral imidazolium bromide **3** was synthesised in a manner similar to **1**, in a 21% yield by heating the readily available S-(+)-1-bromo-2-methylbutane with TMS-imidazole at reflux temperature.



4 R1 = H, R2 = Me

5 R1 = Me, R2 = H

7 R1 = H, R2 = Me

8 R1 = Me, R2 = H

Scheme 1. Reactants and products of the investigated Diels-Alder reactions.

4.2.1 NMR data

¹H-NMR data for **1**:- (400mhz, Acetone d₆) 10.25 [1H, s, 2-CH (Im)], 7.75 [2H, t, J=2.2Hz, 4- and 5-CH(Im)], 4.42 (4H, q, J=9.2Hz, NCH₂), 1.56 (6H, t, J=9.2 Hz, CH₂CH₃) ppm; ¹³C-NMR data for **1**:- (100mhz, Acetone d₆) 15.42, 41.98, 128.42, 136.93 ppm.

¹H-NMR data for **2**:- (400mhz, Acetone d₆) 9.97 [1H, s, 2-CH (Im)], 7.85 [2H, t, J=2.0Hz, 4- and 5-CH (Im)], 4.42 (4H, q, J=9.2Hz, NCH₂), 1.56 (6H, t, J=9.2Hz, CH₂CH₃) ppm; ¹³C-NMR data for **2**:- (100mhz, Acetone d₆) 13.91, 44.35, 121.59, 134.31 ppm.

¹H-NMR data for **3**:- (400mhz, Acetone d₆) 0.93 (6H, t, J=7.4Hz, 4'-CH₃), 1.25 (2H, m, 3'-CH₂), 1.4 (2H, m, 3'-CH₂), 2.1 (6H, d, J=6.9Hz, 2'-CHCH₃ overlapping 2H, m, 2'-CH), 4.38 (4H, m, NCH₂), 7.88 [2H, s, 4- and 5- CH (Im)], 10.03 [1H, s, 2-H (Im)] ppm; ¹³C-NMR data for **3**:- (100mhz, Acetone d₆) 10.47, 15.88, 20.89, 25.83, 35.15, 122.26, 136.56 ppm. [α]_D²⁵ = +19° (c = 6, CHCl₃).

4.2.2 Experimental procedure

The dialkylimidazolium salts, **1**, **2** or **3** (0.2 equivalents) were stirred in dichloromethane for 48 h with the dienophile **4** or **5** (1.0 equivalent) and the diene (5.0 equivalent), at -25°C , under nitrogen. All six reactions produced **7** or **8** (endo or exo) in yields between 35 and 40%. The endo:exo selectivities for the crotonaldehyde/cyclopentadiene reactions were always greater than 15:85 (endo:exo ratios were determined by proton NMR from the integration ratios of the aldehydic protons). The control reactions between methacrolein or crotonaldehyde and cyclopentadiene without the dialkylimidazolium salt present gave no product after 48h at -25°C .

4.3 RESULTS AND DISCUSSION

These results clearly show that these dialkylimidazolium salts act as Lewis acids, both in the way that they catalyse the two Diels-Alder reactions at low temperature and the high endo:exo selectivities relative to the non catalysed reactions.

However, as shown in **Table 32**, the yields show that they are weak Lewis acids, but there is obvious scope to increase the Lewis acidity by the use of electron withdrawing groups, such as chloro, bromo, cyano and nitro, on the carbons of the imidazole ring or an aryl/alkyl sulfonyl group on one of the nitrogen atoms in the ring.

Dienophile

| Dialkylimidazolium Salt | Crotonaldehyde | Methacrolein |
|-------------------------|----------------|--------------|
| 1 | 35%; 95:5 | 40%; 15:85 |
| 2 | 37%; 95:5 | 40%; 13:87 |
| 3 | 36%; 93:7 | 36%; 10:90 |

Table 32. Results (Yield%; Endo:Exo Ratio) for the Diels-Alder reaction between cyclopentadiene and crotonaldehyde or methacrolein in the presence of dialkylimidazolium salts **1**, **2** or **3**.

An interesting property of the dialkylimidazolium salt **1** is the ease with which it can be recycled under heterogeneous conditions. The above reactions were carried out in dichloromethane, in which **1** is soluble. However, ionic liquid **1** does not dissolve in diethyl ether and remains fluid at -25°C . A heterogeneous reaction between crotonaldehyde and cyclopentadiene in the presence of **1**, under the same conditions as before, except substituting diethyl ether for dichloromethane as the reaction solvent, gave a 25% yield of the product **7** (endo and exo). The diethyl ether layer was decanted off and the remaining **1** was washed with further diethyl ether. This process was repeated four more times and gave approximately the same yield of products (24, 23, 23 and 21% respectively).

Attempts at using N,N-di(2'S-2'-methylbutane)imidazolium bromide **3** as a catalyst were not successful as the enantiomeric excesses achieved in the reactions (**Scheme 1**) were less than 5% (as determined by chiral GC).

This class of compound shows great potential as catalysts in a variety of Lewis acid mediated reactions such as Claisen rearrangements [354], the ene reaction [355] and cyanohydrin formation [356]. Research is continuing in these areas.

5 BIBLIOGRAPHY

1. Molecular Mechanics, U. Burkett and N.L. Allinger, ACS Monograph, 1982.
2. Introducing Molecular Mechanics into the Undergraduate Chemistry Curriculum, W.J. Hehre and J.E. Nelson, Wavefunction Inc., 1997.
3. Experiments in Computational Chemistry, W.J. Hehre, L.D. Burke, A.J., Shusterman and W.J. Pietro, Wavefunction Inc., 1993.
4. A Laboratory Book of Computational Organic Chemistry, W.J. Hehre, A.J. Shusterman and W.W. Huang, Wavefunction Inc., 1996.
5. Molecular Interactions, From van der Waals to Strongly Bound Complexes, S. Schiner, (Ed.) Wiley Tutorial Series, 1995.
6. Frontiers in Supramolecular Organic Chemistry and Photochemistry, H.-J. Schneider and H. Dürr, (Eds.) VCH Verlagsgesellschaft mbH, 1991
7. Accurate Molecular Structures. Their Determination and Importance, A. Domenicano and I. Harigittai, (Eds.).
8. Modeling the Hydrogen Bond, D.A. Smith, (Ed.) ACS Symposium Series 569, 1994.
9. Molecular Modelling and Drug Design, J.G. Vinter and M. Gardner, (Eds.) Topics in Molecular and Structural Biology, MacMillan.
10. Computational Chemistry using the PC, D.W. Rogers, VCH Publishers (UK) Ltd., 1990.
11. Chemistry with Computation, W.J. Hehre and W.W. Huang, Wavefunction Inc., 1995.
12. Modelling Molecular Structures, A. Hinchcliffe, Wiley Tutorial Series in Theoretical Chemistry, 1996.
13. Introduction to Computational Chemistry, F. Jensen, John Wiley & Sons Ltd., Chichester, England, 1999.
14. Molecular Modelling. Principles and Applications, A.R. Leach, Longman, 1996.
15. A Computational Approach to Chemistry, D.M. Hirst, Blackwell, 1990.

16. *A Handbook of Computational Chemistry*, T. Clark, Wiley, 1985.
17. *Computational Chemistry*, G.H. Grant and W.G. Richards, Oxford University Press, 1995.
18. *The Determination of Molecular Structure*, P.J. Wheatley, Dover Publications, New York, 2nd Edition, 1968.
19. *Principles and Methods in Supramolecular Chemistry*, H.-J. Schneider and A. Yatsimirsky, Wiley, 2000.
20. *Luminescence Techniques in Chemical and Biochemical Analysis*, W.R.G. Baeyens, D. de Keukeleine and K. Korkidis (Eds.), Marcel Dekker, 1991.
21. *Calixarenes Revisited*, G.D. Gutsche, The Royal Society of Chemistry, 1998.

6 REFERENCES

1. Dirac, P.A.M., *Proc. Roy. Soc.*, **1929**, A123, 714-733.
2. Bauschlicher Jr., C.W. and Langhoff, S.R., *Science*, **1991**, 254, 394-398.
3. Andrews, D.H., *Phys. Rev.*, **1930**, 36, 544-554.
4. (a) Hill, T.L., *J. Chem. Phys.*, **1946**, 14, 465; (b) Dostrovsky, I., Hughes, E.D. and Ingold, C.K., *J. Chem. Soc.*, **1946**, 173-194; (c) Westheimer, F.H. and Mayer, J.E., *J. Chem. Phys.*, **1946**, 14, 733-738; see also, (d) de la Mare, P.B.D., Fowden, L., Hughes, E.D., Ingold, C.K. and Mackie, J.D.H., *J. Chem. Soc.*, **1955**, 3200-3236; (e) Westheimer, F.H., Calculation of the magnitude of steric effects. In: "Steric Effects in Organic Chemistry", Newman, M.S., (Ed.) Wiley, New York, 1956, 523-555.
5. Hendrickson, J.B., *J. Am. Chem. Soc.*, **1961**, 83, 4537-4547.
6. Wilberg, K.B., *J. Am. Chem. Soc.*, **1965**, 87, 1070-1078.
7. CRC Handbook, 74th Edition.
8. Allinger, N.L., *J. Am. Chem. Soc.*, **1977**, 99, 8127.
9. Jensen, F., "Introduction to Computational Chemistry", John Wiley & Sons Ltd., Chichester, England, 1999, p. 31.
10. *ibid*, p. 42.
11. Lipkowitz, K.B., *J. Chem. Ed.*, **1995**, 72, 1070-1075
12. Howard, A.E., Singh, U.C., Billeter, M. and Kollman, P.A., *J. Am. Chem. Soc.*, **1988**, 110, 6984-6991.
13. Hendrickson, J.B., Cram, D.J. and Hammond, G.S., "Organic Chemistry", McGraw-Hill, New York, 1970. For a comprehensive listing of bond lengths see: Allen, F.H. et al. *J. Chem. Soc., Perkins Trans. II*, **1987**, S1-S19.

-
14. Scheraga, H. A., "Peptides: Proceedings of the Fifth American Peptide Symposium", Goodman, M. and Meienhofer, J., (Eds.) John Wiley & Sons, New York, 1977.
 15. Fitzwater, F. and Bartell, L.S., *J. Am. Chem. Soc.*, **1976**, *98*, 5107.
 16. Morley, S.D, Abraham, R.J., Haworth, I.S., Jackson, D.E., Saunders, MR. and Vinter, J.G., *J. Comp. -Aided Mol. Design*, **1991**, *5*, 475.
 17. (a) Schreiber, H. and Steinhauser, O., *Biochemistry*, **1992**, *31*, 5856-5860; (b) Schreiber, H. and Steinhauser, O., *Chem. Phys.*, **1992**, *168*, 75-89.
 18. Steinbach, P.J. and Brooks, B.R., *J. Comput. Chem* , **1993**, *15*, 667-683.
 19. Maple, J.R., Dinur, U. and Hagler, A.T., *Proc. Natl Acad. Sci. USA*, **1988**, *85*, 5350.
 20. Alemán, C. and Orozco, M., *J. Comp-Aided Mol. Design*, **1992**, *6*, 331.
 21. Sharp, K.A. and Honig, B. *Annu. Rev. Biophys. Biophys. Chem.*, **1990**, *19*, 301-332.
 22. Gilson, M.K., *Curr. Biol.*, **1995**, *5*, 216-223.
 23. (a) Allinger, N.L., *J. Am. Chem. Soc.*, **1977**, *99*, 8127-8134 (Conformational analysis on hydrocarbons).
 24. (a) Aped, P. and Allinger, N.L., *J. Am. Chem. Soc.*, **1992**, *114*, 1-16 (Cyclopropanes); (b) Shen, M.Z., Schaefer, H.F., Liang, C.X., et al., *J. Am. Chem. Soc.*, **1992**, *114*, 497-505 (Adamantane); (c) Allinger, N.L., Yuh, Y.H. and Lii, J.H., *J. Am. Chem. Soc.*, **1989**, *111*, 8551-8566.
 25. (a) Allinger, N.L., Chen, K. and Lii, J.H.. *J. Comp. Chem.*, **1996**, *17*, 642-668; (b) Storer. J.W. and Houk, K.N.. *J. Am. Chem. Soc.*, **1992**, *114*, 1165-1168 (Study on triquinacone and its hydrogenation products to see if it is homoaromatic).
 26. (a) Scott, R.A. and Scheraga, H.A., *J. Chem. Phys.*, **1966**, *45*, 2091; (b) Weiner, P. and Kollman, P.A., *J. Comput. Chem.*, **1981**, *2*, 287-303; (c) Weiner, S.J., Kollman, P.A., Case, D.A., Singh, U.C., Ghio, C., Alagona, G., Profeta, S. Jr. and Weiner, P.K., *J. Am. Chem. Soc.*, **1984**, *106*, 765-784; (d)

-
- Singh, U.C., Weiner, P.K., Caldwell, J. and Kollman, P.A., AMBER 3.0, University of California-San Francisco, 1987.
27. Kollman, P.A., Weiner, P. and Dearing, A., *Biopolymers*, **1981**, 20, 2583-2621.
 28. Brooks, B. R., Bruccoleri, R.E., Olafson, B.D., States, D.J., Swaminathan, S. and Karplus, M., *J. Comp. Chem.*, **1983**, 4, 187-217.
 29. Clark, M., Cramer, R.D. and van Opdenbosch, N., *J. Comput. Chem.*, **1989**, 10, 982.
 30. (a) Hermans, J., Berendsen, H.J.C., van Gunstern, W.F. and Postma, J.P.M., *Biopolymers*, **1984**, 23, 1513-1518; (b) van Gunstern, W.F. and Berendsen, H.J.C., "Groningen Molecular Simulation (GROMOS) Library Manual"; Biomos, Nijenborgh 4, 9747 AG Groningen, The Netherlands, 1987.
 31. Pettersson I. and Liljefors, T., "Reviews in Computational Chemistry", Vol. 9, 1996, VCH Publishers, p. 167-189.
 32. (a) van Gunsteren, W.F. and Berendsen, H.J.C. *Angew. Chem., Int. Ed. Engl.*, **1990**, 29, 992-1023; (b) Pillardy J., Czaplowski C., Wedemeyer W.J. and Scheraga H.A., *Helv. Chim. Acta*, **2000**, 83, (9) 2214-2230; (c) Kostrowicki, J. and Scheraga, H.A., *J. Phys. Chem.*, **1992**, 96: (18) 7442-7449.
 33. (a) Straatsma, T.P. and McCammon, J.A., *Annu. Rev. Phys. Chem.*, **1992**, 43, 407-437 (Free energy calculations using MD/MC); (b) Billeter, M., Howard, A.E., Kuntz, I.D. and Kollman, P.A., *J. Am. Chem. Soc.*, **1988**, 110, 8395-8391.
 34. Chang, G., Guida, W.C. and Still, W.C., *J. Am. Chem. Soc.*, **1989**, 111, 4379-4386.
 35. (a) Fischer, S. and Karplus, M., *Chem. Phys. Lett.*, **1992**, 194, 252-261 (Algorithm for finding reaction pathways and transition states); (b) Beusen, D.D., Shands, E.F.B., Karasek, S.F., Marshall, G.R. and Dammkoehler, R.A., *J. Molec. Struct., Theochem*, **1996**, 370, 157-171 (A review of systematic search algorithms).

-
36. Verlet, L., *Phys. Rev.*, **1967**, 159, 98.
 37. Ryckaert, J.P., Ciccotti, G. and Berendsen, H.J.C., *J. Comp. Phys.*, **1977**, 23, 327.
 38. Berendsen, H.J.C., Postma, J.P.M., van Gunsteren, W.F., DiNola, A. and Haak, J.R., *J. Chem. Phys.*, **1984**, 81, 3684.
 39. Auffinger, P. and Wipff, G., *J. Comp. Chem.*, **1990**, 11, 19-31.
 40. Metropolis, N., Rosenbluth, A.W., Rosenbluth, M.N. and Teller, A.H., *J. Chem. Phys.*, **1953**, 21, 1087-1092.
 41. Clementi, E., Corongiu, G., Lie, G.C., Niesar, U. and Procacci, P., In: "Modern Techniques in Computational Chemistry": MOTTECC-89, Clementi, E., (Ed.) 1989, ESCOM, Leiden, p. 368.
 42. Saunders, M., Houk, K.N., Wu, Y.-D., Still, W.C., Lipton, M., Chang, G. and Guida, W.C., *J. Am. Chem. Soc.*, **1990**, 112, 1419-1427.
 43. Treasurywala, A.M., Jaeger, E.P. and Peterson, M.L., *J. Comput. Chem.*, **1996**, 17, 1171-1182.
 44. Leach, A.R., A survey of methods for searching the conformational space of small and medium sized-molecules, In: "Reviews in Computational Chemistry", Lipkowitz, K.B. and Boyd, D.B., (Eds.), Vol. 2, VCH, New York, 1991, p.1-55.
 45. Meza, J.C., Judson, R.S., Faulkner, T.R. and Treasurywala, A.M., *J. Comput. Chem.*, **1996**, 17, 1142-1151.
 46. (a) Judson, R.S., Colvin, M.E., Meza, J.C., Huffer, A. and Gutierrez, *Int. J. Quant. Chem.*, **1992**, 44, 277-290; (b) Meza, J.C. and Martinez, J., *J. Comput. Chem.*, **1994**, 15, 627-632.
 47. (a) Clark, D.E., Jones, G., Willet, P., Kenney, P.W. and Glen, R.C., *J. Chem. Inf. Comput. Sci.*, **1994**, 34, 197; (b) Gunn, J.R., Monge, A., Friesner, R.A. and Marshall, C.H., *J. Phys. Chem.*, **1994**, 98, 702.
 48. Shenkin, P.S., Yarmush, D.L., Fine, R.M., Wang, H. and Levinthal, C., *Biopolymers*, **1987**, 26, 2053.

-
49. (a) Ferguson, D.M. and Raber, D.J., *J. Am. Chem. Soc.*, **1989**, 111, 4371-4378; (b) Saunders, M., Houk, K.N., Wu, Y.-D., Still, W.C., Lipton, M., Chang, G. and Guida, W.C., *J. Am. Chem. Soc.*, **1990**, 112, 1419-1427; (c) Head, M.S., Given, J.A. and Gilson, M.L., *J. Phys. Chem.*, **1997**, 101, 1609-1618.
 50. Kirkpatrick, S, Gelatti, C. D. Jr. and Vecchi, M. P. *Science* (Washington D.C.), **1983**, 220, 671.
 51. Pannetier, J., *Inst. Phys. Conf. Ser. No. 107*, **1990**, Chapter 1, 23-44.
 52. Morley, S.D., Jackson, D.E., Saunders, M.R. and Vinter, J.G., *J. Comp. Chem.*, **1992**, 13, 693-703.
 53. Wilberg, K.B. *J. Am. Chem. Soc.* **1965**, 87, 1070.
 54. Allinger, N.L., Miller, M.A., Van Catledge, F.A. and Hirsch, J.A., *J. Am. Chem. Soc.*, **1967**, 89, 4345.
 55. White, D.N.J. and Ermer, O., *Chem. Phys. Lett.*, **1975**, 31, 111.
 56. Schlick, T., Optimization Methods in Computational Chemistry, In: "Reviews in Computational Chemistry", Vol. 3, Lipkowitz, K.B. and Boyd, D.B., (Eds.) VCH, New York, 1992, p. 1-71.
 57. Simulating Solvent and Dielectric Effects, Warshel A. and Russell S.T. in: Molecular Dynamics and Protein Structure, Herman, J., (Ed.), Polycrystal Book Service, Western Springs, Illinois, 1985, p. 23.
 58. Sciortine, F., Geiger, A. and Stanley, H.E., *Nature*, **1991**, 354, 218-221.
 59. Pitera, J. and Kollman, P., *J. Molec. Graph. Model.*, **1997**, 15, 355-358.
 60. Wong, M.W., Frisch, M.J. and Wiberg, K.B., *J. Am. Chem. Soc.*, **1991**, 113, 4776-4782.
 61. Still, W.C., Tempczyk, A., Hawley, R.C. and Hendrickson, T., *J. Am. Chem. Soc.*, **1990**, 112, 6127-6129.
 62. Eliel, E.L., Allinger, N.L., Angyal, S.J. and Morrison, G.A., "Conformational Analysis", Wiley-Interscience, New York, 1965.

-
63. Briggs, J.M., Matsui, T. and Jorgensen, W.L., *J. Comp. Chem.*, **1990**, 11, 958-971, and References [2-16] therein.
64. (a) Jorgensen, W.L., *J. Am. Chem. Soc.*, **1981**, 103, 335-340; (b) Jorgensen, W.L., *J. Am. Chem. Soc.*, **1981**, 103, 341-345; (c) Jorgensen, W.L., *J. Am. Chem. Soc.*, **1981**, 103, 345-350.
65. Jorgensen, W.L., Madura, J.D. and Swenson, C.J., *J. Am. Chem. Soc.*, **1984**, 106, 6638-6646.
66. (a) Jorgensen, W.L. and Tirado-Rives, J., *J. Am. Chem. Soc.*, **1988**, 110, 1657-1666; (b) Tirado-Rives, J. and Jorgensen, W.L., *J. Am. Chem. Soc.*, **1990**, 112, 2773-2781.
67. Hunter, C.A. and Saunders, J.K.M., *J. Am. Chem. Soc.*, **1990**, 112, 5525-5534.
68. Legon, A.C. and Millen, D.J., *Can. J. Chem.*, **1989**, 67, 1683-1686.
69. (a) Böhm, H.J. and Brode, S., *J. Am. Chem. Soc.*, **1991**, 113, 7129-7135; (b) Wiberg, K.B., Hadad, C.M., Breneman, C.M., Laidig, K.E., Murcko, M.A. and LePage, T.J., *Science*, **1991**, 252, 1266-1272.
70. Mulliken, R.S., *J. Chem. Phys.*, **1955**, 23, 1833, 1841, 2338, 2343.
71. (a) Chirlian, L.E. and Francl, M., *J. Comp. Chem.*, **1987**, 8, 894; (b) Breneman, C.M. and Wilberg, K.B., *ibid*, **1990**, 11, 361.
72. Yates, P.C. and Richardson, C.M., *J. Molec. Struct., Theochem.*, **1996**, 363, 17-22.
73. Reviews: (a) Arnaud-Neu, F. and Schwing-Well, M.-J., *Synth. Metals*, **1997**, 157-164; (b) Shinkai, S., *Tetrahedron*, **1993**, 49, 8933-8968.
74. (a) Araki, K., Iwamoto, K., Shinkai, S. and Matsuda, T., *Chem. Lett.*, **1989**, 1747; (b) Iwamoto, K., Araki, K. and Shinkai, S., *J. Org. Chem.*, **1991**, 56, 4956-4962.
75. (a) Harada, T. and Shinkai, S., *J. Chem. Soc., Perkin Trans. 2*, **1995**, 2231-2242; (b) Bayard, F., Decoret, C., Pattou, D., Royer, J., Satrallah, A. and Vicens, J., *J. Chim. Phys.*, **1989**, 86, 945; (c) Grüttner, C., Böhmer, V., Vogt,

-
- W., Thondorf, I., Biali, S. and Grynszpan, F., *Tetrahedron Lett.*, **1994**, 35, 6267.
76. (a) Varnek, A. and Wipff, G., *J. Mol. Struct., Theochem.*, **1996**, 363, 67-85; (b) Grote Gansey, M.H.B., Verboom, W., van Veggel, F.C.J.M., Vetrogon, V., Arnaud-Neu, F., Schwing-Weill, M.-J. and Reinhoudt, D.N., *J. Chem. Soc., Perkin Trans. 2*, **1998**, 2351-2360; (c) Lamare, V., Dozol, J.-F., Fuangswasdi, S., Arnaud-Neu, F., Thuéry, P., Nierlich, M., Asfari, Z. and Vicens, J., *J. Chem. Soc., Perkin Trans. 2*, **1999**, 271-284; (d) Arnaud-Neu, F., Barbosa, S., Berny, F., Casnati, A., Muzet, N., Pinalli, A., Ungaro, R., Schwing-Weill, M.-J. and Wipff, G., *J. Chem. Soc., Perkin Trans. 2*, **1999**, 1727-1738.
77. Thondorf, I. and Brenn, B., *J. Chem. Soc., Perkin Trans. 2*, **1997**, 2293-2299.
78. Lipkowitz, K.B. and Pearl, G., *J. Org. Chem.*, **1993**, 58, 6729-6736.
79. Thondorf, I. and Brenn, J., *J. Molec. Struct.*, **1997**, 307-314.
80. Gundertofte, K., Palm, J., Pettersson, I. and Stamvik, A., *J. Comput. Chem.*, **1991**, 12, 200-208.
81. Grootenhius, P.D.J., Kollman, P.A., Groenen, L.C., Reinhoudt, D.N., van Hummel, G.J., Ugozzoli, F. and Andreotti, G.D. *J. Am. Chem. Soc.*, **1990**, 86, 945.
82. (a) Bayard, F., Decoret, C., Pattou, D., Royer, J., Satrallah, A. and Vicens, J., *J. Chim. Phys.*, **1989**, 86, 945; (b) Royer, J., Bayard, F. and Decoret, C., *J. Chim. Phys.*, **1990**, 87, 1695.
83. (a) Groenen, L.C., van Loon, J.-D., Verboom, W., Harkema, S., Casnati, A., Ungaro, R., Pochini, A., Ugozzoli, F. and Reinhoudt, D.N., *J. Am. Chem. Soc.*, **1991**, 113, 2385; (b) Groenen, L.C., Brunink, J.A.J., Bakker, W.I.I., Harkema, S., Wijmenga, S.S. and Reinhoudt, D.N., *J. Chem. Soc., Perkin Trans. 2*, **1992**, 1899.
84. Thondorf, I., Brenn, J., Brandt, W. and Bhömer, V., *Tetrahedron Lett.*, **1995**, 36, 6665.

-
85. Neri, P., Ferguson, G., Gallagher, J.F. and Pappalardo, S., *Tetrahedron Lett.*, **1992**, 33, 7403.
86. Drew, M.G.B, In: "Spectroscopic and Computational Studies of Supramolecular Systems", Davies, J.E. (Ed.), Kluwer Academic Publishers, 1992, p. 207.
87. Thondorf, I., Hillig, G., Brandt, W., Brenn, J., Barth, A. and Böhmer, V., *J. Chem. Soc. Perkin Trans.*, **1994**, 2259-2267.
88. (a) Groenen, L.C., van Loon, J.-D., Verboom, W., Hakema, S., Casnati, A., Ungaro, R., Pochini, A., Ugozzoli, F. and Reinhoudt, J., *J. Am. Chem. Soc.*, **1991**, 113, 2385; (b) Grootenhuis, P.D.J., Kollman, P.A., Groenen, L.C., Reinhoudt, D.N., van Hummel, G.J., Ugozzoli, F. and Andreete, G.D., *J. Am. Chem. Soc.*, **1990**, 112, 4165; (c) Fisher, S., Grootenhuis, P.D.J., Groenen, L.C., van Hoorn, W.P., van Veegel, F.C.J., Reinhoudt, D.N. and Karplus, M., *J. Am. Chem. Soc.*, **1995**, 117, 1611-1620.
89. (a) Williams, R.M., Verhoeven, J.W., *Recl. Trav. Chim. Pays-Bas*, **1992**, 11, 531-532; (b) Constable, E.C., *Angew. Chem. Int., Ed. Engl.*, **1994**, 33, 2269-2271; (c) Atwood, J.L., Koutsantonis, G.A. and Raston, C.L., *Nature*, **1994**, 368, 229-231.
90. Schlachter, I., Höweler, U., Iwanek, W., Urbaniak, M. and Mattay, J., *Tetrahedron*, **1999**, 55, 14931-14940.
91. Harada, T. and Shinkai, S., *J. Chem. Soc., Perkin Trans. 2*, **1995**, 12, 2231-2242.
92. (a) Harada, T., Rudzinski, J.M. and Shinkai, S., *J. Chem. Soc. Perkin Trans. 2*, **1992**, 2109-2115; (b) Harada, T., Rudzinski, J.M., Osawa, E. and Shinkai, S., *Tetrahedron*, **1993**, 49, 5941-5954; (c) Thondorf, I. and Brenn, J., 3rd International Calixarene Conference, Texas, May, 1995 (Comparison of 4 force fields).
93. Benevelli, F., Kolodziejcki, W., Wozniak, K. and Klinowski, J., *Chem. Phys. Lett.*, **1999**, 308, 65-70.

-
94. Brzezinski, B., Bartl, F. and Zundel, G., *J. Phys. Chem. B*, **1997**, 101, 5611.
95. (a) Havlicek, I., Tkadlecova, M., Vyhnankova, M., Pinkhassik, E. and Stibor, I., *Coll. Czech. Chem. Commun.*, **1996**, 61, 1783; (b) Israeli, Y. and Detellier, C., *J. Phys. Chem.*, **1997**, 101, 1897.
96. Ahn, S., Chang, S.K., Kim, T. and Lee, J.W., *Chem. Lett.*, **1995**, 297.
97. (a) Ikeda, A., Tsuzuki, H. and Shinkai, S., *J. Chem. Soc., Perkin Trans. 2*, **1994**, 2073; (b) Harrowfield, J.M., Ogden, M.I., Richmond, W.R. and White, A.H., *J. Chem. Soc., Chem. Comm.*, **1991**, 1159-1161.
98. Shinkai, S., Araki, K.J., Matsuda, T. and Manabe, O., *Bull. Chem. Soc. Jpn.*, **1989**, 62, 3856.
99. Harada, T. and Shinkai, S., *J. Chem. Soc., Perkin Trans. 2*, **1995**, 2231.
100. Harrowfield, J.M., Ogden, M.I., Richmond, W.R. and White, A.H., *J. Chem. Soc., Chem. Commun.*, **1991**, 1159-1161.
101. Fenton, D.E., "Comprehensive Coordination Chemistry", McCleverty, J.A., Gillard, R.D. and Wilkinson, G. (Eds.) Pergamon Press, Oxford, 1987, Vol. 3, p. 1.
102. Asmuss, R., Böhmer, V., Harrowfield, J.M., Ogden, M.I., Richmond, W.R., Skelton B.W. and White, A.H., *J. Chem. Soc., Dalton Trans. 2*, **1993**, 2427.
103. Cox, B.G. and Schneider, H., "Coordination and Transport Properties of Macrocyclic Compounds in Solution", Elsevier, Amsterdam, 1992, Chapter 1.
104. Hamada, F., Robinson, K.D., Orr, G.W. and Atwood, J.L., *Supramol. Chem.*, **1993**, 2, 19.
105. Abidi, R., Baker, M.V., Harrowfield, J.M., Ho, D.S.C., Richmond, W.R., Skelton, B.W., White, A.H., Varnek, A. and Wipff, G., *Inorg. Chim. Acta*, **1996**, 246, 275-286.
106. Amino acid receptor: Tye, H., Eldred, C. and Wills, M., *J. Chem. Soc., Perkin Trans. 1*, **1998**, 457-465.

-
107. Current review: "Chemosensors of Ions and Molecular Recognition", Desvergne, J.-P. and Czarnik, A.W., (Eds.) NATO ASI Series C, Vol. 492, Kluwer Academic Press, Dordrecht, 1997.
108. Kyba, E.P. et al., *J. Am. Chem. Soc.*, **1977**, 99, 2564-2571.
109. (a) Kubo, Y., Marayama, S., Ohhara, N., Nakamura, M. and Tokita, S., *J. Chem. Soc. Chem. Commun.*, **1995**, 1727, and references therein; (b) Bauer, L.J. and Gutsche, C.D., *J. Am. Chem. Soc.*, **1985**, 107, 6063-6069; (c) Gutsche, C.D., Iqbal, M. and Alam, I., *J. Am. Chem. Soc.*, **1987**, 109, 4314-4320.
110. Zhang, X.X., Bradshaw, J.S. and Izatt, R.M., *Chem. Rev.*, **1997**, 97, 3313-3361.
111. Chung, T.D., Kang, S.K., Kim, J., Kim, H. and Kim, H., *J. Electro. Chem.*, **1997**, 438, 71-78.
112. Mohammed-Ziegler, I., Kubinyi, M., Grofcsik, A., Grün, A. and Bitter, I., *J. Molec. Struct.*, **1999**, 480-481, 289-292. Previous work: Kubinyi, M., Mohammed-Ziegler, I., Grofcsik, A., Bitter, I. and Jones, W.J., *J. Molec. Struct.*, **1997**, 408/409, 543-546.
113. (a) Arena, G., Contino, A., Gulino, F.G., Madri, A., Sansone, F., Sciotto, D. and Ungaro, R., *Tetrahedron Lett.*, **1999**, 40, 1597-1600; (b) Arena, G., Casnati, A., Contino, A., Sciotto, D. and Ungaro, R., *Chem. Eur. J.*, **1999**, 5, 738-744.
114. Previously synthesised sulfonated calixarenes: (a) Shinkai, S., Mori, S., Koreishi, H., Tsubaki, T. and Manabe, O., *J. Am. Chem. Soc.*, **1986**, 108, 2409; (b) Shinkai, S., Kawabata, H., Arimura, T., Matsuda, T., Satoh, H. and Manabe, O., *J. Chem. Soc. Perkin Trans. I*, **1989**, 1073; (c) Zhang, L., Macias, A., Lu, T., Gordon, J.I., Gokel, G.W. and Kaifer, A., *J. Chem. Soc., Chem. Comm.*, **1993**, 1017; 235; (d) Castro, R., Godnez, L.A., Criss, C.M. and Kaifer, A., *J. Org. Chem.*, **1997**, 62, 4928.

-
115. Sansone, F., Barbosa, S., Casnati, A., Sciotto, D. and Ungaro, R., *Tetrahedron Lett.*, **1999**, 40, 4741-4744.
116. Arduini, A., Fabbi, M., Mantovani, M., Mirone, L., Pochini, A., Secchi, A. and Ungaro, R., *J. Org. Chem.*, **1995**, 60, 1454-1457.
117. Unpublished results.
118. (a) Shimizu, K.D. and Rebek, J., Jr., *Proc. Natl. Acad. Sci. USA*, **1995**, 92, 12403-12407; (b) Mogck, O., Pons, M., Böhmer, V. and Vogt, W., *J. Am. Chem. Soc.*, **1997**, 119, 5706-5712; (c) Böhmer, V., Mogck, O., Pons, M. and Paulus, E.F., Reversible Dimerization of Tetraureas Derived from Calix[4]arenes, In: "NMR in Supramolecular Chemistry", Pons, M., (Ed.) NATO ASI Series, Ser. C, Kluwer Academic Publishers, Dordrecht, The Netherlands, 1999, Vol. 526, p. 45-60.
119. Castellano, R.K., Nuckolls, C. and Rebek, J., Jr., *J. Am. Chem. Soc.*, **1999**, 121, 11156-11163.
120. Crabbé, P., "ORD and CD in Chemistry and Biochemistry", Academic Press, New York, 1972.
121. (a) Dowden, J., Edwards, P.D., Flack, S.S. and Kilburn, J.D., *Chem. Eur. J.*, **1999**, 5, 79-89; (b) Costante-Crassous, J., Marrone, T.J., Briggs, J.M., McCammon, J.A. and Collet, A., *J. Am. Chem. Soc.*, **1997**, 119, 3818-3823.
122. Mogck, O., Böhmer, V. and Vogt, W., *Tetrahedron*, **1996**, 52, 8489.
123. Review: Rebek, J. Jr., *Chem. Commun.*, **2000**, 637-643.
124. Shimizu, K.D. and Rebek, J., Jr., *Proc. Nat. Acad. Sci.*, **1995**, 92, 12403-12407.
125. Mogck, O., Paulus, E.F., Böhmer, V., Thondorf, I. and Vogt, W., *Chem. Commun.*, **1996**, 253.
126. Scheerder, J., Vreekamp, R.H., Engbersen, J.F.J., Verboom, W., van Duynhoven, J.P.M. and Reinhoudt, D.N., *J. Org. Chem.*, **1996**, 61, 3476.
127. Chapman, K.T. and Still, W.C., *J. Am. Chem. Soc.*, **1989**, 111, 3075.

-
128. Castellano, R.K., Nuckolls, C. and Rebek, J. Jr., *J. Am. Chem. Soc.*, **1999**, 121, 11156-11163.
129. Pochini, A. and Ungaro, R., In: "Comprehensive Supramolecular Chemistry", Vol. 2, Vögtle, F., (Ed.) Pergamon Press, 1996, p. 103-142.
130. Alvarez, J., Wang, Y., Gómez-Kaifer, M. and Kaifer, A., *J. Chem. Soc., Chem. Comm.*, **1998**, 1455-1456.
131. Haino, T., Matsumura, K., Harano, T., Yamada, K., Saijyo, Y. and Fukazawa, Y., *Tetrahedron*, **1998**, 54, 12185-12196.
132. (a) "Comprehensive Supramolecular Chemistry", Vols. 2 and 4, Atwood, J.L., Davies, J.E.D., MacNicol, D.D., Vögtle, F. and Murakami, Y., (Eds.) Pergamon, Oxford, 1996; (b) Chen, H., Weiner, W.S. and Hamilton, A.D., *Curr. Opinion Chem. Biol.*, **1997**, 1, 458-466.
133. Peña, M.S., Zhang, Y., Thibodeaux, S., McLaughlin, M.L., del la Peña, A.M. and Warner, I.M., *Tetrahedron Lett.*, **1996**, 37, 5841-5844.
134. Sanchez-Peña, M., Zhang, Y. and Warner, I.M., *Anal. Chem.*, **1997**, 69, 3239.
135. Healy, L.O., McEnery, M.M., McCarthy, D.G., Harris, S.J. and Glennon, J.D., *Anal. Lett.*, **1998**, 31, 1543.
136. Mnuk, P., Feltl, L. and Schurig, V., *J. Chromatogr. A*, **1996**, 732, 63.
137. (a) Zhang, H., Dai, R., Ling, Y., Wen, Y., Zhang, S., Fu, R. and Gu, J., *J. Chromatogr. A*, **1997**, 787, 161-169; (b) Gross, B., Jauch, J. and Schurig, V., *J. Microcol. Sep.*, **1999**, 11, 4, 313-317.
138. Lai, X.H., Lin, L. and Wu, C.Y., *Chromatographia*, **1999**, 50, 1-2, 82-88.
139. Iki, N., Narumi, F., Suzuki, T., Sugawara, A. and Miyano, S., *Chem. Lett.*, **1988**, 10, 1065.
140. Pfeiffer, J. and Schurig, V., *J. Chromatogr. A*, **1999**, 840, 145-150.
141. Chen, L.-x., He, X.-w., Hu, X.-b. and Xu, H., *Analyst*, **1999**, 124, 1787-1790.
142. Bernardino, R.J., Costa Cabral, B.J. and Pereira, J.L.C., *J. Molec. Struct. Theochem*, **1998**, 455, 23-32.
143. Dhawan, D. and Gutsche, C.D., *J. Org. Chem.*, **1983**, 48, 1536.

-
144. Bavoux, C., Vocason, F., Perrin, M. and Lamartine, R., *J. Incl. Phenom. Mol. Recog. Chem.*, **1995**, 22, 119.
145. Marcos, P., Ascenso, J., Lamartine, R. and Pereira, J.L.C., *Tetrahedron*, **1997**, 53, 11791.
146. Santos, M.A., Marcos, P.M. and Pereira, J.L.C., *J. Molec. Struct.*, **1999**, 463, 21-26.
147. Thondorf, I., Brenn, J. and Böhmer, V., *Tetrahedron*, **1998**, 54, 12823-12828.
148. Review: Timmerman, P., Verboom, W. and Reinhoudt, D.N., *Tetrahedron*, **1996**, 52, 2663-2704.
149. Schalley, C.A., *Int. J. Mass Spec.*, **2000**, 194, 11-39.
150. Inokuchi, F., Miyahara, Y., Inazu, T. and Shinkai, S., *Angew. Chem., Int. Ed. Engl.*, **1995**, 35, 1364.
151. Armentrout, P.B., *Int. J. Mass Spec.*, **1999**, 193, 227-240.
152. (a) More, M.B., Glendening, E.D., Ray, D., Feller, D. and Armentrout, P.B., *J. Phys. Chem.*, **1996**, 100, 1605; (b) Ray, D., Feller, D., More, M.B., Glendening E.D. and Armentrout, P.B., *J. Phys. Chem.*, **1996**, 100, 16116; (c) More, M.B., Ray, D. and Armentrout, P.B., *J. Phys. Chem., A*, **1997**, 101, 831; (d) More, M.B., Ray, D. and Armentrout, P.B., *J. Phys. Chem., A*, **1997**, 101, 4254; (e) More, M.B., Ray, D. and Armentrout, P.B., *J. Phys. Chem., A*, **1997**, 101, 7007; (f) More, M.B., Ray, D. and Armentrout, P.B., *J. Phys. Chem. Soc.*, **1999**, 121, 417.
153. Hill, S.E., Glendening, E.D. and Feller, D., *J. Phys. Chem. A*, **1997**, 101, 6125.
154. Izatt, R.M., Terry, R.E., Haynmore, B.L., Hansen, L.D., Dalley, N.K., Avondet, A.G. and Christensen, J.J., *J. Am. Chem. Soc.*, **1976**, 98, 7620.
155. (a) More, M.B., Ray, D. and Armentrout, P.B., *J. Phys. Chem. A*, **1999**, 121, 417; (b) Glendening, E.D., Feller, D. and Thompson, M.A., *J. Am. Chem. Soc.*, **1994**, 116, 10657.

-
156. More, M.B., Ray, D. and Armentrout, P.B., *J. Phys. Chem. A*, **1997**, 101, 7007.
157. Feller, D., *J. Phys. Chem. A*, **1997**, 101, 2723.
158. Grootenhuis, P.D.J. and Kollman, P.A., *J. Am. Chem. Soc.*, **1989**, 111, 2152-2158.
159. (a) Salvatierra, D., et al., *Tetrahedron*, **2000**, 56, 3035-3041; (b) Li, X.-S., Liu, L., Guo, Q.-X., Chu, S.-D. and Liu, Y.-C., *Chem. Phys. Lett.*, **1999**, 307, 117-120.
160. Rizzarelli, E. and Vecchio, G., *Coord. Chem. Rev.*, **1999**, 118, 343-364.
161. Alvira, E., García, J.I. and Mayoral, J.A., *Chem. Phys.*, **1999**, 240, 101-108.
162. (a) Lipkowitz, K.B., *Chem. Rev.*, **1998**, 98, 1829; (b) Lipkowitz, K.B., Corner, B. and Peterson, M.A., *J. Am. Chem. Soc.*, **1997**, 119, 11269; (c) Black, D.R., Parker, C.G., Zimmerman, S.S. and Lee, M.L., *J. Comput. Chem.*, **1996**, 17, 931.
163. Cozzini, P., Domiano, P., Musini, P.C., Palla, G. and Zanardi, E., *J. Incl. Phenom. Mol. Recogn. Chem.*, **1996**, 26, 295-302.
164. Alberts, B., Bray, D., Lewis, J., Raff, M., Roberts, K. and Watson, J.D., "Molecular Biology of the Cell", Garland Pub., Inc., New York, 1983.
165. Ehrlich, P., Croonian Lecture. *Proc. Roy. Soc.*, London, **1900**, 66, 424-428.
166. Fischer, E. *Ber. Detsch. Chem. Ges.*, **1894**, 27, 2985.
167. Koshland, D.E. Jr., *Proc. Natl. Acad. Sci.* **1958**, 44, 98.
168. "Principles of Molecular Recognition", Buckingham, A.D., Legon, A.C. and Roberts, S.M., (Eds.) Blackie Academic, Glasgow, 1993.
169. Atwood, J.L., Davies, J.E.D., MacNicol, D.D. and Vgtle, F., (Eds.) "Comprehensive Supramolecular Chemistry", Elsevier, Exeter, 1996.
170. (a) Cram, D.J., *Angew. Chem., Int. Ed. Engl.*, **1988**, 27, 1009; (b) Pirkle, W.H. and Pochapsky, T.C., *Chem. Rev.*, **1989**, 89, 347; (c) Easton, C.J. and Lincoln, S.F., *Chem. Soc. Rev.*, **1996**, 163.

-
171. Crossley, R., "Chirality and the Biological Activity of Drugs", CRC Press, New York, 1995.
172. Baum, S.T. and Scaife, C.W.J., "Chemistry, A Life Science Approach", MacMillan Publishers, New York, 1980, p. 519.
173. (a) Allenmark, S.G., "Chromatographic Enantioseparation: Methods and Applications", 2nd Edition, Ellis Horwood, Chichester, 1991; (b) White, C.A., "A Practical Approach to Chiral Separations by Liquid Chromatography", Subramanian, G. (Ed.) VCH, New York, 1994.
174. Lipkowitz, K.B., *J. Chromatogr. A*, **1995**, 694, 15.
175. Faerman, C.H. and Price, S.L. *J. Am. Chem. Soc.*, **1990**, 112, 4915-4926.
176. Williams, D.H. and Westwell, M.S., *Chem. Soc. Rev.*, **1998**, 27, 57-63.
177. Topiol, S. and Sabio, M., *Enantiomer*, **1996**, 1, 251-265.
178. Dalglish, C.E., *J. Chem. Soc.*, **1952**, 3940.
179. Salem, L., Chapuisat, X., Segal, G., Hiberty, P.C., Monet, C., Leforestier, C. and Sautet, P., *J. Am. Chem. Soc.*, **1987**, 109, 2887-2894.
180. Meyer, V.R. and Rais, M., *Chirality*, **1989**, 1, 167-169.
181. Topiol, S. and Sabio, M., *J. Am. Chem. Soc.*, **1989**, 111, 4109-4110.
182. (a) Lochmuller, C.H., Harris, J.M. and Souter, R.W., *J. Chromatogr.*, **1972**, 71, 405-413; (b) Lochmuller, C.H. and Ryall, R.R., *J. Chromatogr.*, **1978**, 150, 511-514.
183. Pirkle, W.H. and Pochapsky, T.C., *J. Am. Chem. Soc.*, **1987**, 109, 5975-5982.
184. Topiol, S., Sabio, M., Moroz, J. and Caldwell, W.B., *J. Am. Chem. Soc.*, **1988**, 110, 8367-8376.
185. Lipkowitz, K.B. and Baker, B., *Anal. Chem.*, **1990**, 62, 774-777.
186. Easson, L.H. and Stedman, E., *Biochem. J.*, **1993**, 27, 1257-1266.
187. Topiol, S., *Chirality*, **1989**, 1, 69-79.
188. Buda, A.B., Auf der Heyde, T. and Mislow, K., *Angew. Chem., Int. Ed. Engl.*, **1992**, 31, 989-1007.

-
189. Breckenridge, R.J., *Experientia*, **1991**, 47, 1148-1161.
190. Filippi, A., Giardini, A., Piccirillo, S. and Speranza, M., *Int. J. Mass. Spectrom.*, **2000**, 198, 137-163.
191. Schneider, H.J., *Angew. Chem., Int. Ed. Engl.*, **1991**, 30, 1417-1436.
192. Reviews on metal-ion complexes: (a) Hancock, R.D. and Martell, A.E., *Chem. Rev.* **1989**, 89, 1875; (b) Hancock, R.D. *Pure Appl. Chem.*, **1986**, 58, 1445.
193. (a) Lehn, J.M., *Accts. Chem. Res.*, **1978**, 11, 49; for reviews on ligand conformations, etc, see (b) Lehn, J.M. *Struct. Bonding* (Berlin), **1973**, 16, 1; (c) Lehn, J.M., *Angew. Chem., Int. Ed. Engl.*, **1988**, 27, 89-112.
194. Reviews of molecular mechanics calculations on metal complexes: (a) Brubaker, G.R. and Johnson, D.W., *Coord. Chem. Rev.*, **1984**, 53, 1-36; (b) Hancock, R.D., *Progr. Inorg. Chem.* **1989**, 37, 187; (c) Landis, C.R., Root, D.M. and Cleveland, T., Molecular mechanics force fields for modeling inorganic and organometallic compounds, "Reviews in Computational Chemistry", Lipowitz, K.B. and Boyd, D.B., (Eds.) Vol. 6, 1995, p. 73-148; (d) Hay, B.P., *Coord. Chem. Rev.*, 126, **1993**, 177-236.
195. (a) Cram, D.J., *Angew. Chem., Int. Ed. Engl.*, **1986**, 25, 1039-1134; (b) Cram, D.J., *Angew. Chem., Int. Ed. Engl.*, **1988**, 27, 1009-1020 [*Angew. Chem.*, **1988**, 100, 1041]; (c) Reinhoudt, D.N., Dijkstra, P.J., in't Veld, P.J.A., Bugge, K.E., Harkema, S., Ungaro, R. and Ghidini, E., *J. Am. Chem. Soc.*, **1987**, 109, 4761; (d) Review of host molecules: Cram, D.J., *Nature*, **1992**, 356, 29-36.
196. Cram, D.J., Kaneda, T., Helgeson, R.C., Brown, S.B., Knobler, C.B., Maverick, E. and Trueblood, K.N., *J. Am. Chem. Soc.*, **1985**, 107, 3645-3657.
197. Comba, P., *Coord. Chem. Rev.*, **1999**, 185-186, 81-98.
198. Comba, P., *Coord. Chem. Rev.*, **1998**, 182, 343.
199. Rebek, J., Jr., *Science* (Washington D.C.) **1987**, 235, 1478-1483.
200. Helgeson, R.C., Koga, K., Timko, J.M. and Cram, D.J., *J. Am. Chem. Soc.*, **1973**, 95, 3021-3023.

-
201. (a) Cram, D.J., Hegelsson, R.C., Sousa, L.R., Timko, J.M., Newcomb, M., Moreau, P., de Jong, F., Gokel, G.W., Hoffman, D.H., Domeier, L.A., Peacock, S.C., Madan, K. and Kaplan, L., *Pure Appl. Chem.*, **1975**, 43, 327-349; (b) Helgesson, R.C., Koga, K., Timko, J.M. and Cram, D.J., *J. Am. Chem. Soc.*, **1973**, 95, 3021-3023.
202. Finkelstein, A.V. and Janin, J., *Protein Eng.*, **1989**, 3, 1-3.
203. Weiner, P.K., Langridge, R., Blaney, J.M., Schaefer, R. and Kollman, P.A., *Proc. Natl. Acad. Sci. USA*, **1982**, 79, 3754-3758.
204. Spichiger-Keller, U.E., *Anal. Chim. Acta*, **1999**, 400, 65-72.
205. Inoue, Y., Hakushi, T. and Liu, Y., In: "Cation Binding by Macrocycles", Inoue, Y. and Gokel, G.W., (Eds) Marcel Dekker, New York, Basel, 1990, p. 1.
206. (a) Stix, G., *Sci. Am.*, **1991**, 264, 116; (b) Robinson A.J. and Hardy B.J., *Theochem-J. Mol. Struct.*, **1996**, 368, 111-117; (c) Ihlenfeldt W.D., *J. Mol. Mod.*, **1997**, 3, 9, 386-402; (d) Cruz-Neira C., Langley R. and Bash P.A., SAR and QSAR in Environmental Research, **1998**, 9, (1-2), 39-51.
207. Available from, amongst others, Argus VR International http://www.argusvr.com/core/company/co_toc.htm.
208. Rzepa, H.S., *J. Molec. Struct., Theochem.*, **1997**, 398-399, 27-33.
209. Moore, T.S. and Winmill, T.F., *J. Chem. Soc.*, **1912**, 101, 1635.
210. Latimer, W.M. and Rhodebush, W.H., *J. Am. Chem. Soc.*, **1920**, 42, 1431.
211. (a) Huggins, M.L., *J. Org. Chem.*, **1936**, 1, 407-456; (b) Huggins, M.L., *J. Phys. Chem.*, **1936**, 40, 723-731.
212. Pauling, L., "The Nature of the Chemical Bond", Cornell University Press, Ithaca, NY, 1939.
213. (a) Abboud, J.L.M., Notario, R. and Botella, V., "Quantitative Treatments of Solute/Solvent Interactions, Theoretical and Computational Chemistry", 1994, p. 1, 135 and references therein; (b) Gal, J.-F. and Maria, P.-C., *Prog. Phys. Org. Chem.*, **1990**, 17, 159 and references therein

-
214. Schneider, H.-J., Juneja, R.K. and Simova, S., *Chem. Ber.*, **1989**, 122, 1211.
215. Chapman, K.T. and Still, W.C., *J. Am. Chem. Soc.*, **1989**, 111, 3075.
216. Subramanian, S. and Zaworotko, M.J., *Coord. Chem. Rev.*, **1994**, 137, 357-401.
217. Watson, J.D., "The Importance of Weak Interactions; Molecular Biology of the Gene", Benjamin, New York, Chapter 4, p. 102-140, 1965.
218. Hibbert, F. and Emsley, J., *Adv. Phys. Org. Chem.*, **1990**, 26, 255.
219. (a) MacDonald, J.C. and Whitesides, G.M., *Chem. Rev.*, **1994**, 94, 2383; (b) Bernstein, J., Etter, M.C. and Leiserowitz, L., The Role of Hydrogen Bonding in Molecular Assemblies, In: "Structure Correlation", Bürgi, H.-B. and Dunitz, J.D., (Eds.) VCH, Weinheim, 1994, p. 431; (c) Koch, U. and Popelier, P.L.A., *J. Phys. Chem.*, **1995**, 99, 9747.
220. Desiraju, G.R. and Steiner, T., "The Weak Hydrogen Bond", 1999, Oxford University Press, New York.
221. Alkorta, I., Rozas, I. and Elguero, J., *Chem. Soc. Rev.*, **1998**, 27, 163-170.
222. (a) Desiraju, G.R., *Acc. Chem. Res.*, **1996**, 29, 441; (b) Steiner, T., Starikov, E.B., Amado, A.M. and Teixeira-Dias, J.J.C., *J. Chem. Soc., Perkin Trans. 2*, **1995**, 1321; (c) Seiler, P., Isaacs, L. and Diederich, F., *Helv. Chim. Acta*, **1996**, 79, 1047.
223. Rozas, I., Alkorta, I. and Elguero, J., *J. Phys. Chem., A*, **1997**, 101, 9457.
224. Platts, J.A. and Howard, S.T., *J. Chem. Soc., Perkin Trans. 2*, **1997**, 2241.
225. (a) Alkorta, I., Elguero, J. and Foces-Foces, C., *Chem. Commun.*, **1996**, 1633; (b) Liu, Q. and Hoffmann, R., *J. Am. Chem. Soc.*, **1995**, 117, 10108.
226. Alkorta, I. and Elguero, J., *J. Phys. Chem.*, **1996**, 100, 19367.
227. (a) Tang, T.-H., Hu, W.-J., Yan, D.-Y. and Cui, Y.-P., *Theochem*, **1990**, 207, 319; (b) Rozas, I., Alkorta, I. and Elguero, J., *J. Phys. Chem., A*, **1997**, 101, 9457.
228. Romas, M., Alkorta, I., Elguero, J., Golubev, N.S., Denisov, G.S., Benedict, H. and Limbach, H.-H., *J. Phys. Chem. A*, **1997**, 101, 9791.

-
229. Rozas, I., Alkorta, I. and Elguero, J., *Chem. Phys. Lett.*, **1997**, 275, 423.
230. Rozas, I., Alkorta, I. and Elguero, J., *J. Phys. Chem. A*, **1997**, 101, 4236.
231. (a) Hankins, D., Moskowitz, J.W. and Stillinger, F.H., *J. Chem. Phys.*, **1970**, 53, 4544-4554; (b) Del Bene and J., Pople, J.A., *J. Chem. Phys.*, **1970**, 52, 4858-4866; (c) Del Bene, J. and Pople, J.A., *J. Chem. Phys.*, **1973**, 58, 3605-3608; (d) Newton, M.D., Jeffrey, G.A. and Takagi, S., *J. Am. Chem. Soc.*, **1979**, 101, 1997-2002.
232. Saenger, W., *Nature (Lond.)*, **1979**, 279, 343-344.
233. (a) Lesyng, B. and Saenger, W., *Biochim. Biophys. Acta*, **1981**, 678, 408-413; (b) Koehler, J.E.H., Lesyng, B. and Saenger, W., *J. Comput. Chem.*, **1987**, 8, 1090-1098.
234. Oki, M. and Iwamura, H., *J. Am. Chem. Soc.*, **1967**, 89, 576.
235. Miyata, M., Shibakami, M., Chirachanchai, S., Takemoto, K., Kasai, N. and Miki, K., *Nature*, **1990**, 343, 446.
236. (a) Lord, R.C. and Merrifield, R.E., *J. Chem. Phys.*, **1953**, 21, 166; (b) Kato, T., Frechet, J.M.J., Wilson, P.G., Saito, T., Uryu, T., Fujishima, A., Jin, C. and Kaneuchi, F., *Chem. Mater.*, **1993**, 5, 1094.
237. (a) Endo, S., Chino, T., Tsuboi, S. and Koto, K., *Nature*, **1989**, 340, 452; (b) Sugiura, K., Toyoda, J., Okamoto, H., Okaniwa, K., Mitani, T., Kawamoto, A., Tanaka, J. and Nakasuji, K., *Angew. Chem., Int. Ed. Engl.*, **1992**, 31, 852.
238. Singh, U.C. and Kollman, P.A., *J. Chem. Phys.*, **1985**, 83, 4033-4040.
239. Levitt, M. and Perutz, M.F., *J. Molec. Biol.*, **1988**, 201, 751-754.
240. Atwood, J.L., Hamada, F., Robinson, K.D., Orr, G.W. and Vincent, R.L., *Nature*, **1991**, 349, 683-684.
241. Allerhand, A. and Schleyer, P.v.R., *J. Am. Chem. Soc.*, **1963**, 85, 1233-1237.
242. Taylor, R., Kennard, O. and Versichel W., *Acta Cryst. B*, **1984**, 40, 280-288.
243. (a) Shan, S. and Herschlag, D., *J. Am. Chem. Soc.*, **1996**, 118, 5515; (b) Schwartz, B. and Drueckhammer, D.G., *J. Am. Chem. Soc.*, **1995**, 117, 11902; (c) Perrin, C.L. and Nielson, J.B., *Annu. Rev. Phys. Chem.*, **1997**, 48,

-
- 511; (d) Kato, Y., Toledo, L.M. and Rebek, J., Jr., *J. Am. Chem. Soc.*, **1996**, 118, 8575.
244. (a) Garcia-Viloca, M., Gonzalez-Lafont, A. and Lluch, J.M., *J. Am. Chem. Soc.*, **1997**, 119, 1081; (b) Chen, J., McAllister, M.A., Lee, J.K. and Houk, K.N., *J. Org. Chem.*, **1998**, 63, 4611.
245. Kumar, G.A. and McAllister, M.A., *J. Am. Chem. Soc.*, **1998**, 120, 3159-3165.
246. Kumar, G.A. and McAllister, M.A., *J. Org. Chem.*, **1998**, 63, (20), 6968-6972.
247. Gronert, S., *J. Am. Chem. Soc.*, **1993**, 115, 10258-10266.
248. Del Bene J.E., Frisch, M.J. and Pople, J.A., *J. Phys. Chem.*, **1985**, 89, 3669-3674.
249. Del Bene, J.E., *J. Phys. Chem.*, **1988**, 92, 2874-2880.
250. Neuheuser, T., Hess, B.A., Reutel, C. and Weber, E., *J. Phys. Chem.*, **1994**, 98, 6459-6467.
251. Hinchcliffe, A., *J. Molec. Struct.*, **1984**, 106, 361-366.
252. Feyereisen, M.W., Feller, D. and Dixon, D.A., *J. Phys. Chem.*, **1996**, 100, 2993-2997.
253. Turi, L. and Dannenberg, J.J., *J. Phys. Chem.*, **1993**, 97, 7899-7909.
254. Malone, J.F., Murray, C.M., Charlton, M.H., Docherty, R. and Lavery, A.J., *J. Chem. Soc., Faraday Trans.*, **1997**, 93, 3429-3436.
255. Howard, J.A.K., Hoy, V.J., O'Hagan, D. and Smith, G.T., *Tetrahedron*, **1996**, 52, 12613-12622.
256. Philp, D. and Robinson, D.M.A., *J. Chem. Soc., Perkin Trans. 2*, **1998**, 1643-1649.
257. Woodbridge, E.L., Tso, T.-L., McGrath, M.P., Hehre, W.J. and Lee, E.K.C., *J. Chem. Phys.*, **1986**, 85, 6991-6994.
258. Novoa, J.J., Tarron, B., Whangbo, M.H. and Williams, J.M., *J. Chem. Phys.*, **1991**, 95, 5179-5186.

-
259. Rovira, C. and Novoa, J.J., *Chem. Phys. Lett.*, **1998**, 279, 140-150.
260. (a) Taylor, R., Kennard, O. and Versichel, W., *J. Am. Chem. Soc.*, **1983**, 105, 5761-5766; (b) Murray-Rust, P. and Glusker, J.P., *J. Am. Chem. Soc.*, **1984**, 106, 1018-1025.
261. (a) Pedersen, B., *Acta Cryst. B*, **1974**, 30, 289-291; (b) Kroon, J., Kanters J.A., Van-Duijneveldt-Van der Rijdt, J.G.C.M., Van-Duijneveldt, F.B. and Vliegthart, J.A., *J. Molec. Struct.*, **1975**, 24, 109-129; (c) Olovsson, I. and Jönsson, P.G., "The Hydrogen Bond - Recent Developments in Theory and Experiments", Schuster, P., (Ed.) North-Holland, Amsterdam, 1976, p. 393-456.
262. Taylor, R., Kennard, O. and Versichel, W., *J. Am. Chem. Soc.*, **1984**, 106, 244-248.
263. Jeffrey, G.A. and Maluszynska, H., *Int. J. Biol. Macromol.*, **1982**, 7, 173-185.
264. Albrecht, G. and Corey, R.B., *J. Am. Chem. Soc.*, **1939**, 61, 1087-1103.
265. Jönsson, P.G. and Kviick, A., *Acta Cryst. B*, **1972**, 28, 1827-1833.
266. Jeffrey, G.A., Maluszynska, H. and Mitra, J., *Int. J. Biol. Macromol.*, **1985**, 7, 336-348.
267. (a) Jeffrey, G.A. and Takagi, S., *Accts. Chem. Res.*, **1978**, 11, 244-248; (b) Ceccarelli, C., Jeffrey, G.A. and Taylor, R., *J. Molec. Struct.*, **1981**, 70, 255-271; (c) Jeffrey, G.A. and Mitra, J., *Acta Cryst. B*, **1983**, 39, 468-480; (d) Jeffrey, G.A. and Maluszynska, H., *Int. J. Biol. Macromol.*, **1982**, 4, 173-185; (e) Jeffrey, G.A. and Mitra, J., *J. Am. Chem. Soc.*, **1984**, 106, 5546-5553.
268. (a) Franks, F., "The Chemistry and Physics of Water, A Comprehensive Treatise", Franks, F., (Ed.) Vol. 4, Plenum Press, New York, p. 1-94; (b) Scheraga, H.A., *Acc. Chem. Res.*, **1978**, 12, 7-14; (c) Hildebrand, J.H., *Proc. Nat. Acad. Sci. USA*, **1979**, 76, 194; (d) Tanford, C., "The Hydrophobic Effect. Formation of Micelles and Biological Membranes", 2nd Edition, Wiley, New York, 1980; (e) Cantor, C.R. and Schimmel, P.R., "Biophysical Chemistry. Part I: Conformation of Biological Macromolecules", Chapter 5,

-
- Freeman & Co., San Francisco, 1980, p. 279-288; (f) Creighton, T.E., "Proteins. Structure and Molecular Principles", Chapter 4, Freeman & Co., New York, 1984, p.133-158.
269. (a) Chothia, C., *Nature*, **1974**, 248, 338-339; (b) Richards, F.M., *Annu. Rev. Biophys. Bioeng.*, **1977**, 6, 151-176; (c) Miller, S., Janin, J., Lesk, A.M. and Chothia, C., *J. Mol. Biol.*, **1987**, 196, 641-656.
270. Jiang, X.-K., *Accts. Chem. Res.*, **1988**, 21, 362-367.
271. Taylor, R. and Kennard, O., *Acta Cryst. Sect. B*, **1983**, 39, 133-138.
272. Jeffrey, G.A. and Lewis, L., *Carbohydr. Res.*, **1978**, 60, 179-182.
273. Dauben, P. and Hagler, A.T., *Acc. Chem. Res.*, **1980**, 13, 105-112.
274. Pedersen, B., *Acta Cryst. B*, **1974**, 30, 289-291.
275. (a) Kollman, P.A., *J. Am. Chem. Soc.*, **1977**, 99, 4875-4894; (b) Kollman, P.A., *J. Am. Chem. Soc.*, **1978**, 100, 2974-2984; (c) Došen-Micovic, L., Jeremic, D. and Allinger, N.L., *J. Am. Chem. Soc.*, **1983**, 105, 1716-1722; (d) Momany, F.A., *J. Phys. Chem.*, **1978**, 82, 592-601; (e) Abraham, R.J. and Hudson, B., *J. Comput. Chem.*, **1985**, 6, 173-181; (f) Singh, U.C. and Kollman, P.A., *J. Comput. Chem.*, **1984**, 5, 129-135; (g) Kar, T., Sannigrahi, A.B. and Mukherjee, D.C., *J. Molec. Struct. (Theochem)*, **1987**, 153, 93-101; (h) Cox, S.R. and Williams, D.E., *J. Comput. Chem.*, **1981**, 2, 304-323.
276. (a) Barnes, P., Finney, J.L., Nicholas, J.D. and Quinn, J.E., *Nature (London)*, **1979**, 282, 459-464; (b) Goodfellow, J.M., Finney, J.L. and Narnes, P., *Proc. R. Soc. Lond.*, **1982**, B214, 213-228.
277. (a) Melberg, S., Rasmussen, K., Scordamaglia, R. and Tosi, C., *Carbohydr. Res.*, **1979**, 76, 23-37; (b) Pertsin, A.J. and Kitaigorodsky, A.I., "The Atom-Atom Potential Method. Application to Organic Molecular Solids", Springer, Berlin, Heidelberg, New York. Tokyo, 1987; (c) Taylor, R., *J. Molec. Struct.*, **1981**, 71, 311-325; (d) Taylor, R., *J. Molec. Struct.*, **1982**, 72, 125-136; (e) KroonBatenberg, L.M.J. and Kanters, J.A., *J. Molec. Struct. (Theochem)*, **1983**, 105, 417-418.

-
278. (a) Hunter, C.A. and Sanders, J.K.M., *J. Am. Chem. Soc.*, **1990**, 112, 5525; (b) Jorgenson, J.L. and Severance, D.L., *J. Am. Chem. Soc.*, **1990**, 112, 4768.
279. Gilli, P., Bertolasi, V., Ferretti, V. and Gilli, G., *J. Am. Chem. Soc.*, **1994**, 116, 909.
280. (a) Saenger, W., Betzel, C.H., Hingerty, B.E. and Brown, G.M., *Nature*, **1982**, 296, 581-583; (b) Betzel, C.H., Saenger, W., Hingerty, B.E. and Brown, G.M., *J. Am. Chem. Soc.*, **1984**, 106, 7545-7557.
281. Vögtle, F. and Knops, P., *Angew. Chem., Int. Ed. Engl.*, **1991**, 30, 958-960.
282. (a) Kubo, Y., Hamaguchi, S., Niimi, A., Yoshida, K. and Tokita, S., *J. Chem. Soc., Chem. Comm.*, **1993**, 305-307; (b) Kubo, Y., Maruyama, S., Ohhara, N., Nakamura, M. and Tokita, S., *J. Chem. Soc., Chem. Comm.*, **1995**, 1727-1728; (c) Kubo, Y., Tokita, S., Kojima, Y., Osano, Y. and Matsuzaki, T., *J. Org. Chem.*, **1996**, 61, 375.
283. Jin, T. and Monde, K., *Chem. Commun.*, **1998**, 1357-1358 and references following in this Section.
284. (a) Czarnik, A.W., *Acc. Chem. Res.*, **1994**, 27, 302-308; (b) Fabrizzi, L. and Poggi, A., *Chem. Soc. Rev.*, **1995**, 24, 197-202; (c) de Silva, A.P., Gunaratne, N., Gunnlaugsson, T., Huxley, A.J.M., McCoy, C.P., Rademacher, J.T. and Rice, T.E., *Chem. Rev.*, **1997**, 97, 1515-1566.
285. (a) Matsumoto, H. and Shinkai, S., *Tetrahedron Lett.*, **1996**, 37, 77-80; (b) Jin, T., Ichikawa, K. and Koyama, T., *J. Chem. Soc., Chem. Comm.*, **1992**, 499-501; (c) Aoki, I., Sakaki, T. and Shinkai, S., *J. Chem. Soc., Chem. Comm.*, **1992**, 730-732; (d) Aoki, I., Kawabata, H., Nakashima, K. and Shinkai, S., *J. Chem. Soc., Chem. Comm.*, **1991**, 1771-1773; (e) Ji, H.-F., Brown, G.M. and Dabestani, R., *J. Chem. Soc., Chem. Comm.*, **1999**, 609-610.
286. Unob, F., Asfari, Z. and Vicens, J., *Tetrahedron Lett.*, **1988**, 39, 2951-2954.

-
287. Bugler, J., Sommerdijk, N.A.J.M., Visser, A.J.W.G., van Hoek, A., Nolte, R.J.M., Engbersen, J.F.J. and Reinhoudt, D.N., *J. Am. Chem. Soc.*, **1999**, 121, 28-33.
288. Talanova, G.G., Elkarim, N.S.A., Talanov, V.S. and Bartsch, R.A., *Anal. Chem.*, **1999**, 71, 3106-3109.
289. Kubo, Y., Maeda, S., Tokita, S. and Kubo, M., *Nature*, **1996**, 382, 522-524; Review: Kubo, Y., *Synlett*, **1999**, 2, 161-174.
290. Kyba, E.B., Koga, K., Sousa, L.R., Siegel, M.G. and Cram, D.J., *J. Am. Chem. Soc.*, **1973**, 95, 2692
291. Helgeson, R.C., Timko, J.M., Moreau, P., Peacock, S.C., Mayer, J.M. and Cram, D.J., *J. Am. Chem. Soc.*, **1974**, 96, 6762.
292. Anderson, S., Neidlein, U., Gramlich, V. and Diederich, F., *Angew. Chem., Int. Ed. Engl.*, **1995**, 34, 1596.
293. Martinborough, E., Denti, T.M., Castro, P.P., Wyman, T.B., Knobler, C.B. and Diederich, F., *Helv. Chim. Acta*, **1995**, 78, 1037.
294. Reichwein, A.M., Verboom, W. and Reinhoudt, D.N., *Recl. Trav. Chim. Pays-Bas.*, **1993**, 112, 358.
295. James, T.D., Sandanayake, K.R.A.S. and Shinkai, S., *Nature*, **1995**, 374, 345-347.
296. Grady, T., Harris, S.J., Smyth, M.R. and Diamond, D., *Anal. Chem.*, **1996**, 68, 3775-3782.
297. Grady, T., Joyce, T., Smyth, M.R., Harris, S.J. and Diamond, D., *Anal. Commun.*, **1998**, 35, 123.
298. Snowden, T.S. and Anslyn, E.V., *Curr. Opin. Chem. Biol.*, **1999**, 3, 740-746.
299. Kammerer, K., Happel, P. and Caeses, L., *Makromol. Chem.*, **1972**, 162, 179.
300. Bauer, J.L. and Gutsche, C.D., *J. Am. Chem. Soc.*, **1985**, 107, 6059.
301. (a) Coruzzi, M., Andretti, G.D., Bocchi, A. and Ungaro, R., *J. Chem. Soc. Perkin Trans. 2*, **1982**, 1133; (b) Perrin, M. and Lecocq, S., *J. Include. Phenom. Mol. Recog.*, **1991**, 11, 171; (c) Juneja, R.K., Robinson, K.D., Orr,

-
- G.W., Dubois, R.H., Belmore, K.A., Atwood, J.L., Ripmeester, J.M. and Ratcliffe, C.I., *J. Include. Phenom. Mol. Recog.*, **1992**, 13, 93; (d) Gallagher, J. F., Ferguson, G., Böhmer, V. and Kaft, D., *Acta Cryst. C*, **1994**, 50, 73; (e) Pappalardo, S. and Ferguson, G., *J. Org. Chem.*, **1996**, 61, 2407.
302. Bell, S.E.J., McKerverey, M.A., Fayne, D., Kane, P. and Diamond, D., *J. Mod^e Model.*, **1998**, 4, 44-52.
303. CambridgeSoft Corporation, MA, USA. www.camsoft.com.
304. Kane, P., Kincaid, K., Fayne, D., Diamond, D. and McKerverey, M.A., *J. Mol. Mod.*, **2000**, 6, 272-281.
305. HyperChem is available from Hypercube, Inc., 419 Philips St., Waterloo, Ontario, N2L 3X2 Canada.
306. Cambridge Crystallographic Data Centre (CCDC), 12 Union Road, Cambridge CB2 1EW, UK, E-mail: deposit@ccdc.cam.ac.uk.
307. Izatt, S.R., Hawkins, R.T., Christensen, J.J. and Izatt, R.M., *J. Am. Chem. Soc.*, **1985**, 107, 63-66.
308. Harrowfield, J.M., Ogden, M.I., Richmond, W.R. and White, A.H., *J. Chem. Soc., Chem. Commun.*, **1991**, 1159-1161.
309. De Namor, A.F.D., de Sueros, N.A., McKerverey, M.A., Barrett, G., Anaud Neu, F. and Schwing-Well, M.J., *J. Chem. Soc., Chem. Commun.*, **1991**, 1546-1548.
310. Andreetti, G.D., Pochini, A. and Ungaro, R., *J. Chem. Soc., Perkin Trans. 2*, **1983**, 1773-1778.
311. Ikeda, A., Tsuzuki, H. and Shinkai, S., *J. Chem. Soc., Perkin Trans. 2*, **1997**, 575.
312. Stewart, J.J.P., *J. Comput. Chem.*, **1991**, 12, 320-341.
313. Bott, S.G., Coleman, A.W. and Atwood, J.L., *J. Am. Chem. Soc.*, **1986**, 108, 1709-1710.
314. (a) Diamond, D., In: Smyth, M.R. and Vos, J.G., (Eds.) "Electrochemistry, Sensors and Analysis", Analytical Chemistry Symposium Series, Vol. 25,

-
- Elsevier, Amsterdam, 1986, p. 155; (b) Diamond, D., Svehla, G., Seward, E.M. and McKervey, M.A., *Anal. Chim. Acta*, **1988**, 204, 223-231; (c) McKervey, M.A., Seward, E.M., Ferguson, G., Ruhl, B. and Harris, S.J., *J. Chem. Soc., Chem. Commun.*, **1984**, 388; (d) Cadogan, A.M., Diamond, D., Smyth, M.R., Deasy, M., McKervey, M.A. and Harris, S.J., *Analyst*, **1989**, 114, 1551-1554.
315. (a) Diamond, D., Svehla, G., Seward, E.M. and McKervey, M.A., *Anal. Chim. Acta*, **1988**, 204, 223; (b) Cadogan, A.M., Diamond, D., Smyth, M.R., Deasy, M., McKervey, M.A. and Harris, S.J., *Analyst*, **1989**, 114, 1551; (c) Arnaud-Neu, F., Collins, E.M., Deasy, M., Ferguson, G., Harris, S.J., Kaitner, B., Lough, A.J., McKervey, M.A., Marques, E., Ruhl, B.L., Schwing-Weill, M.J. and Seward, E.M., *J. Am. Chem. Soc.*, **1989**, 111, 8681-8691.
316. Ikeda, A., Tsuzuki, H. and Shinkai, S., *J. Chem. Soc., Perkin Trans. 2*, **1994**, 2073.
317. (a) Calestani, G., Uggozoli, F., Arduini, A., Ghidini, E. and Ungaro, R. *J. Chem. Soc., Chem. Commun.*, **1987**, 344-346. (b) Arduini, A., Ghidini, E., Pochini, A., Ungaro, R., Andreetti, G., Calestani, G.D. and Uggozoli, F. *J. Incl. Phenom.*, **1988**, 6, 119.
318. Guilbaud, P., Varnek, A. and Wipff, G., *J. Am. Chem. Soc.*, **1993**, 115, 8298.
319. Wolf, N.J., Georgiev, E.M., Yordanov, A.T., Whittlesey, B.R., Koch, H.F. and Roundhill, D.M., *Polyhedron*, **1999**, 885-896.
320. Ikeda, A., Tsuzuki, H. and Shinkai, S., *Tetrahedron Lett.*, **1994**, 35, 8417.
321. Kane, P., Fayne, D., Diamond, D., Bell, S.E.J. and McKervey, M.A., *J. Mod. Model.*, **1998**, 4, 259-267.
322. (a) Dewar, M.J.S. and Thiel, W., *J. Am. Chem. Soc.*, **1977**, 99, 4899. (b) Dewar, M.J.S. and McKee, M.L., *ibid*, **1977**, 99, 5231; (c) Dewar, M.J.S. and Rzepa, H., *ibid*, **1978**, 100, 58.
323. Thiel, W., *Tetrahedron*, **1988**, 44, 7393.

-
324. (a) Stewart, J.J.P., *J. Comp. Chem.*, **1989**, 10, 209; (b) Stewart, J.J.P., *ibid*, 221.
325. Pople, J.A., Santry, D.P. and Segal, G.A., *J. Chem. Phys.*, 1967, 47, 2026.
326. (a) Pople, J.A., Santry, D.P. and Segal, G.A., *J. Chem. Phys.*, **1965**, 43, S129; (b) Pople, J.A., Santry, D.P. and Segal, G.A., *ibid.*, S136; (c) Pople, J.A., Santry, D.P. and Segal, G.A., *ibid*, 3289.
327. Anderson, W.D., Edwards, W.P. and Zerner, M.C., *Inorg. Chem.*, **1986**, 28, 2732.
328. Ikeda, A. and Shinkai, S., *J. Am. Chem. Soc.* **1994**, 116, 3102.
329. Bell, S.E.J., Browne, J.K., McKee, V., McKervey, M.A., Malone, J.F., O'Leary, M., Walker, A., Arnaud-Neu, F., Boulangeot, O. Mauprivez O. and Schwing-Weill, M.-J., *J. Org. Chem.*, **1998**, 63, 489-501.
330. Gutsche, C.D., Muthukrishnan, R. and No, K.H., *Tetrahedron Lett.*, **1979**, 2213-2216.
331. A review on the stereochemistry of calix[n]arenes: Otsuka, H. and Shinkai, S., *Supramolecular Sci* , **1996**, 3, 189-205.
332. (a) Muthukrishnan, R. and Gutsche, C.D., *J. Org. Chem.*, **1979**, 44, 3962-3964; (b) Bayard, F., Fenet, B., Lamartine, R., Petit-Ramel, M. and Royer, J., *J. Chim. Phys.*, **1995**, 92, 13.
333. (a) First water soluble lower rim functionalised chiral calixarene: Arimura, T., Kawabata, H., Matsuda, T., Maramatsu, T., Satoh, H., Fujio, K., Manabe, O. and Shinkai, S., *J. Org. Chem.* **1991**, 56, 301-306; (b) Marra, A., Schermann, M.-C., Dondoni, A., Casnati, A., Minari, P. and Ungaro, R., *Angew. Chem. Int. Ed. Engl* , **1994**, 33, 2479-2481; (c) Yashima, E. and Okamoto, Y., *Bull. Chem. Soc. Jpn.*, **1995**, 68, 3289-3307; (d) Neri, P., Bottino, A., Geraci, C. and Piattelli, M., *Tetrahedron Asymm.*, **1996**, 7, 17-20; (e) Shinkai, S., Araki, K., Kubota, M., Arimura T. and Matsuda, T., *J. Org. Chem.*, **1991**, 56, 295-300.

-
334. First synthesised: Casabianca, H., Royer, J., Satrallah, A., Taty-C, A. and Vicens, J., *Tetrahedron Lett.*, **1987**, 28, 6595.
335. For a review on inherently chiral calixarenes, see: (a) Böhmer, V., Kraft, D. and Tabatabai, M., *J. Incl. Phenom. Mol. Recogn.*, **1994**, 19, 17-39; Recent work: (b) Caccamese, S., Notti, A., Pappalardo, S., Parisi, M.F. and Principato, G., *Tetrahedron*, **1999**, 55, 5505-5514.
336. No, K. and Gutsche, C.D., *J. Org. Chem.*, **1982**, 47, 2713.
337. Shinkai, S., Arimura, T., Kawabata, H., Murakami, H., Araki, K., Iwamoto, K. and Matsuda, T., *J. Chem. Soc., Chem. Comm.*, **1990**, 1734-1736.
338. Recent review: Webb, T. and Wilcox, C.S., *Chem. Soc. Rev.*, **1993**, 22, 383-395; Recent topics: (a) Cristofaro, M.F. and Chamberlin, A.R., *J. Am. Chem. Soc.*, **1994**, 116, 5089-5098; (b) Gasparrini, F., Misiti, D., Villani, C., Borchardt, A., Burger, M.T. and Still, W.C., *J. Org. Chem.*, **1995**, 60, 4314-4315; (c) Araki, K., Inada, K. and Shinkai, S., *Angew. Chem. Int. Ed. Engl.*, **1996**, 35, 72-74; (d) Martín, M., Raposo, C., Almaraz, M., Crego, M., Caballero, C., Grande, M. and Morán, J.R., *Angew. Chem. Int. Ed. Engl.*, **1996**, 35, 2386-2388; (e) Reetz, M.T., Rudolph, J. and Mynott, R., *J. Am. Chem. Soc.*, **1996**, 118, 4494-4495; (f) Naemura, K., Ogasahara, K., Hirose, K. and Tobe, Y., *Tetrahedron Asymm.*, **1997**, 8, 19-22; (g) Dowden, J., Edwards, P.D. and Kilburn, J.D., *Tetrahedron Lett.*, **1997**, 38, 1095-1098; (h) Das, G. and Hamilton, A.D., *Tetrahedron Lett.*, **1997**, 38, 3675-3678; (i) Mizutani, T., Ema, T., Tomita, T., Kuroda, Y. and Ogoshi, H., *J. Am. Chem. Soc.*, **1994**, 114, 4240; (j) Galán, A., Andreu, D., Echavarren, A.M., Prados, P., and de Mendoza, J., *J. Am. Chem. Soc.*, **1992**, 114, 1511-1512; (k) Metzger, A., Gloe, K., Stephan, H. and Schmidtchen, F.P., *J. Org. Chem.*, **1996**, 61, 2051.
339. Mohamadi, F., Richards, N.G.J., Guida, W.C., Liskamp, R., Lipton, M., Caufield, C., Chang, G., Hendrickson, T. and Still, W.C., *J. Comput. Chem.*, **1990**, 11, 440.

-
340. (a) Scott, R.A. and Scheraga, H.A., *J. Chem. Phys.*, **1966**, 45, 2091; (b) Weiner, P. and Kollman, P.A., *J. Comput. Chem.*, **1981**, 2, 287-303; (c) Weiner, S.J., Kollman, P.A., Case, D.A., Singh, U.C., Ghio, C., Alagona, G., Profeta, S. Jr. and Weiner, P.K., *J. Am. Chem. Soc.*, **1984**, 106, 765-784; (d) Singh, U.C., Weiner, P.K., Caldwell, J. and Kollman, P.A., AMBER 3.0,² University of California-San Francisco, 1987.
341. Allinger, N.L., Yuh, Y.H. and Lii, J.H., *J. Am. Chem. Soc.*, **1989**, 111, 8551-8566.
342. Polak, E. and Ribiere, G., *Revue Francaise Informat., Recherche Operationelle*, **1969**, 16, 35.
343. Nadin, A., Derrer, S., McGeary, R.P., Goodman, J.M., Holmes, A.B. and Raithby, P.R., *Mater. Sci. Engineer. C*, **1996**, 4, 59-62.
344. Wavefunction, Inc., Irvine, CA, USA.
345. <http://www.povray.org/>
346. (a) Diamond, D., *J. Incl. Phenom. Mol. Recogn. Chem.*, **1994**, 19, 149; (b) Diamond, D. and McKerverey, M.A., *Chem. Soc. Rev.*, **1996**, 15-24.
347. Howarth, J., Fayne, D., Hanlon, K. and McCormac, P., *Tetrahedron Lett.*, **1997**, 38, 17, 3097-3100.
348. Carmichael, H., *Chem. Brit.*, **2000**, 36, 1, 36-38.
349. Bonhote, P., Dias, A.-P., Papageorgiou, N., Kalyanasundaram, K. and Gratzel, M., *Inorg. Chem*, **1996**, 35, 1168.
350. Koch, V.R., Nanjundiah, C., Appetechi, G.B. and Scrosati, B., *J. Electrochem. Soc.*, **1995**, 142, L116.
351. Abdul-Sada, A.A.K., Ambler, P.W., Hodgson, P.K.G., Seddon, K.R. and Stewart, N.J., Pat., WO 9521871 A1 950817.
352. Suarez, P.A.Z., Dullius, J.E.L., Einloft, S., Desouza, R.F. and Dupont, J., *Polyhedron*, **1996**, 15, 1217.
353. Harlow, K.J., Hill, A.F. and Welton, T., *Synthesis*, **1996**, 697.
354. Maruoka, K. and Yamamoto, H., *Synlett*, **1991**, 793.

-
355. Terada, M., Mikami, K. and Nakai, T., *Tetrahedron Lett.*, **1991**, 32, 935.
356. Minamikawa, H., Hayakawa, S., Yamada, T., Iwasawa, N. and Narasaka, K.,
Bull. Chem. Soc. Jpn., **1988**, 61, 4379.

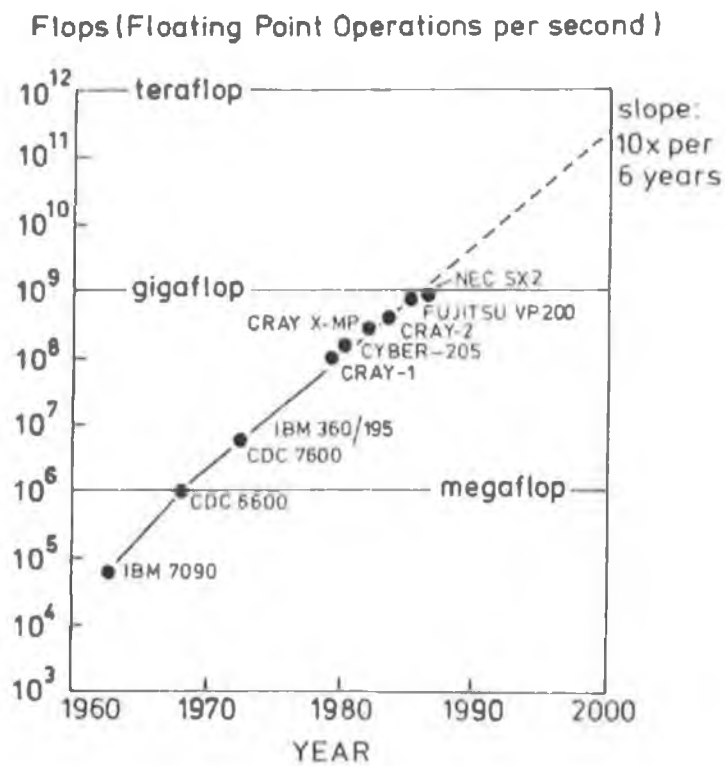


Figure 1. Graph depicting the rate of increase in computational power as time progresses.

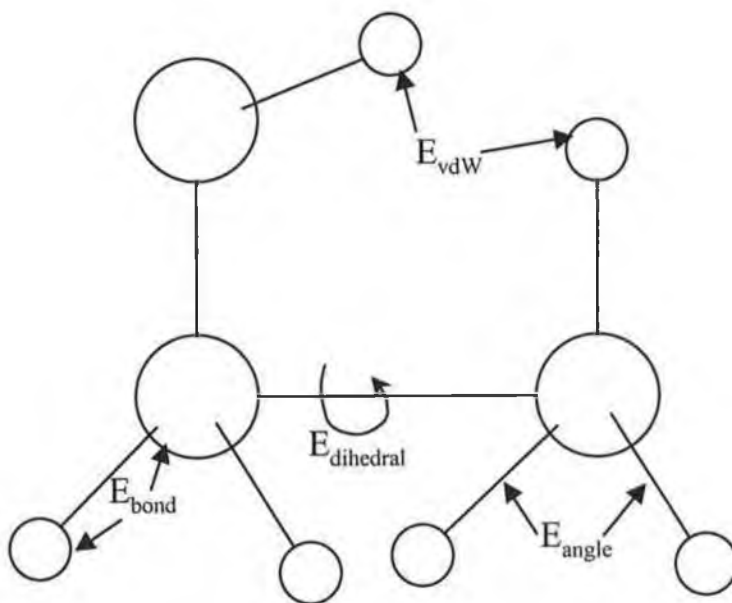


Figure 2. Four of the main interactions included in force field equations.

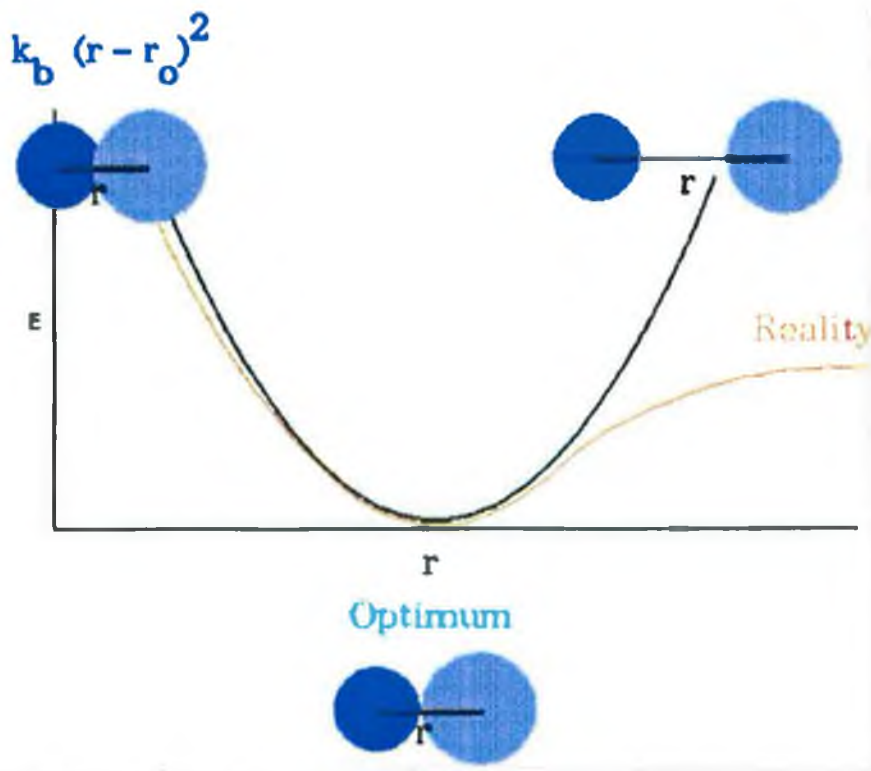


Figure 3. A schematic demonstrating how atomic distance effects bond energy.

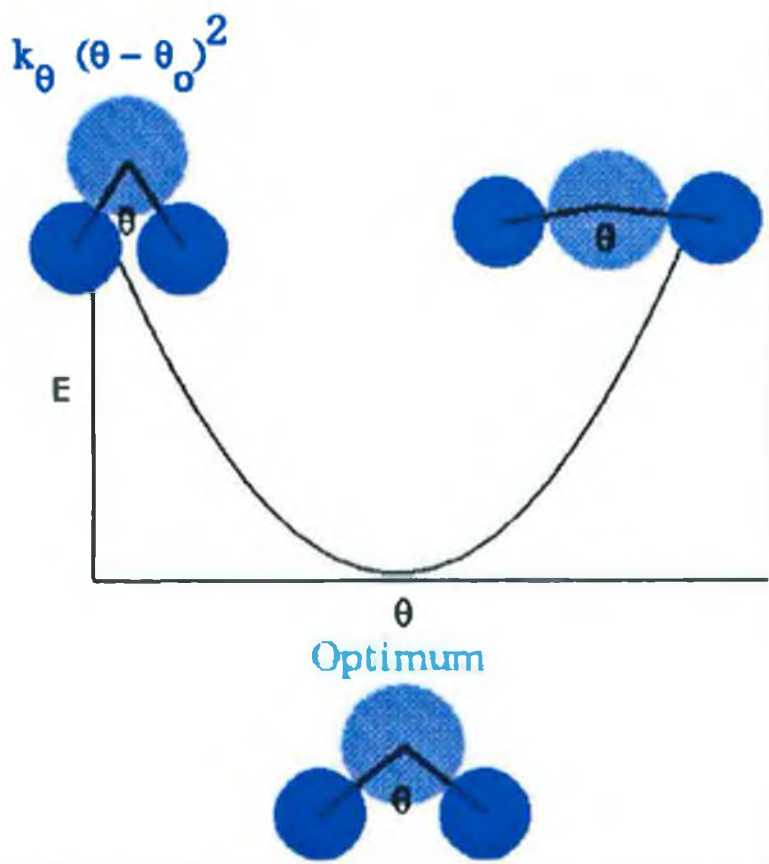


Figure 4. A display of how a change in the orientation of bonded atoms effects the energy yielded by the Hookes law representation of the angle bending function.

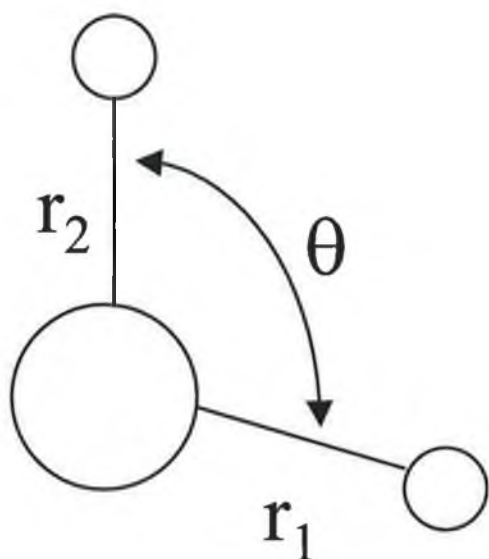


Figure 5. The coupling of bond length and bond angle potentials.

$$k_{\theta} (\theta - \theta_0)^2 \text{ or } k_b (r - r_0)^2$$

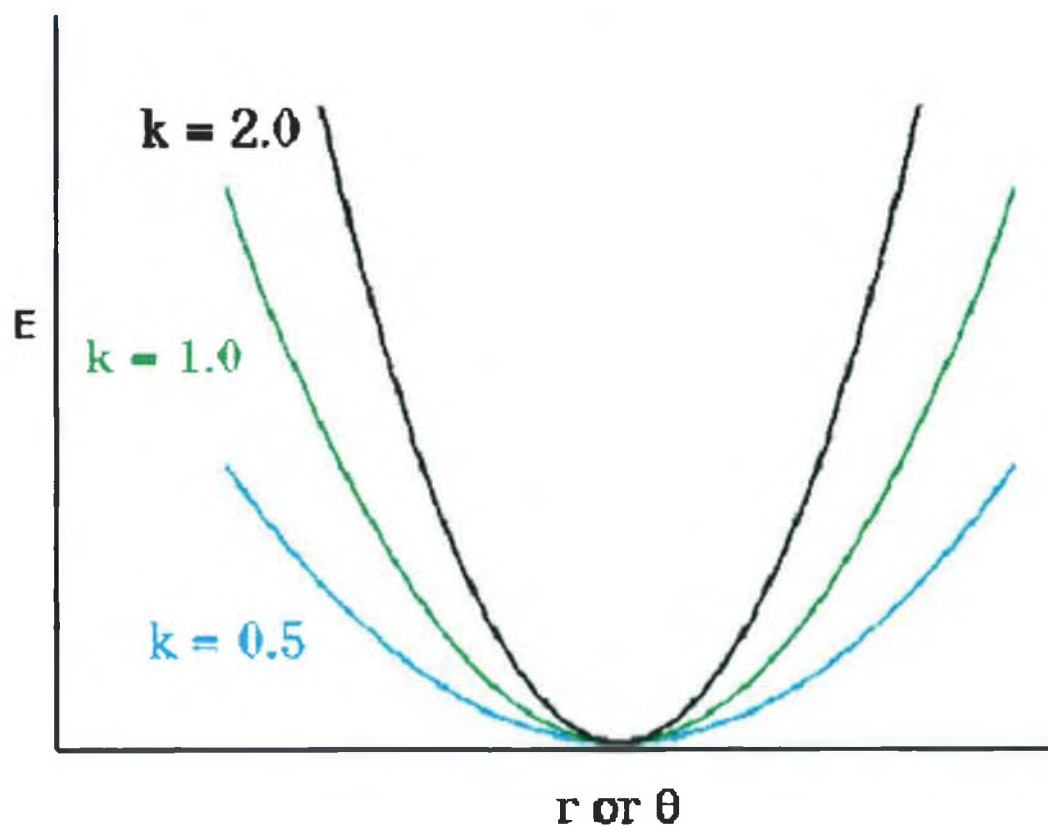


Figure 6. How a change in the potential constants effects the degree of curvature of the Hooke law generated energy curves.

$$A [1 + \cos(n\tau - \phi)]$$

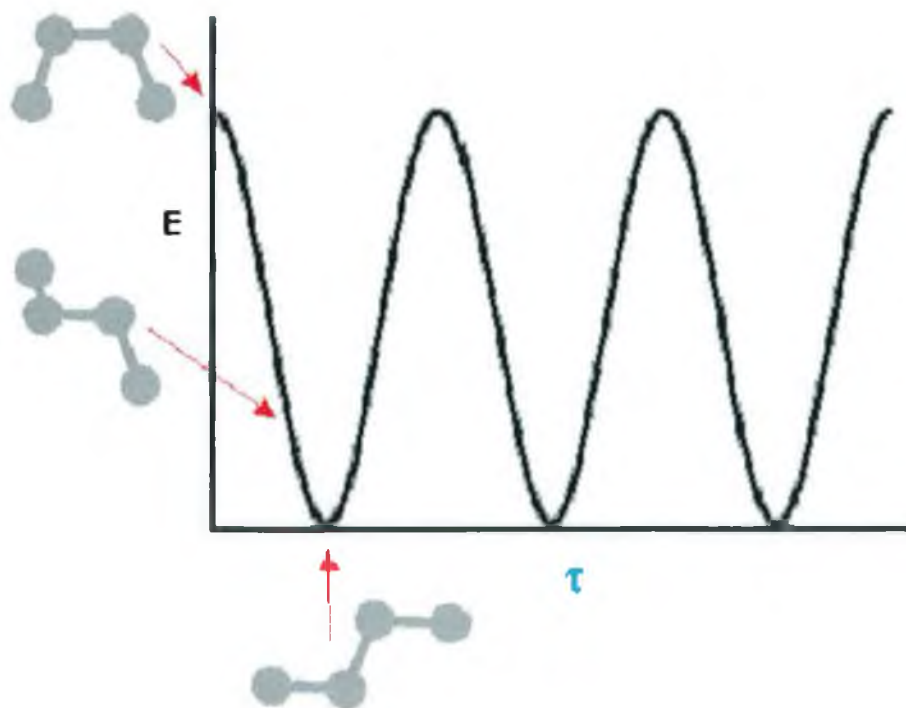


Figure 7. An illustration of how the torsional energy varies as the torsional angle, τ , changes for a simple alkane.

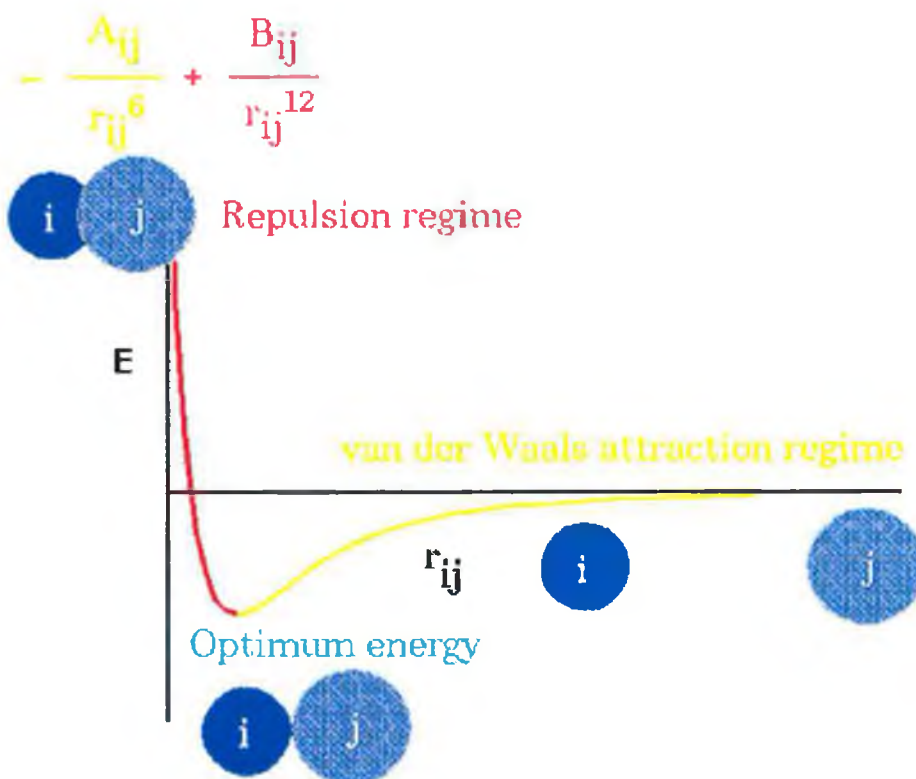


Figure 8. A schematic of the effect that the van der Waals radii of atoms have on the attractive and repulsive interactions.

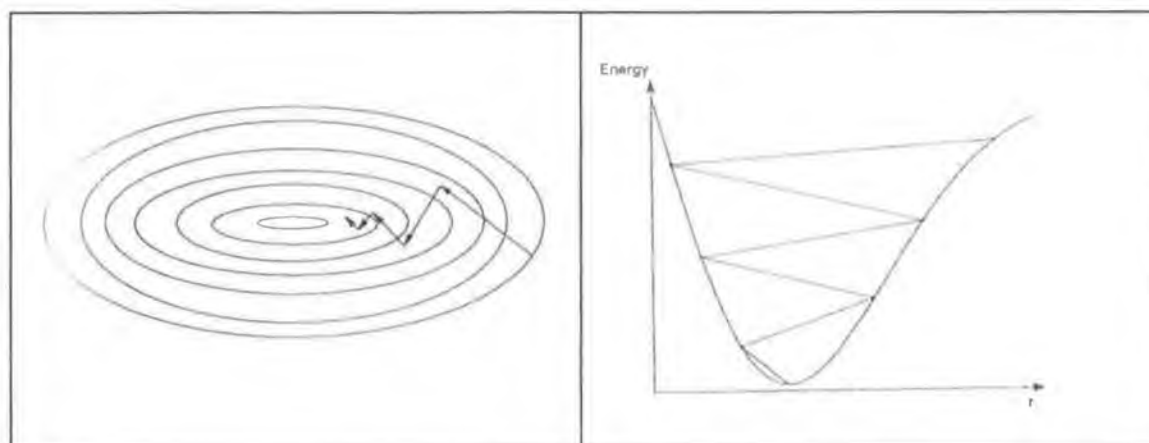


Figure 9. An illustration of the steepest descent minimisation method.

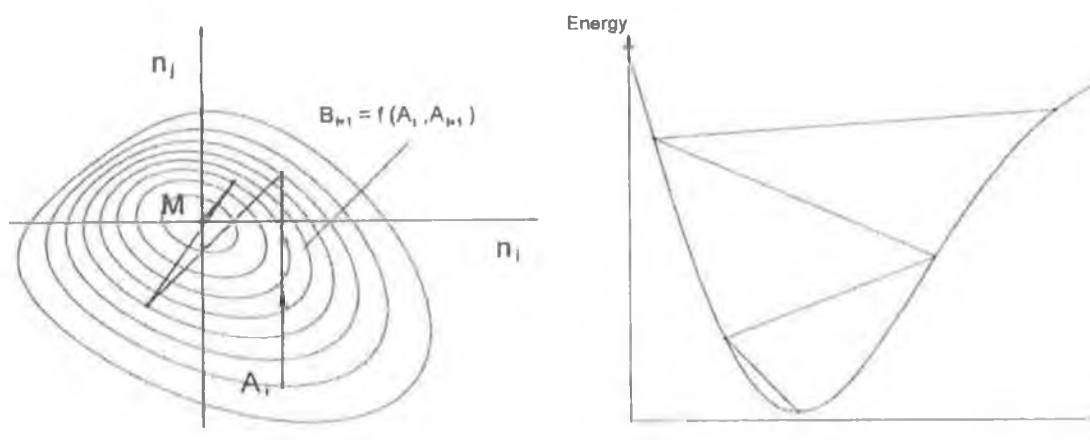


Figure 10. An illustration of the Polak-Ribiere minimisation method.

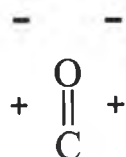
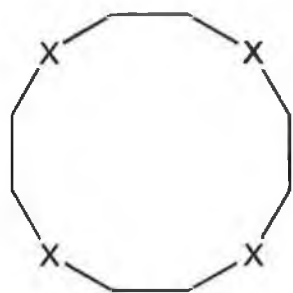
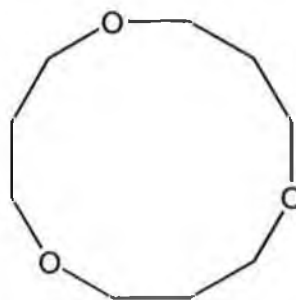


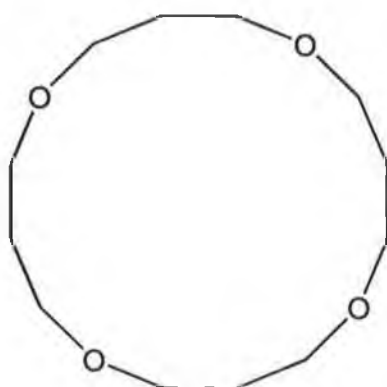
Figure 11. A schematic of partial charge placement around a carbonyl group to increase the accuracy of lone pair portrayal.



- [1] X=C Cyclododecane
- [2] X=O 12-crown-4
- [3] X=S [12]aneS₄

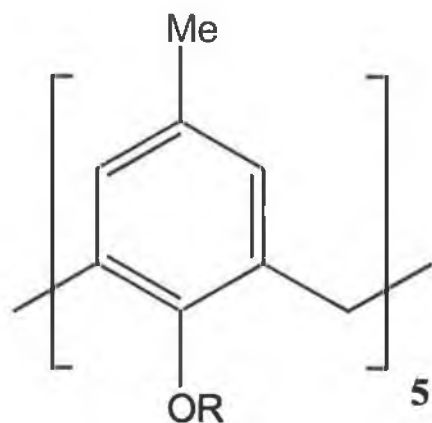


[4] 12-crown-3



[6] 16-crown-4

Figure 12. Crown ethers studied by Yates and Richardson.



- R=H (phenolic)
- R=Me (methyl ether)

Figure 13. The two calix[5]arenes studied utilising molecular mechanics methods by Thondorf and Brenn.

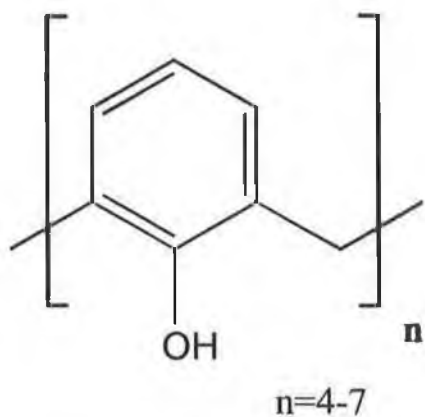


Figure 14. The unmodified calix[n]arenes studied by Harada and Shinkai.

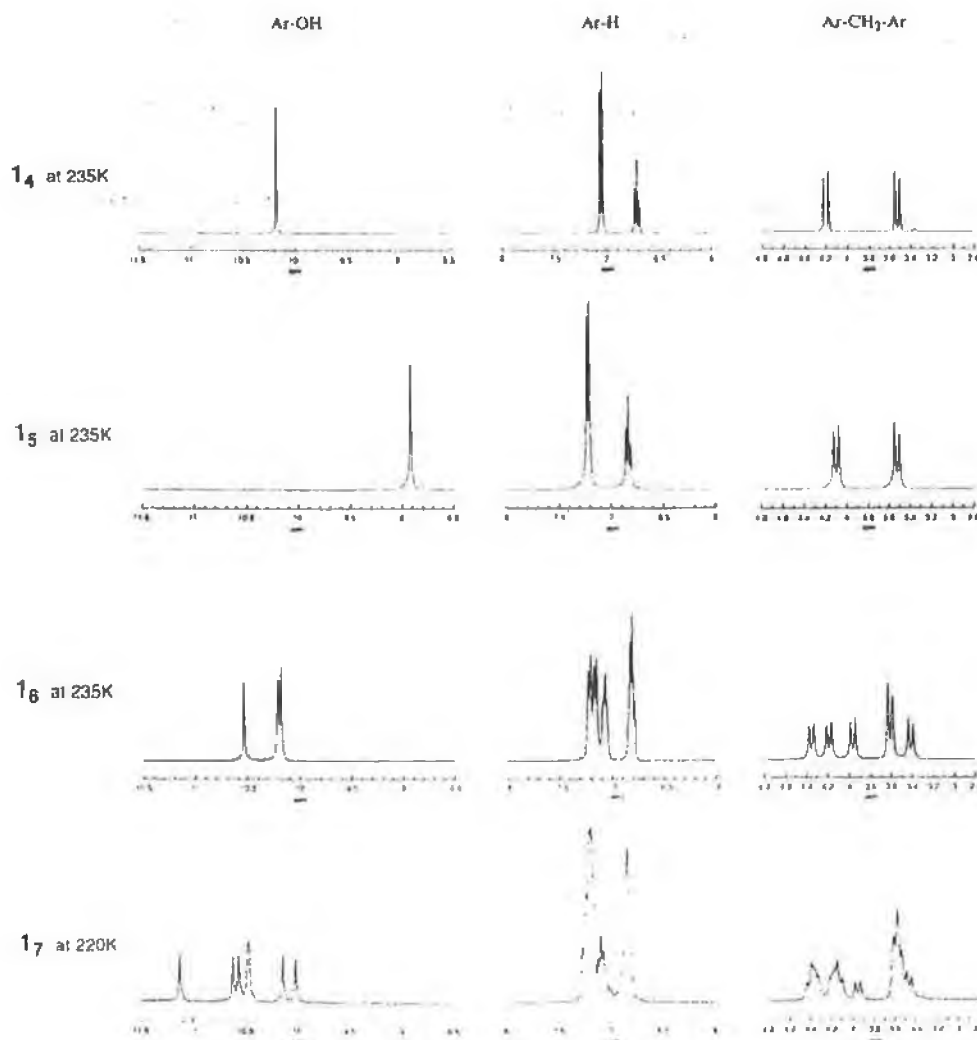


Figure 15. Partial ^1H NMR spectra of calix[4-7]arenes in the low temperature region (300 MHz, solvent CD_2Cl_2). $\mathbf{1}_n$ corresponds to the calix[n]arene.

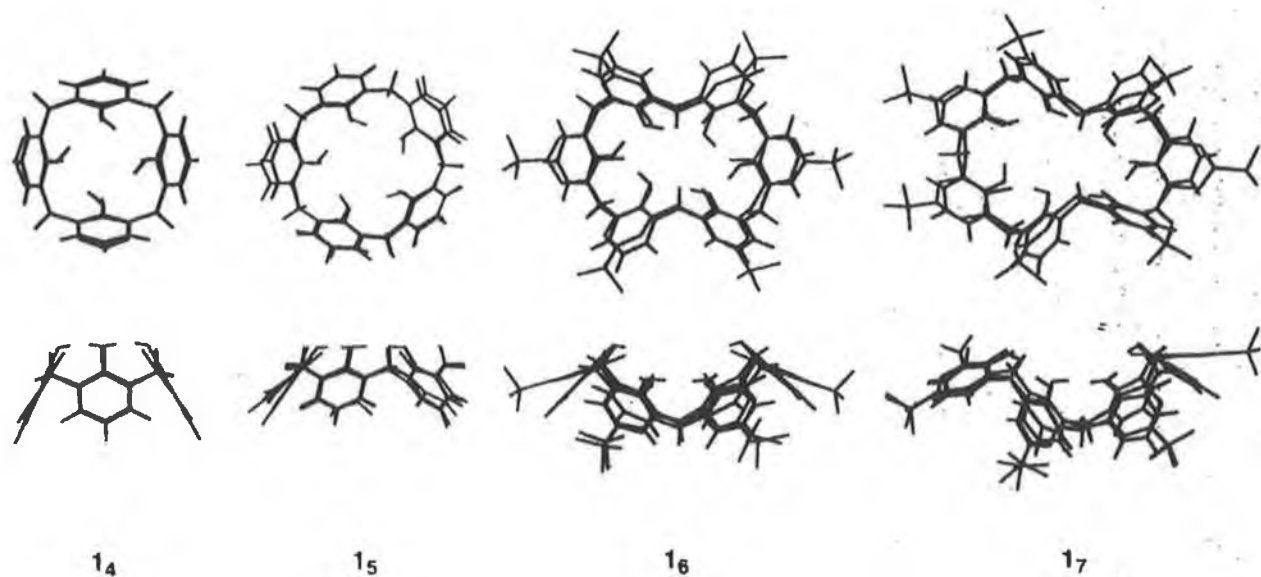


Figure 16. Superimposed displays of the X-ray crystallographic and the MM3(92) calculated structures. The RMS values corresponding to the methylene bridge carbons are: 0.02 Å for calix[4]arene; 0.14 Å for calix[5]arene; 0.33 Å for calix[6]arene and 0.49 Å for calix[7]arene.

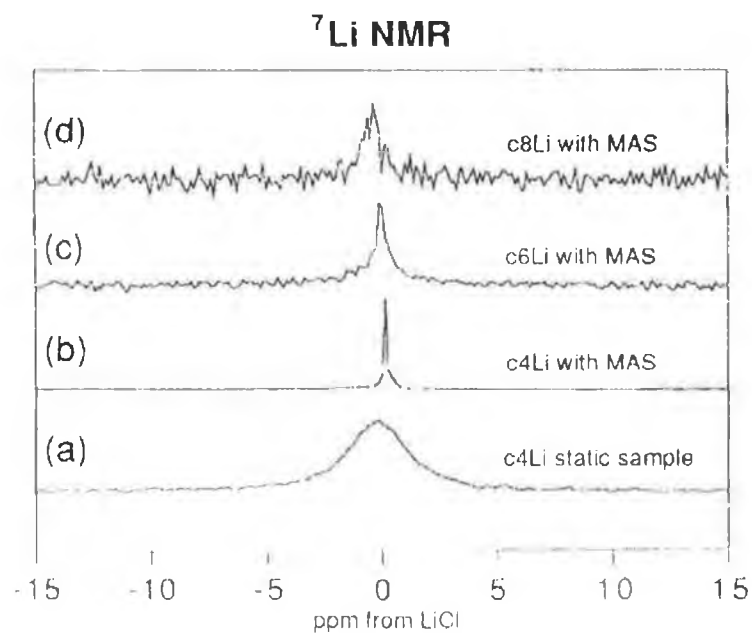


Figure 17. Solid state ^7Li NMR spectra of the calix[4-8]arenes (a)-(d) complexing Li^+ .

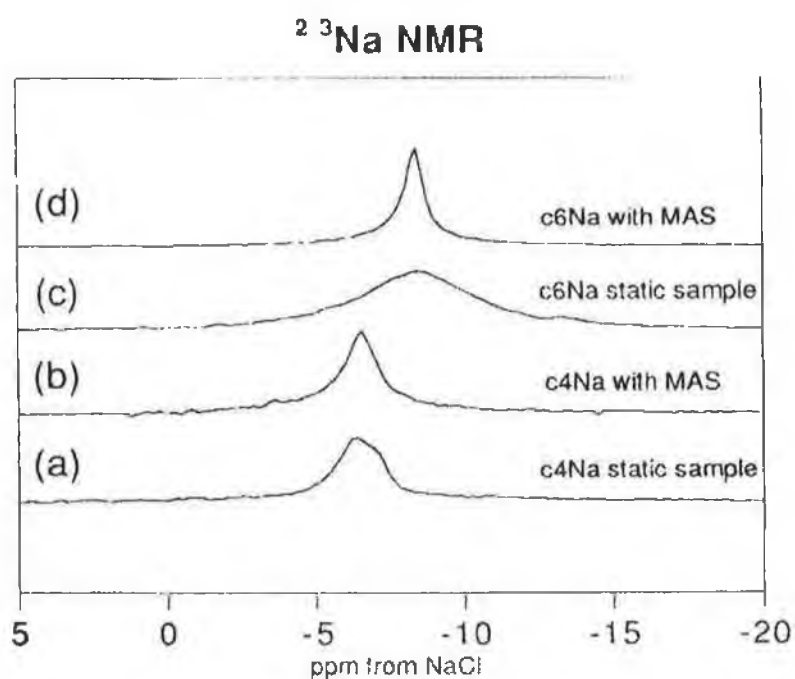


Figure 18. Solid state ^{23}Na NMR spectra of the calix[4,6]arenes (a)-(d) complexing Na^+ .

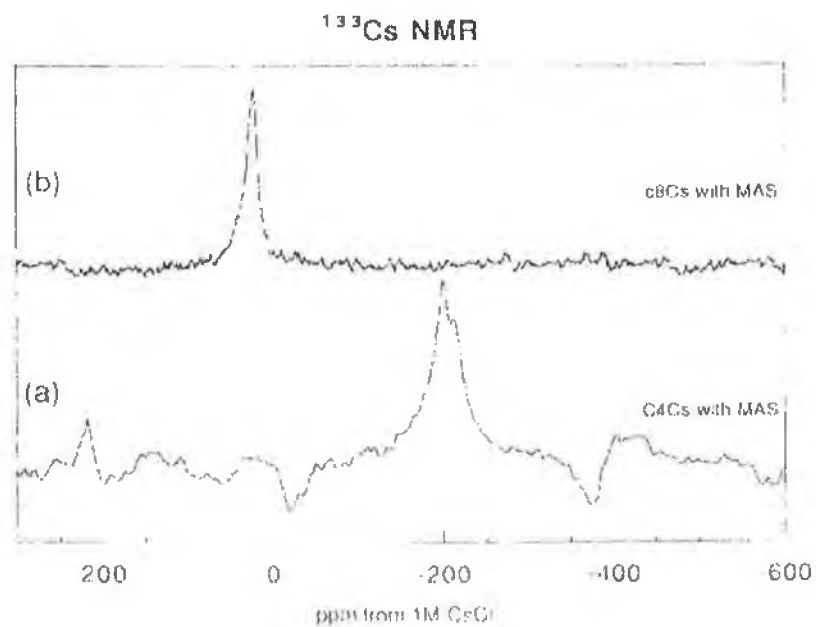


Figure 19. Solid state ^{133}Cs NMR spectra of the calix[4,8]arenes (a) and (b) complexing Cs^+ .

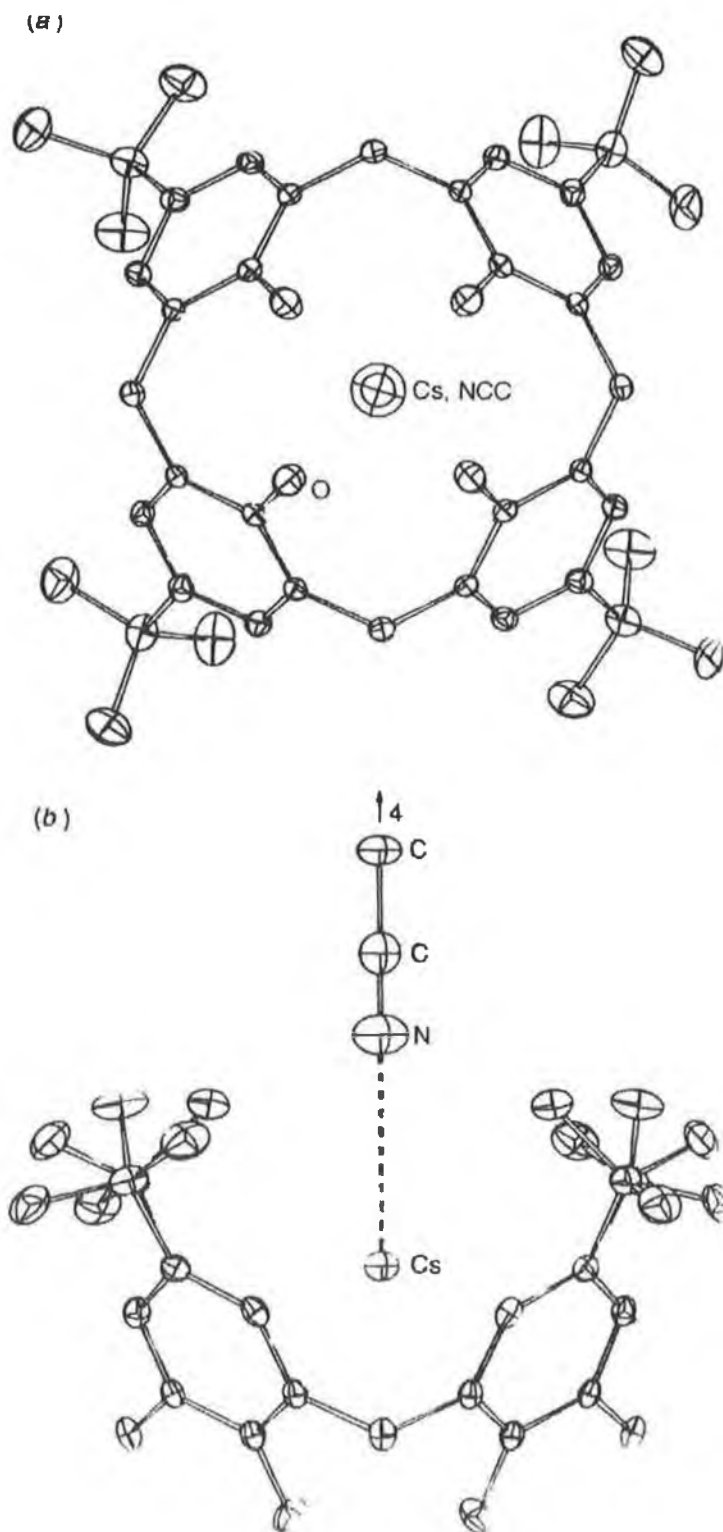


Figure 20. X-ray structure of the 1:1 Cs^+ complex of *p*-*tert.*-butyl-calix[4]arene monoanion. (a) A through the cavity view; (b) Side on view.

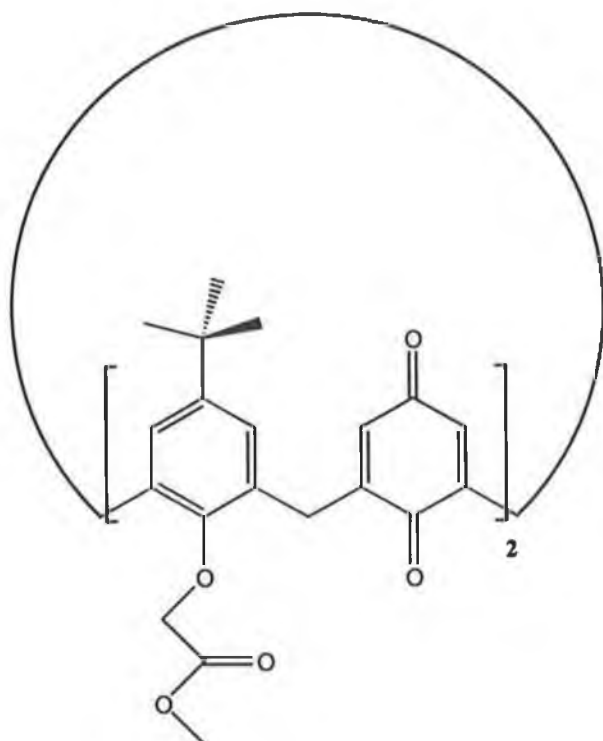
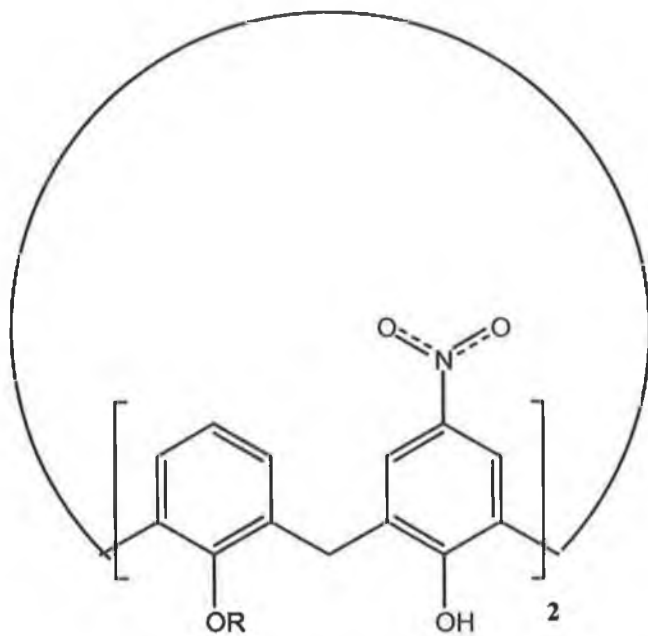


Figure 21. The calix[4]-26,28-diquinone used in complexation studies of amines by Chung et al.



- (1) $R+R = \text{CH}_2\text{CONH}(\text{CH}_2)_2\text{NHCOCH}_2$
 (2) $R = \text{CH}_2\text{COOEt}$

Figure 22. Nitro calix[4]arene used in complexation studies of amines and cations by Mohammed-Ziegler et al.

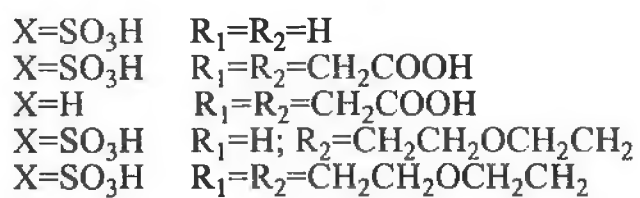
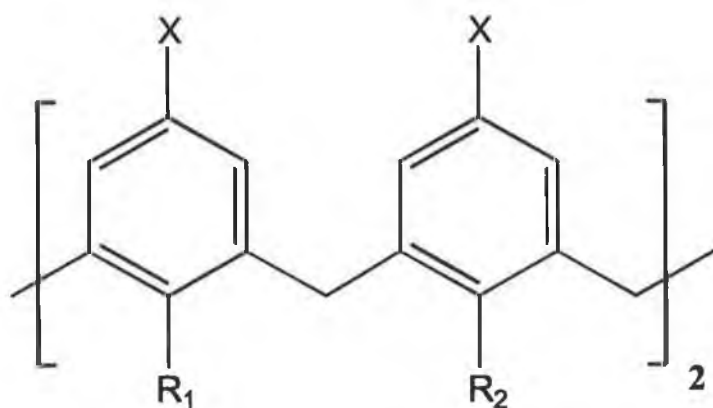


Figure 23. Tetrasulfonatocalix[4]arenes used in studied on complexation with L- α -amino acids.

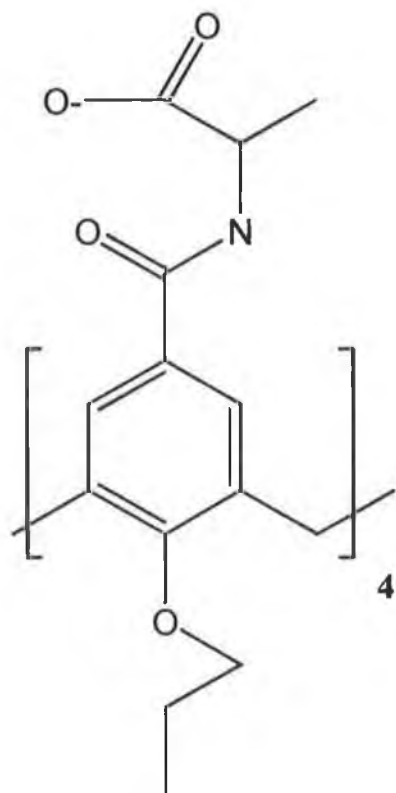


Figure 24. L-alanine upper rim functionalised calix[4]arene.

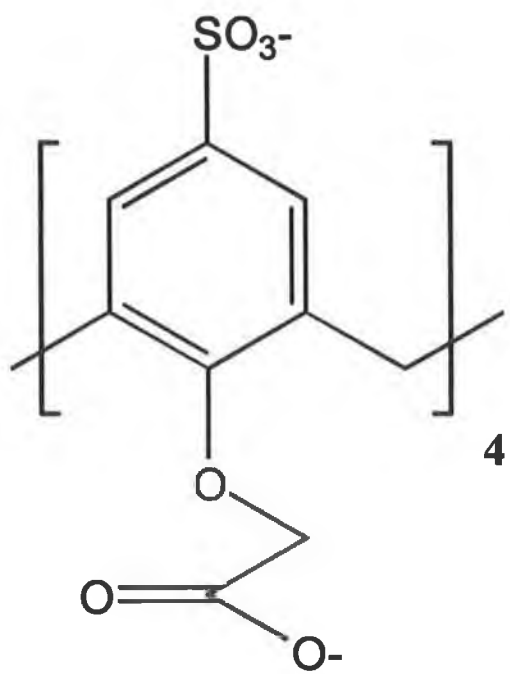


Figure 25. Tetrasulfonatecalix[4]arene utilised by Sansone et al.

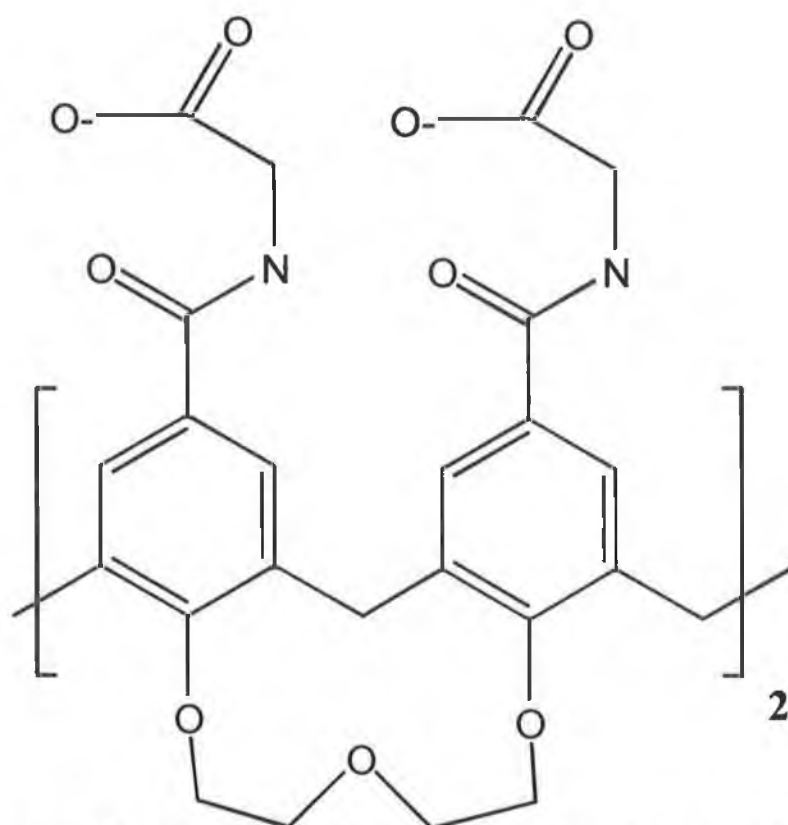


Figure 26. Glycol modified calix[4]arene for the binding of amines.

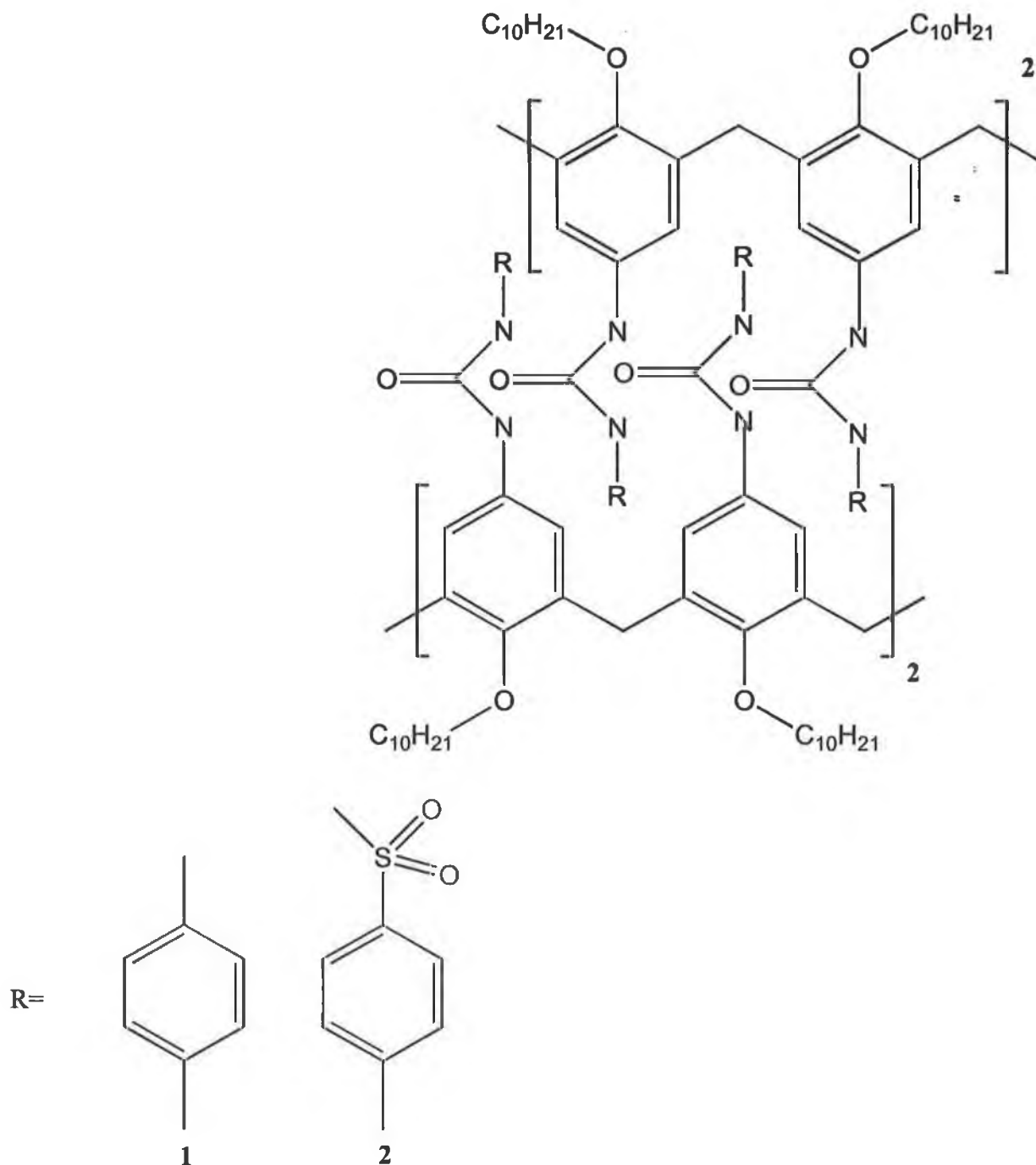


Figure 27. The "tongue-in-groove" interaction in urea modified calix[4]arenes.

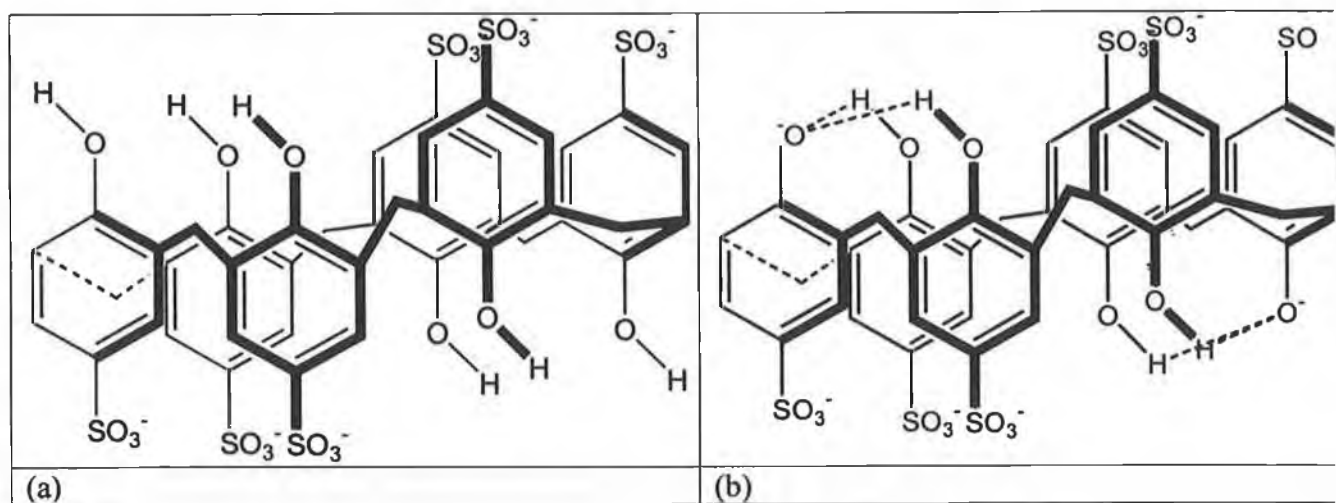


Figure 28. Lower rim unsubstituted sulfonated calix[6]arenes, (a) protonated and (b) deprotonated, demonstrating the preorganisation attained due to intramolecular hydrogen bonding.

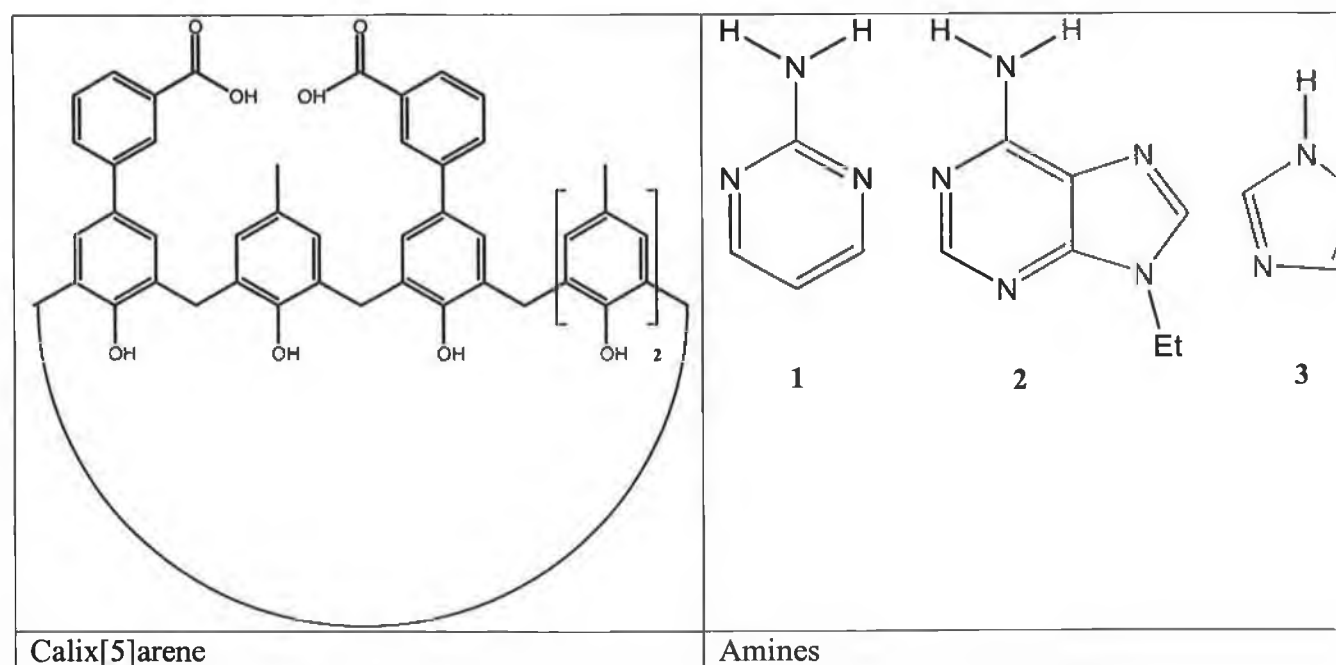
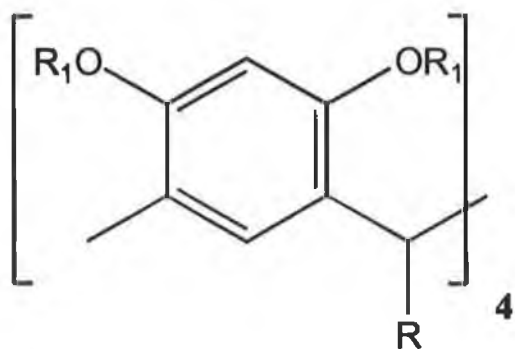


Figure 29. A functionalised calix[5]arene-pentahydroxy and the guest amines studied.



R=phenyl
 $R_1=n-C_5H_{11}$

Figure 30. A resorc[4]arene modified with long alkyl chains to improve solubility in organic (non-polar) solvents.

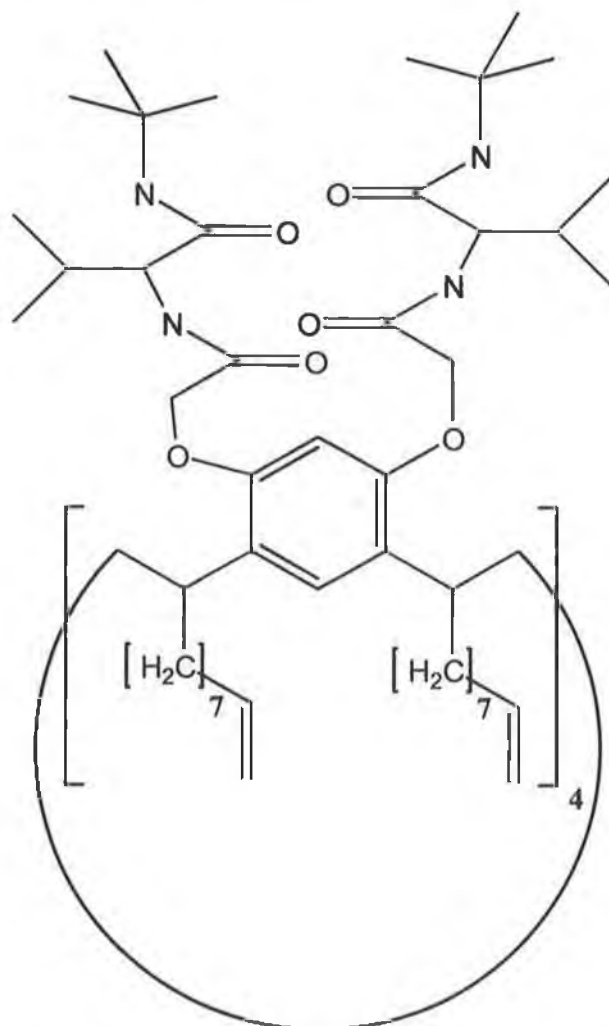


Figure 31. A L-valine-tert-butylamide resorc[4]arene used in resolving amino acid methyl esters.

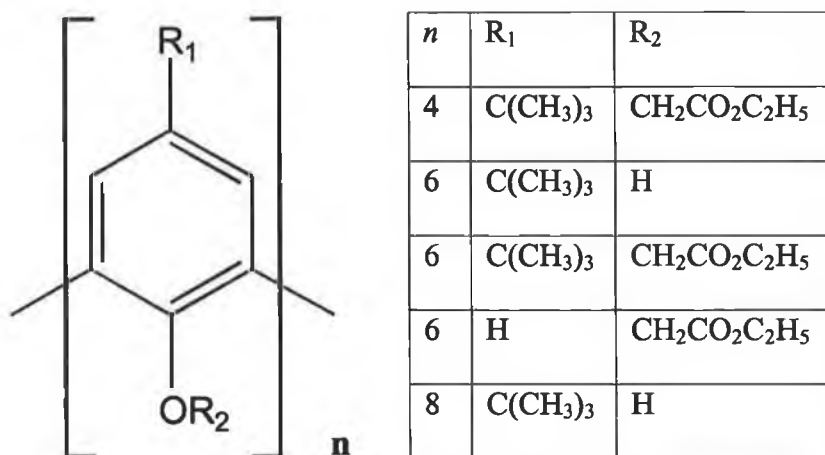


Figure 32. The five calix[n]arenes used as PQC sensors.

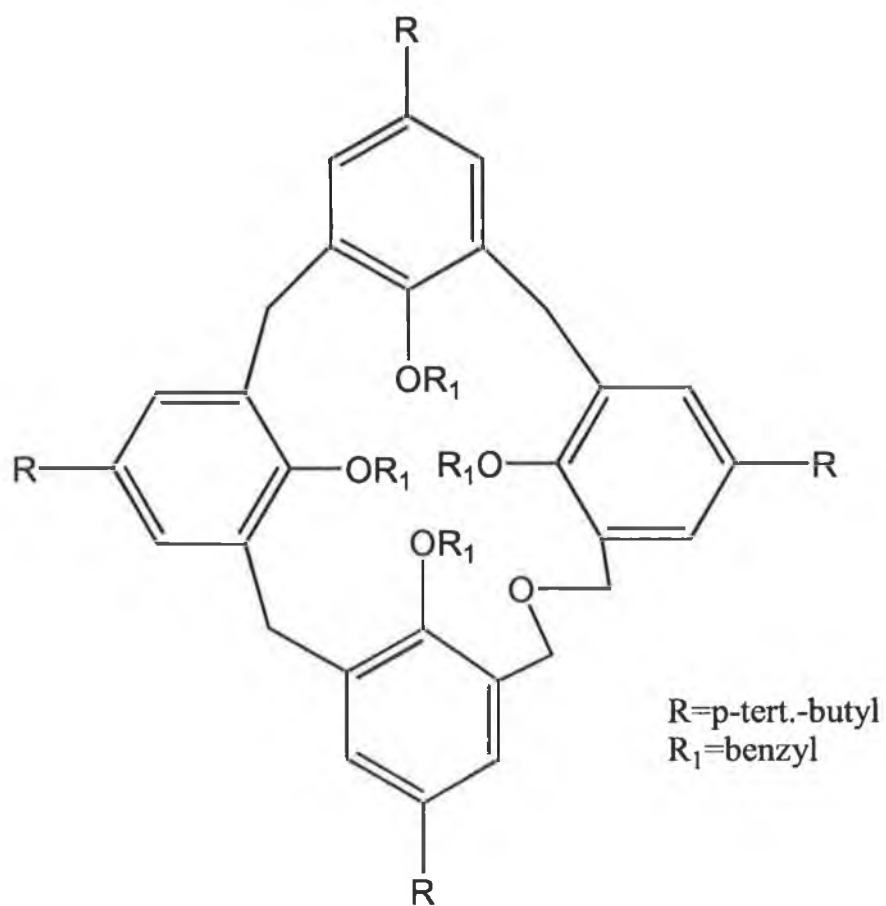


Figure 33. The tetra-tert-butyl ether of *p-tert.*-butyl-dihomooxalix[4]arene.

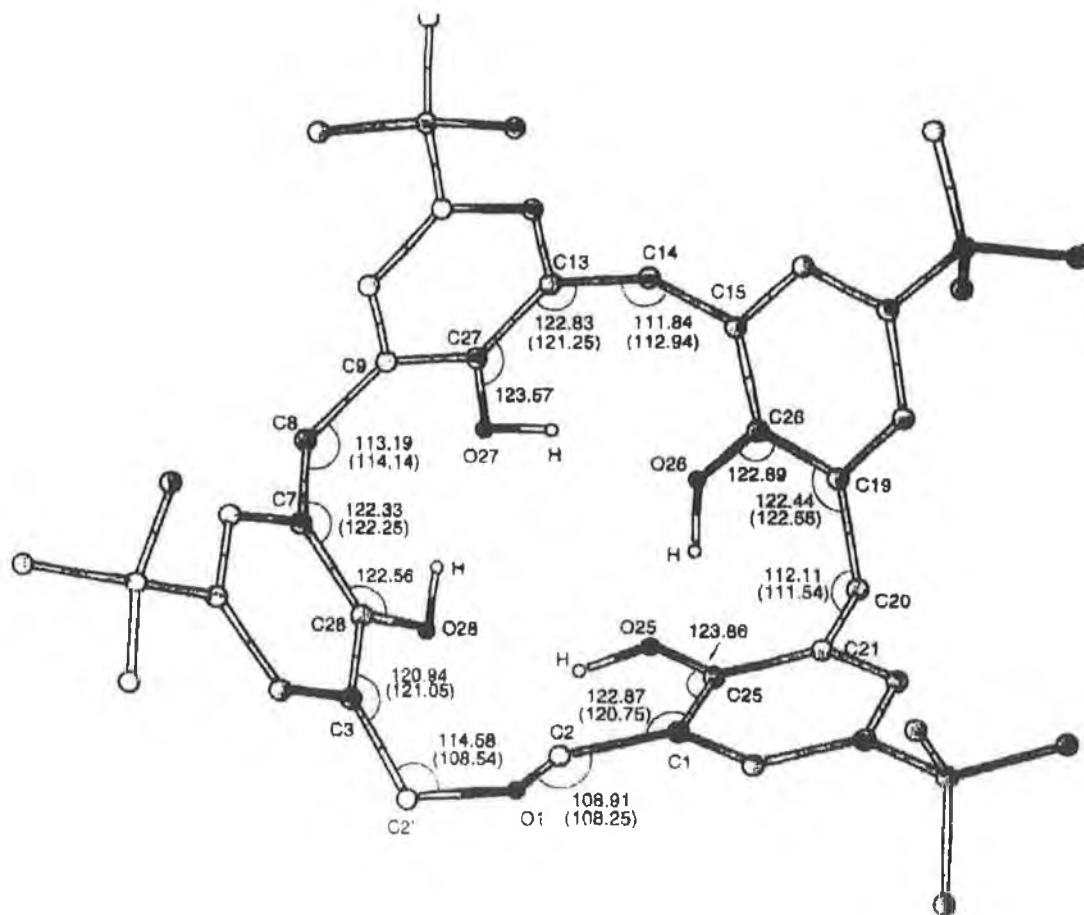
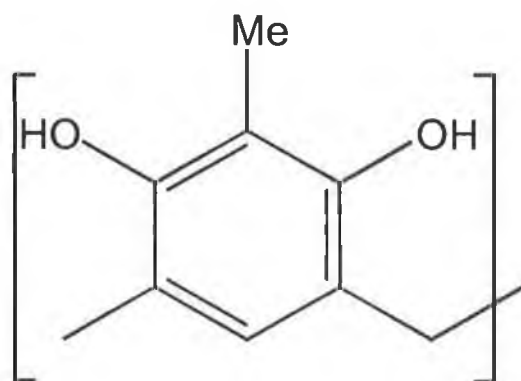


Figure 34. A through the cavity view of the cone shaped conformation showing a comparison between the AM1 valence angles and X-ray crystallography data (values in parentheses).



4

Figure 35. Thondorf et al. performed molecular mechanics calculations on this p-methylresorcarene.

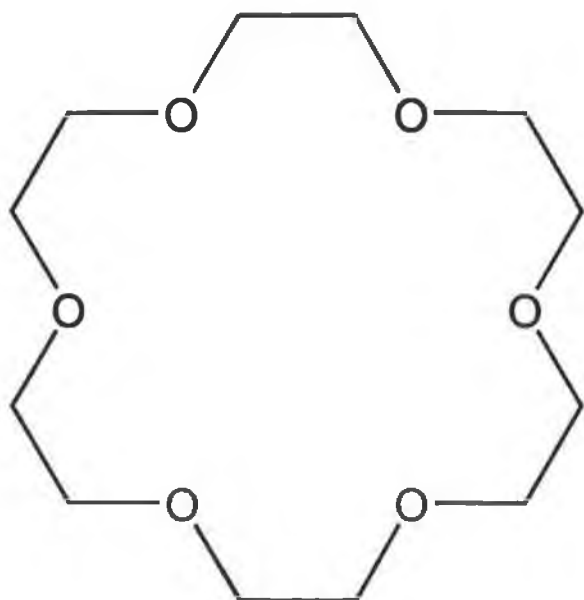


Figure 36. 18-crown-6: Investigated by Schalley et al. with reference to alkali cation binding.

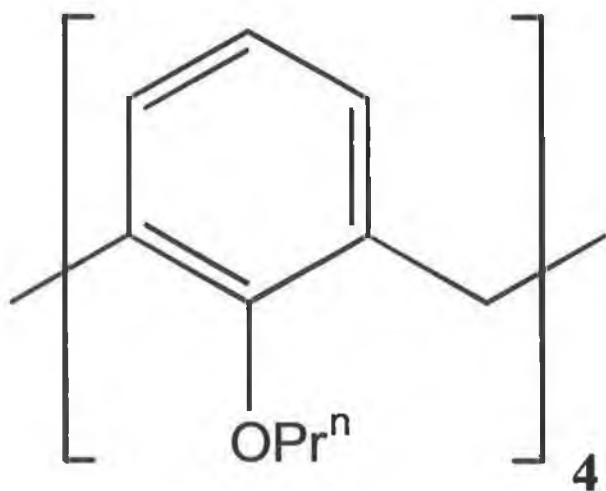


Figure 37. Calix[4]arene studied by Inokuchi et al. displayed cation- π interactions (Pr^n : neo-propyl).

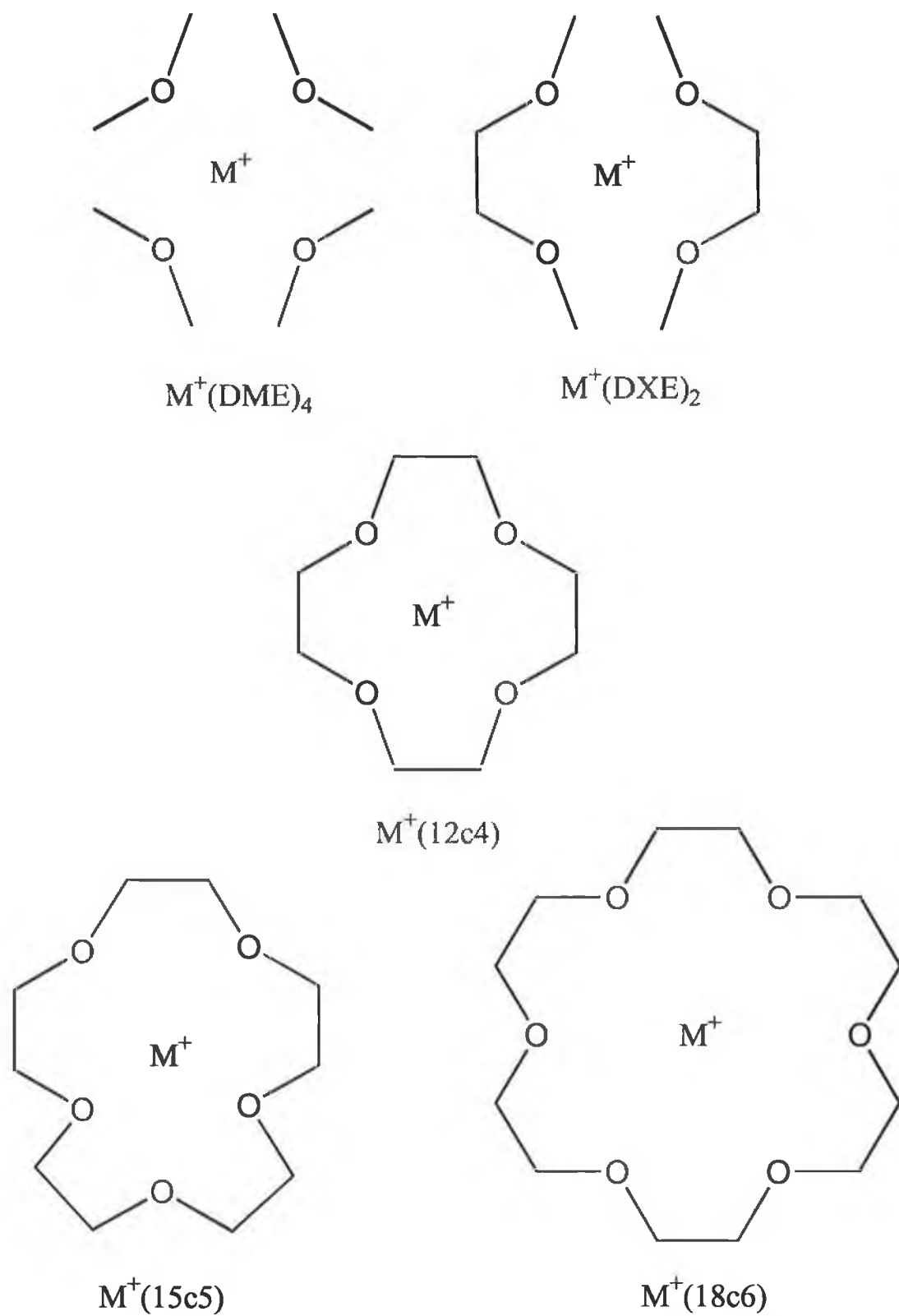


Figure 38. The series of ethers and crown ethers used in studying host:alkali metal cation interactions.

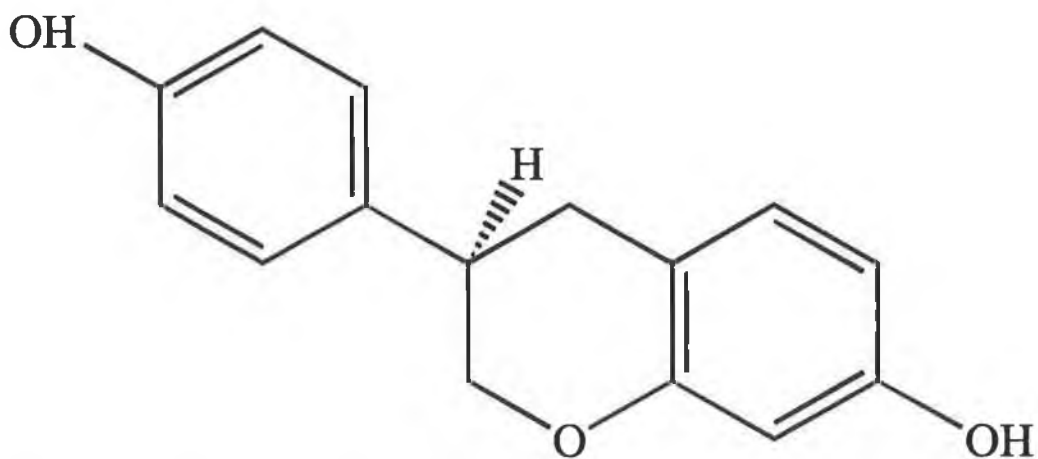


Figure 39. A 2D representation of R-equol.

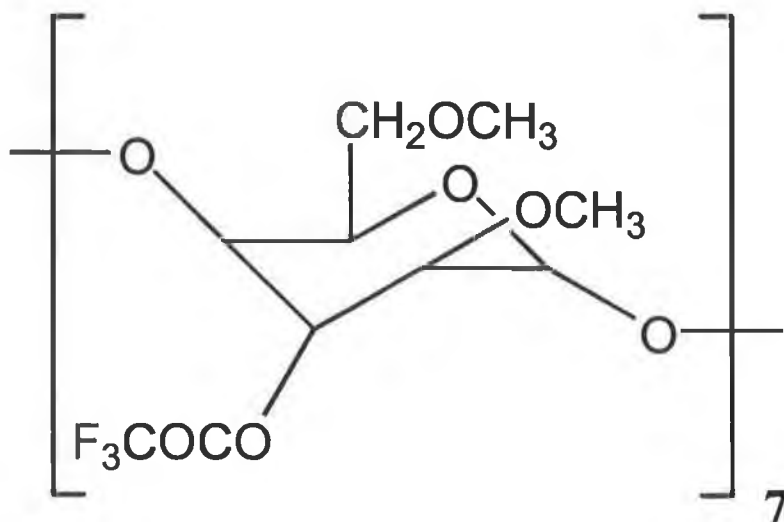


Figure 40. The modified β -cyclodextrin that was studied both experimentally and computationally interacting with 20 chiral guest molecules.

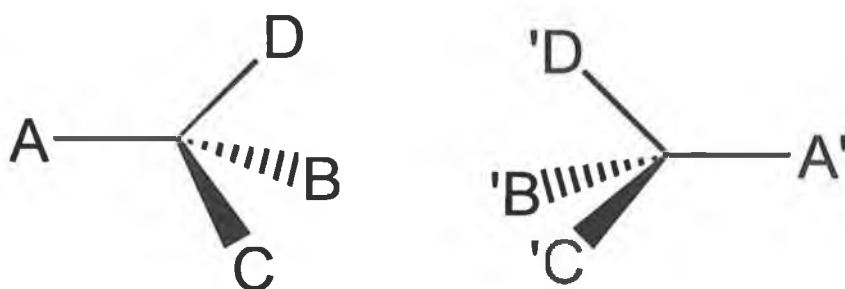


Figure 41. The classic 3-point model enantiodiscriminatory interaction.

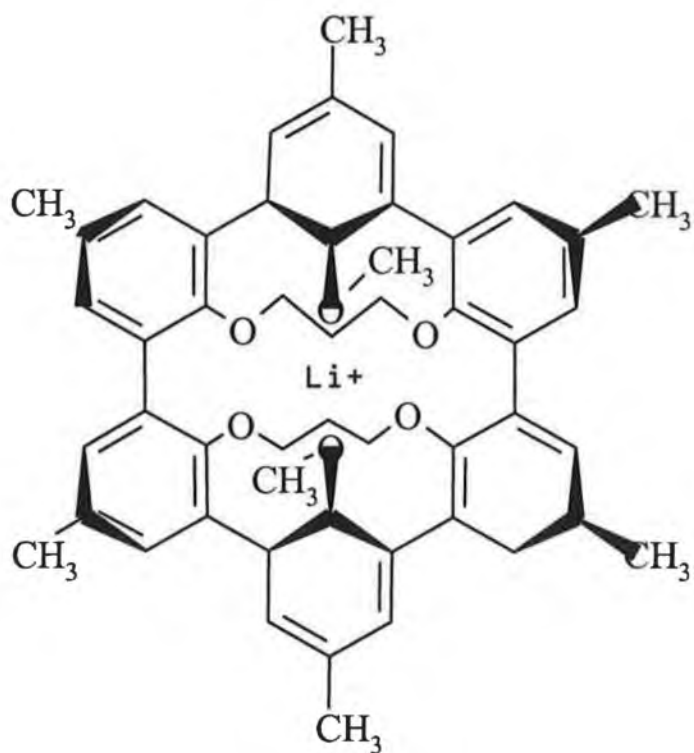


Figure 42. Complexation of a Li⁺ cation by a spherand with six potential chelating sites.

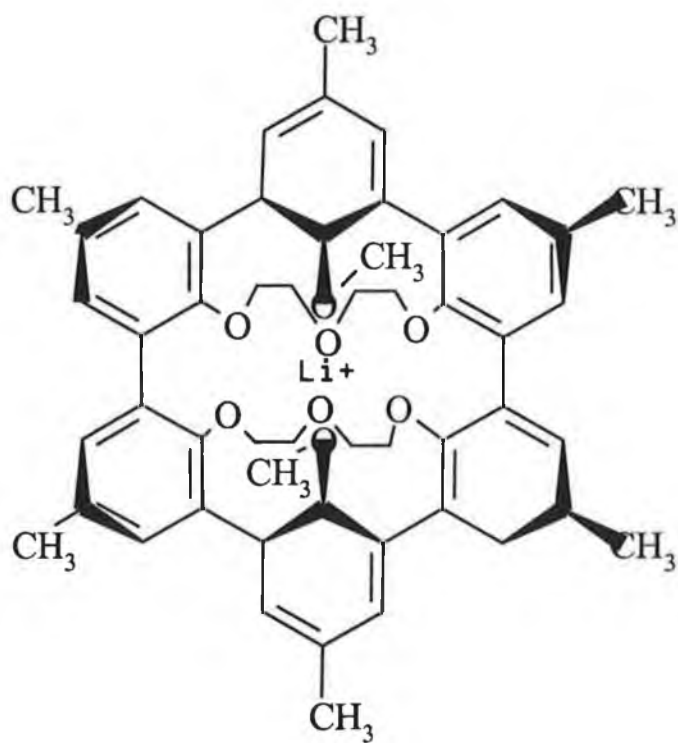


Figure 43. Complexation of a Li⁺ cation by a spherand with eight potential chelating sites.

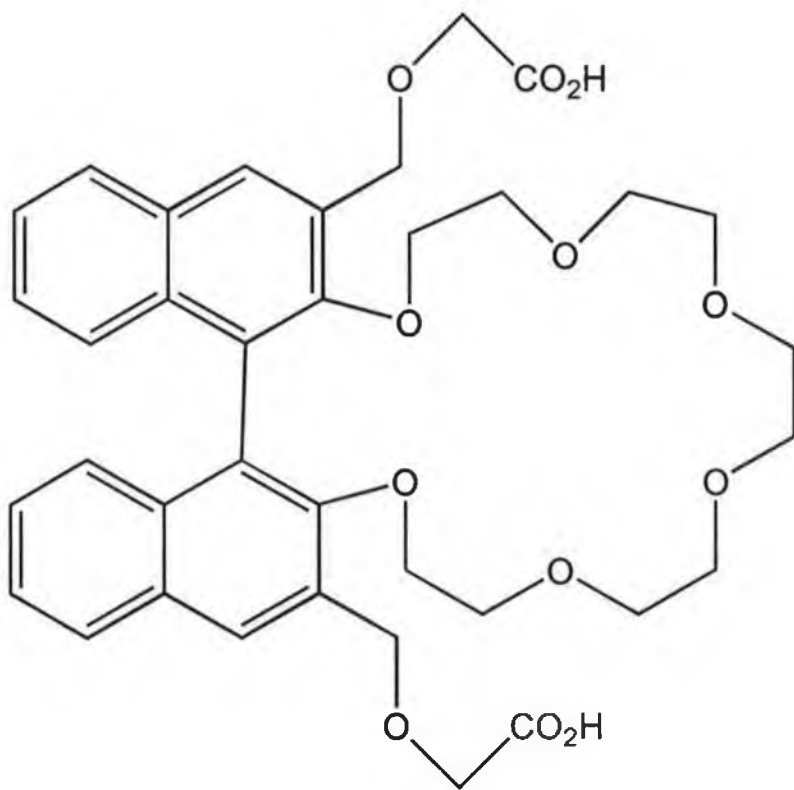


Figure 44. A binaphthyl crown ether with enantioselectively complexes valine.

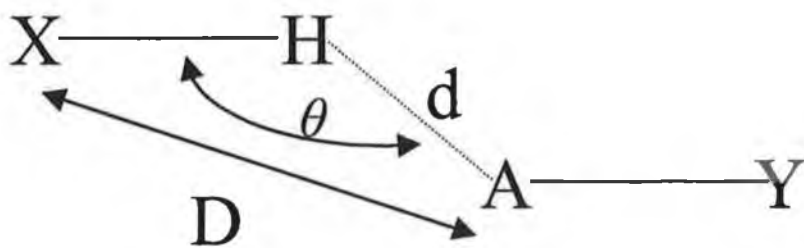


Figure 45. Definition of the variables used in Table 13.

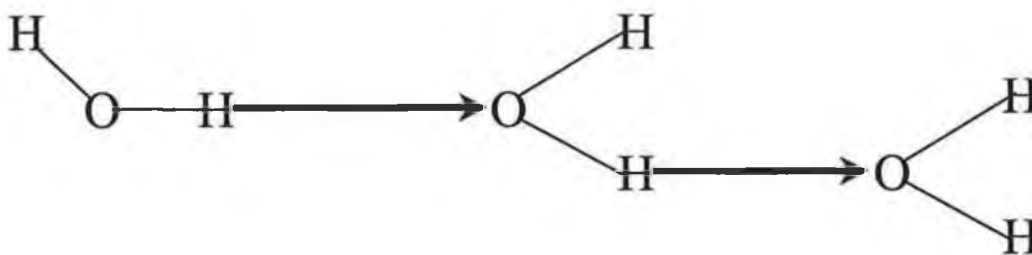
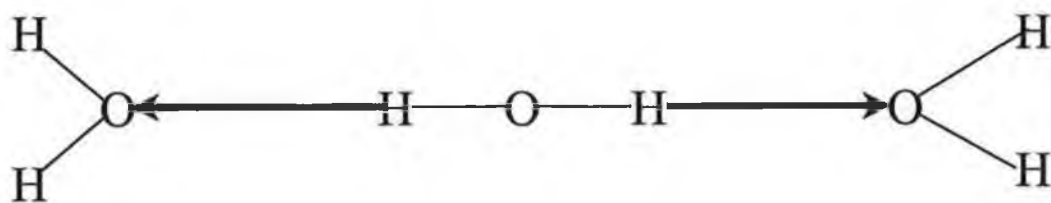
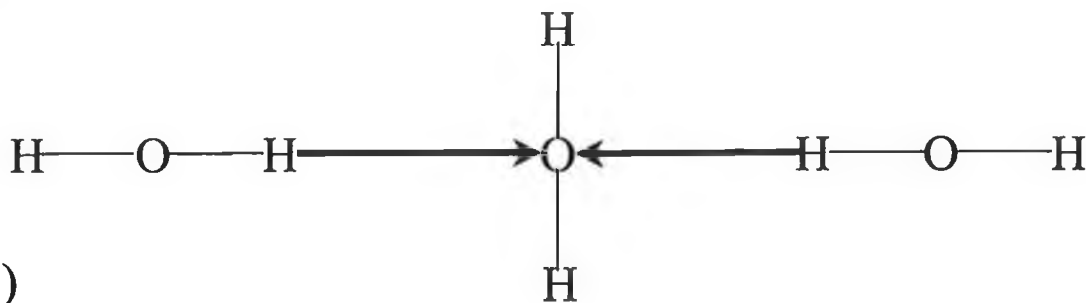


Figure 46. The most favourable, theoretically, hydrogen bonding patterns formed; the sequential double donor (The thick arrow represents the hydrogen bond).



(a)



(b)

Figure 47. Alternative hydrogen bonding patterns that could be formed.

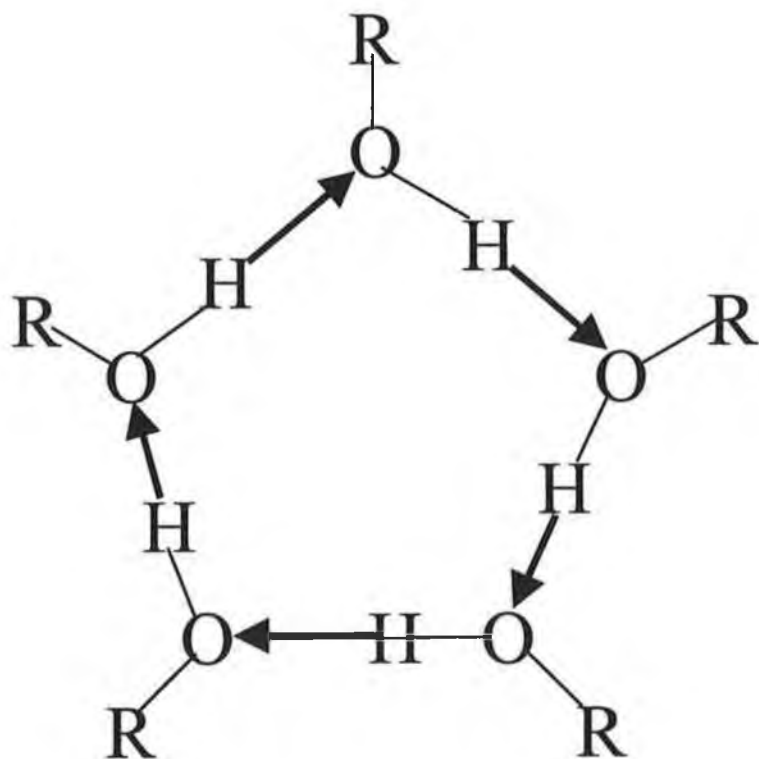


Figure 48. The theoretically most stable cyclic hydrogen bonding pattern calculated to form.

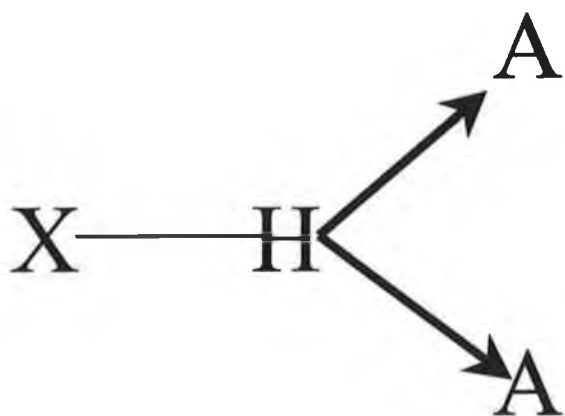


Figure 49. Hydrogen bond formation with multiple acceptor atoms.

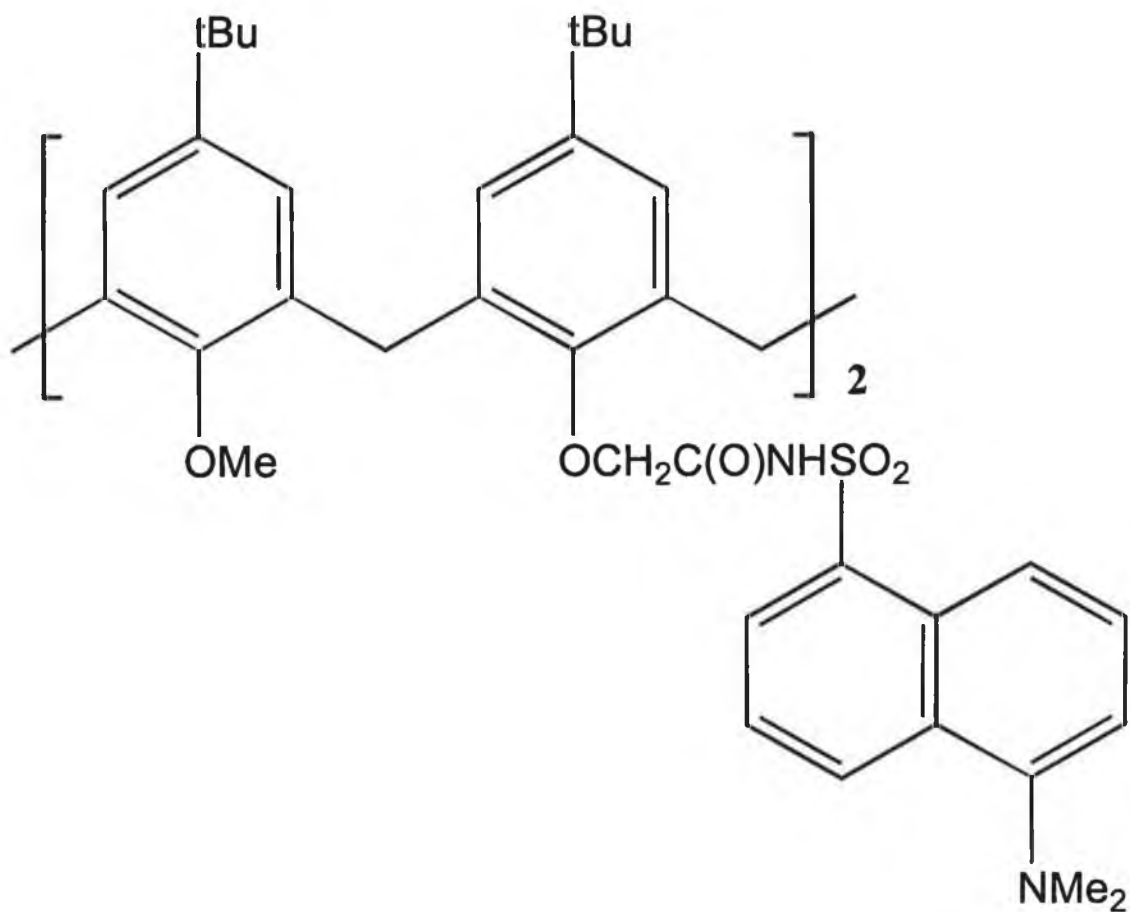


Figure 50. The first fluorogenic calixarene for Hg(II) recognition.

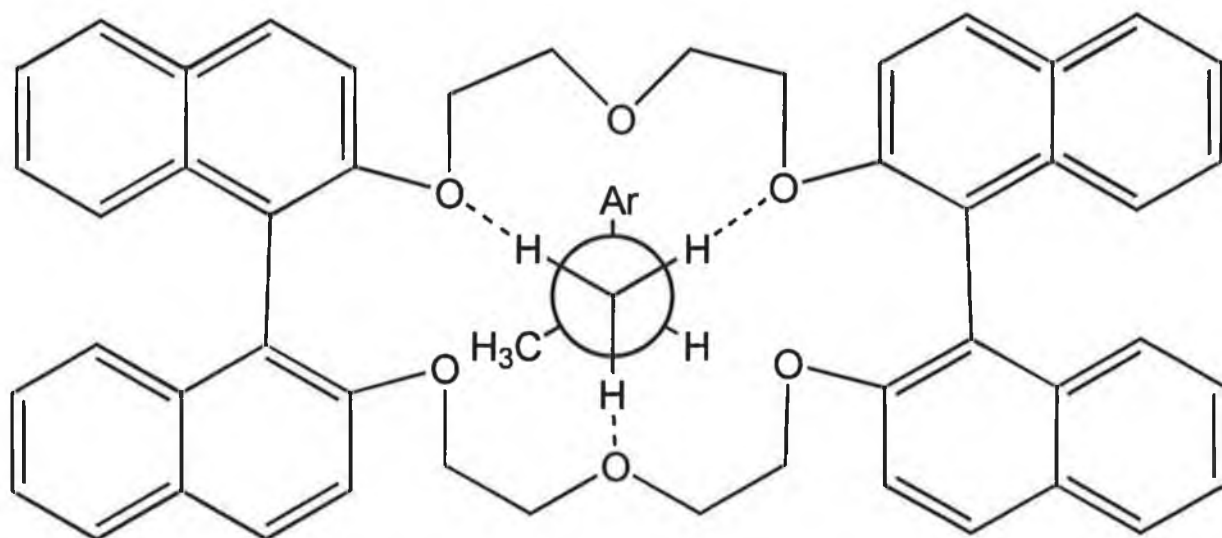


Figure 51. Projection down C-N bond of the R-phenylethylamine salt complexed with a binaphthyl modified crown ether.

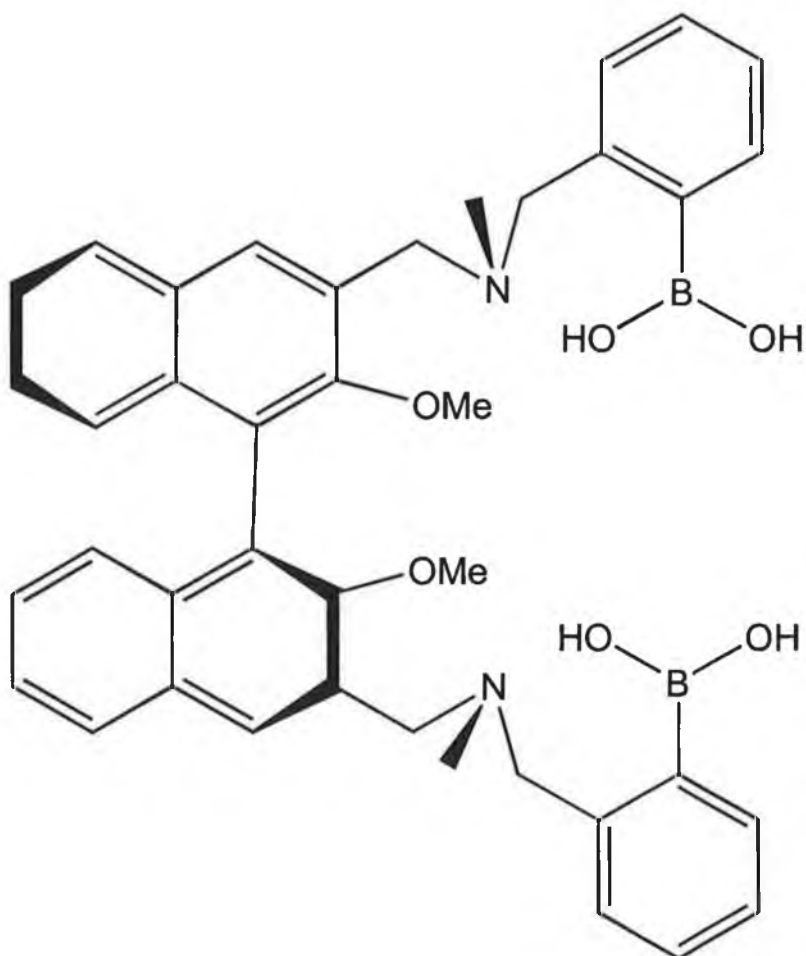


Figure 52. A binaphthyl derived molecule that can enantiodiscriminate between certain sugars.

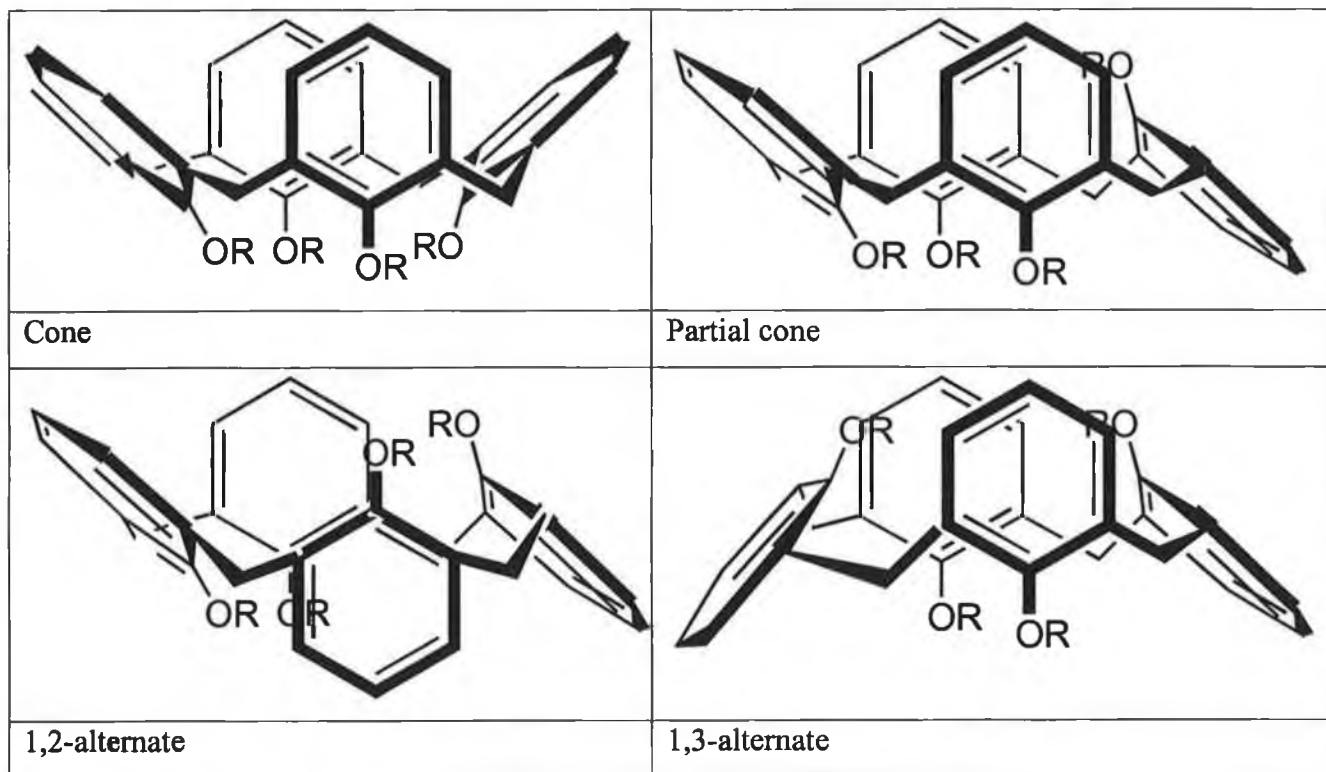


Figure 53. The four possible conformations of the calix[4]arene.

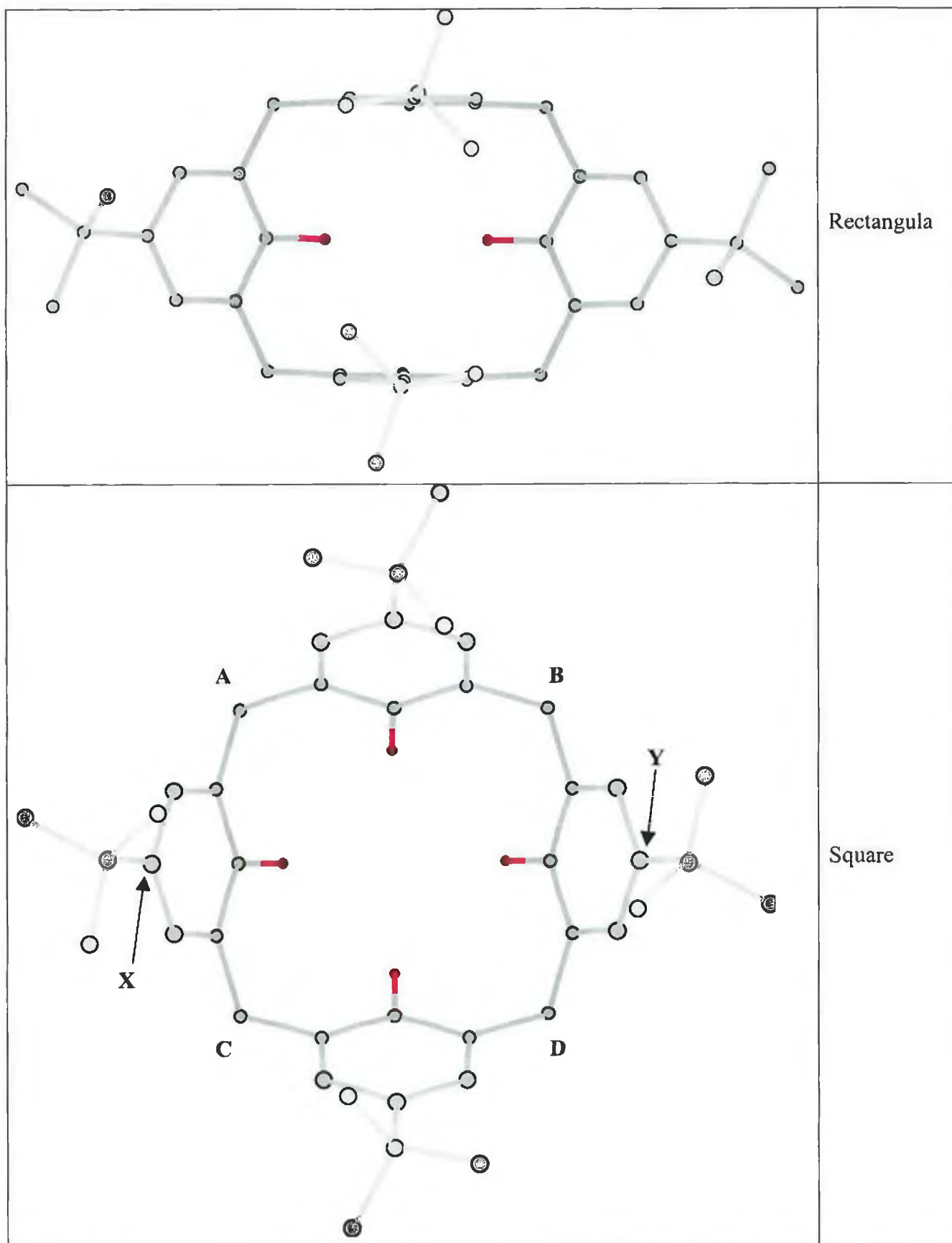
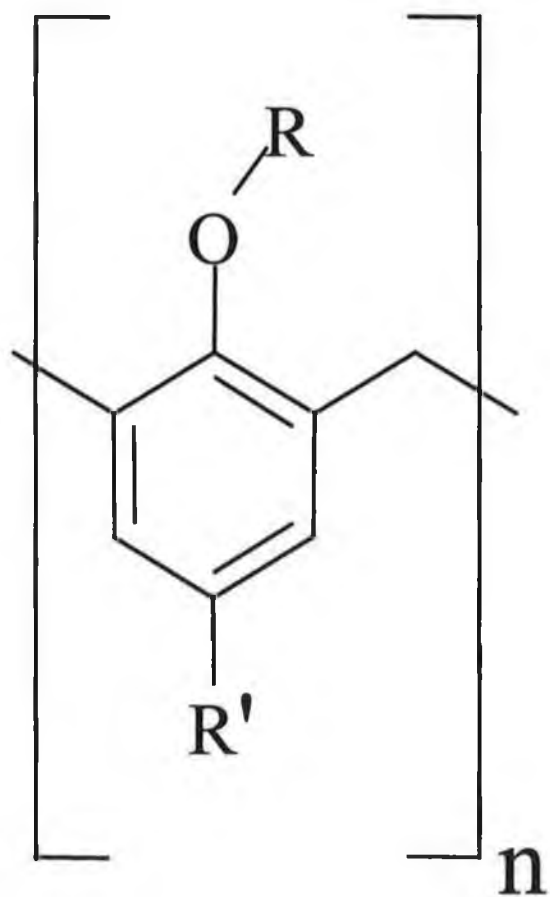


Figure 54. The C_{2v} (rectangular) and C_{4v} (square) views of a calix[4]arene.



| | R | R' | <i>n</i> |
|----------|--------------------------------------|-----------------|----------|
| 1 | CH ₂ CON(Et) ₂ | ^t Bu | 4 |
| 2 | CH ₂ CO ^t Bu | ^t Bu | 5 |
| 3 | CH ₂ COOMe | ^t Bu | 4 |
| 4 | CH ₂ COOEt | ^t Bu | 4 |
| 5 | CH ₃ | ^t Bu | 4 |
| 6 | H | ^t Bu | 4 |

Figure 55. A schematic diagram of the six non-chiral calix[4]arenes studied.

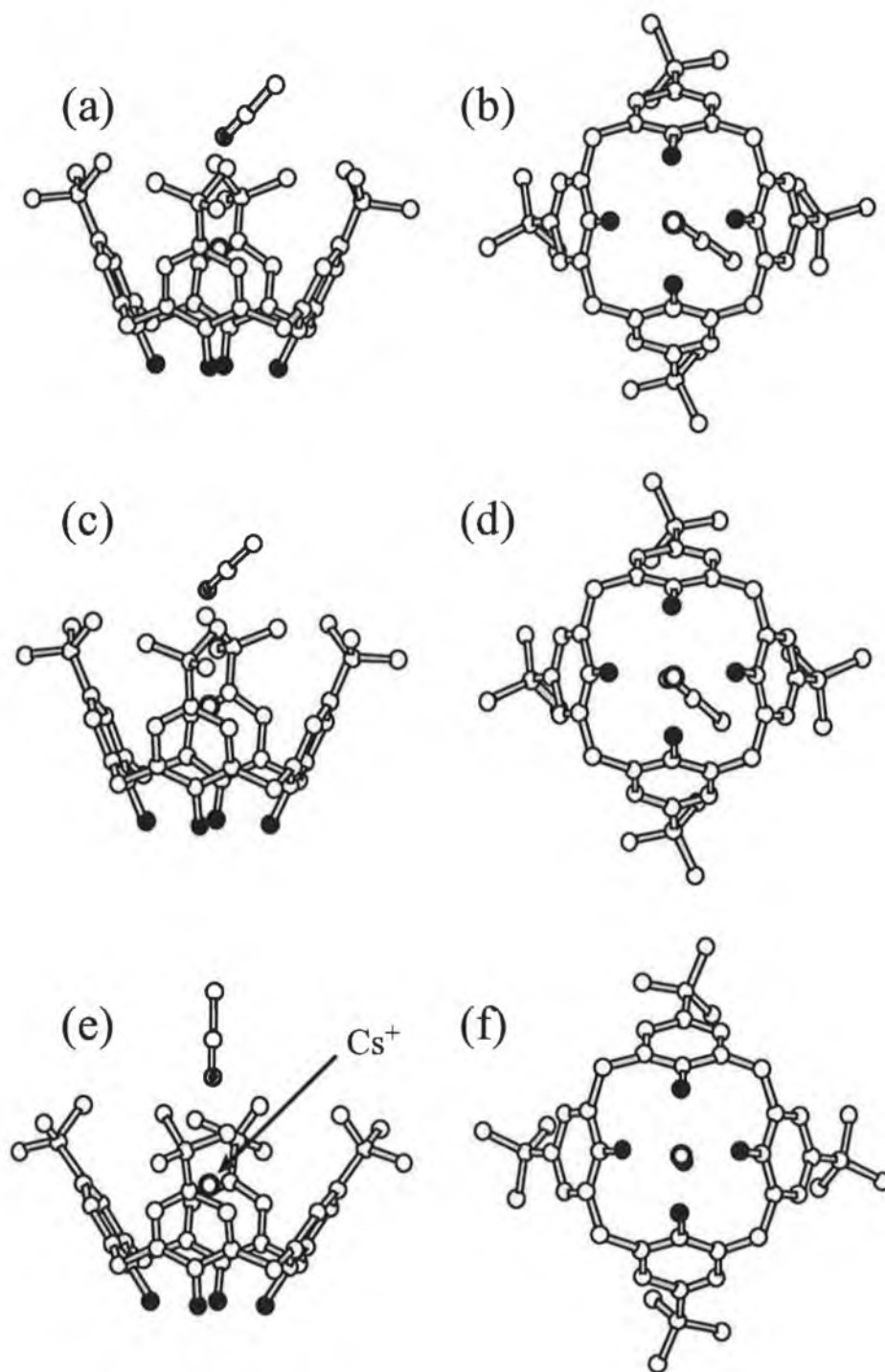


Figure 56. Orthogonal views of : (a), (b) the model structure of the Cs⁺ complex of 6 using partial charges for a singly-ionised complex; (c), (d) a similar model structure obtained using partial charges for a neutral calixarene; (e), (f) the X-ray structure of the complex. An acetonitrile solvate is shown in each of the structures. Dark gray ball: Nitrogen; black ball: Oxygen; white ball: Carbon.

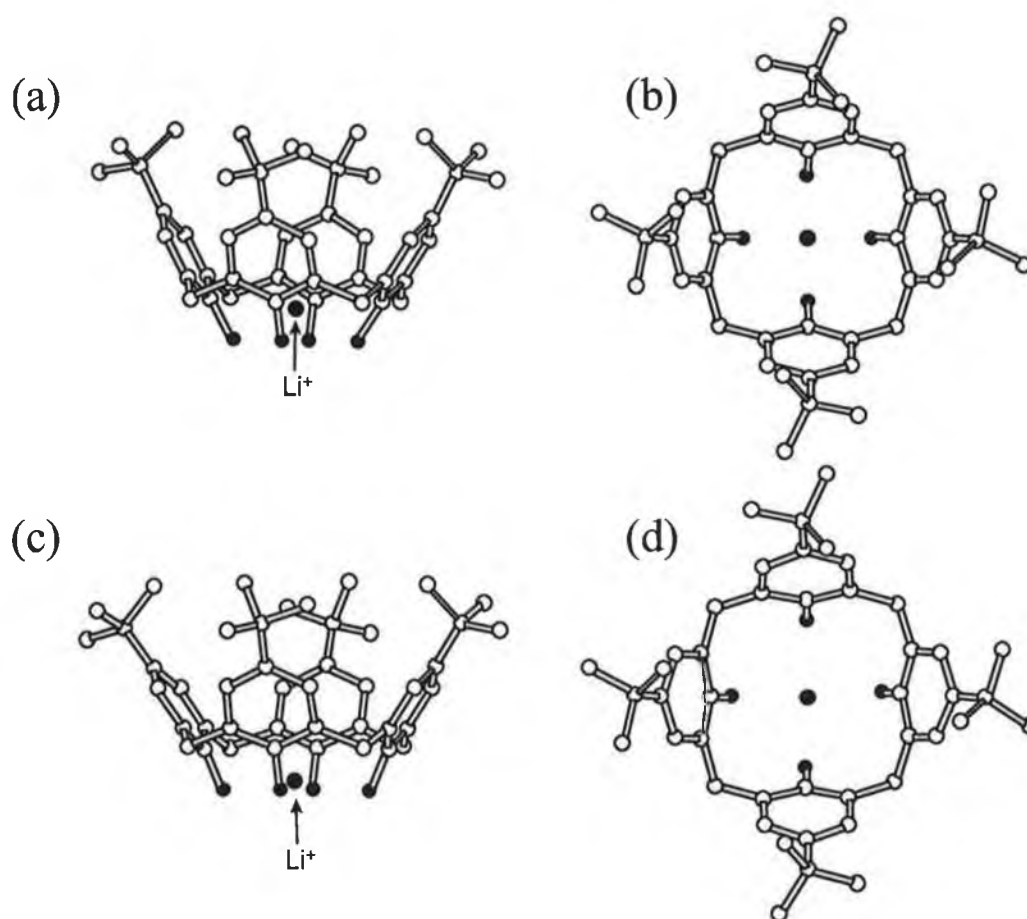


Figure 57. Orthogonal views of model structures of the Li^+ complex of **6**: (a), (b) modelled using molecular mechanics; (c), (d) modelled using the PM3 semi-empirical method.

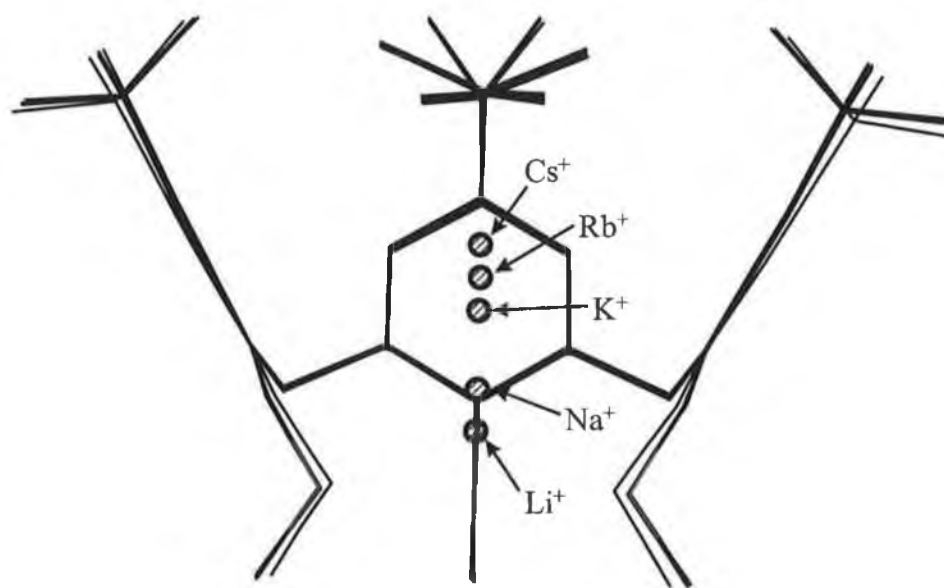


Figure 58. Overlaid model structures of the complexes of **5** with Li^+ , Na^+ , K^+ , Rb^+ and Cs^+ . The red lines indicate oxygen atoms.

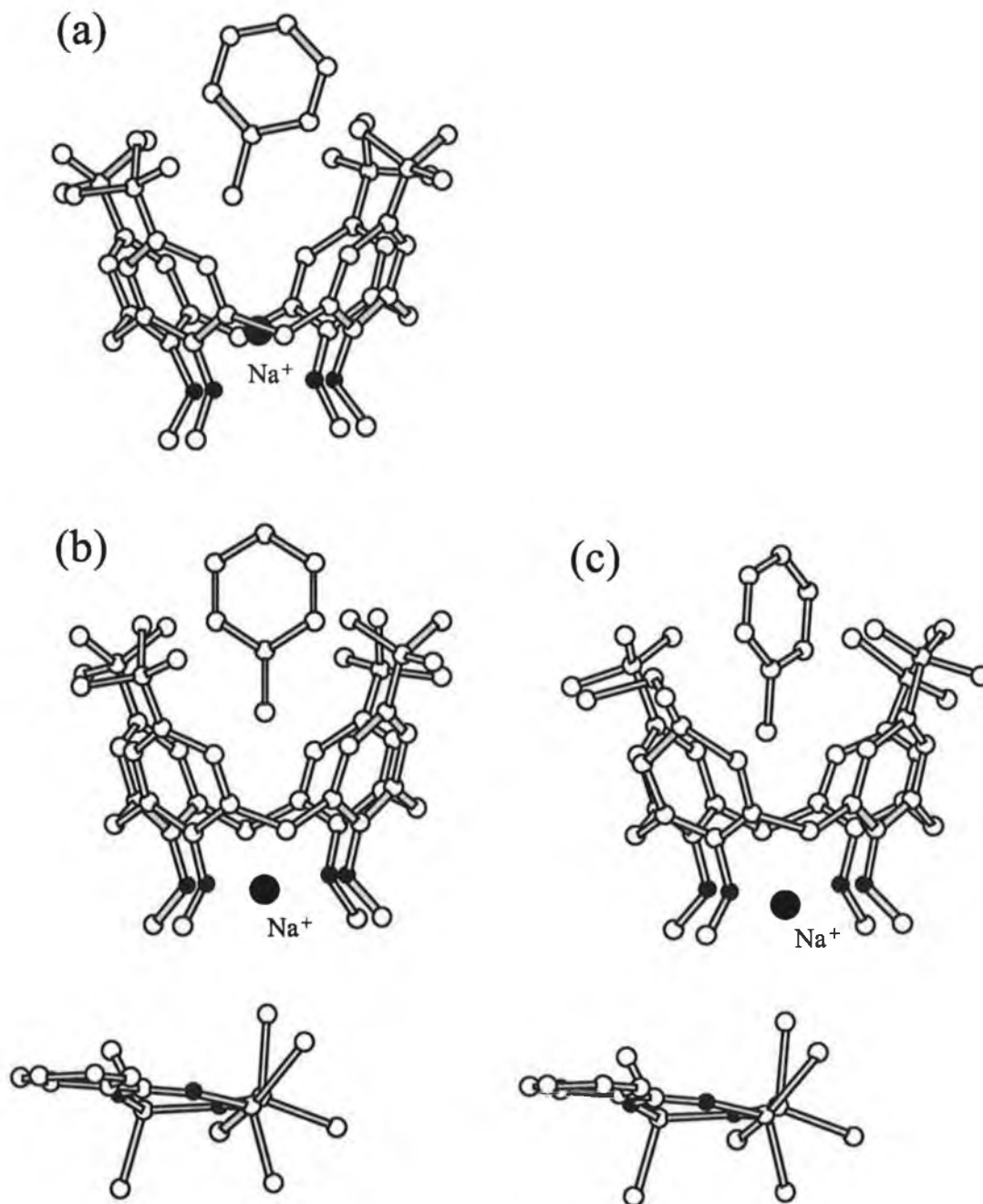


Figure 59. The model structure of (a) the Na^+ complex of **5** with a toluene solvate (b) after inclusion of a fixed counter-ion and (c) the X-ray structure of the complex.

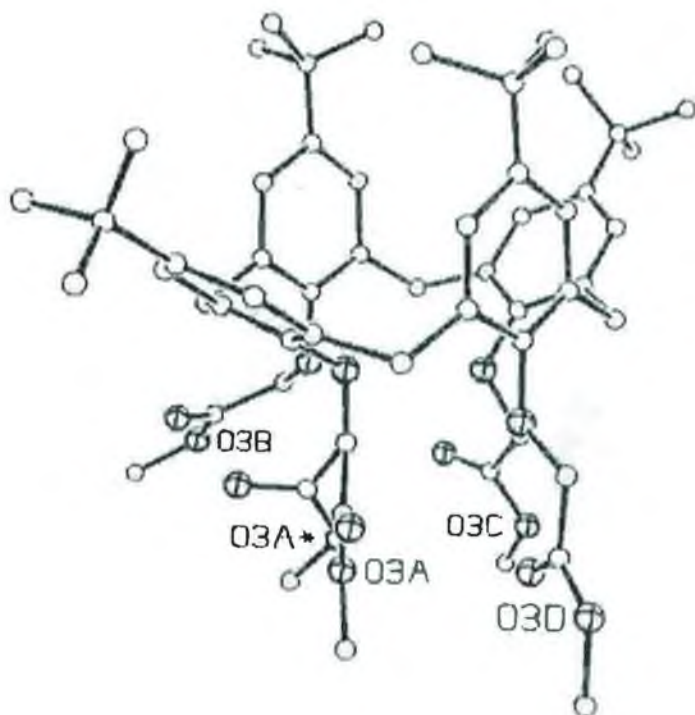


Figure 60. A side on view of 3. The oxygen atoms are the larger circles and are marked with a cross.

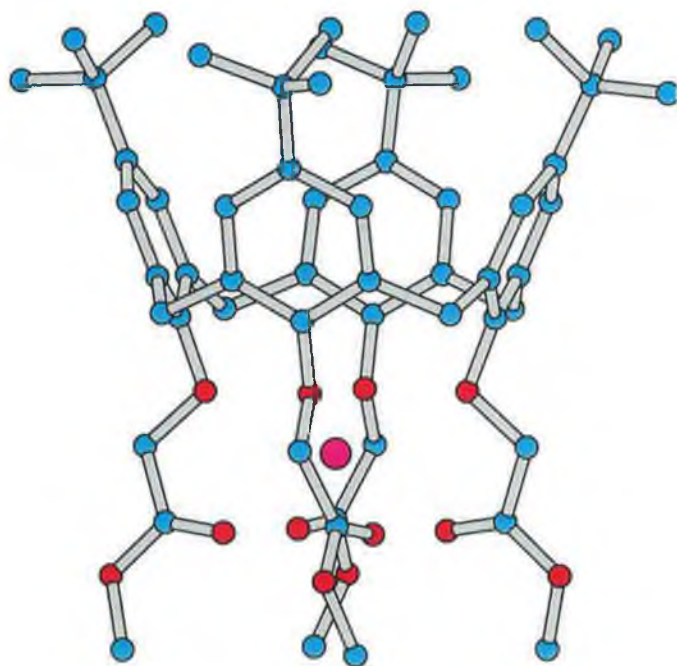


Figure 61. Ball and tube rendering of the side-on view of the optimised structure of 3:Na⁺. PM3 partial charges were placed on the ligand with Method 2 and by initially placing the ion close to the optimised position. The initial geometry used for the ligand was that of the optimised structure of the free ligand. Colour code: cyan: Carbon; red: Oxygen; magenta: Sodium.

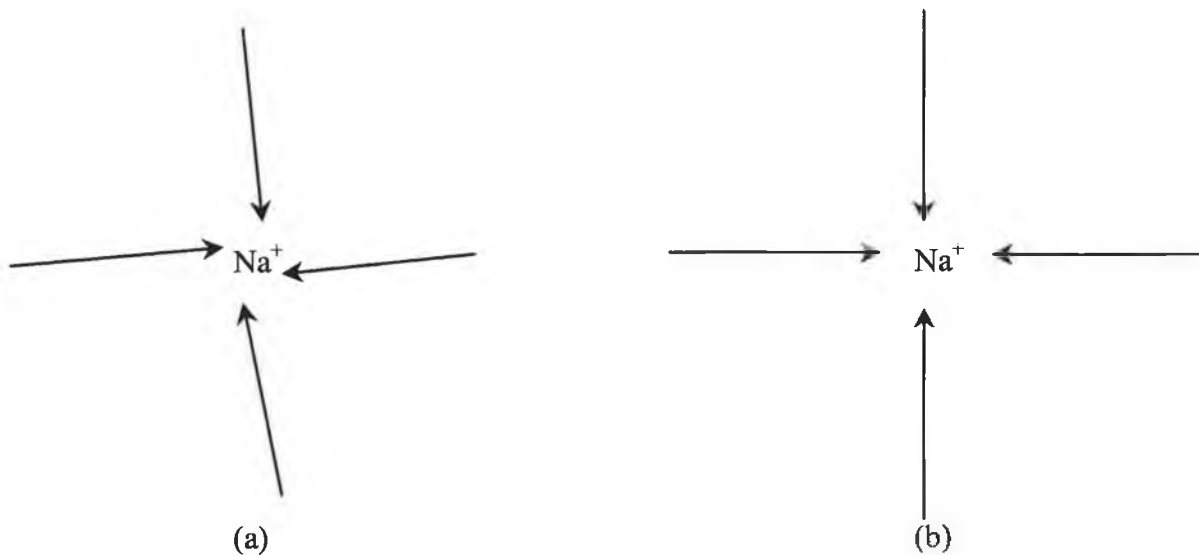


Figure 62. An illustration of how the carbonyl complexing groups are positioned around the included cation Na^+ (The CO oxygen atom is at the arrow head).

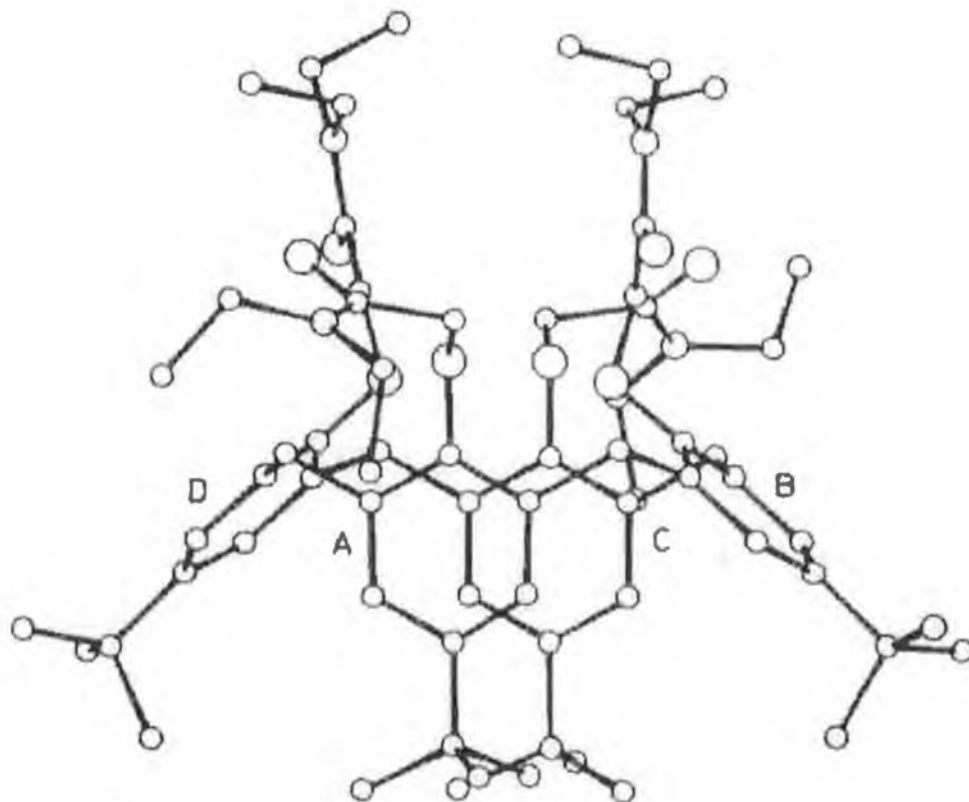


Figure 63. A side on view of 1

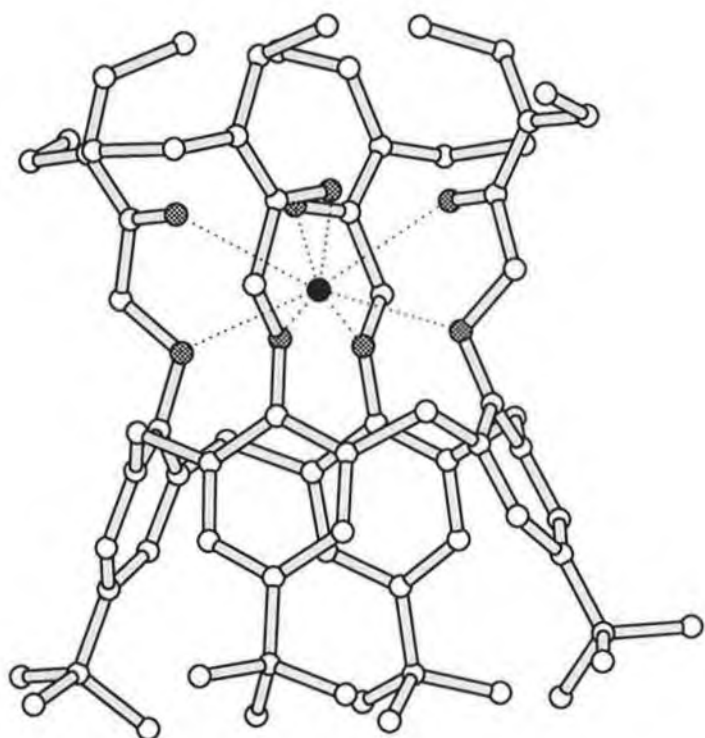


Figure 64. The model structure of the K^+ complex of 1.

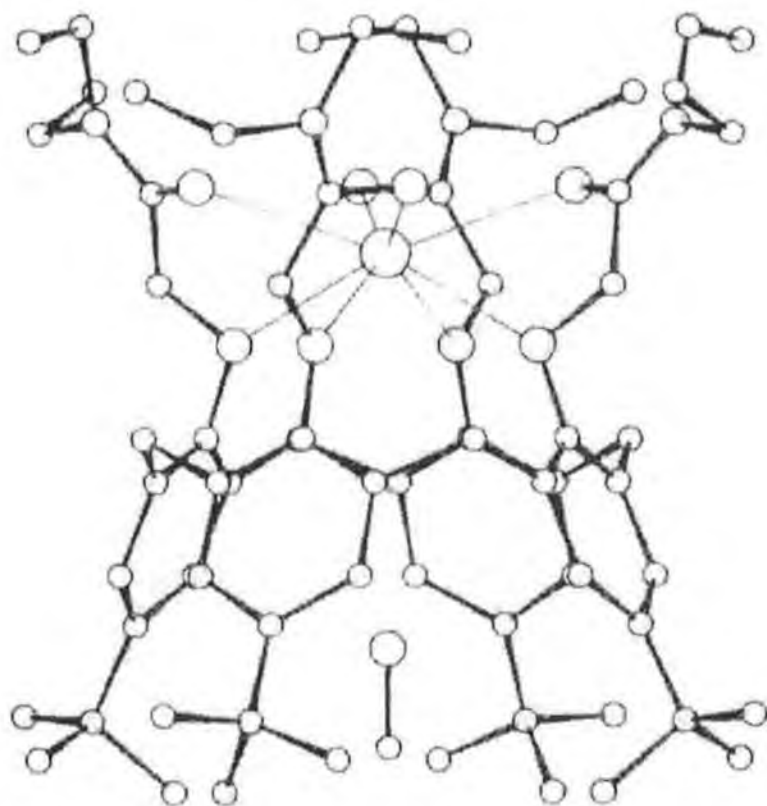


Figure 65. The X-ray crystal structure of the 1·KSCN·MeOH complex.

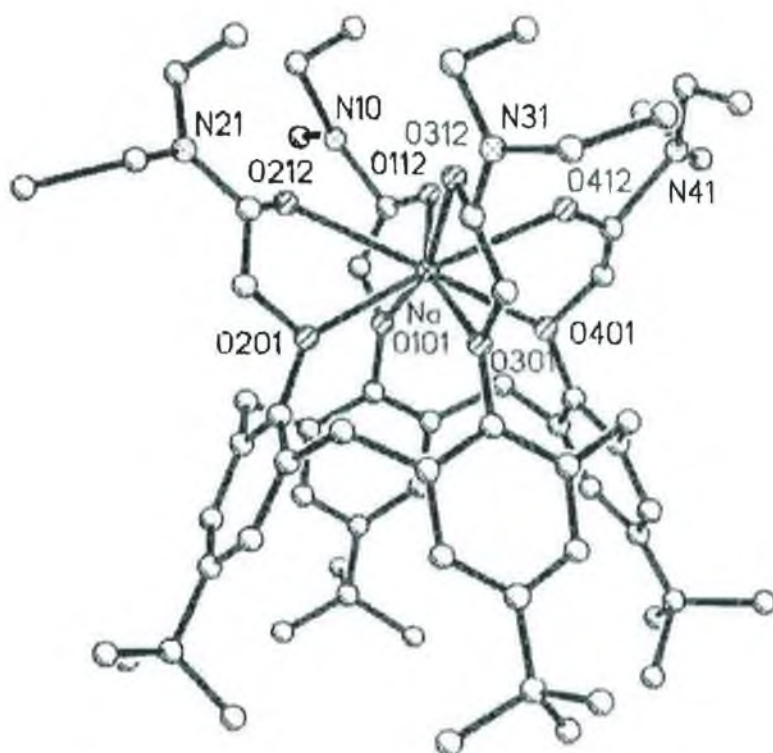


Figure 66. X-ray structure of the 1:Na⁺ complex

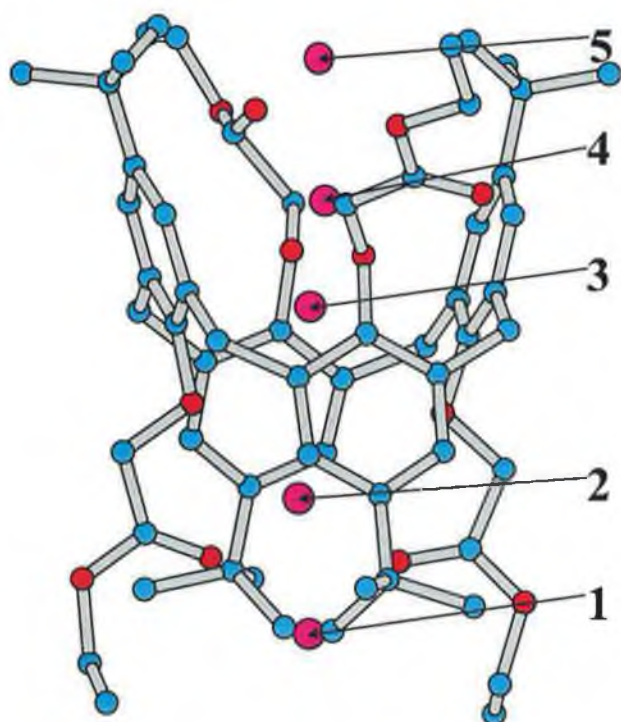


Figure 67. Ball and tube rendering of the side-on view of the X-ray structure of 4:Na⁺, showing the different positions in which the Na⁺ ion was initially placed when carrying out the optimisations. In the X-ray structure, the Na⁺ ion is in Position 2.

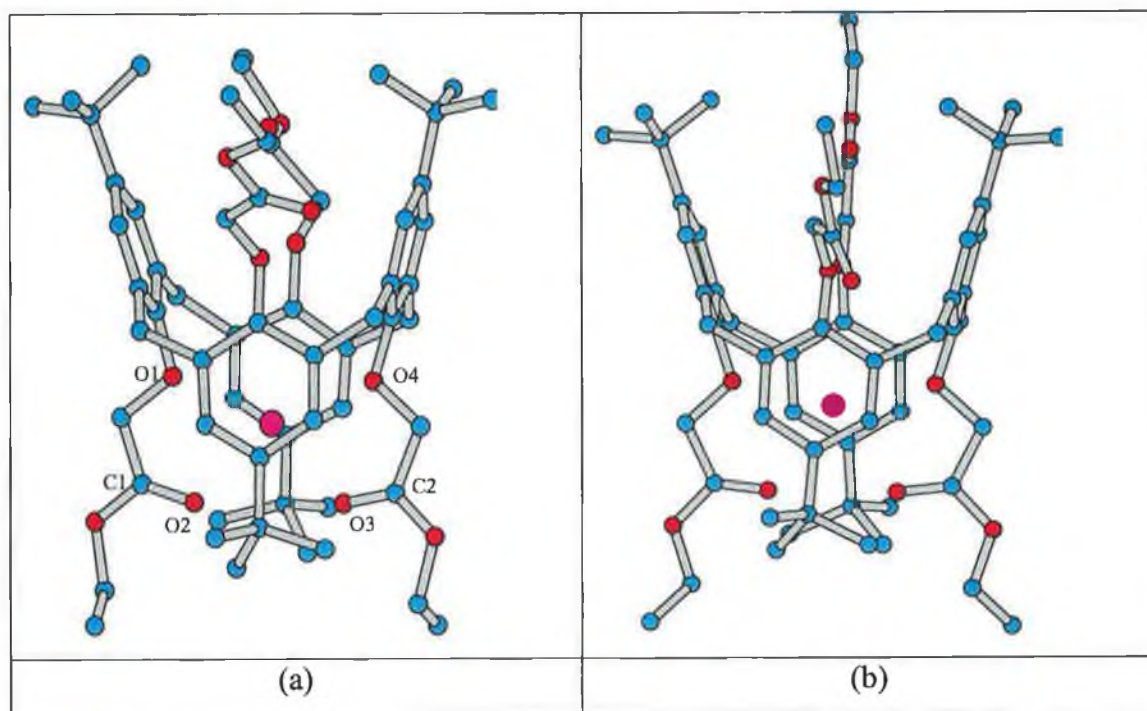


Figure 68. Ball and tube rendering of the side-on views of (a) the X-ray, and (b) the optimised, structures of $4:\text{Na}^+$. Colour code: Cyan - carbon, red - oxygen, magenta - sodium.

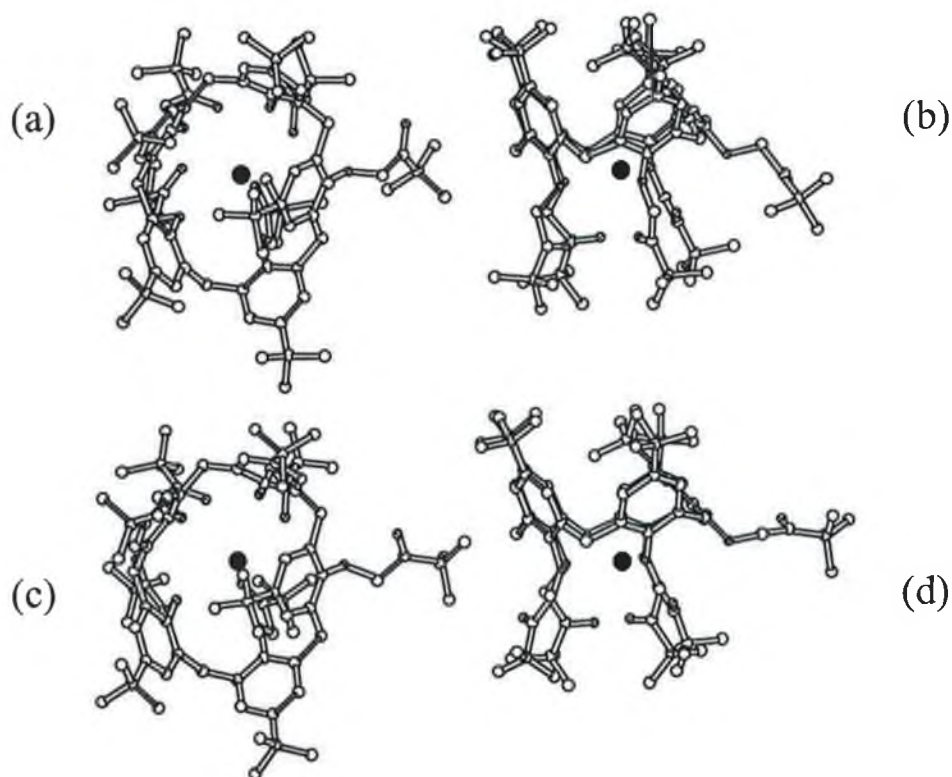


Figure 69. Orthogonal views of (a), (b) the modelled structure and (c), (d) the X-ray structure of the Rb^+ complex of **2**.

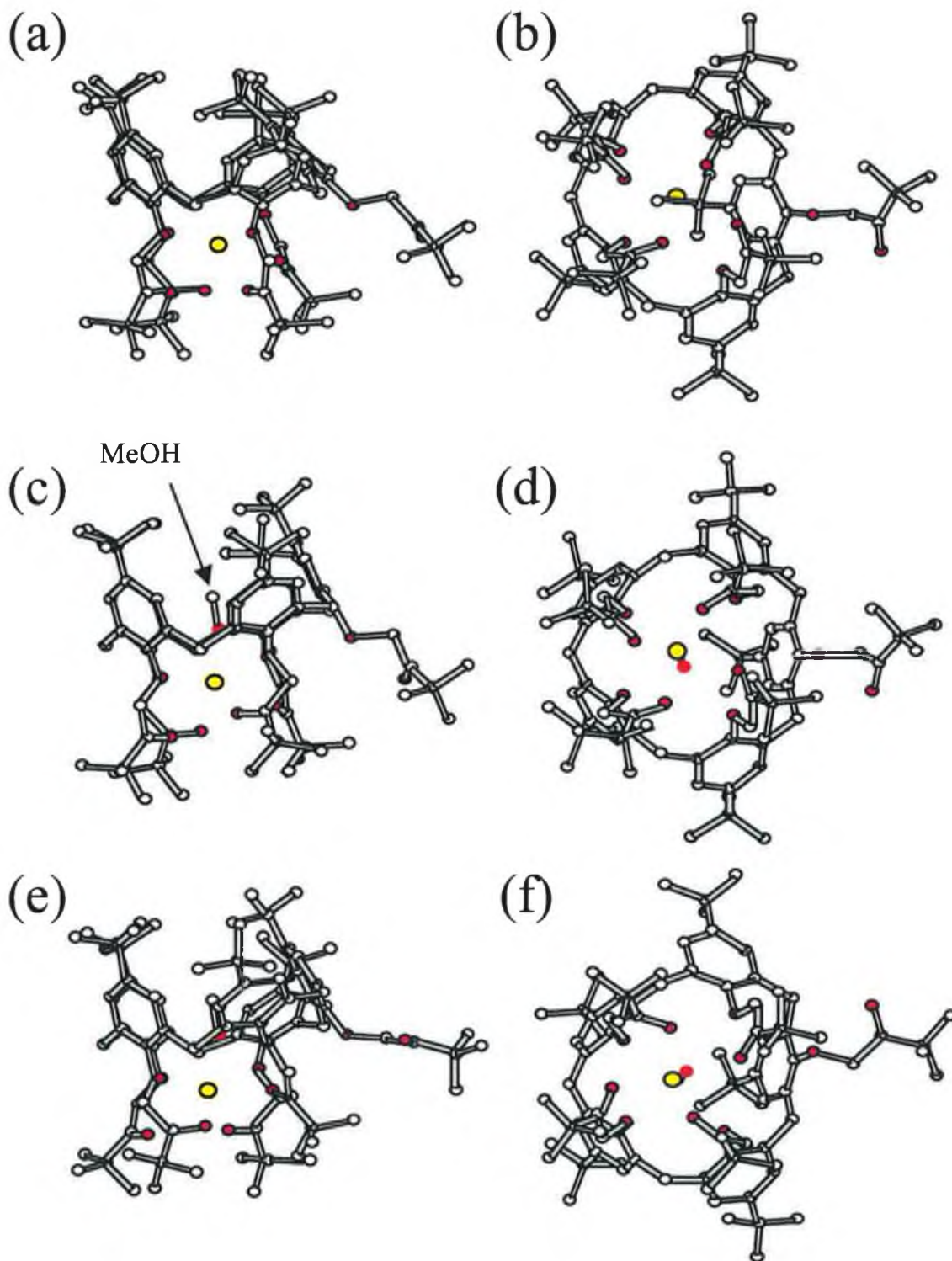


Figure 70. Orthogonal views of: (a), (b) the modelled structure of the Na⁺ complex of **2** with no solvent included in the model: (c), (d) the modelled structure of the Na⁺ complex of **2** with a methanol solvent molecule included: (e), (f) the X-ray structure of the Na⁺ complex of **2**. Legend: Red: Oxygen; Yellow: Sodium; White: Carbon.

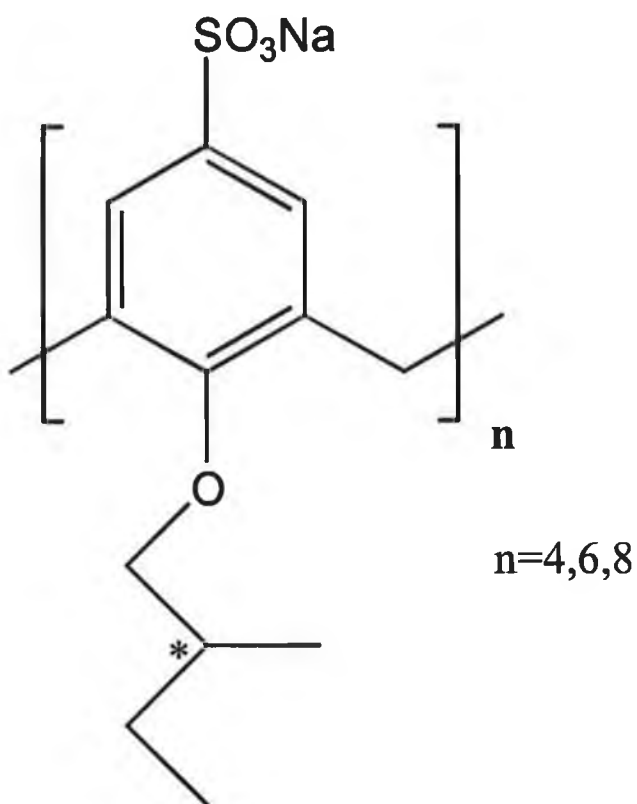


Figure 71. p-Sulfonatocalix[n]arene. * denotes the chiral centre.

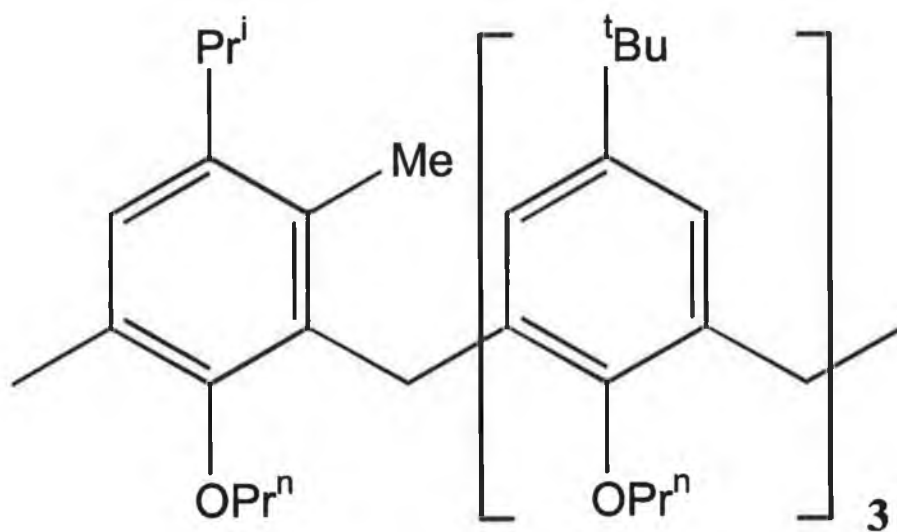
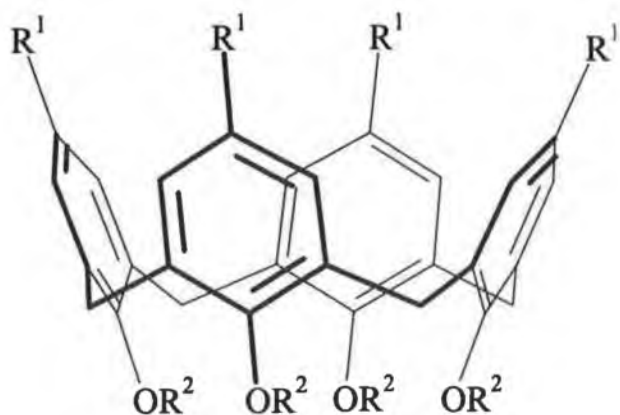


Figure 72. Shinkai first resolved this enantiomerically pure calixarene (Pr^n : neo-propyl; Pr^i : iso-propyl).



| Calix[4]arene | R ¹ | R ² |
|---------------------------------|----------------|----------------|
| (S) dinaphthyl prolinol (L1) | <i>t</i> -Bu | |
| (S) propranolol amide (L2) | | |

Figure 73. A 2D schematic of the two chiral calix[4]arenes used in this study. The 'squiggle' indicates the bond joining the R group to the phenolic oxygen /aromatic carbon atom. The asterisk indicates the chiral carbon atoms.

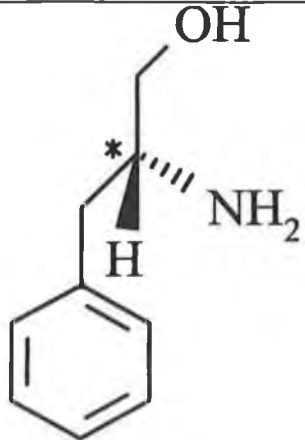
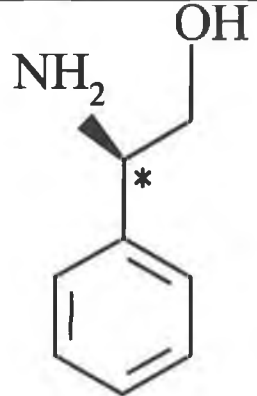
| Chiral amine | 2D structure |
|--------------------------------|--|
| R-phenylalaninol (pa) |  |
| R-phenylglycinol (pg) |  |

Figure 74. A 2D representation of the two chiral amines used in this study. The asterisk indicates the chiral carbon atoms.

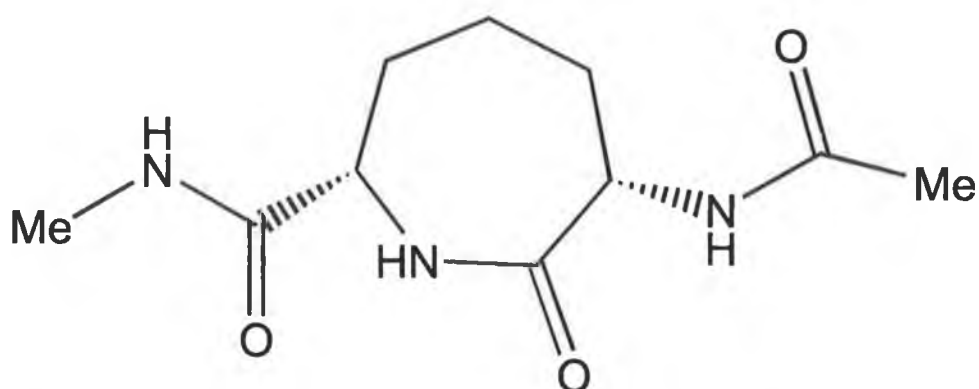


Figure 75. The lactam use in the study of inter(intra)molecular hydrogen bonding.

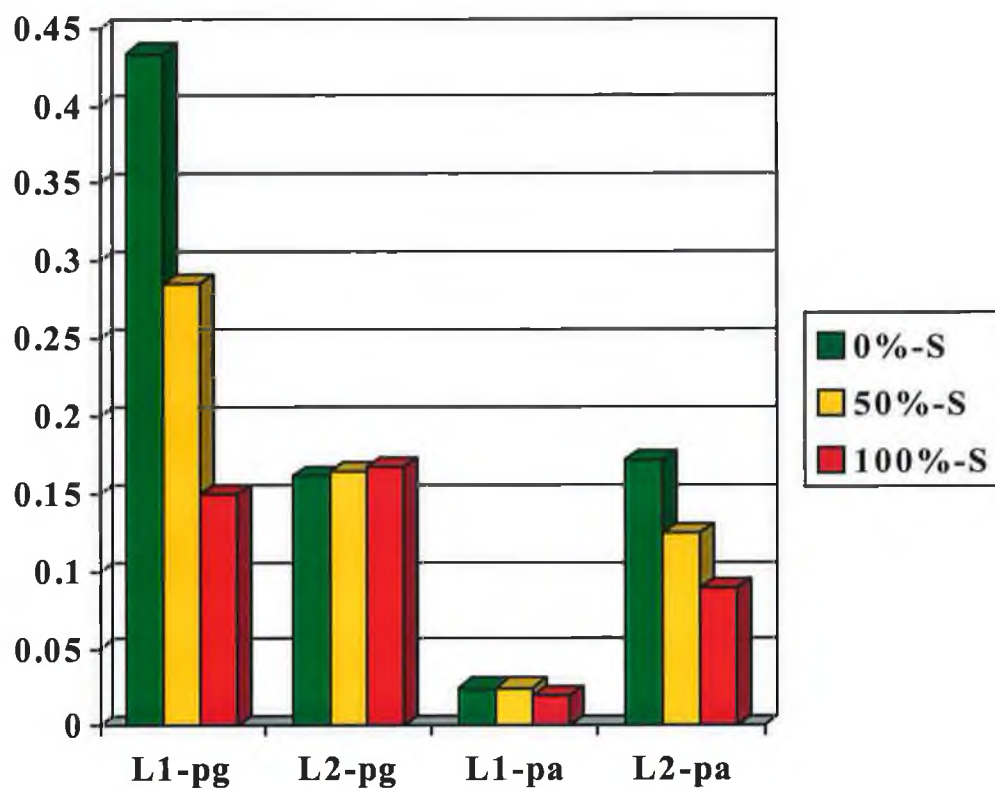


Figure 76. Stern-Volmer constants (K_{sv}) for L1 and L2 interacting with pg and pa.

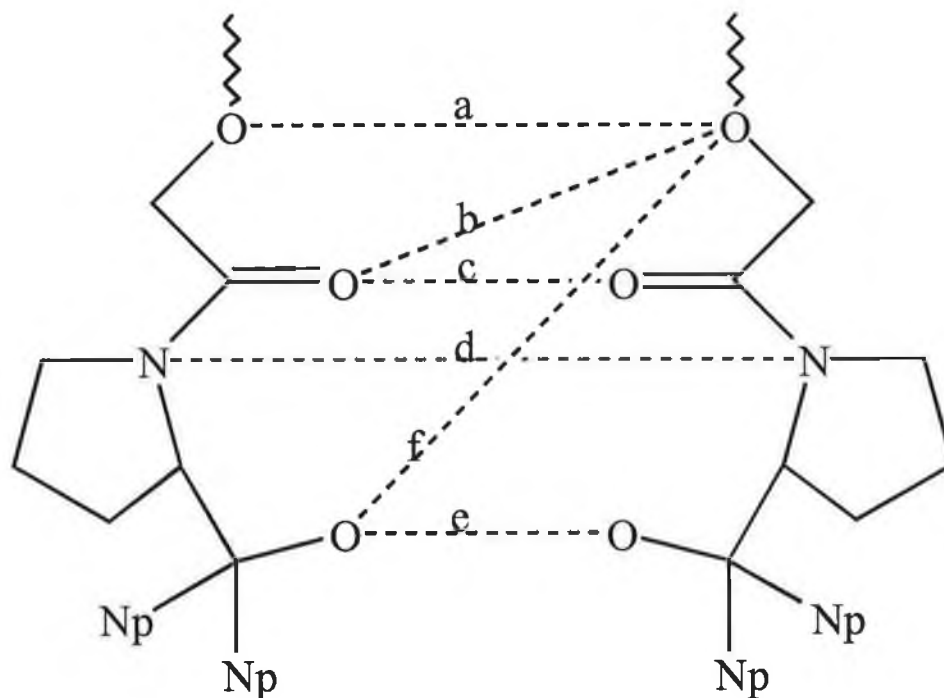


Figure 77. A diagram of two of the pendant groups of L1 illustrating the distances mentioned in Section 3.3.

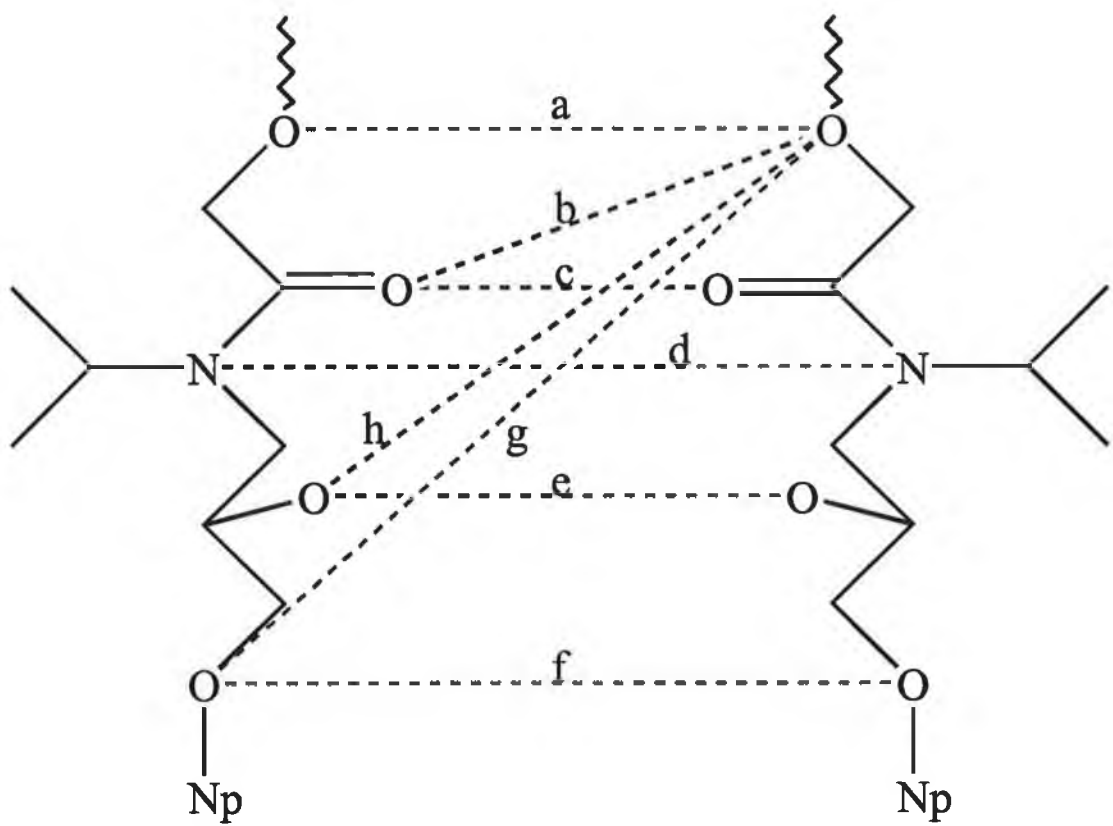


Figure 78. An illustration of two of the pendant groups of L2 demonstrating the distances mentioned in **Section 3.3**.

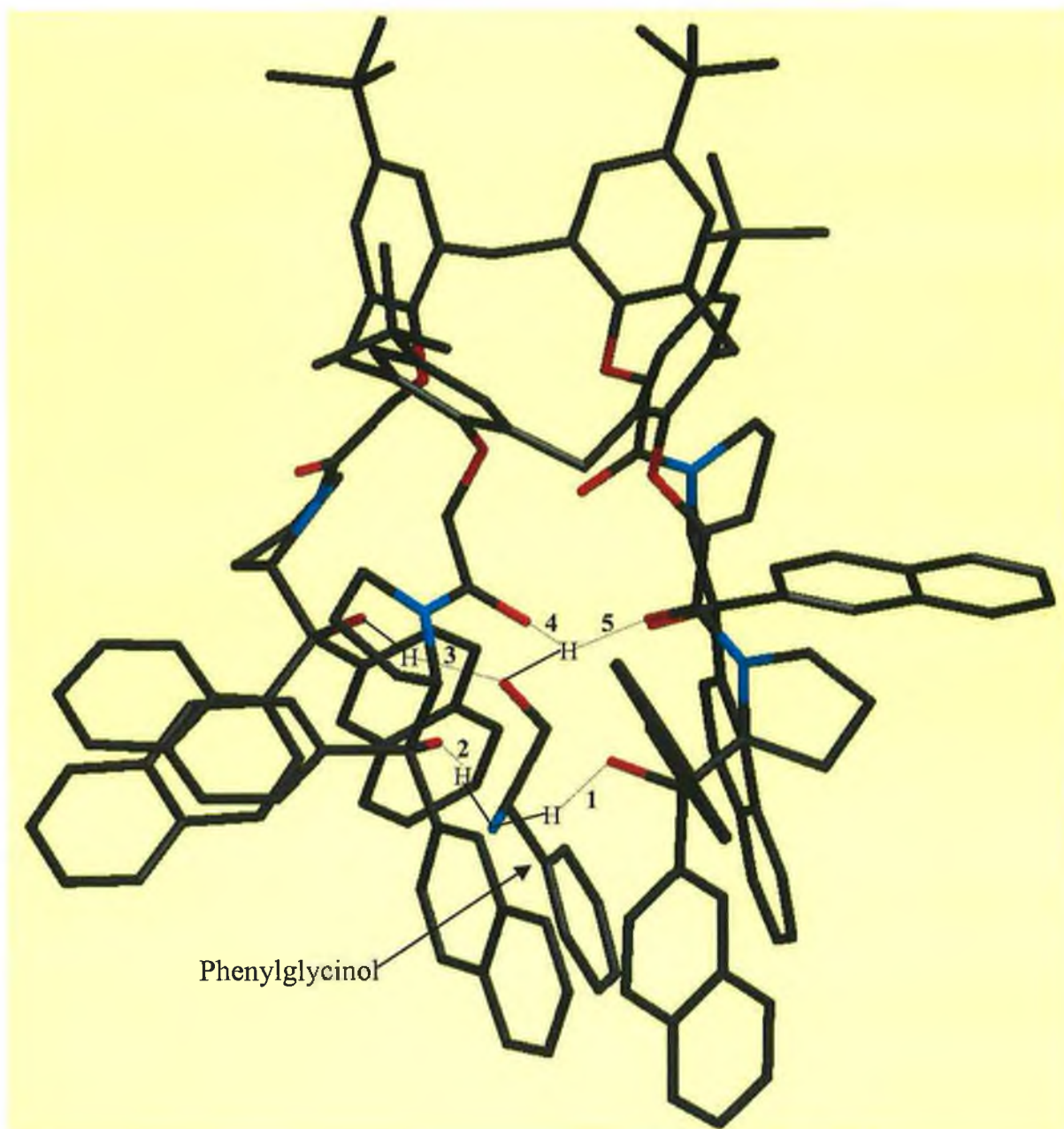


Figure 79(a). A view through the side of the R-pg : L1 inclusion complex. Grey: Carbon; Blue: Nitrogen; Red: Oxygen. Hydrogen atoms not in the complexation region omitted for clarity. Dotted line: Hydrogen bond; Full black line: O-H, N-H₂ bonds.

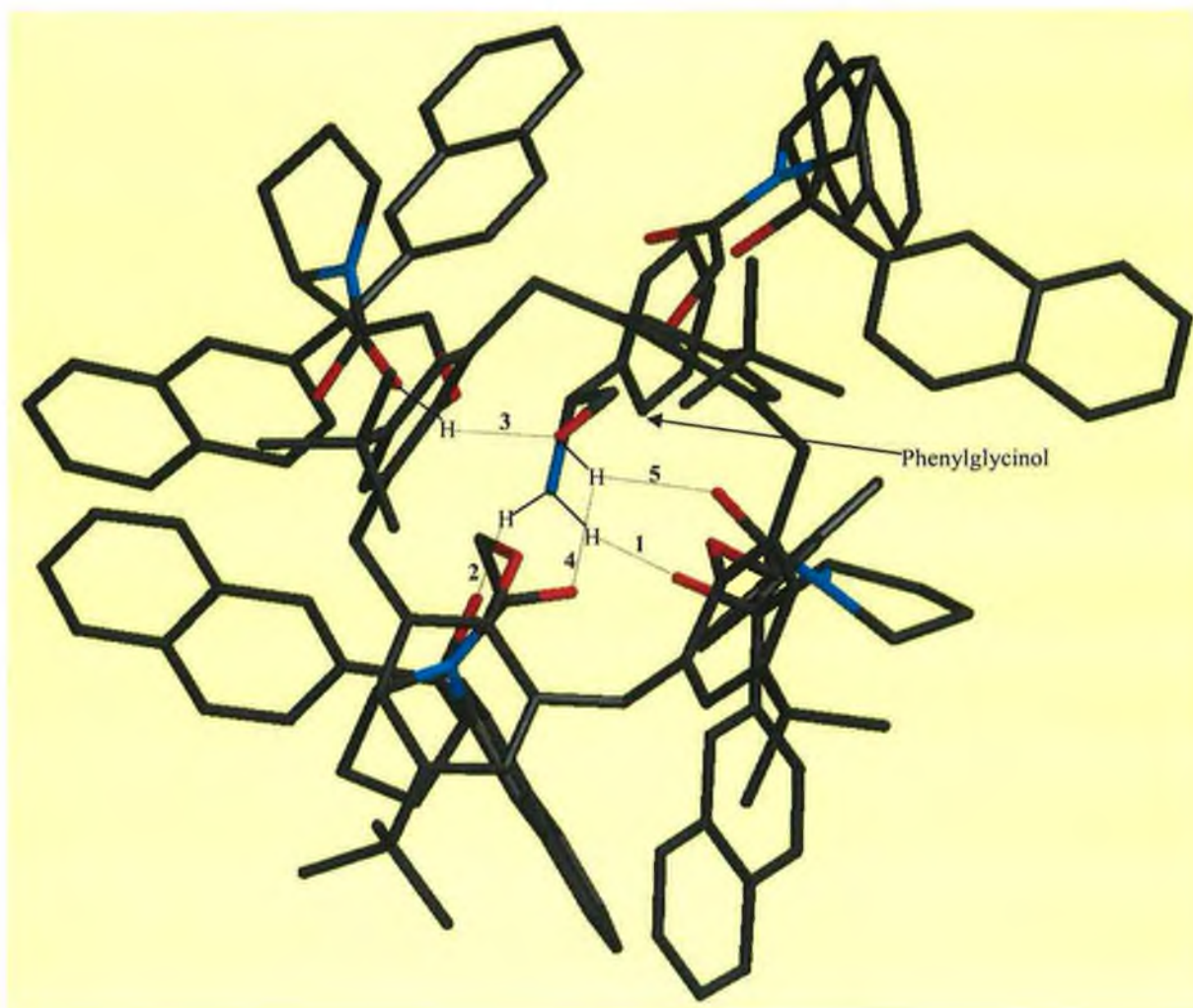


Figure 79(b). A view through the cavity (from above the tert.-butyl groups) of the R-pg : L1 inclusion complex. Designations as in Fig. 79(a).

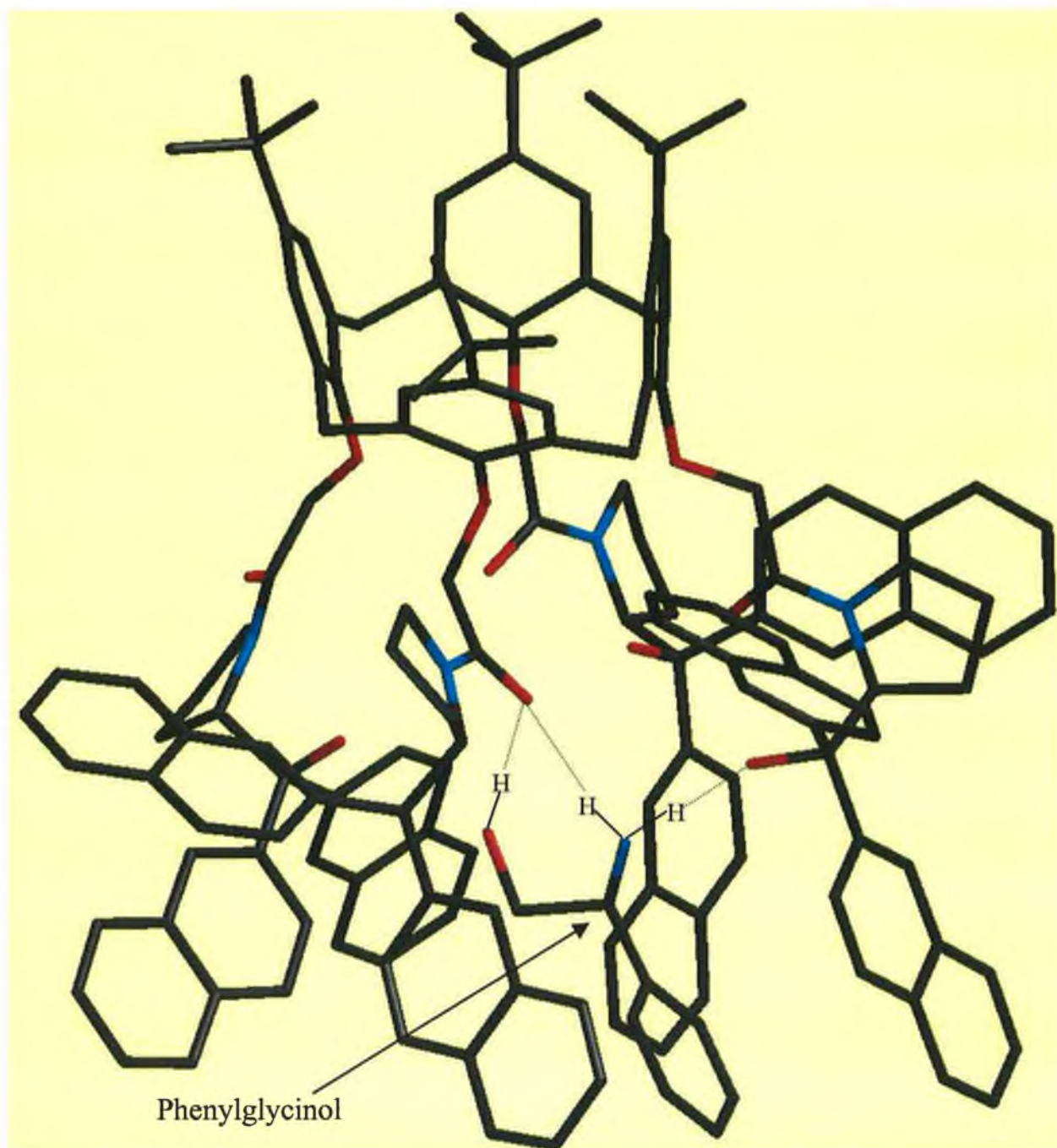


Figure 80(a). A view through the side of the S-pg : L1 inclusion complex. Designations as in Fig. 79(a).

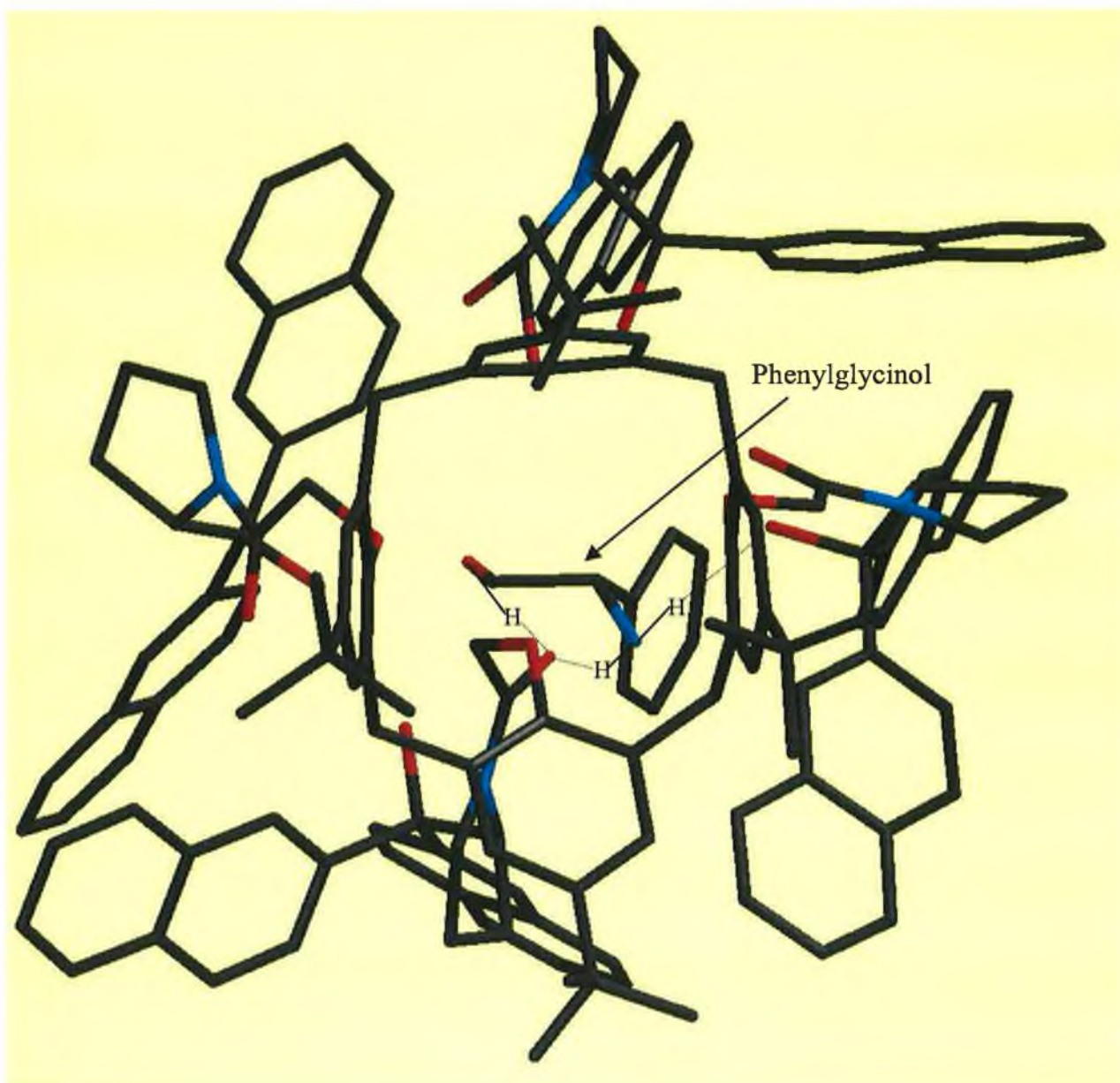


Figure 80(b). A view through the cavity (from above the tert.-butyl groups) of the S-pg : L1 inclusion complex. Designations as in Fig. 79(a).

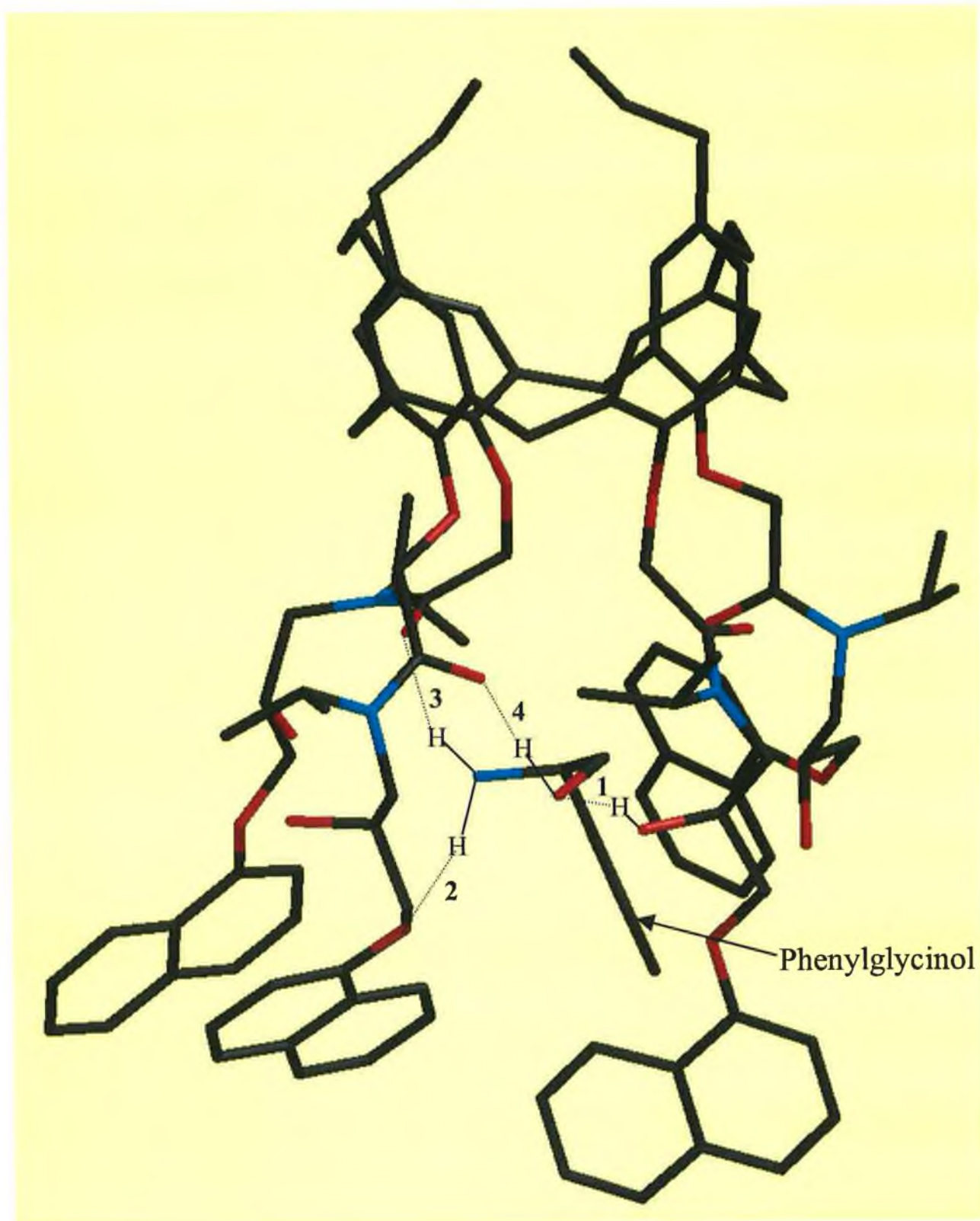


Figure 81(a). A view through the side of the R-pg : L2 inclusion complex. Designations as in Fig. 79(a).

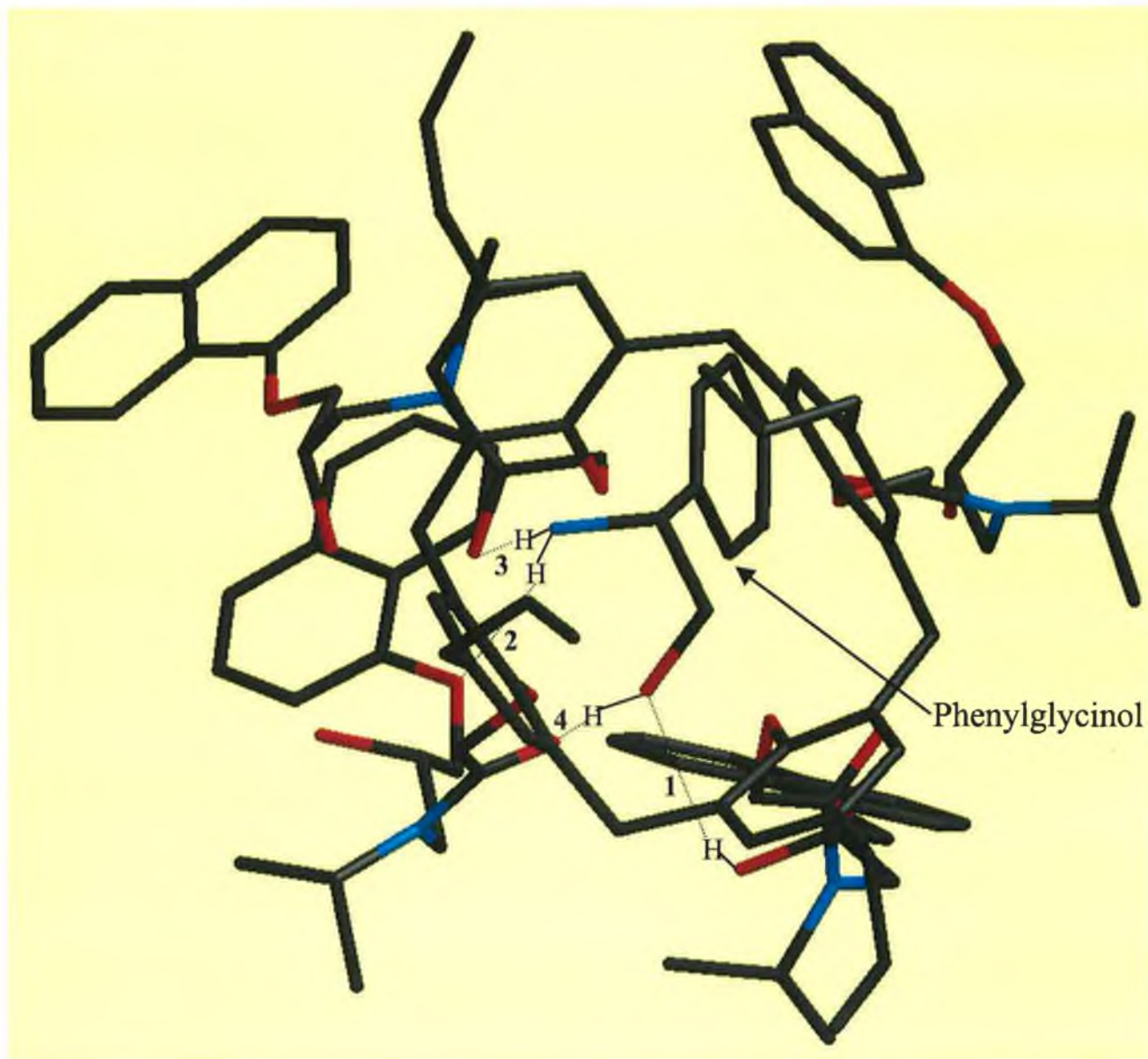


Figure 81(b). A view through the cavity (from above the tert.-butyl groups) of the R-pg : L2 inclusion complex. Designations as in Fig. 79(a).

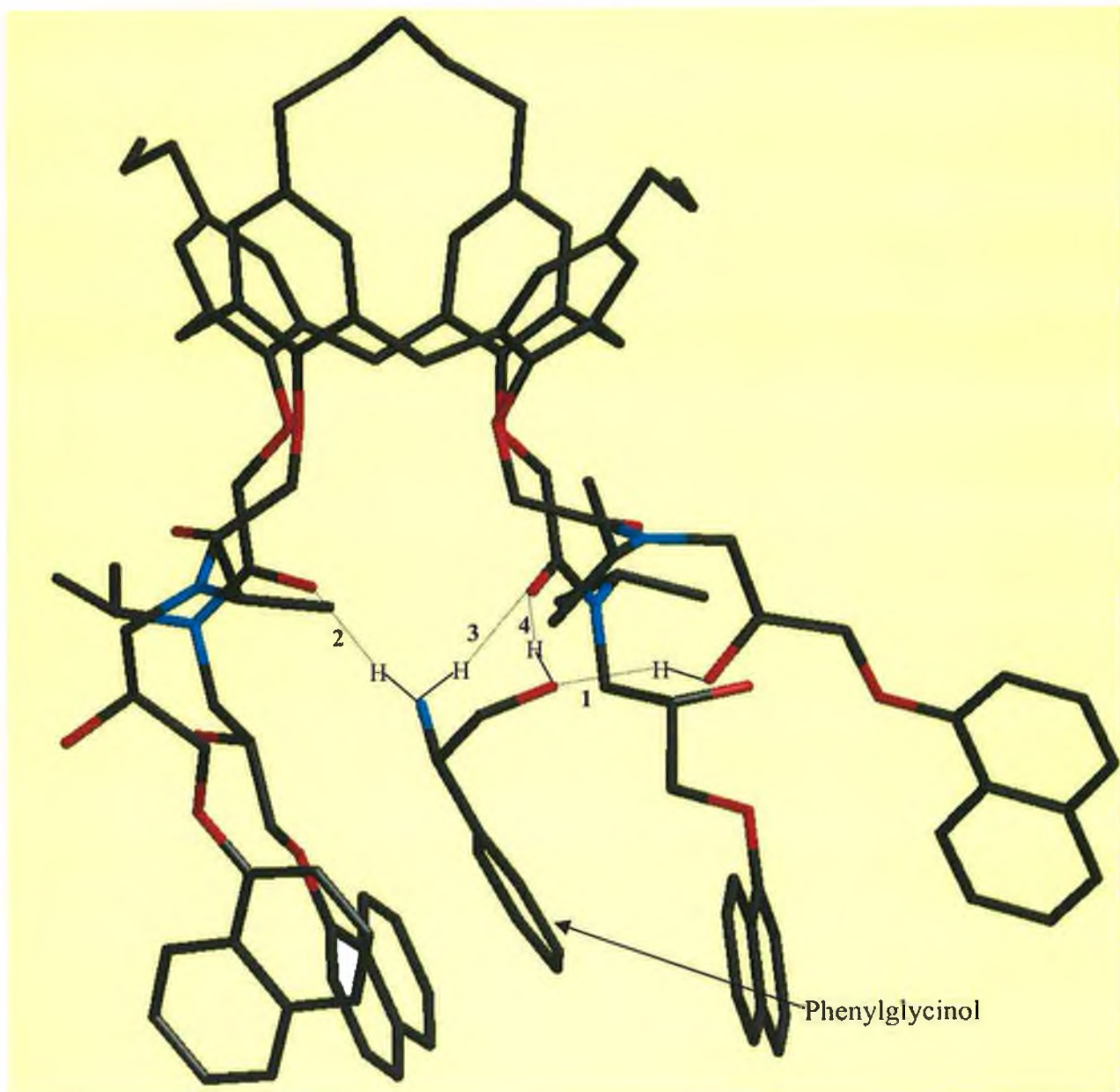


Figure 82(a). A view through the side of the S-pg : L2 inclusion complex. Designations as in Fig. 79(a).

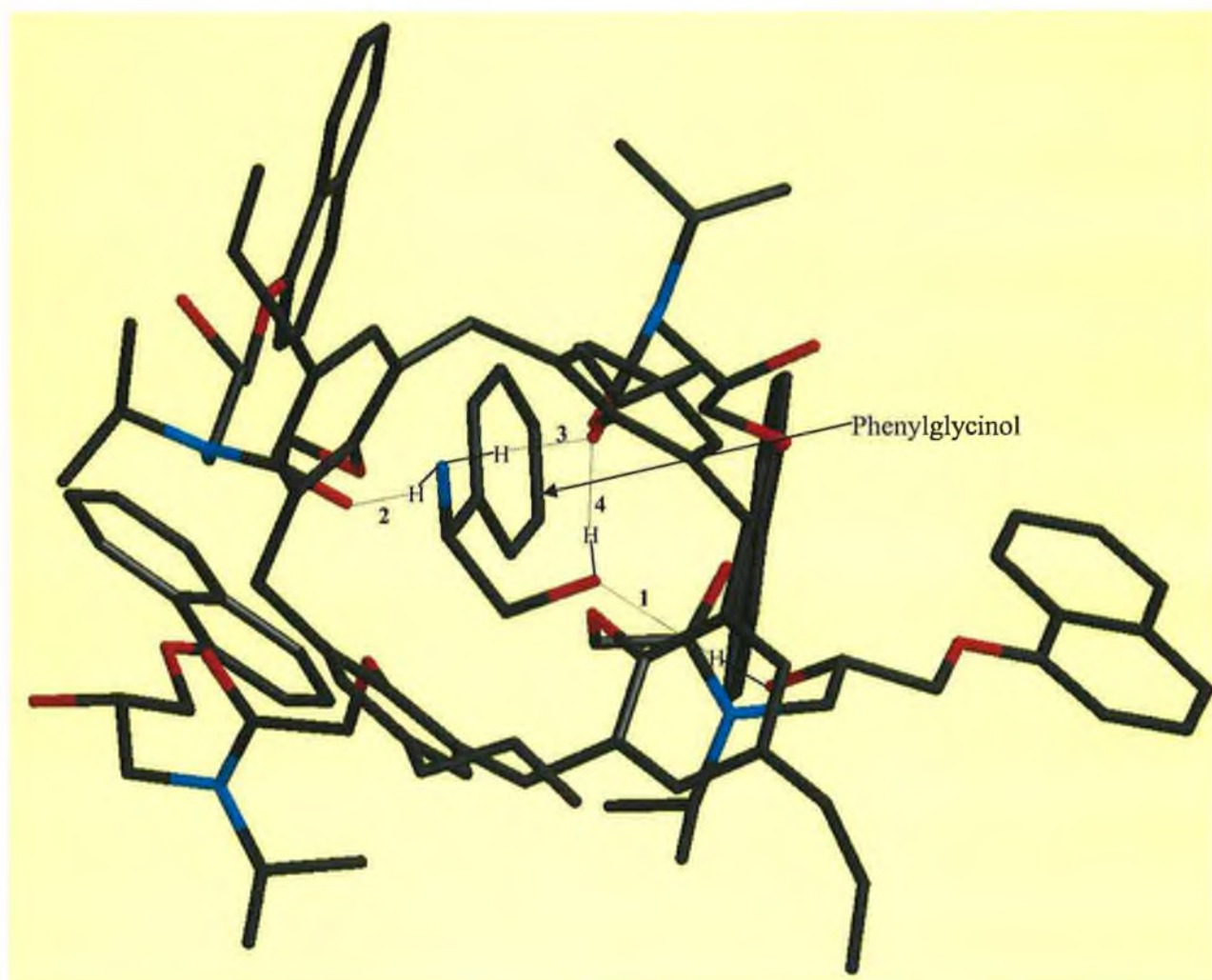


Figure 82(b). A view through the cavity (from above the tert.-butyl groups) of the S-pg : L2 inclusion complex. Designations as in Fig. 79(a).

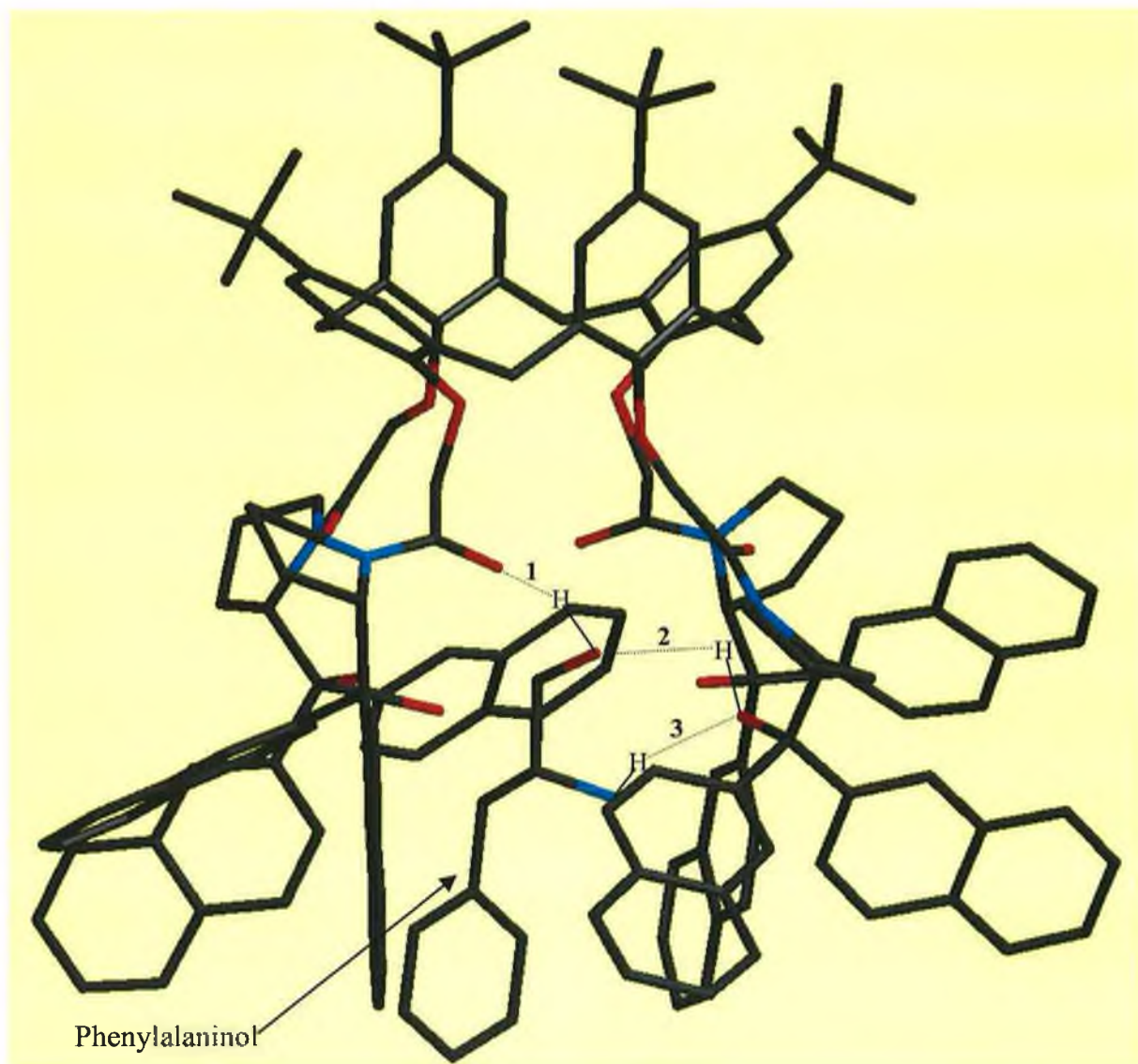


Figure 83(a). A view through the side of the R-pa : L1 inclusion complex. Designations as in Fig. 79(a).

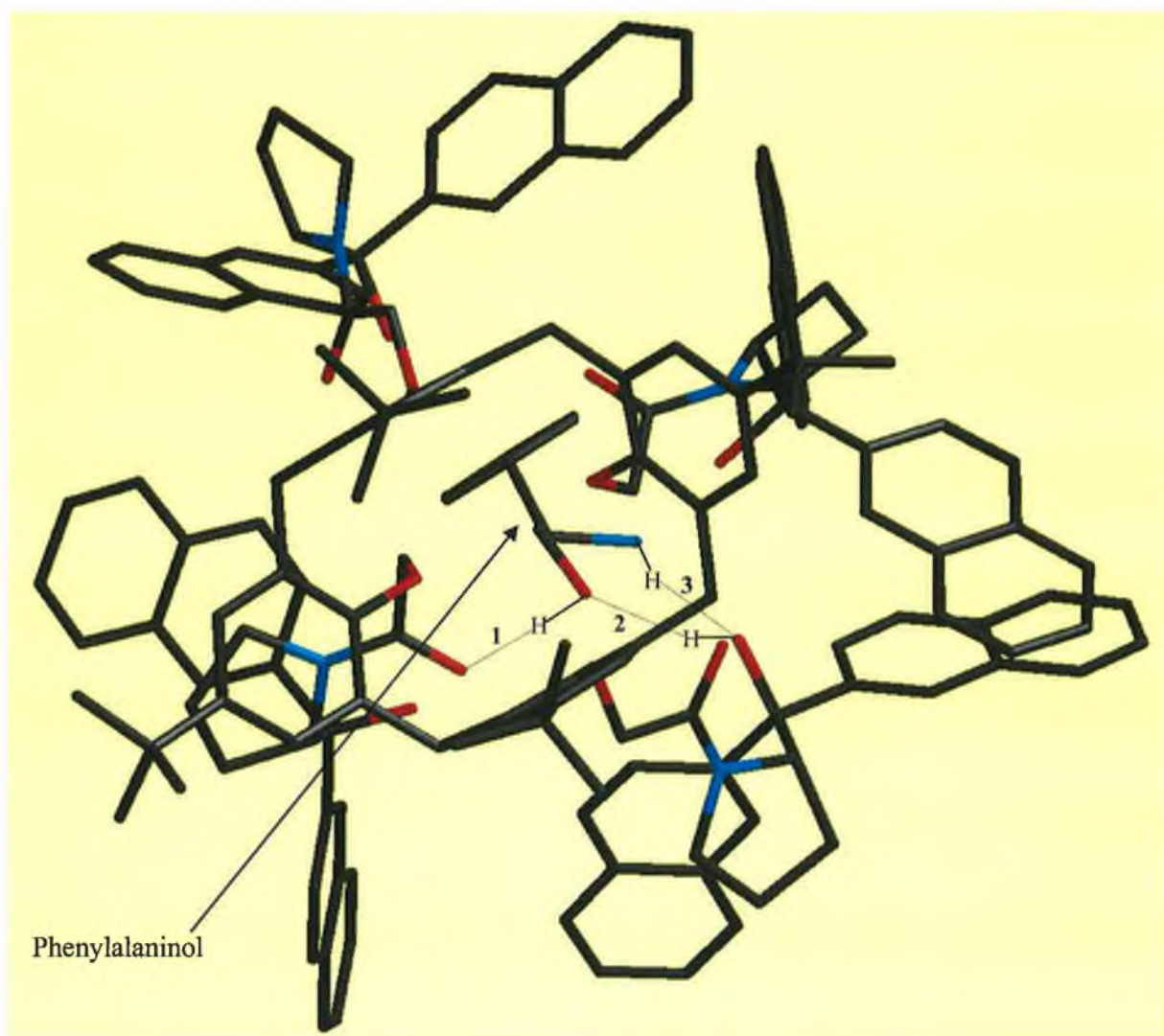


Figure 83(b). A view through the cavity (from above the tert.-butyl groups) of the R-pa : L1 inclusion complex. Designations as in Fig. 79(a).

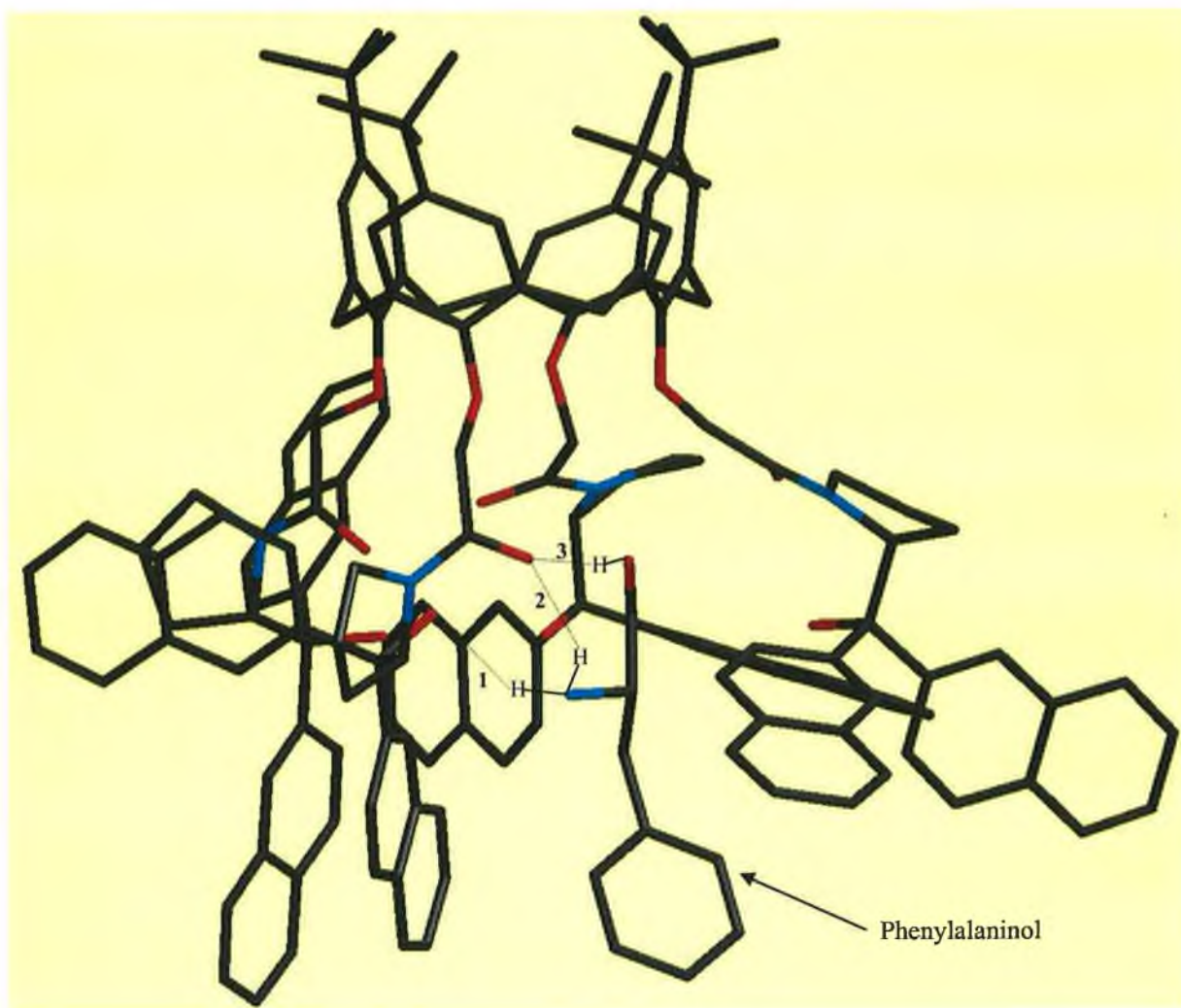


Figure 84(a). A view through the side of the S-pa : L1 inclusion complex. Designations as in Fig. 79(a).

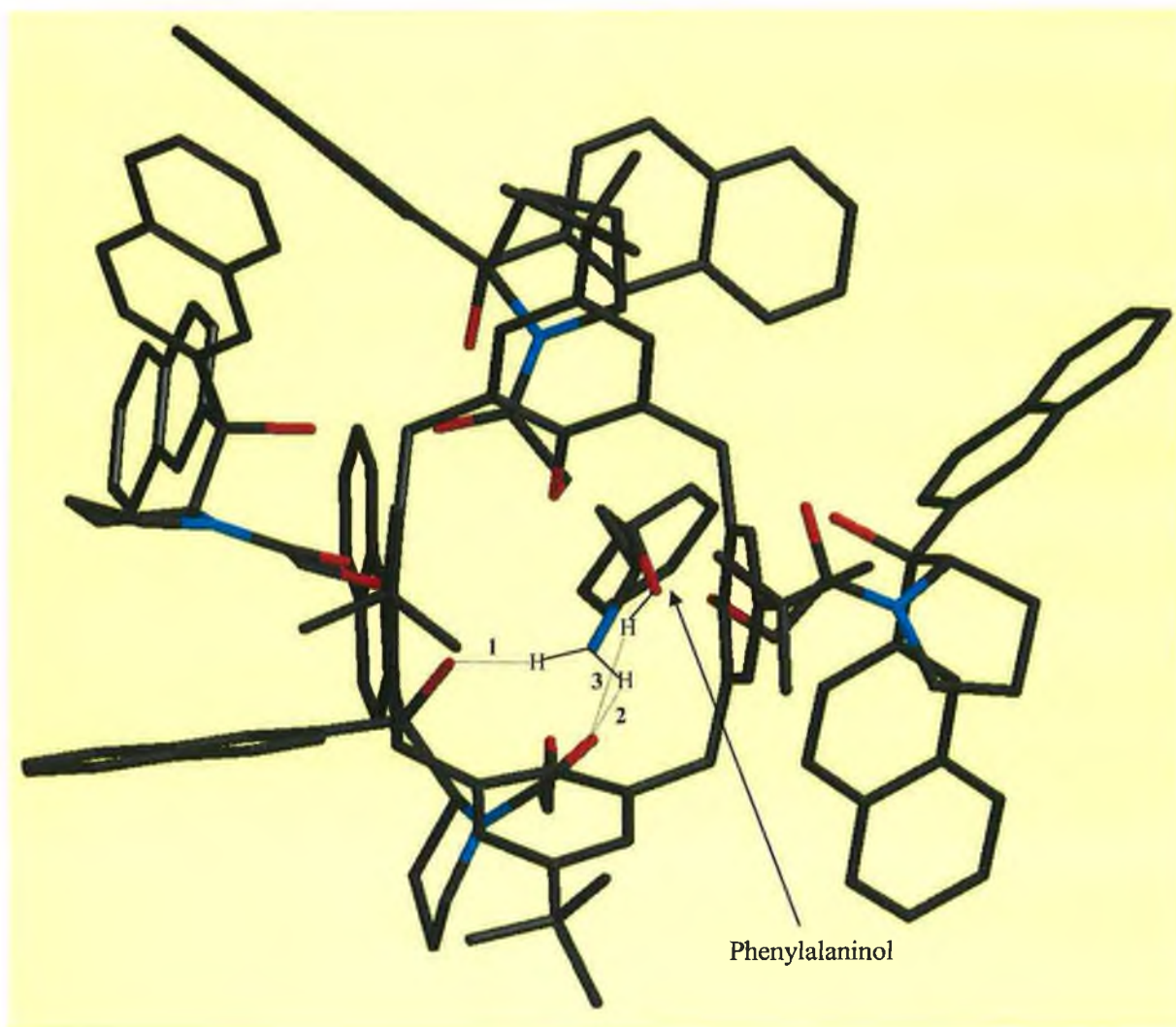


Figure 84(b). A view through the cavity (from above the tert.-butyl groups) of the S-pa : L1 inclusion complex. Designations as in **Fig. 79(a)**.

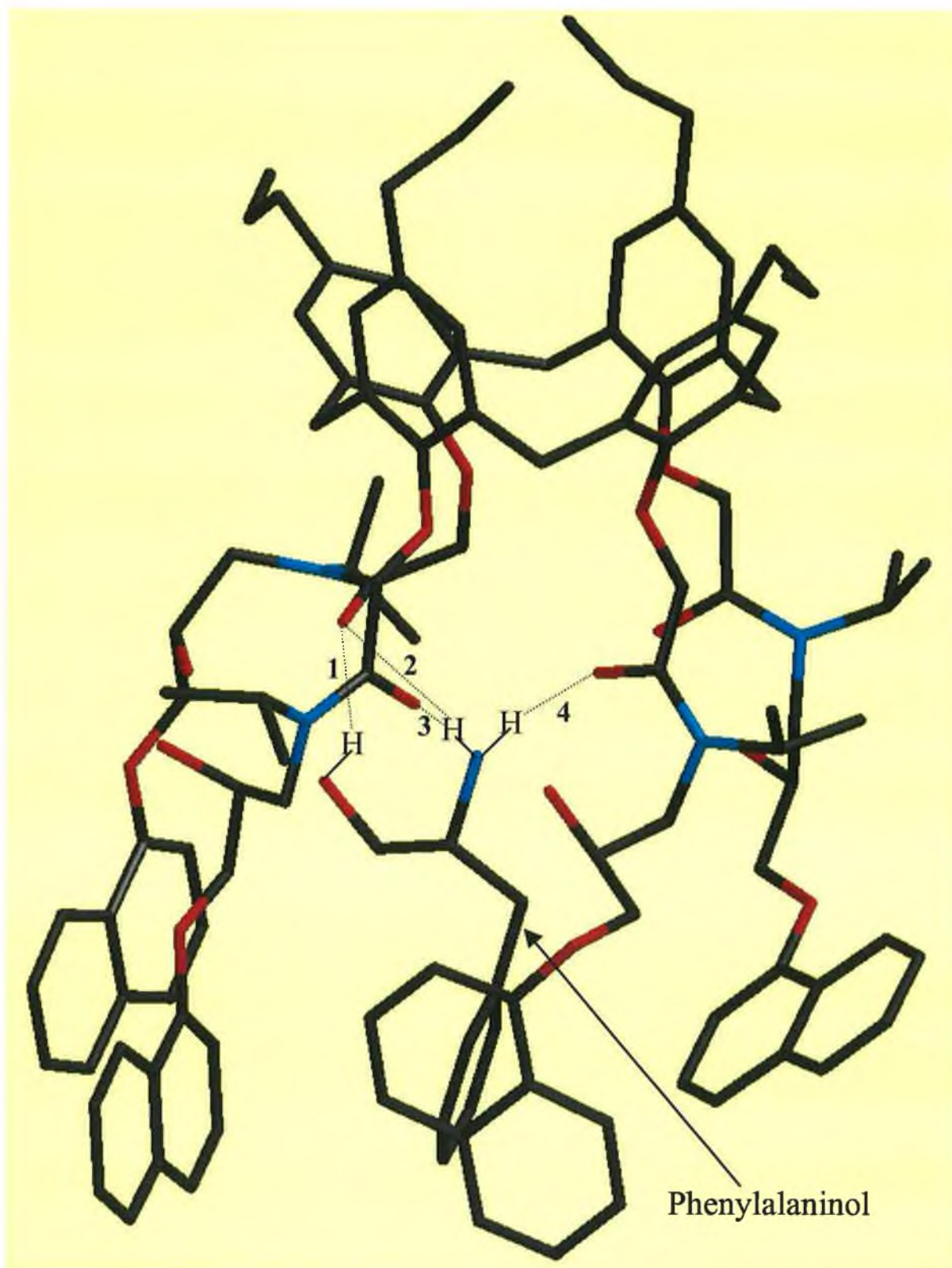


Figure 85(a). A view through the side of the R-pa : L2 inclusion complex. Designations as in **Fig. 79(a)**.

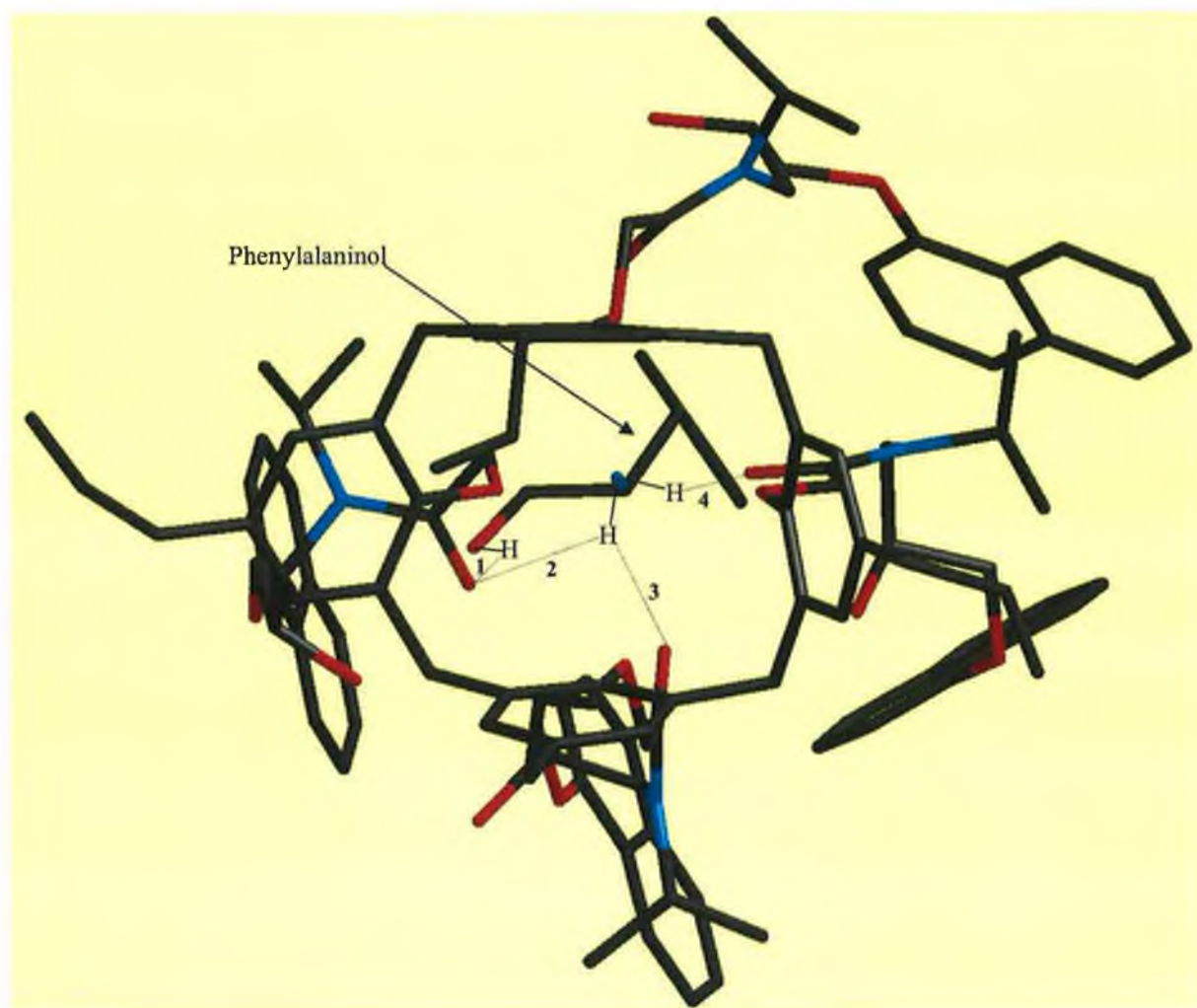


Figure 85(b). A view through the cavity (from above the tert.-butyl groups) of the R-pa : L2 inclusion complex. Designations as in Fig. 79(a).

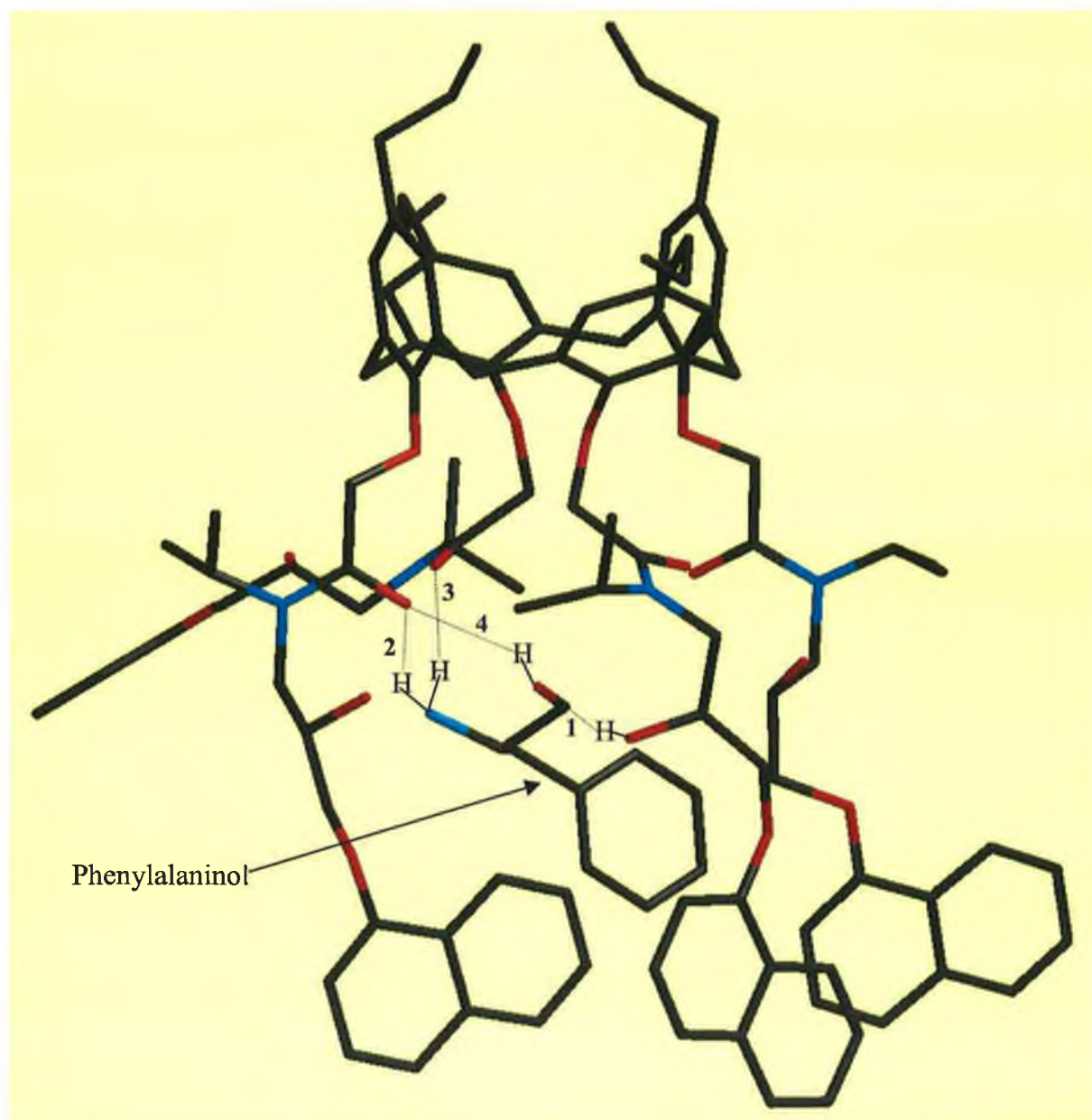


Figure 86(a). A view through the side of the S-pa : L2 inclusion complex. Designations as in **Fig. 79(a)**.

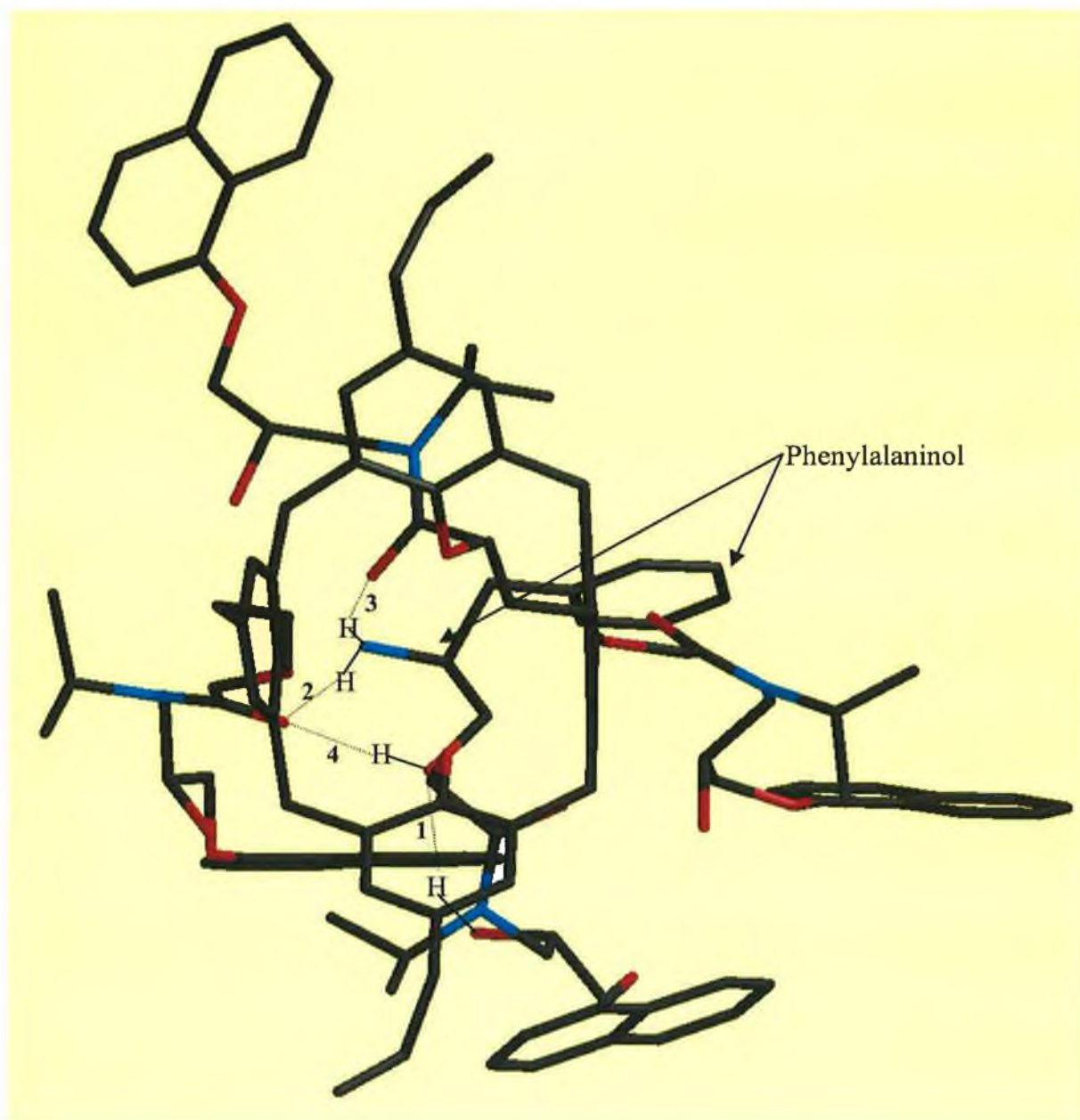


Figure 86(b). A view through the cavity (from above the tert.-butyl groups) of the S-pa : L2 inclusion complex. Designations as in **Fig. 79(a)**.

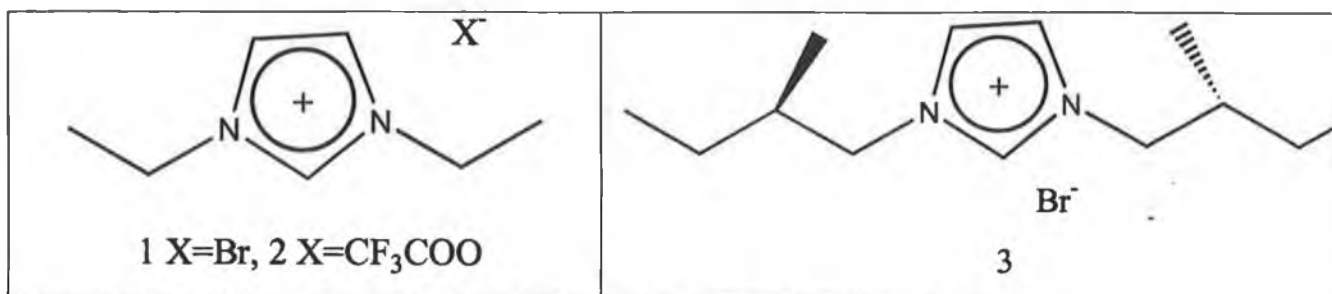


Figure 87. An illustration of the three ionic liquids utilised in this study.